"STUDIES OF DOUBLE-DIFFUSED TRANSISTOR STRUCTURES"

A THESIS

presented for the degree of

DOCTOR OF PHILOSOPHY of the UNIVERSITY OF LONDON

by

RAYE EDWARD THOMAS

June 1966

ABSTRACT

The solid-state diffusion process is examined with particular reference to the idealized classical impurity distributions normally assumed to apply in diffused structures. The peculiar properties of the double-diffused structure (graded junctions and a maximum in base doping) are shown to effect an overall improvement in frequency performance. Methods used to derive information on the impurity profile both in large area devices (destructive techniques) and in small area devices (physical model derived from terminal measurements) are discussed. Early models are shown to be inadequate and strictly limited in applicability.

A physical model (double exponential) is proposed to apply generally to double-diffused transistors. A detailed study of classical distributions establishes that the assumed model not only is a good representation of such distributions in the base region, but also accurately predicts depletion layer and base transport properties.

The proper interpretation of terminal measurements allows the constants of the model to be successfully determined for actual transistors. Within the accuracy of the above-mentioned measurements, the derived model is concluded to be a good representation for actual devices. In conclusion, suggestions for further work are offered.

ACKNOWLEDGEMENTS

The author wishes to express his gratitude to his Supervisor, Professor A.R. Boothroyd of The Queen's University of Belfast, (formerly of Imperial College) for his support, guidance and encourangement during the course of the work described in this thesis.

Grateful thanks are extended to his fellow research students for friendly and stimulating discussions, in particular, to Viphandh Roengpithya for additional assistance in the reproduction stage of the thesis. The friendly interest of the staff, and the facilities of the Electrical Engineering Department of the Queen's University during the latter stages of the work are appreciated.

Financial assistance provided for 1961-1963 by the Board of Trade in the form of an Athlone Fellowship, and for 1963-1966 by the National Research Council of Canada is gratefully acknowledged.

Finally, the author pays tribute to Elda, his wife, for her steadfast and affectionate support throughout the study, and for her invaluable assistance in preparing the final product.

TABLE OF CONTENTS

	Page
Abstract	2
Acknowledgements	3
Table of Contents	4
Location of Figures	9
Location of Tables	9
List of Principal Symbols	10
1. INTRODUCTION	13
1.1 Historical Background	13
1.2 Formulation of the Problem	17
1.3 Original Contribution	20
2. FORMATION OF THE DOUBLE-DIFFUSED TRANSISTOR AND EARLY CHARACTERIZATION ATTEMPTS	21
2.1 Introduction	21
2.2 The Diffusion Equation and its Solution	24
2.2.1 General Form	24
2.2.2 Diffusion from Vapour of Constant Impurity Concentration	27
2.2.3 Diffusion from a Planar Source	28
2.2.4 Modifications due to Outward Diffusion and Rate Limitations	31
2.3 Double-Diffused Structures	33
2.3.1 The Planar Process	33
2.3.2 Classical Distributions	36
2.3.3 Practical Device Profiles	39
2.3.4 The Planar Epitaxial Transistor	41

Page

2.4 Influence of Diffused Structure on Transistor Performance 45

2.4.1 General Considerations 45

2.4.2 Influence of Base Impurity Profile on Diffusion Coefficient 51

2.4.3 Minority Carrier Density in Base Region 56

2.4.4 Base Transit Time 60

2.4.5 Equivalent Circuit for Transistor 63

2.4.6 Cutoff Frequency Considerations 68

2.5 Basic Approaches to Device Characterization 69

2.6 The Classical Distribution Approach 71

2.7 Equivalent Circuit Approach 78

2.7.1 Direct Derivation of Actual Distributions from Terminal Measurement 78

2.7.2 Single Exponential Model for Base Region 83

2.7.3 Linear Plus Exponential Model for Base Region 86

2.7.3.1 Equations for the Model 86

2.7.3.2 Results and Criticisms 93

2.7.4 Intrinsic Input Admittance Y_{ee} 96

3. TREATMENT OF CLASSICAL DISTRIBUTIONS AND APPROXIMATION BY DOUBLE EXPONENTIAL MODEL 98

3.1 Introduction 98

3.2 The Double ERFC Distribution 100

3.2.1 Form of Impurity Distribution 100

3.2.2 Depletion Region Distribution 101

		Page
3.2.3	Base Region Properties	108
3.2.4	Emitter Doping	110
3.2.5	Representative Example	112
3.3	Double Gaussian Distribution	118
3.3.1	Impurity Distribution	118
3.3.2	Depletion Region Equations	119
3.3.3	Base Region Properties	122
3.3.4	Emitter Region	123
3.3.5	Representative Example	123
3.4	Planar Epitaxial Transistor	129
3.4.1	Collector Substrate	129
3.4.2	Extensions to Junction Equations	130
3.4.3	Base Region Properties	137
3.4.4	Representative Example	138
3.5	Double Exponential Model to Approximate Base	144
3.5.1	Justification of the Model and Choice of Exponentials	144
3.5.2	Collector Junction	149
3.5.3	Emitter Junction	152
3.5.4	Minority Carrier Density in the Base Region	158
3.5.5	Base Transit Time	161
3.5.6	Model Applied to Representative Double ERFC and Double Gaussian Examples	163
3.5.7	Model Extended to Epitaxial Structure	166
3.6	Numerical Techniques	169

Page

4. TERMINAL CHARACTERISTICS AND CIRCUIT ELEMENTS OF ACTUAL TRANSISTORS BASED ON THE DOUBLE EXPONENTIAL MODEL 173

4.1 Introduction 173

4.2 Collector and Emitter Junctions 174

4.2.1 Collector Depletion Region 174

4.2.2 Emitter Depletion Region 178

4.2.3 Measurement of Transition Capacitances 183

4.2.4 Emitter and Collector Areas 192

4.2.5 Estimate of N_B from Collector Breakdown 199

4.3 Emitter Diode Characteristics 205

4.3.1 General Equations 205

4.3.2 $\overline{D}_R$ and $\overline{D}_A$ Approximation 207

4.3.3 Approximation Based on $\overline{D}_R$ only 208

4.3.4 Measurement of Diode Characteristic 209

4.4 Base Transit Time 212

4.4.1 General Equations 212

4.4.2 Simplification when N_B is Negligible in the Base 217

4.4.3 Transit Time Measurement 223

5. DETERMINATION OF THE PHYSICAL CONSTANTS OF THE DOUBLE EXPONENTIAL MODEL FOR ACTUAL DEVICES 230

5.1 Introduction 230

5.2 Evaluation of Constants of Model 231

5.2.1 Emitter and Collector Areas Known 231

Page

5.2.2 A_e/A_c Known from r'_{bb} and $r'_{bb}C_{tc1}$ Measurement 238

5.2.3 Checks on Parameters Determined 240

5.2.4 Discussion of Results 244

5.3 Evaluation from Emitter Capacitance Data 249

5.3.1 Derivation of Parameters 249

5.3.2 Discussion of Results 251

5.4 Numerical Techniques 256.

6. CONCLUSIONS 259

6.1 General Conclusions 259

6.2 Suggestions for Further Work 264

REFERENCES 267

APPENDICES

A.1 Determination of Parameters of Linear-Exponential Model 274

A.2 Attempt to Measure Y_{ee} 277

A.3 Determination of L and L when both Exponentials are Significant at Collector Junction 282

A.4 Program for Double ERFC 285

A.5 Program for Double Gaussian 297

A.6 Double Exponential for Double ERFC 304

A.7 Detailed Equations for Input and Output Admittance 320

A.8 Evaluation of Integral in Transit Time Expression 322

A.9 Program to Determine Double Exponential Model 324

Location of Figures

Fig.	Page	Fig.	Page	Fig.	Page
2.1	29	3.3	115	4.7	194
2.2	30	3.4	115	4.8	198
2.3	35	3.5	116	4.9	200
2.4	35	3.6	117	4.10	200
2.5	37	3.7	117	4.11	201
2.6	37	3.8	125	4.12	211
2.7	40	3.9	126	4.13	215
2.8	40a	3.10	126	4.14	215
2.9	44	3.11	127	4.15	221
2.10	44	3.12	127	4.16	221
2.11	53	3.13	128	4.17	222
2.12	64	3.14	141	4.18	222
2.13	64	3.15	142	4.19	224
2.14	73	3.16	143	4.20	224
2.15	75	3.17	143	4.21	228
2.16	77	3.18	155	4.22	228
2.17	80	3.19	155	5.1	241
2.18	80	4.1	174	5.2	253
2.19	84	4.2	174	A.1	279
2.20	84	4.3	184	A.2	281
2.21	90	4.4	184	A.3	285
3.1	102	4.5	190	A.4	304
3.2	114	4.6	194	A.5	324

Location of Tables

Table	Page	Table	Page	Table	Page
2.1	92	4.3	191	5.3	237
2.2	92	4.4	195	5.4	241
2.3	92	4.5	213	5.5	252
2.4	92	5.1	235	5.6	252
4.1	187	5.2	236	5.7	253
4.2	189				

LIST OF PRINCIPAL SYMBOLS

A_e, A_c	=	Emitter and Collector areas.
Arg	=	Argument or phase-angle of complex quantity.
a	=	Common-base intrinsic short-circuit current gain.
a_o	=	Low-frequency asymptote of a.
α	=	Extrinsic (measured) common-base short-circuit current gain.
a_{1e}, a_{2e}	=	Depletion layer semi-widths on emitter and base sides respectively of emitter junction.
a_{1c}, a_{2c}	=	Depletion layer semi-widths on base and collector sides respectively of collector junction.
C_{te}, C_{tc}	=	Emitter and collector transition capacitances.
C_{tc1}, C_{tc2}	=	Fractions of collector transition capacitance under the emitter area and outside this area respectively.
C_{de}	=	Emitter diffusion capacitance.
$C_{seb}, C_{sec}, C_{scb}$	=	Stray capacitances between emitter-base, emitter-collector, and collector-base leads respectively.
D	=	Impurity diffusion coefficient.
$D_n(N_A;N_D)$	=	Minority carrier (electron) diffusion coefficient dependent on the distribution of donors and acceptors in the base.
$\overline{D}_R, \overline{D}_A$	=	Equivalent diffusion coefficients in the retarding and aiding field regions of the base.
D_1, D_2, D_3	=	Diffusion coefficients of emitter, base and substrate impurity elements respectively.

d_e, d_c	=	Width of emitter and collector depletion layers.
$E_1(x)$, $E_2(x)$	=	Electric fields in the depletion layer to left and right of a junction respectively.
F_0, F_1, F_2, F_3	=	Functions defined as required.
f_τ	=	Frequency at which $R_e[\alpha] = 0.5$, assuming a 6 db/octave fall-off of gain with frequency.
i_e, i_b, i_c	=	Small-signal emitter, base, and collector currents.
I_e, I_b, I_c	=	D.C. Emitter, base, and collector currents.
J_n, J_p	=	Current density of holes and electrons.
k	=	Boltzmann's constant.
K	=	Constant defining rate limitations at surface of a semiconductor wafer.
L_1, L_2	=	Characteristic length of the two exponentials
m_2	=	W/L_2.
N_A, N_D	=	Density of acceptors and donors respectively.
N_{S1}, N_{S2}	=	Surface concentrations of base and emitter diffusants.
N_B	=	Background doping (collector body doping) of a transistor.
N_0	=	Impurity density reached at emitter junction by the exponential defined at the collector junction.
N_0'	=	Density of either emitter or base diffusant at emitter junction.
n	=	Minority carrier density (electrons) in base region.
n_i	=	Intrinsic carrier density.
q	=	Unit electronic charge.
Q	=	Charge density.

r'_{cc}	=	Collector body resistance
S_1	=	Impurity gradient at the emitter junction.
T	=	Temperature (^oK)
v_s	=	Limiting drift velocity in an electric field.
V_e, V_c	=	Emitter and collector bias voltages referred to base. (Also use V_{te}, V_{tc})
V_{oe}, V_{oc}	=	Equilibrium barrier potentials at emitter and collector junctions.
W	=	Distance from emitter metallurgical junction to base edge of collector depletion layer.
W_b	=	Physical base width.
x	=	Position variable-origin at surface of wafer.
x'	=	Position variable-origin at emitter metallurgical junction.
x_e, x_c	=	Positions of emitter and collector junctions.
Y	=	x/W
Y_1	=	a'_{2e}/W.
Y_m	=	x_m/W - Position of maximum doping in the base.
Y_{ee}	=	Emitter admittance
γ	=	L_2/L_1
ε	=	Dielectric constant
η	=	N_B/N_o
τ	=	Terminal transit time.
τ_b	=	Base transit time.
τ_c	=	$d_c/2v_s$
ω	=	Angular frequency (= $2\pi f$)
Σ_1, Σ_2 Σ_3	=	Functions defined as required.

1. INTRODUCTION

The expression "double-diffused transistor" refers to a transistor formed by the successive introduction of both types of impurity atoms (donors and acceptors) by solid-state diffusion in sufficient concentrations to form p-n junctions where equal concentrations of each type exist. Depending on the initial doping of the wafer, the transistor may be of either p-n-p or n-p-n structure.

The nature of the diffusion process (discussed in Chapter 2) is such that in a double-diffused transistor the following characteristic properties obtain: junctions are graded (or diffused), the emitter has low resistivity (highly doped), the base consists of a region which opposes the transport of minority carriers (retarding field region) followed by a region which enhances the transport of minority carriers (aiding field region), and the collector has high resistivity (doping is largely governed by the initial doping of the wafer).

A double-diffused transistor is often referred to simply as a "diffused" transistor, or as a "planar" transistor - a term descriptive of the process used in fabrication[1]. Both terms will be used in this thesis.

1.1 Historical Background

Since the experimental discovery of transistor action[2] in 1948, much effort has been spent in effecting technical innovations to improve the quality and performance of transistors. The first junction transistors, described theoretically by Shockley[3] in 1949 and realised

physically in 1951 by the grown junction technique[4], were low frequency devices. To increase the frequency response, fabrication processes were developed which greatly reduced base width and emitter and collector areas. The most important of these, junction preparation by an alloying process[5] realised its physical limit in minimizing base width in the "surface barrier transistor"[6].

The double-diffused transistor was a consequence of further efforts to increase the upper frequency limit. Krömer[7,8] considered theoretically the effect on performance of the introduction of an exponential impurity gradient falling from a high concentration on the emitter side of the base to a low concentration at the collector side. Considerable drift enhancement of the transport of minority carriers across the base was indicated, leading to an improvement in transit time and frequency response. Experimental work on the diffusion of impurities into germanium and silicon[9-11] had already produced sufficient quantitative information on solid-state diffusion to enable this process to be used to fabricate photocells[12] and power rectifiers[13]. Subject to certain idealizations, the form of the concentration profile from diffusion could be predicted theoretically[14-19]: thus assuming the process to be linear at a constant temperature and to be from a constant source concentration, a complimentary error function (ERFC) profile was to be expected, decreasing with depth of penetration from the source surface. The diffusion process was recognized as a possible means of obtaining a graded base profile similar in nature to the exponential studied by Krömer[7,8].

The first two transistors realised by diffusion techniques were

announced in 1956[20,21]. That described by Lee[20] was of the alloyed-emitter diffused-base type, while that described by Tanenbaum and Thomas[21] was the first to be fabricated solely by two diffusion processes. Both differed from the structure described by Krömer[7,8] by having diffused collector junctions and high resistivity collector regions. ("Drift" transistors with alloyed emitter and collectors and graded bases were not physically realised until later[22].)

Further refinements in the diffusion process, including the development of the deposition drive-in procedure for carrying out diffusions[23], provided detailed information on the diffusion coefficients involved in the process over a wide range of conditions and for a wide range of impurity elements[24-26]. The introduction of the planar process[1] in 1961 proved to be a major advance in diffusion technology, providing the basis for the present dominance of the transistor market by silicon planar devices and for development of integrated circuits. A further important technological development was the process of epitaxial growth introduced in 1960[27]. Using this process it was possible to reduce the value of the parasitic collector body resistance, often a serious problem in double-diffused transistors due to the necessarily high resistivity of the silicon wafer prior to processing.

As with each technological development, much effort has been devoted to characterizing the structure produced by the diffusion process. Techniques used earlier to study single-diffused layers were extended to double-diffused transistors. Junctions could be located by staining techniques[23] and their depths measured by optical interference techniques[28]. The four-point probe measurement of sheet resistivity[29]

was also used to locate junction positions and, with the lapping of surface layers, was used to determine the variation of impurity concentration with position. To provide the basis for these evaluations, Backenstoss[30] and, later, Irvin[31] presented charts which gave surface concentrations as sheet resistivity with junction depth as a parameter, computed for ERFC and Gaussian* concentration distributions. Radioactive tracer techniques[32] were also developed to aid in the evaluation of impurity distributions, but like the other measurements mentioned were applicable only to diffusions in large areas and were essentially destructive.

Correlation between idealized theoretical impurity concentrations and those actually resulting from fabrication processes is very difficult to ostablish. The theoretical distributions are complex analytically even after considerable idealization of the situation has been made. However, in actual impurity diffusion processes there are several major departures from such idealizations: in particular, the process is not linear and conditions at the semiconductor surface differ greatly from those assumed in analysis and are not fully understood. As a consequence, the known relationships between the fabrication process and the impurity concentration distributions produced in the device are somewhat qualitative and empirical in nature. Studies that have been made on actual small-area devices have been restricted to single-diffused junctions, e.g. extraction of junction depth and depletion layer width from transition capacitance measurements[33]. The absence of specific information

---

* As mentioned above, an ERFC distribution results under idealized conditions of linear diffusion from a surface source of constant temperature and concentration. A Gaussian distribution is ideally produced if a constant total number of impurity atoms, previously predeposited on the surface, undergoes linear diffusion at constant temperature[14-19,23].

on the impurity concentration distribution in the base region of transistors, and specifically of devices of the double-diffused type, poses the problem of determining this distribution from terminal properties of the device itself,as discussed below.

1.2 Formulation of the Problem

The base impurity profile defines all internal electrical processes in a transistor consequent upon carrier injection into the base. Therefore, knowledge of the impurity profile is essential to the analysis of internal electronics and, in particular, the prediction or understanding of performance characteristics and the derivation of equivalent circuit models (related to internal electrical processes) to characterize the device as a basis for circuit design. A "physical model", in which the basic ingredient is the impurity density profile, may be used to represent the essentials of the device structure with permissible idealizations (e.g. device is essentially one-dimensional under appropriate circumstances). It is possible, if the impurity density profile can be determined, to establish a better quantitative connection between the device and its fabrication process.

Two possibilities exist for determining the impurity profile nondestructively in practical devices:

(1) a point-by-point determination from terminal measurements (impractical as discussed further below), and

(2) to define a simple, yet adequate, analytic approximation characterized by a small number of parameters, and determine these parameters from terminal measurements on the device.

The point-by-point determination is possible only from interpretation of transition capacitance measurements[34,35]. The difficulty of establishing the position of the edge of the depletion layer on either side of a junction (hence doping at the edge of the depletion layer) of arbitrary impurity density distribution limits the usefulness of this method either to highly asymetrical or symmetrical linear junctions. (See Chapter 2, Section 2.7.1). The second approach is therefore adopted in this thesis.

Two early analytical approximations proposed to represent the base impurity density profile of a double-diffused transistor were a single exponential[36] and a linear retarding field region followed by an exponential aiding field region[37,38]. These are discussed in Chapter 2, Sections 2.7.2 and 2.7.3. Although the exponential is a good approximation to the individual components of the impurity profile when they have fallen substantially from their initial values, and is also the simplest function that has the same properties (i.e. rapid decrease over several orders of magnitude) as these components, it is strictly applicable as a model only to a single-diffused structure. The linear-exponential model is limited to a device in which the retarding field region is a small fraction of the total base width, and is therefore not applicable to the general case in which the retarding field region can occupy any fraction of the total base width.

The extent of the retarding field region is determined by the relationship the two diffusions bear to each other; the impurity profile is essentially the difference of the two diffusions added to a constant "background" doping density. The limitations to the

approximations mentioned above points out the need for an approximate model which represents the general case where the two diffusions may bear any relation to each other. In order to provide the basis for the choice of such a model, the nature of the impurity distributions produced by diffusion must be thoroughly understood. In the absence of complicating factors, classical distributions such as the ERFC[14-19] or the Gaussian[14-19,23] represent the diffused profiles for the boundary conditions normally used in the fabrication of diffused devices. The double-diffused impurity profile should ideally be the difference of two such distributions superimposed on the background doping. The diffusion process is studied in Chapter 2. Base region and depletion layer properties of double-diffused transistors in which the above classical distributions apply are studied in Chapter 3. These properties are then used in the form of a representative example to indicate the accuracy of similar quantities computed for the double exponential model chosen later in the chapter to approximate the base region. Where necessary, extensions to theory are included to account for the presence of a substrate layer in an epitaxial transistor.

The inter-relationship between the various electrical properties of the device, e.g. base transport and depletion layer properties, may be represented by an equivalent circuit model[39] whose elements may be expressed in terms of the physical model. Terminal measurements of the electrical properties may be interpreted with the aid of this equivalent circuit model to yield the constants of the physical model (see Chapters 4 and 5).

In brief, the specific objectives of this thesis may be stated as: (1) to determine the simplest approximate model to give accurate representation of general classical diffusion profiles which are the difference of two ERFCs or two Gaussians, and (2) to establish that the model can also characterize actual devices over a wide range of operating conditions (bearing in mind that the diffusion profiles involved may depart from classical distributions owing to the nonlinear nature of the actual diffusion process). The first of the two objectives is carried out in Chapter 3, while the second is carried out in Chapters 4 and 5.

1.3 Original Contribution

Except where reference is made to the work of others, the research and conclusions reported in this thesis are original as far as the author is aware.

2. FORMATION OF THE DOUBLE-DIFFUSED TRANSISTOR AND EARLY CHARACTERIZATION ATTEMPTS

2.1 Introduction

This chapter deals with the processes involved in the fabrication of double-diffused transistors and with early attempts to physically and electrically characterize the completed device.

In order to provide a basis for description of the internal configuration of double-diffused transistors, the solid state diffusion process must be thoroughly understood. Therefore, the general form of the diffusion equation is discussed, and solutions are given for two cases where the diffusion has proceeded ideally - subject only to the initial boundary conditions most commonly encountered in practical diffusions. The non-linear nature of the diffusion process and the possibility of violation of the ideal boundary conditions can lead to considerable modification of the classical distributions; so a section is devoted to consideration of modified impurity distributions.

The most common fabrication process in diffusion technology is the planar process[1] which restricts diffusion to pre-selected areas. It is considered here as the standard process for fabricating double-diffused transistors, which are essentially formed by successive diffusions, into an initially doped wafer, of opposite and same type impurities respectively. Classically, the impurity distributions should be the difference of two ERFCs or two Gaussians, (depending on the boundary conditions used) subject to modifications by non-ideal conditions. Factors which may cause deviation from non-ideality are considered briefly. Epitaxy[27] is often

used in conjunction with the diffusion process to improve high-frequency performance, so the implications in terms of impurity profile are discussed.

Proper understanding of the external characteristics of the double-diffused transistor requires an adequate knowledge of the physical parameters of the internal transistor structure. The inherent properties of graded junctions and a base consisting of both a retarding and an aiding field region exert considerable influence on depletion layer width for any bias voltages and on minority carrier density in the base - hence on base transit time. Since depletion layer characteristics and base transit time occupy unique positions in transistor characterization, they are considered here in general terms in order to point out the effect of the diffused structure on transistor performance. (Specific cases are considered throughout the thesis as required). An equivalent circuit model is presented, and the effect of the diffused structure on the individual circuit elements is qualitatively discussed. It is concluded that the diffused structure results in a general improvement in frequency characteristics.

Considerable effort has in the past been devoted to determination of the dimensional quantities of base width, junction areas, and depletion layer width, as well as those that characterize impurity density distribution. The earliest of these were directed towards the establishment of a fund of information sufficient for design of future devices and prediction of the internal structure of the fabricated device from knowledge of the boundary conditions used in fabrication. They invariably involved the assumption of classical distributions and measurement of

junction depth and sheet resistivity. This approach, applied to large numbers of devices, has produced graphical data which is useful either for design of or evaluation of double-diffused transistors. The more important aspects of this approach - limited to those with facilities for device fabrication - are considered briefly.

The above evaluation procedure, implying destruction of the device, is unattractive to the consumer who encounters the device in encapsulated form in small quantities. Having access only to the device terminals, his assessment of the internal configuration must, necessarily, be based on terminal measurements. This assessment may involve: (a) a direct determination of the actual impurity profile from terminal measurements, or (b) the assumption of a simple yet accurate, approximate model for the actual distribution, derivation of circuit elements and terminal characteristics in terms of this model, and, subsequently, determination of the physical constants of the model from terminal measurements.

Both cases (a) and (b) are discussed qualitatively in this chapter. Quantitatively, attempts to determine the impurity profile [case (a)] based on transition capacitance data[34,35] are shown to be inadequate for reasons of accuracy and limited applicability. Previous approximation of the base region [case (b)] by a single exponential[36] and by a linear retarding field region and an exponential aiding field region[37,38] are discussed. They are shown to have limited applicability, pointing out the need for a more accurate representation applicable to most double-diffused transistors.

2.2 The Diffusion Equation and its Solution

2.2.1 General Form

Although considered early in the development of transistors as a possible fabrication technique, solid-state diffusion could not be utilized until (a) sufficient quantitative information on the diffusion of impurities into semiconductors could be amassed and (b) practical problems of apparatus, material preparation, and the degradation of carrier lifetime as a consequence of the heat treatment required for diffusion could be overcome. Many investigators[9-11] have been involved in amassing diffusion information; their efforts were rewarded with the announcement of the first double-diffused transistor in 1956[21]. Since that time solid-state diffusion has become virtually the standard fabrication technique for transistors.

The distribution of impurities is the most important aspect of a diffused layer. It is determined by the boundary conditions imposed on the diffusion, and is described mathematically by the solution of the diffusion equation under these boundary conditions. Two boundary conditions are of special interest in device fabrication by diffusion and will be considered in Sections 2.2.2 and 2.2.3. First, however, consideration must be given to the general diffusion equation and certain aspects of the diffusion process.

The diffusion equation was described originally in 1855 by Fick[14] in terms of a constant of proportionality relating the number of solute atoms per square crossing an arbitrary plane to the concentration gradient at this plane. Stated mathematically, Fick's first law is:

$$\vec{F} = -D\vec{\nabla}N$$

where $\vec{F}$ is the flow density of diffusing atoms,

$\vec{\nabla}N$ is the concentration gradient,

and D is the constant of proportionality called the diffusion coefficient. The negative sign indicates that diffusion is down the concentration gradient.

Several fortuitous properties of semiconductors simplify the solution of the diffusion equation for diffusion into these materials: (1) the semiconductor structure is mono-crystalline so grain boundary diffusion does not exist; (2) the crystal lattice is cubic, so D is a scalar; (3) the amounts of diffusant are generally small enough so that changes in crystal dimensions may be neglected; (4) in most cases we are interested in plane-parallel junctions, so treatment can be restricted to diffusion in one dimension only.

Applying the continuity equation in one dimension to eqn. 2.2.1 yields Fick's second law:

$$\frac{\partial N}{\partial t} = \frac{\partial}{\partial x}\left(D\frac{\partial N}{\partial x}\right) \qquad 2.2.2$$

If D is a constant this simplifies to:

$$\frac{\partial N}{\partial t} = D\frac{\partial^2 N}{\partial x^2} \qquad 2.2.3$$

Equation 2.2.3 is of fundamental importance in solid-state diffusion and has been solved by various authors[15-19] for a number of boundary conditions including those commonly imposed during semiconductor device fabrication.

The assumption of constant D, although applied generally in semiconductor work, can lead to serious errors for high impurity concentrations.

Smits[40] shows that only electrical fields appear to cause departure from an ideal solution. This consideration yields (for one diffusing impurity):

$$D = kTG\left(1 + \frac{N}{\sqrt{(2n_i)^2 + N^2}}\right) \qquad 2.2.4$$

where k is Boltzmann's constant, T is absolute temperature, G is microscopic mobility (i.e. the velocity attained by an atom under unit applied force), N is the concentration of diffusing impurities, and n_i is the intrinsic carrier density. Eqn. 2.2.4 indicates that D can vary with N by a factor of two. For low concentrations ($N < 2n_i$) the assumption of constant D introduces negligible error; while for high concentrations ($N \geq 2n_i$) solution of eqn. 2.2.3 instead of 2.2.2. may lead to appreciable error in the impurity distribution. With non-constant D it may be necessary to solve 2.2.2 by numerical means.

Diffusion of groups three and five elements is by lattice substitution. The mechanism is highly temperature dependent, requiring temperatures approaching the melting point of the semiconductor. This temperature dependence is reflected quantitively by:

$$D = D_o e^{-\Delta Q/kT} \qquad 2.2.5$$

where D_o is a constant and ΔQ is the activation energy for the particular element in the semiconductor. Diffusion coefficients for different elements have been determined from experimental diffusions of known diffusion depths, time, temperature and sheet resistivity. Equations which are solutions of eqn. 2.2.3 were assumed to represent the diffusions and D determined by solution of these equations. Fig. 2.1, reproduced from Fuller[24], represents the best results available for the elements

commonly used in silicon diffusion. Similar curves are available for germanium. Practical difficulties have limited the usefulness of germanium for double-diffused structures, so silicon devices will be tacitly assumed throughout this study. Solution of eqn. 2.2.3 provides the basis for the theoretical distributions commonly used to characterize diffused devices.

2.2.2 Diffusion from Vapour of Constant Impurity Concentration

When a vapour of constant impurity concentration is passed over the surface of a semiconductor wafer which has been raised to a temperature near the melting point, impurity atoms will diffuse from the vapour state into the wafer. The impurities in the wafer assume a distribution decreasing (from an equilibrium surface concentration N_s) with distance into the wafer. N_s is related to the impurity concentration in the vapour (N_g) by a constant K defining the rate limiting properties of the surface. Equating the flow of atoms across the surface to the flow away from the surface defines K.

$$- D\frac{\partial N}{\partial x}\Big|_{x=0} = K(N_g - N_s) \qquad 2.2.6$$

If $K = \infty$, $N_s = N_g$ at all times and no rate limitation occurs.

For cases where no rate limitation occurs or N_s is constant with time t, the boundary conditions are:

(1) N_g is constant for $0 \leq t \leq \infty$;

(2) $N(x) = 0$ at $t = 0$;

(3) Equilibrium of reactions at the wafer surface is achieved in times short in comparison with diffusion times. (N_s is constant for all $t > 0$).

Solution of eqn. 2.2.3 for these boundary conditions gives:

$$N(x) = N_s\,(1 - \mathrm{erf}(x/\sqrt{4Dt})) \qquad 2.2.7$$

"Erf" is an abbreviation for error function and is defined by:

$$\mathrm{erf}\left(\frac{x}{\sqrt{4Dt}}\right) = \frac{2}{\sqrt{\pi}} \int_0^{x/\sqrt{4Dt}} e^{-\lambda^2}\, d\lambda \qquad 2.2.8$$

where λ is an integration variable. Eqn. 2.2.7 is normally expressed in the complimentary error function (ERFC) form:

$$N(x) = N_s\,\mathrm{erfc}(x/\sqrt{4Dt}) \qquad 2.2.9$$

where erfc = 1 - erf.

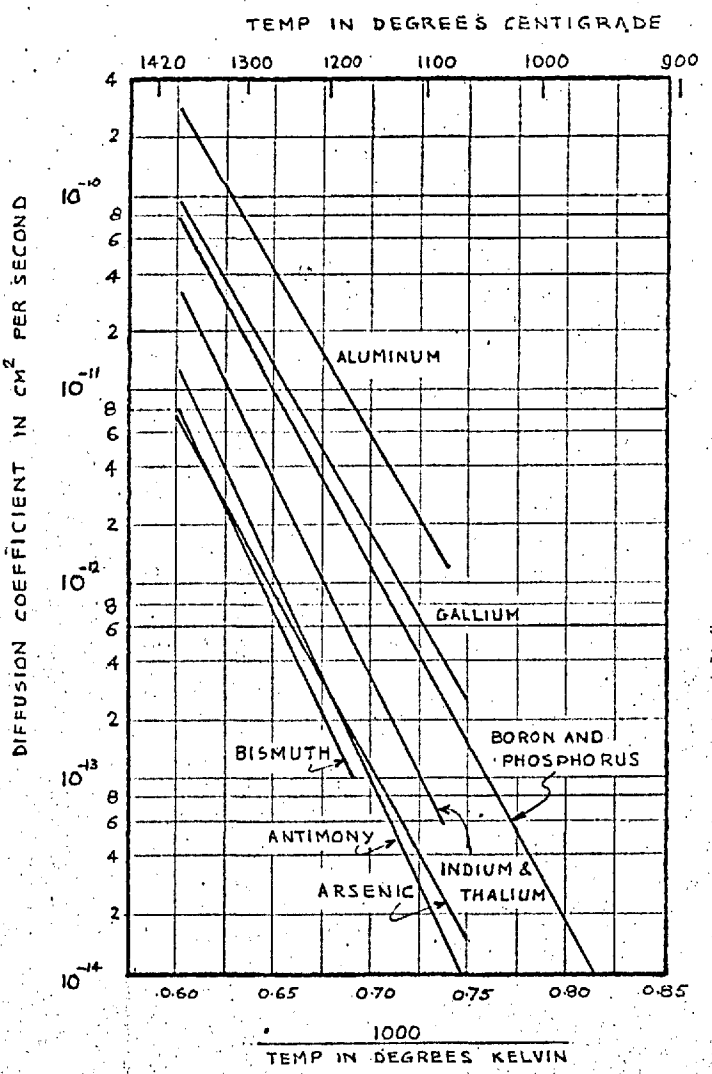
Eqn. 2.2.9 is of special interest for diffused devices and is plotted in Fig. 2.2. Log-linear paper is used to cover the range of magnitudes normally encountered. The normalizing factor is N_s. The distribution can be seen to approach an exponential when it has fallen below 10^{-3} of its initial value.

If the third boundary condition does not apply it is replaced as a boundary condition by eqn. 2.2.6. The modifications introduced by the consideration of rate limitations are discussed in Section 2.2.4.

2.2.3 Diffusion from a Planar Source

The alternative to the vapour diffusion of the previous section is a two step process involving deposition of a fixed amount of impurity $\overline{N}_o$ on the surface of the wafer prior to the actual diffusion. An oxide layer is then grown over the surface and the diffusant driven inwards under this oxide at temperatures near the melting point of the semiconductor. The oxide layer prevents outward diffusion during the "drive-in" stage. Obviously during the deposition stage some diffusion

Fig. 2.1. Diffusion Coefficients of Donor and Acceptor Elements in Silicon (from Ref. 24).



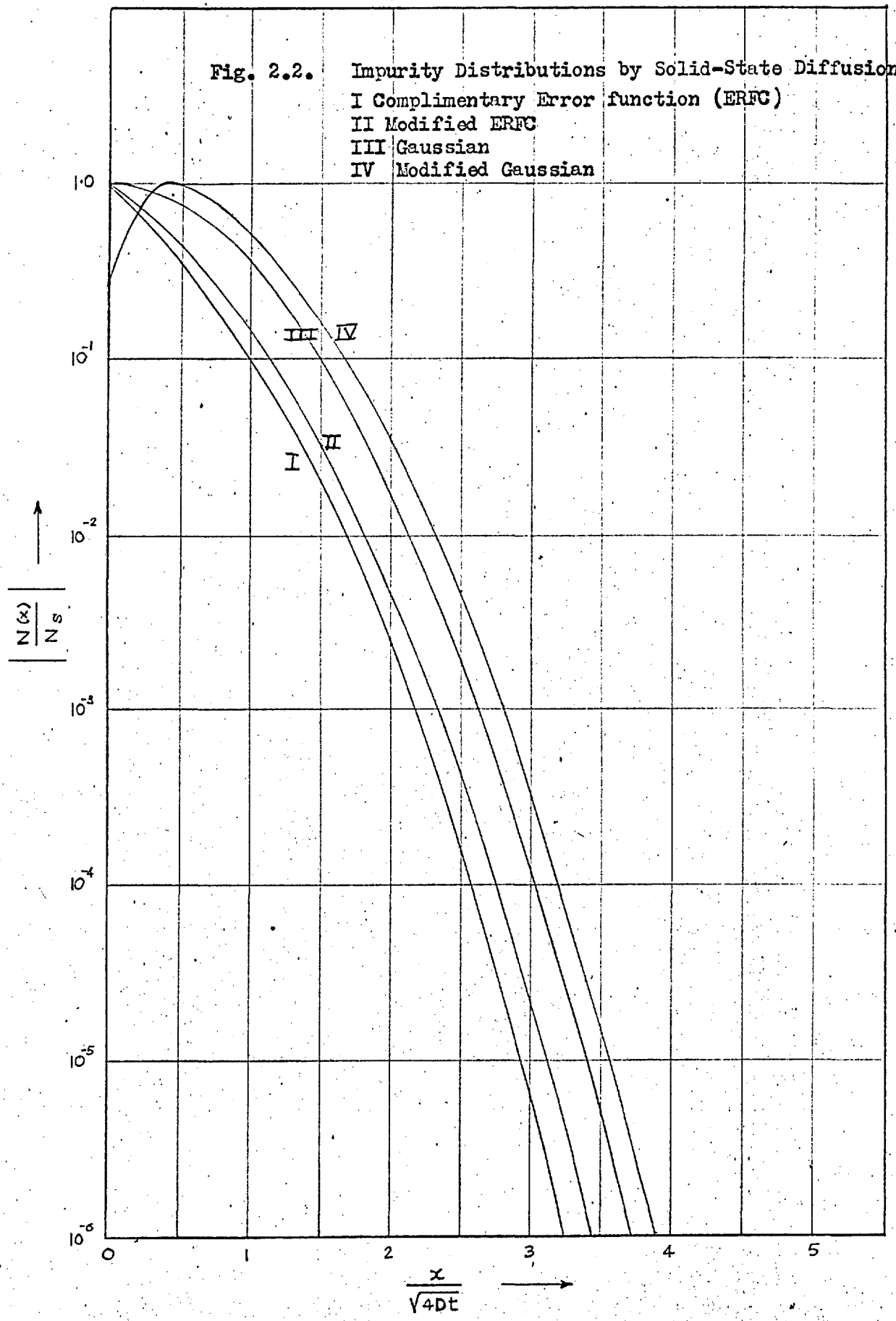


Fig. 2.2. Impurity Distributions by Solid-State Diffusions

occurs into the semiconductor. This may be neglected, however, owing to the short times and fairly low temperatures involved; so the diffusant effectively forms a planar source.

The boundary conditions for the drive-in stage are:

(1) $N(0) = \bar{N}_o$ at $t = 0$,

(2) $N(x) = 0$ for $0 < x \leq \infty$ at $t = 0$

Neglecting rate limitation and outward diffusion into the oxide layer gives a Gaussian distribution as a solution to eqn. 2.2.3:

$$N(x) = \frac{\bar{N}_o}{\sqrt{\pi Dt}} e^{-x^2/4Dt} \qquad 2.2.10$$

where $\bar{N}_o$ is the initial sheet density for the diffusant at the surface. Clearly the N_s of Section 2.2.2 corresponds to $\bar{N}_o/\sqrt{\pi Dt}$ in eqn. 2.2.10.

Eqn. 2.2.10 is plotted in Fig. 2.2 to facilitate comparison with the ERFC distribution. Although for fixed values of N_s and $\sqrt{4Dt}$ the Gaussian falls less rapidly than the ERFC, the exponential approximation is valid when the Gaussian has fallen below 10^{-3} of its initial value.

2.2.4 Modifications Due to Outward Diffusion and Rate Limitations

The classical ERFC and Gaussian distributions of Sections 2.2.2 and 2.2.3 are generally assumed in device fabrication by solid-state diffusion. The possible existence of rate limitations and outward diffusion were ignored in their derivation. Practically, these factors may appreciably modify the classical distributions.

Should rate limitation occur at the surface during vapour diffusion (i.e. approach to equilibrium conditions is slow) a finite difference will exist between surface concentration N_s and vapour concentration N_g.

Application of the boundary condition of eqn. 2.2.6 to the solution of eqn. 2.2.3 yields:

$$N(y,z) = N_s \left[\operatorname{erfc}(y) - e^{(2yz + z^2)} \operatorname{erfc}(y + z)\right] \qquad 2.2.11$$

where $N(y,z)$ is the variable concentration of the diffusant, $y = x/\sqrt{4Dt}$, and $z = K\sqrt{t/D}$. All other terms are as previously defined. Eqn. 2.2.11 reduces to 2.2.9 when $z \to \infty$.

During the drive-in stage of the two-step process (Section 2.2.3) out-diffusion may occur depending largely on whether the oxide layer accepts or rejects the impurity. With complete rejection, eqn. 2.2.10 applies; with incomplete rejection out-diffusion occurs and the Gaussian distribution must be modified. Consideration of out-diffusion and rate limitation in the solution of eqn. 2.2.3[40,41] leads to:

$$N(y,z) = \frac{\bar{N}_o}{\sqrt{\pi Dt}} e^{-y^2} \left[1 - \sqrt{\pi} z\, e^{(y+z)^2} \cdot \operatorname{erfc}(y+z)\right] \qquad 2.2.12$$

where all terms are as previously defined. When $z = K\sqrt{t/D} \to 0$, eqn. 2.2.12 approaches the Gaussian distribution. When K has a finite value the distribution has a maximum. This maximum can be observed in Fig. 2.2 where eqn. 2.2.12 is plotted for $z = 2.5$. Eqn. 2.2.11 is also plotted for the same value of z.

Although for practical diffusions rate limitation and out-diffusion are often unavoidable, diffused devices have generally been characterized by the classical distributions of eqns. 2.2.9 and 2.2.10. Other modifying effects such as variable D and changing position of the surface during diffusion are also generally ignored. The complicated nature of these departures from ideality necessitates treatment by numerical

techniques. Detailed study of the modified distributions and the factors involved in the modification is beyond the scope of this thesis. Classical distributions (ERFC and Gaussian) will be assumed to describe practical diffusions throughout this chapter - except where specific approximations are assumed for purposes of device characterization.

2.3 Double-Diffused Structures

2.3.1 The Planar Process

Assume as a starting point a silicon wafer uniformly doped with n-type impurities. Successive diffusions into this wafer of p- and n-type impurities respectively produces the n-p-n configuration with junctions occurring where complete compensation of impurities takes place. The earliest double-diffused transistors were mesa types fabricated in steps as shown in Fig. 2.3. Briefly, these steps are: diffusion of p-type impurities into the entire top surface of the wafer with accompanying oxide growth, photoetching of the oxide to form apertures through which emitter diffusion is carried out, removal of the oxide, masking and deposition of metal to form emitter and base contacts, and etching away of part of the wafer to form a mesa.

For reasons of superior performance (elimination of surface effects, improved reliability, and reduction of leakage currents by an order of magnitude) the silicon planar transistor introduced in 1961[1] has virtually completely replaced the mesa structure. Both diffusions are carried out under a protective oxide layer with lateral diffusion ensuring that junctions are formed under this oxide and are thus protected from contamination. Fabrication steps are shown in Fig. 2.4. The original

n-type wafer is oxidized to a thickness of about one micron (10^{-4} cm.). A photoetching process with suitable masks opens windows through the oxide for the base diffusion which is then carried out with reoxidization of the previously exposed area. A similar process opens windows for emitter diffusion which is carried out with accompanying reoxidization. Photoetching again opens windows for base and emitter contacts. Metal is deposited over the whole of the surface and removed from all but the contact areas by photoengraving. The protective photo-resist is then removed from the contacts leaving the device ready for connection to the outside world.

The diffusions involved in fabrication of both the mesa and the planar transistor can be either from a vapour source or by the two step process (section 2.2.3). Suitable p-type diffusants (Group III) are boron or aluminium; suitable n-type impurities (Group V) are antimony, arsenic or phosphorus. Boron and phosphorus are preferred because of their high solid solubilities, i.e. the maximum concentrations which can be dissolved in the semiconductor at any specified temperature. Fig. 2.5, reproduced from Trumbore[42] gives the solid solubilities of different impurities in silicon. For sharply-defined junctions to be formed the surface concentration of each subsequent diffusant must be more than an order of magnitude greater than the impurity concentration already in the wafer. The high solubilities of boron and phosphorus are thus advantageous when either of these elements are used for the emitter diffusion.

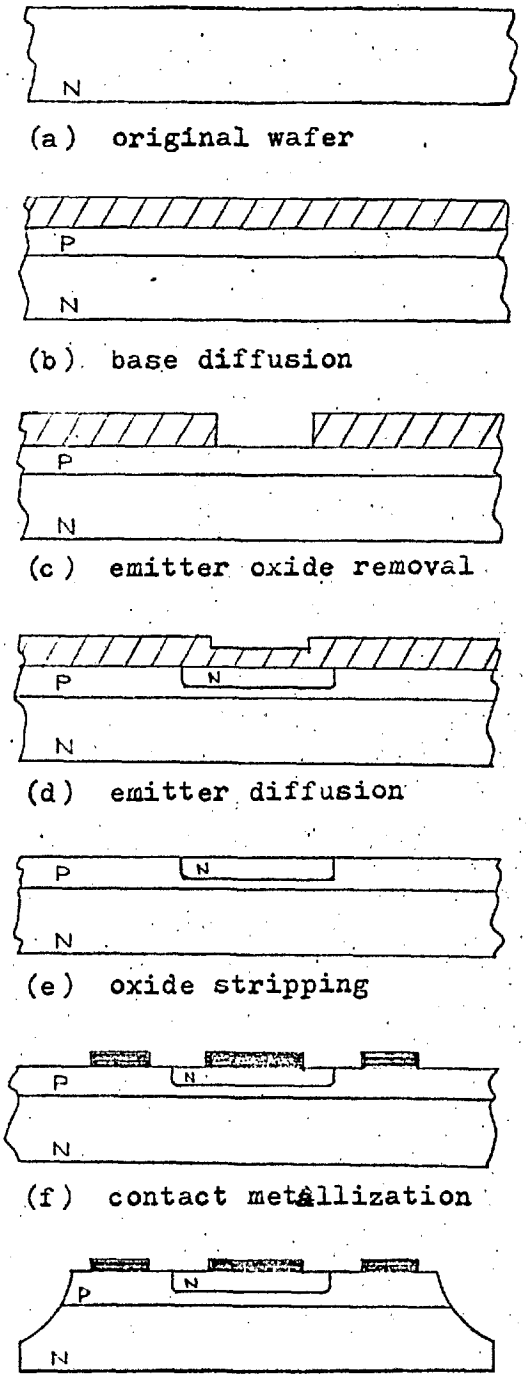


Fig. 2.3. Fabrication Steps for Double-Diffused Mesa Transistors.

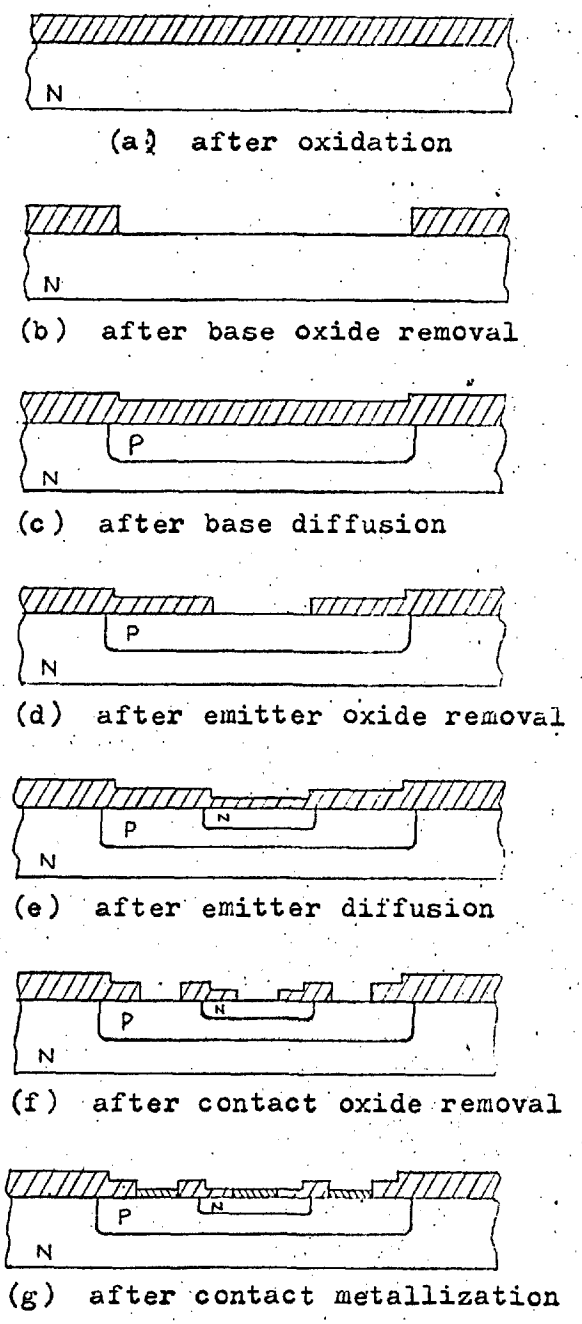


Fig. 2.4. Fabrication Steps for Double-Diffused Planar Transistors.

Current transport through the base region of transistors is by minority carriers which are delayed in transit by various scattering mechanisms (see Section 2.4.2). The extent of the delay governs the frequency response of the device. Since electrons have higher mobility than holes, it is advantageous for base transit to be by electrons which, for a given base width, suffer less delay than holes in a similar device. It is therefore, possible to fabricate higher-frequency transistors in the n-p-n structure than in the p-n-p structure. Most silicon planar devices are n-p-n and, since they are in such preponderance in double-diffused transistors, discussion throughout the thesis will be limited to silicon planar n-p-n devices. The usefulness of germanium in fabricating planar transistors has, in any case, been limited by technical considerations such as the difficulty of producing an oxide on its surface.

2.3.2 Classical Distributions

In Sections 2.2.2 and 2.2.3 an undoped wafer was the starting point for the diffusions. For a wafer already lightly doped with impurities, background doping should have negligible effect on base diffusion, since this impurity density is small in comparison with the density of states. Similarly, the presence of the base diffusant should have negligible effect on the emitter diffusion. Junctions are formed where "compensation" of donors N_D (n-type impurities) and acceptors N_A (p-type impurities) is complete, i.e. where $N_D = N_A$. The general form of the double-diffused impurity profile is represented in Fig. 2.6. For convenience the base is assumed to have positive impurity distribution.

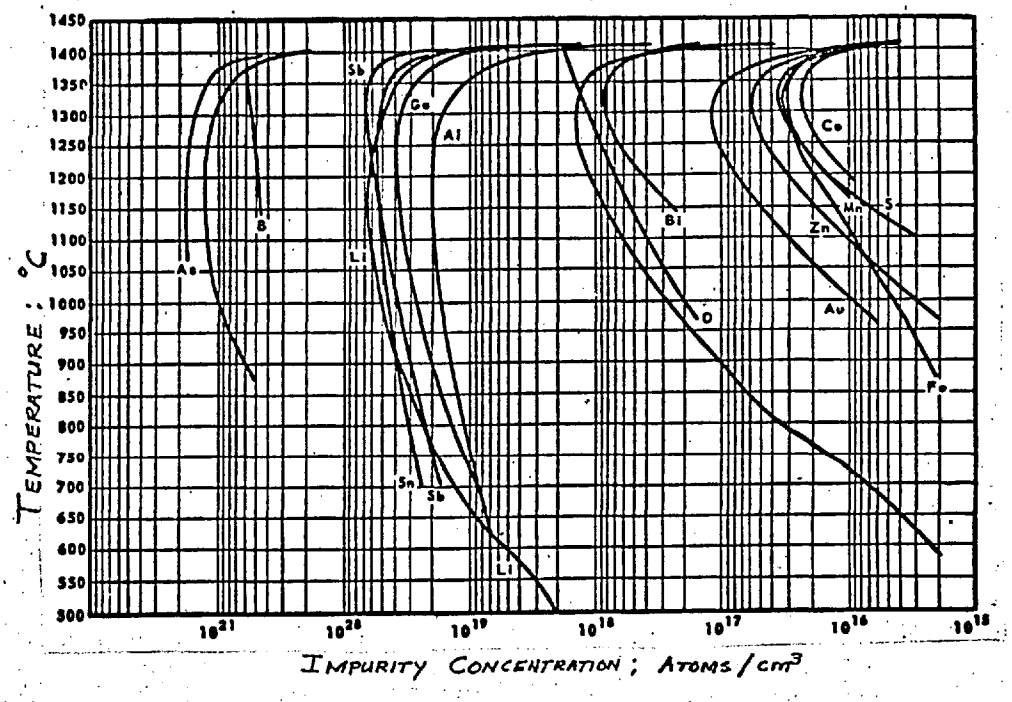


Fig. 2.5. Solid Solubilities of Impurity Elements in Silicon. Reproduced from Trumbore[42].

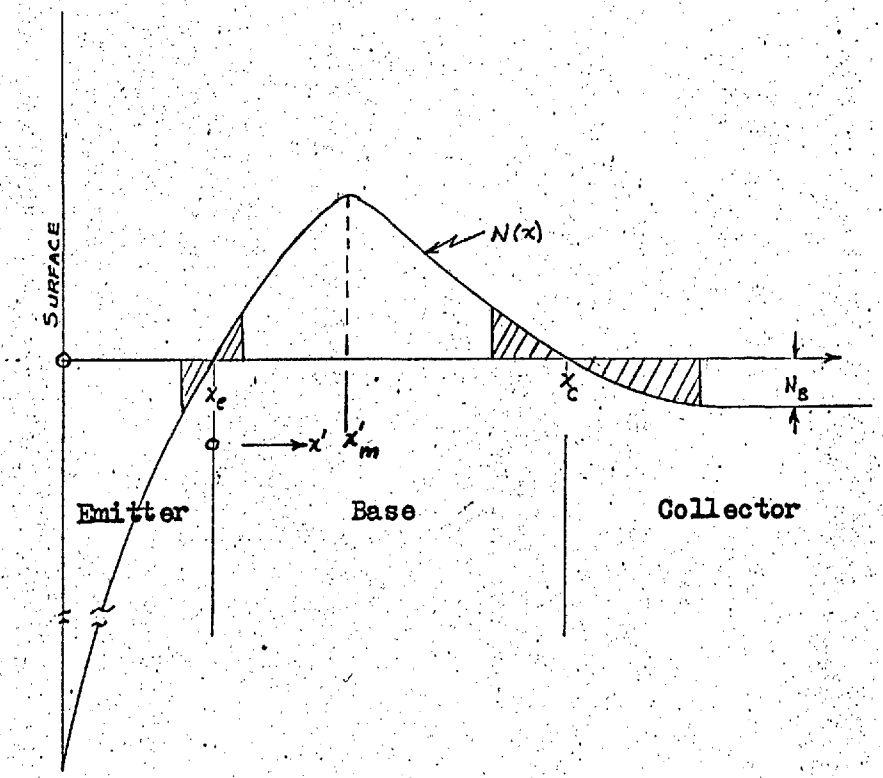


Fig. 2.6. General Representation of Double-Diffused Impurity Profile.

If both diffusions are from vapour sources subject to the boundary conditions of Section 2.2.2, the resulting uncompensated impurity distribution should be the difference of two ERFCs:

$$N(x) = N_A - N_D = -N_{S1}\,\mathrm{erfc}(x/\sqrt{4D_1t_1}) + N_{S2}\mathrm{erfc}(x/\sqrt{4D_2t_2}) - N_B \qquad 2.3.1$$

where the subscripts "1" and "2" refer to the emitter and base diffusants respectively. N_B is the background doping of the wafer.

For diffusion from two planar sources subject to the boundary conditions of Section 2.2.3, the uncompensated impurity distribution would be the difference of two Gaussians:

$$N(x) = N_A - N_D = -N_{S1}\,e^{-x^2/4D_1t_1} + N_{S2}\,e^{-x^2/4D_2t_2} - N_B \qquad 2.3.2$$

In this case $N_{S1} = \bar{N}_{O1}/\sqrt{\pi D_1 t_1}$ and $N_{S2} = \bar{N}_{O2}/\sqrt{\pi D_2 t_2}$, where $\bar{N}_{O1}$ and $\bar{N}_{O2}$ are the initial sheet densities of the deposited material in atoms/cc.

The classical distributions of eqns. 2.3.1 and 2.3.2 have occupied a central position in studies of double-diffused transistors. Most design information and most characterization attempts have been based on these distributions - except for cases where specific approximations have been assumed. Although the impurity distributions of practical devices may depart significantly from ideality (see Section 2.3.3), this study will assume for simplicity that practical profiles are either double ERFC or double Gaussian.

Eqns. 2.3.1 and 2.3.2 are plotted in Figs. 2.7 and 2.8 respectively where diffusion lengths are in the ratio $\sqrt{4D_2t_2}/\sqrt{4D_1t_1} = 3$ and surface densities are in the ratio $N_{S1}/N_{S2} = 100$. N_B is assumed to be = $N_{S2}/1000$. Log-linear paper is used and magnitudes only are plotted.

Consideration of the magnitudes of the two diffusions at the junctions indicates two possible simplications to the treatment of double-diffused transistors. With little error the collector junction may be assumed to occur where $|N_2(x_c)| = |N_B|$, and the emitter junction can be assumed to occur where $|N_1(x_e)| = |N_2(x_e)|$. $N_1(x)$ and $N_2(x)$ are the values of emitter and base diffusion respectively, while x_e and x_c are the positions of the emitter and collector junctions respectively.

2.3.3 Practical Device Profiles

Departures from classical distributions due to rate limitations and out diffusion were discussed in Section 2.2.4. Since the pre-deposit, drive-in process now finds wide application in device fabrication, the modified ERFC distribution of eqn. 2.2.11 has little significance in practical devices. Out-diffusion during the drive-in stage of the two-step process is much more significant. The amount of modification introduced by this factor depends on the oxide, with a dry oxide rejecting the diffusant more completely than a wet oxide. The double-diffused distribution with out-diffusion would be

$$N(y,z) = -N_{S1} e^{-y_1^2} [1 - \sqrt{\pi} z_1 e^{(y_1 + z_1)^2} \operatorname{erfc}(y_1 + z_1)] + N_{S2} e^{-y_2^2} [1 - \sqrt{\pi} z_2 e^{(y_2 + z_2)^2} \operatorname{erfc}(y_2 + z_2)] - N_B \qquad 2.3.3$$

where y and z are as defined in section 2.2.4, and the subscripts "1" and "2" refer to emitter and base diffusions respectively.

Variation of diffusion coefficient D with impurity density (eqn. 2.2.4) can lead to departures from the classical distributions based on the existence of constant D. Technical considerations such as

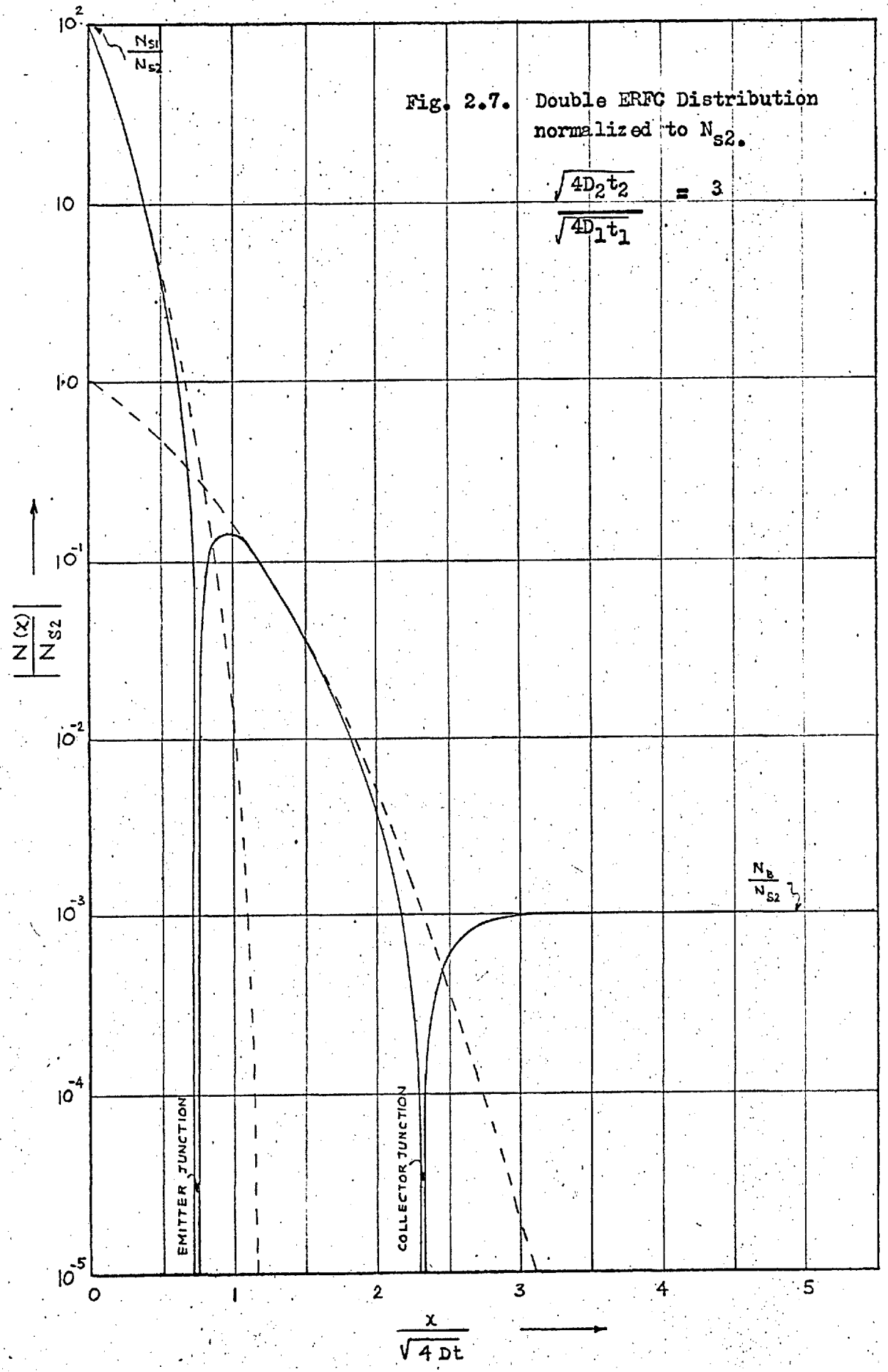


Fig. 2.7. Double ERFC Distribution normalized to N_{S2}.

$$\frac{\sqrt{4D_2t_2}}{\sqrt{4D_1t_1}} = 3$$

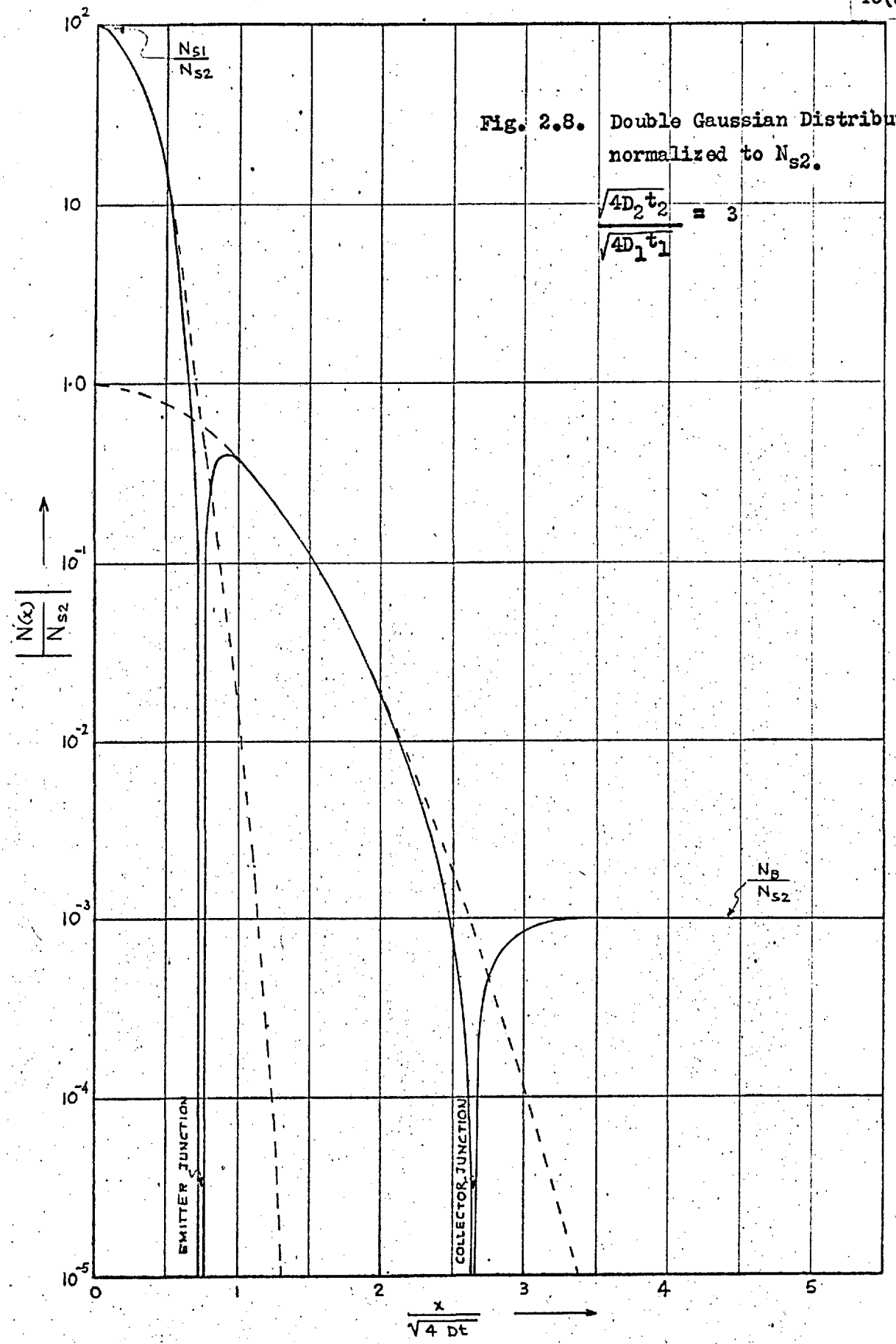


Fig. 2.8. Double Gaussian Distribution normalized to N_{S2}.

$$\frac{\sqrt{4D_2t_2}}{\sqrt{4D_1t_1}} = 3$$

inadequate control of temperature, surface contamination, or crystal imperfections can also lead to departures from ideality. In addition, further diffusion of the base impurity during emitter diffusion modifies the classical double-diffused distribution[43,44]. Consideration of the inevitable technical variations from one manufacturer to another leads to the conclusion that practical distributions are unique to a particular manufacturer. The degree of standardization is such, however, that individual variations may be neglected and the same general distributions be assumed to describe double-diffused impurity profiles - bearing in mind that these are not necessarily intended to cover extreme deviations from ideality but are intended to serve only as general representations.

2.3.4 The Planar Epitaxial Transistor

Epitaxial growth, introduced in 1960[27], provides a convenient means of reducing collector series resistance with subsequent improvement in switching speed and high-frequency gain of the transistor. A thin high-resistivity layer is grown on to a low resistivity substrate of the same material, with the single crystal nature of the substrate being propogated into the epitaxial layer. The planar transistor is then formed in the epitaxial layer in the normal manner.

Growth of an epitaxial film is always accompanied by diffusion of impurities from the substrate into the growing film. A gradual transition replaces an otherwise sharp transition. A natural phenomenon of epitaxial growth is a decrease in impurity density from the substrate interface, a mechanism separate from the accompanying diffusion[45,46]. This decrease approximates a slowly-decreasing

exponential. The impurity distribution prior to the planar process is given mathematically by:

$$N(x) = -N_B\left(1 + a\, e^{-b(x_s-x)}\right) - \tfrac{1}{2}N_C \operatorname{erfc}\left(\frac{x_s - x}{\sqrt{4D_o t_o}}\right) \qquad 2.3.4$$

where N_B, a, and b are constants describing the exponential nature of the epitaxial layer, x_s is the position of the original substrate interface, N_C is original substrate doping, D_o is the diffusion coefficient of the substrate impurity, and t_o is time of epitaxial growth ($\sqrt{4D_o t_o}$ is diffusion length).

During formation of the planar structure, additional diffusion takes place from the substrate into the epitaxial layer. Nomura[44] has shown that, provided concentration at the origin remains constant, (as in this situation) additional diffusion from an ERFC distribution results in an ERFC distribution with increased diffusion length. This is independent of whether this second diffusion is carried out at the same termperature or at a different temperature. After formation of the planar structure by diffusion from vapour sources, the impurity distribution would be

$$\begin{aligned} N(x) = &- N_{S_1}\operatorname{erfc}\left(x/\sqrt{4D_1 t_1}\right) + N_{S_2}\operatorname{erfc}\left(x/\sqrt{4D_2 t_2}\right) \\ &- N_B\left(1 + a e^{-b(x_s-x)}\right) - \tfrac{1}{2} N_C \operatorname{erfc}\left((x_s-x)/\sqrt{4D_3 t_3}\right) \end{aligned} \qquad 2.3.5$$

where $D_3 t_3 = D_o t_o + D_{o2} t_2$. Where diffusion temperature is the same as temperature used in epitaxial growth, $D_3 = D_o = D_{o2}$, and $t_3 = t_o + t_2$; where different temperatures are used, D_3 is an average value and $t_3 = t_o + t_2$. All other terms are as previously defined.

If the planar structure is formed by two-step diffusions, the first

two expressions of eqn. 2.3.5 are replaced by the Gaussians of eqn. 2.3.2. The planar epitaxial transistor is represented in cross section in Fig. 2.9(a) with the different regions indicated. A general representation for the impurity distributions in the different regions is given in Fig. 2.9(b). The original abrupt nature of the substrate interface is also indicated.

The expressions given for impurity distribution apply only up to the original substrate interface. For descriptive purposes the interface represents a discontinuity. Beyond the interface the distribution may be represented, with little error, by:

$$N(x) = - N_B (1 + a) - \tfrac{1}{2}N_C \left[1 + \text{erf } (x-x_s)/\sqrt{4D_3 t_3} \right] \qquad 2.3.6$$

The effect of the diffusions from the wafer surface is neglected, a reasonable supposition when the distance between the collector and the substrate is sufficiently large. (If this assumption does not hold either the double ERFC or the double Gaussian is added to eqn. 2.3.6.)

Lack of information on the constants of the slowly-decreasing exponential of the epitaxial layer precludes its consideration in detail here. For the purposes of this study, epitaxial growth will be assumed to be uniform with a background impurity density N_B. Eqn. 2.3.5 then becomes:

$$N(x)\Big|_{x< x_s} = - N_{s_1}\text{erfc } (x/\sqrt{4D_1 t_1}) + N_{s_2}\text{erfc } (x/\sqrt{4D_2 t_2}) - N_B - \tfrac{1}{2}N_C\text{erfc}((x_s - x)/\sqrt{4D_3 t_3}) \qquad 2.3.7$$

For diffusion from two planar sources,

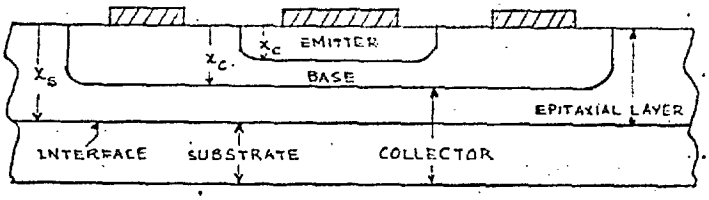


Fig. 2.9(a) Cross-sectional view of Planar Epitaxial transistor showing different regions.

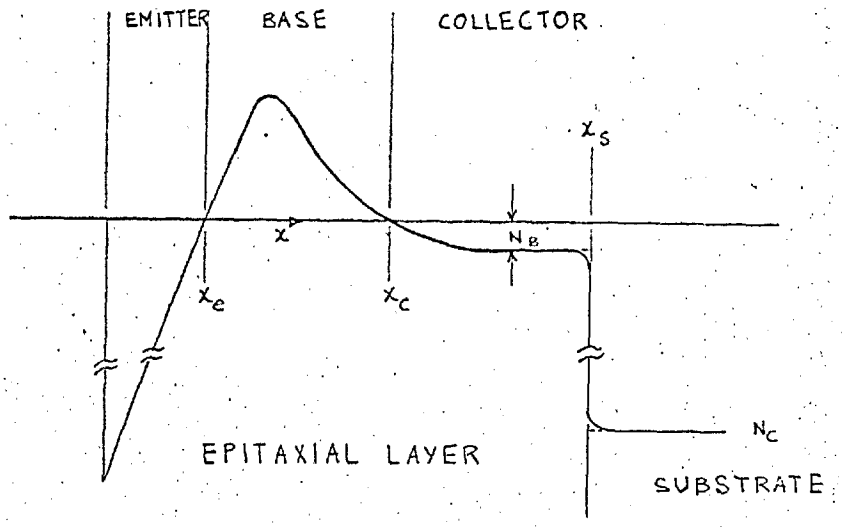


Fig. 2.9(b) General Impurity Profile in Planar Epitaxial transistor.

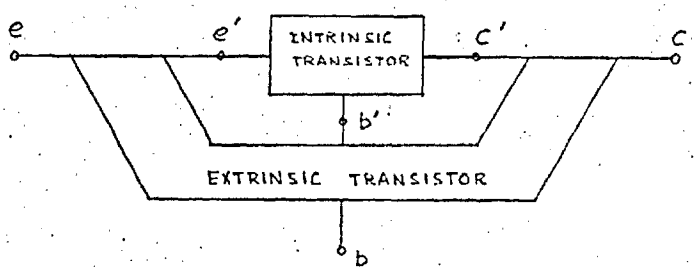


Fig. 210. Representation of Transistor by Intrinsic and Extrinsic Regions.

$$N(x) = - N_{s_1} e^{-x^2/4D_1t_1} + N_{s_2} e^{-x^2/4D_2t_2} - N_B - \tfrac{1}{2}N_C \operatorname{erfc} \frac{x_s - x}{\sqrt{4D_3t_3}} \qquad 2.3.8$$

Beyond the interface, the distribution will be given by:

$$N(x)\Big|_{x>x_s} \simeq - N_B - \tfrac{1}{2} N_C \left(1 + \operatorname{erf} \frac{x - x_s}{\sqrt{4D_3t_3}}\right) \qquad 2.3.9$$

Eqns. 2.3.7, 2.3.8 and 2.3.9 will be considered in more detail in Section 3.4 (Chapter 3) and approximations to it in Section 3.5.7.

2.4 Influence of Diffused Structure on Transistor Performance

2.4.1 General Considerations

Perhaps the major consideration influencing the evolution of transistors has been the search for methods of extending the upper frequency limit. The factors determining the frequency response have long been known; optimization has been limited by fabrication techniques. The utilization of the diffusion process to produce devices within close dimensional tolerances and with accurately gauged impurity concentrations has proved a major breakthrough in the optimization of frequency performance.

Frequency response, a terminal characteristic, is largely dependent on two factors, base transit time τ_b and depletion layer considerations. A "terminal transit time" τ, dependent on both these factors, may be considered as a delay time associated with the small signal common-base current transfer function α. At low frequencies ($\omega \to 0$):

$$\alpha = - \frac{i_c}{i_e}\Bigg|_{\delta V_{cb} \to o} = \frac{\alpha_o}{1 + j\omega\tau} \simeq \alpha_o e^{-j\omega\tau} \qquad 2.4.1$$

where i_c and i_e are small-signal collector and emitter currents respectively, α_o is the terminal current transfer function when $\omega = 0$, (ω has the usual definition of angular frequency) and $\tau = 1/2\pi f_\tau$.

'f_τ' is normally defined as the frequency at which Re [α] = 0.5, assuming a 6 db/octave fall-off of gain with frequency. On this basis f_τ may be predicted from a relatively low frequency measurement of α and subsequent use of the 6 db/octave relationship. At frequencies approaching f_τ, fall-off is often less rapid in practical devices, so that Re [α] = 0.5 occurs at a higher frequency f_1. Eqn. 2.4.1 is, however, sufficiently accurate at low frequencies, giving f_τ validity as a figure of merit in describing frequency performance.

Eqn. 2.4.1 allows determination of τ as follows:

$$\tau = -\lim_{\omega \to o} \frac{\text{Arg}\,\alpha}{\omega} = -\lim \frac{\text{Im}\,\alpha}{\omega |\alpha|} \qquad 2.4.2$$

where Argα refers to the phase angle and Imα refers to the imaginary component of α. In practice, ω must be sufficiently low that Arg$\alpha \leq 5^o$ for 2.4.2 to be applicable. Application of Kirchhoff's current law yields:

$$\tau = -\lim_{\omega \to o} \frac{\text{Im}\, i_b/i_e}{\omega |i_c/i_e|} = -\lim_{\omega \to o} \frac{\text{Im}\, i_b}{\omega |i_c|} \qquad 2.4.3$$

since the phases of i_b and i_c are referred to that of i_e. (i_b is the small-signal base current). Eqn. 2.4.3 provides the basis for the measurement of τ by the small-signal low frequency bridge techniques of Chapter 4 (Sect. 4.4.3).

Since τ represents, in effect, the delay between the emitter and collector currents, it must include the delays associated with the charging of the emitter depletion layer, carrier transit through the base, and collector depletion layer charging. It is worthwhile at this stage of the discussion to appreciate in qualitative terms the origin of these components.

To properly describe base transit time the concept of an "intrinsic transistor", representing the physical mechanism of base transport and separate from the parasitic effects associated with depletion layers, stray capacitances and body resistances, is introduced. This is represented schematically in Fig. 2.10. Base transit time τ_b may be considered as the delay time associated with the small-signal intrinsic short-circuit current gain a. For very low frequency ($\omega \to o$) an expression analogous to eqn. 2.4.1 applies:

$$a = \frac{-i_{c'}}{i_{e'}} = \frac{a_o}{1 + j\omega\tau_b} \simeq a_o e^{-j\omega\tau_b} \qquad 2.4.4$$

where a_o is the intrinsic current gain when $\omega = o$, $i_{c'}$ and $i_{e'}$ are small-signal currents related to terminals c' and e' respectively of the intrinsic transistor. Following a similar argument to that for terminal transit time, τ_b may be determined from:

$$\tau_b = -\lim_{\omega \to o} \frac{\text{Im } i_{b'}}{\omega |i_{c'}|} \qquad 2.4.5$$

where b' is the "base" terminal of the intrinsic transistor.

In the absence of recombination in the base region ($a_o \simeq 1$) it has been shown[47] that the above definition of base transit time

is equal to the charge control definition*:

$$\tau_b = \frac{\delta Q_b}{|i_{c'}|} = \left| \frac{d Q_b}{d I_{c'}} \right| \qquad 2.4.6$$

where Q_b is the excess minority carrier charge in the base ($-Q_b$ is the excess majority carrier charge injected from the "base" terminal). Eqn. 2.4.6 is quite general and applies irrespective of the injection level. For low-level injection:

$$\tau_b = Q_b / |I_{c'}| \qquad 2.4.7$$

where $|I_{c'}|$ ($=|I_e|$) is the steady-state minority carrier current across the base.

Eqn. 2.4.7 is in a form which can be readily discussed in terms of the effect of impurity distribution on the base charge. Strictly speaking, the charge control definition applies only to the base region, so no similar expression exists for τ. To aid discussion, however, it is helpful to visualize a total charge ($-Q$) which defines terminal transit time by:

$$\tau = \frac{-Q}{|I_{c'}|} = \frac{-Q_e}{|I_c|} + \frac{-Q_b}{|I_c|} + \frac{-Q_c}{|I_{c'}|} \qquad 2.4.8$$

where $-Q_e$ and $-Q_c$ are the charges associated with changes of voltage across the emitter and collector depletion layers respectively, and $-Q_b$ is the base charge. The minus signs appear because charging of the depletion layers is by majority carriers supplied from the base terminal.

---

* Charge control transit time is defined as the average time taken for minority carriers to cross the effective base width, regardless of the device geometry.

Collector current, determined by carrier density in the base, is independent of the charge required to charge the depletion layers. Corresponding to any change in collector current there is a change in voltage across the emitter junction. This voltage increment causes an incremental change in the charge dipole of the depletion layer - a capacitive effect. For small-signals the voltage increment is small, hence the charge increment is generally insufficient to appreciably change the width of the emitter depletion layer. The effective capacitance is, therefore, analogous to that of a parallel plate capacitor, and remains relatively constant over the voltage increment - determined by the total current (I_c) which governs total voltage across the emitter junction. A transit time analogous to the charge control definition thus exists for the emitter depletion layer, represented by $-Q_e/|I_c|$ in eqn. 2.4.8.

A similar consideration applies to the collector depletion layer. Flow of collector current causes a voltage drop across the collector body resistance which changes the total voltage across the collector depletion layer. This change causes an increment in the total charge contained in the depletion layer, a capacitive effect controlled by I_c and thus analogous to charge control transit time (in fact, an RC time constant). This is represented in eqn. 2.4.8 by $-Q_c/|I_c|$.

Derivation of terminal transit time in Section 2.4.6 in terms of an assumed small-signal equivalent circuit supports the above arguments

for the emitter and collector depletion layers*. The rest of this section will be devoted to discussion in general terms of the effect of the planar structure on τ_{ru}.

Charge Q is a volume quantity, dependent on both the dimensions of the device and the impurity distribution. Minimization of Q for a given current therefore minimizes τ. In planar structures emitter and collector areas can be made extremely small, limited only by photo-lith techniques and the necessity of making connections to the outside world. The other important dimensional quantity, base width, may be reduced in diffused transistors to a fraction of the wave length of light. In practice,'punch-through' of the base with reverse bias on the collector, provides a limitation on minimum base width. As pointed out, charging of the emitter and collector depletion regions implies capacitive effects. These transition capacitances have been shown[48] to be analogous to parallel plate capacitors with separation d between plates:

$$C_t = \epsilon A/d \qquad 2.4.9$$

where A is the junction area, C_t is transition capacitance, and ϵ is the permittivity of the material (1.0625×10^{-13} farad/cm in silicon). The diffused junctions of the planar structure allow for large values of d at either junction for given bias voltages. Coupled with the small

---

* A significant correction to τ exists when, as in the case for large reverse bias on the collector junction of a double-diffused transistor, minority carriers entering from the base region require a finite time to cross the collector depletion layer. This gives an added delay to τ: viz, there is a delay before i_c after passing through the collector depletion layer, causes voltage drop across collector body resistance, hence change in depletion layer charge.

areas possible in planar devices, large depletion layer width d results in low values of transition capacitances, hence low associated delay effects.

The retarding field region of the base of planar transistors leads to build-up of minority carriers in order to overcome the potential barrier. This has an adverse effect on transit time through the base. However, this is more than compensated for by the very narrow base widths possible in planar devices. The net effect is a decrease in base transit time from that of diffusion and drift transistors. The net reductions in transition capacitances and base transit time made possible by the planar structure, therefore, cause a significant reduction in τ. Certain other parameters of double-diffused transistors are slightly degraded in planar transistors, but the enhancement of frequency characteristics and the elimination of surface effects (see Section 2.3.1) far outweigh these minor effects.

2.4.2 Influence of Base Impurity Profile on Diffusion Coefficient

Determination of base transit time requires a knowledge of minority carrier density distribution in the base at any time. The base transport equations form the basis for this determination:

$$J_n = qD_n \left(\nabla n + \frac{q}{kT} \mathcal{E}.n\right) \qquad 2.4.10$$

and

$$J_p = - qD_p \left(\nabla p - \frac{q}{kT} \mathcal{E}.p\right) \qquad 2.4.11$$

where J_n and J_p are current densities due to electrons and holes respectively, n is excess electron density, p is excess hole density,

D_n and D_p are diffusion coefficients, $\mathcal{E}$ is the built-in electric field, and ∇ is the vector operator ($\nabla = \frac{\partial}{\partial x} a_x + \frac{\partial}{\partial y} a_y + \frac{\partial}{\partial z} a_z$ in Cartesian co-ordinates). Before minority carrier density in the base can be determined from eqns. 2.4.10 and 2.4.11, the nature of the diffusion coefficients must be understood.

Various investigators[49-54] have studied carrier mobility in semiconductors-both experimentally and theoretically. Their results were compiled and adjusted by Conwell[55] and point out the strong dependence of carrier mobility on impurity density, as well as differences between "drift" (minority carrier) and "conductivity" (majority carrier) mobilities. Diffusion coefficients may be determined from these results by utilizing the Einstein relationship:

$$D = \frac{kT}{q} \mu \qquad 2.4.12$$

where μ is mobility. Fig. 2.11 is a plot of diffusion coefficients vs impurity density for electrons in silicon. Drift diffusion coefficients in this figure are based largely on data presented by Prince[49-50], while majority carrier diffusion coefficients were computed from eqn. 2.4.12 with the values of conductivity mobility presented by Conwell[55].

Essentially, carrier mobility in semiconductors is determined by scattering mechanisms of the following types:

(1) scattering by thermal lattice vibrations,

(2) coulomb scattering by ionized donors (N_D) and acceptors (N_A),

(3) coulomb scattering by other charge carriers,

(4) scattering by lattice imperfections and dislocations.

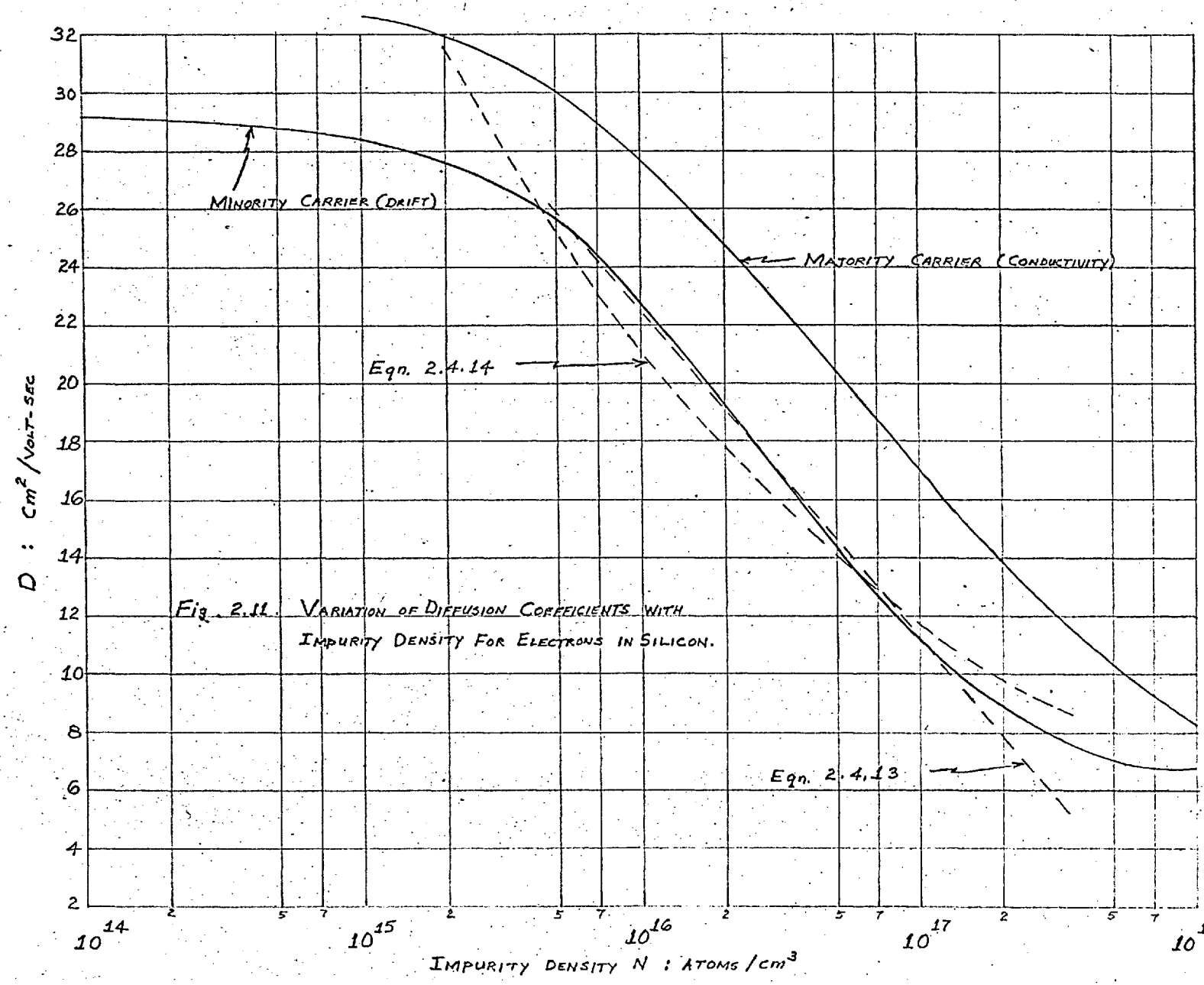


Fig. 2.11. Variation of Diffusion Coefficients with Impurity Density For Electrons in Silicon.

The relative importance of the different scattering mechanisms is not the same for majority and minority carriers, so differences would be expected to exist between conductivity and drift mobilities. The following qualitative discussion should explain the form of the curves of Fig. 2.11 and the differences between the two curves.

Thermal lattice vibrations dominate scattering in a high resistivity sample (low impurity concentration). As impurity concentration is increased, the diffusion coefficient remains relatively constant at first, then decreases as other scattering mechanisms come into play. In low resistivity samples (high impurity concentration) coulomb scattering by ionized donors and acceptors causes considerable reduction in mobility, hence in diffusion coefficient. Like-charge carrier scattering has no first order effect on mobility. Minority-majority carrier scattering has, in general, been treated only theoretically by adopting as a first approximation the Conwell-Weisskopf formula[56] for computing the effect of fixed scattering centres. Prince[49,50] used this approximation to fit his experimental data assuming, however, an unrealistically high value for the effective mass of carriers. Scattering by lattice imperfections and dislocations is normally negligible in the high-quality grown crystals used today. At very high impurity concentrations degeneracy sets in and subsequent increase in concentration results in little change in diffusion coefficients.

In a p-type semiconductor minority carriers undergo coulomb scattering by $N_A + N_D$ fixed scattering centres when complete ionization

is assumed. They are also scattered by $N_A - N_D + n$ majority carriers (charge neutrality assumed) where n is the number of minority carriers. Majority carriers, on the other hand, "see" only $N_A + N_D$ fixed scattering centres (if low-level injection of minority carriers obtains), and are thus less seriously scattered than minority carriers.

The base of a double-diffused transistor is formed by the complete "compensation" of donors and acceptors at the junctions, and by their partial "compensation" throughout the rest of the base. The fixed scattering centres in the base may be considered to be composed of $2N_D$ "compensated" scattering centres and $N_A - N_D$ majority scattering centres. Since, however, compensation is an averaging effect involving total numbers of donors and acceptors in a given reg ion and not "pairing" of specific donors and acceptors, each impurity ion scatters independently of other ions. Moreover, scattering effects of individual donors and acceptors are equal. The drift curves of Fig. 2.11 strictly apply to p-type material doped with acceptors only. The effect of donors in the base of a double-diffused transistor (n-p-n) is to reduce the density of majority carriers, hence scattering effects due to majority carriers. Since acceptors dominate in the base region of an n-p-n transitor, over much of the base this reduction in the number of majority carriers can be neglected. For simplicity, this effect will be neglected altogether in this thesis, and diffusion coefficients will be determined from Fig. 2.11 using the sum of donors and acceptors ($N_A + N_D$) at any point - unless otherwise specified.

To facilitate analytical treatment it is often convenient to

approximate the diffusion coefficient curve by an empirical mathematical expression applicable over a specified range of concentrations. Two such approximations are represented in Fig. 2.11. Over a limited region (5×10^{15} to 1×10^{17} atoms/cc) the following expression may be used:

$$D_n/D_{(10^{17})} = 1 - 0.435 \ln (N_A.10^{-17}) \qquad 2.4.13$$

where an impurity density of 10^{17} atoms/cc was chosen as a reference density and $D_{(10^{17})}$ is the diffusion coefficient at this concentration. A second approximation originally proposed by Sugano and Koshiga[57] and used also by Boothroyd and Trofimenkoff[37,38] is given by:

$$D_n = D_\gamma (N_\gamma/N)^\theta \qquad 2.4.14$$

where the diffusion coefficient is D_γ at reference doping N_γ, and N is the actual doping. θ is a positive fractional index. With values as follows:

$$D_\gamma = 13.5, \quad \theta = 0.25, \text{ and } \quad N_\gamma = 6 \times 10^{16} \text{ atoms/cc},$$

the approximation is adequate over the range 5×10^{15} to 5×10^{18} atoms/cc. Although not very accurate, the approximation of eqn. 2.4.14 has the advantage that it can be simply treated analytically for many impurity distributions. Where greater accuracy is required, the actual drift curve of Fig. 2.11 will be used.

2.4.3 Minority Carrier Density in Base Region

Subject to certain conditions the transport equations (2.4.10 and 2.4.11) may be solved to yield the minority carrier density. Assume a one dimensional n-p-n structure with high emitter efficiency, i.e. current

carried by holes injected into the emitter is neglibible ($J_p \approx 0$). Equating eqn. 2.4.11 to zero and substituting the value of built-in field thus obtained into the one-dimensional form of eqn. 2.4.10 gives:

$$J_n/qD_n = \frac{dn}{dx'} + \left(\frac{1}{p} \cdot \frac{dp}{dx'}\right)n \qquad 2.4.15$$

The further assumptions of base charge neutrality, complete ionization of impurities, and low-level injection allows substitution of the density of uncompensated impurities (N_A-N_D) for majority carrier density p:

$$p \approx N_A - N_D \qquad 2.4.16$$

Eqn. 2.4.15 becomes:

$$\frac{J_n}{qD_n(N_A;N_D)} = \frac{dn}{dx'} + \left(\frac{1}{N_A - N_D}\right) \cdot \frac{d(N_A - N_D)}{dx'} \cdot n \qquad 2.4.17$$

To indicate that diffusion coefficient is dependent on both acceptor and donor density, D_n has been replaced by $D_n(N_A;N_D)$. Eqn. 2.4.17 is a first order linear differential equation which, when solved across the base subject to the boundary condition n = o, at $x' = W$, yields

$$n = \frac{-J_n}{q} \cdot \frac{1}{(N_A - N_D)} \int_{x'}^{W} \frac{N_A - N_D}{D_n(N_A;N_D)}\, dx' \qquad 2.4.18$$

The origin of x' is at the emitter metallurgical junction. (see Fig. 2.6). Normalizing with respect to W (base width from emitter junction to edge of collector depletion region) gives:

$$n = -\frac{J_n W}{q} \cdot \frac{1}{(N_A - N_D)} \int_{Y}^{1} \frac{N_A - N_D}{D_n(N_A;N_D)}\, dY \qquad 2.4.19$$

where $Y = x'/W$. Eqn. 2.4.19 is quite general and will apply to any base impurity distribution. The region of interest is between $Y_1 = a_{ze}/W$ and 1, where a_{ze} is the edge of the emitter depletion region in the base.

Eqn. 2.4.19 is simplified in the "diffusion transistor" by substitution of constant base doping N_A for $N_A - N_D$ and constant D_n for $D_n(N_A;N_D)$. In many practical transistors with variable doping of only one type of impurity in the base (e.g. "drift" transistors), an average diffusion coefficient $\overline{D}_n$ is often sufficient to describe base characteristics. Such an average diffusion coefficient is determined by:

$$\overline{D}_n = \frac{1}{Y_b - Y_a} \int_{Y_a}^{Y_b} D(N)\, dY \qquad 2.4.20$$

where Y_a and Y_b are the limits of the region considered and N is the impurity density distribution. $\overline{D}_n$ could also be determined by finding average doping in the region considered and using Fig. 2.11 to determine $\overline{D}_n$. This approximation is also applicable when $N_D \ll N_A$. For greater accuracy eqn. 2.4.14 may be substituted for $\overline{D}_n$ to give:

$$n \approx -\frac{J_n W}{q D_\gamma} \cdot \frac{1}{N_A} \int_Y^1 \left(\frac{N_A}{N_\gamma}\right)^{1+\theta} dY \qquad 2.4.21$$

where D_γ is the diffusion coefficient at reference impurity density N_γ, θ is a positive fractional index, and N_A is doping in the base region (acceptors only). This approximation was applied by Trofimenkoff[37] (See Section 2.7.2) for the aiding region of a linear-exponential model for the base region of a double-diffused transistor.

Rigorous treatment of the base region of a double-diffused transistor requires solution of eqn. 2.4.19. Such a base consists of two distinct regions - a retarding field region followed by an aiding field region. In Fig. 2.6 the retarding field exists up to x'_m, the position of maximum uncompensated impurity density. Total impurity density $N_A + N_D$ in the retarding field region is considerably higher than that in the aiding field region. Over a large part of the aiding field region impurity density $\approx N_A$. The average diffusion coefficient in the aiding field region is appreciably larger than that in the retarding field region. A reasonable approximate approach, therefore, would seem to be to treat the two regions separately on the basis of an average diffusion coefficient $\bar{D}_R$ for the retarding field region and an average diffusion coefficient $\bar{D}_A$ for the aiding field region. Eqn. 2.4.19 becomes for the retarding field region:

$$n = -\frac{J_n W}{q \bar{D}_R} \cdot \frac{1}{N_A - N_D} \left[\int_Y^{Y_m} (N_A - N_D)\, dY + \frac{\bar{D}_R}{\bar{D}_A} \int_{Y_m}^{1} (N_A - N_D)\, dY \right] \qquad 2.4.22$$

$Y_1 \leq Y \leq Y_m$ where $Y_m = x'_m/W$.

For the aiding field region:

$$n = -\frac{J_n W}{q \bar{D}_A} \cdot \frac{1}{N_A - N_D} \int_Y^1 (N_A - N_D)\, dY \qquad 2.4.23$$

$Y_m \leq Y \leq 1$

This approximation is adopted in Chapters 3, 4, and 5 to simplify calculations of minority carrier density and transit time for the

double exponential model. Comparison for a specific example in Chapter 3 of minority carrier density computed from the above equations with that computed from eqn. 2.4.19 indicates that the approximation is reasonably accurate. It was, therefore, used in Chapters 4 and 5 in the determination of physical constants of actual devices.

2.4.4 Base Transit Time

Transit time across the effective base region between the emitter and collector depletion layers ($Y_1 \leq Y \leq 1$) plays an important role in determining frequency response of a transistor. In Section 2.4.1 the charge control definition was shown to be directly applicable to the base region in the absence of recombination. For low level injection:

$$\tau_b = Q_b / |I_c| \qquad 2.4.24$$

For any base impurity profile, minority carrier density is given by eqn. 2.4.19. The total minority carrier charge Q_b in a base of area A_e (equal to emitter area) is given by:

$$Q_b = qA_eW \int_{Y_1}^{1} n \, dY \qquad 2.4.25$$

Substituting the value of n from eqn. 2.4.19 gives:

$$Q_b = - J_n A_e W^2 \int_{Y_1}^{1} \frac{1}{N_A - N_D} \int_{Y}^{1} \frac{N_A - N_D}{D_n(N_A;N_D)} \, dY \, dY \qquad 2.4.26$$

The electron current density, $J_n = - I_c/A_e$. Thus,

$$\tau_b = Q_b / |I_c| = W^2 \int_{Y_1}^{1} \frac{1}{N_A - N_D} \int_{Y}^{1} \frac{N_A - N_D}{D_n(N_A;N_D)} \, dY \, dY \qquad 2.4.27$$

Eqn. 2.4.27 provides a starting point for the derivation of base transit

time for any specific impurity distribution.

With constant base doping (hence constant D_n) the origin may be taken at the base edge of the emitter depletion layer. Solution of eqn. 2.4.27 results in the well-known intrinsic base transit time of the 'diffusion' transistor.

$$\tau_b = W_{eff}^2/2D_n$$

Where W_{eff} is the effective base width between depletion layer. With average diffusion coefficient $\overline{D}_n$ determined from eqn. 2.4.20 and exponential base distribution,

$$\tau_b = \frac{L^2}{\overline{D}_n} (m - 1 + e^{-m}) \qquad 2.4.29$$

where L is characteristic length of the exponential and $m = W_{eff}/L$. Eqn. 2.4.29 has found considerable application in "drift" and " alloy-diffused" transistors.

The complicated impurity distributions of double-diffused transistors almost invariably necessitate solution of eqn. 2.4.27 by numerical means. In specific cases where an average diffusion coefficient is used, it is often possible to evaluate the inner integration analytically; however, it is seldom possible to evaluate the outside integral except by numerical techniques. For simplicity, the utilization of an approximation to the actual distribution is often attractive. Two early approximations are presented in Section 2.7, while a more accurate approximation is introduced in Chapter 3 (Section 3.5).

In Section 2.4.3 it was suggested that the retarding and aiding field regions be treated individually with average diffusion coefficients

$\overline{D}_R$ and $\overline{D}_A$ applicable in the respective regions. Making this approximation and determining minority carrier density from eqn. 2.4.22, transit time across the retarding field region becomes:

$$\tau_R = \frac{W^2}{\overline{D}_R}\left[\int_{Y_1}^{Y_m} \frac{1}{N_A - N_D}\left\{\int_{Y}^{Y_m} (N_A - N_D)dY + \frac{\overline{D}_R}{\overline{D}_A}\int_{Y_m}^{1} (N_A - N_D)dY\right\} dY\right] \qquad 2.4.30$$

$Y_1 < Y < Y_m$

Transit time across the aiding field region, derived from the minority carrier density of eqn. 2.4.23, is given by:

$$\tau_A = \frac{W^2}{\overline{D}_A}\int_{Y_m}^{1} \frac{1}{N_A - N_D}\int_{Y}^{1} (N_A - N_D)\, dY\, dY \qquad 2.4.31$$

where $Y_m \leq Y \leq 1$

The total base transit time, $\tau_b = \tau_R + \tau_A$, is given by:

$$\tau_b = \frac{W^2}{\overline{D}_R}\left[\int_{Y_1}^{Y_m} \frac{1}{N_A - N_D}\left\{\int_{Y}^{Y_m} (N_A - N_D)dY\right\} + \frac{\overline{D}_R}{\overline{D}_A}\int_{Y_m}^{1} (N_A - N_D)dY\right\}dY$$

$\leftarrow Y < Y_m$

$$+ \frac{\overline{D}_R}{\overline{D}_A}\int_{Y_m}^{1} \frac{1}{N_A - N_D}\int_{Y}^{1} (N_A - N_D)\, dY\, dY\Bigg] \qquad 2.4.32$$

$Y \geq Y_m$

Although, in appearance, eqn. 2.4.32 is more complicated than the general expression (eqn. 2.4.27), it is less complicated in fact. For most impurity distributions the inside integrals of eqn. 2.4.32 may be evaluated analytically, leaving only the outside integral to be evaluated by numerical means. This "two-diffusion coefficient" approximation is adopted in Chapters 4 and 5 as the standard to be used in evaluation of physical parameters of double-diffused transistors.

2.4.5 Equivalent Circuit for Transistor

The interpretation of terminal measurements provides valuable information on transistor internal configuration. To aid this interpretation it is convenient to postulate an equivalent circuit whose elements represent individual effects in the transistor and which can be easily derived from terminal measurements. The small-signal common-base equivalent circuit of Fig. 2.12 has been found[39] to accurately represent a transistor over a wide range of operating conditions and a wide range of frequencies. The elements of this circuit may be derived in terms of impurity distribution and physical dimensions and can be measured by standard techniques (see Chapter 4). A brief discussion of the individual circuit element follows.

A. Stray capacitances. C_{seb}, C_{sec}, and C_{scb} are stray capacitances between the emitter-base, emitter-collector, and collector-base leads respectively. These parasitic elements limit performance at higher frequencies. In planar structures where the collector is normally 'tied' to the can, $C_{sec} \approx C_{scb}$ and are of the order of 0.6pF for the TO-5 can and 0.7pF for the TO-18 can. C_{seb} is generally considerably smaller (order of 0.04pF) and can normally be neglected.

B. Body Resistances. Emitter, base, and collector body resistances are represented by the circuit elements r'_{ee}, r'_{bb} and r'_{cc} respectively. They are lumped equivalents of distributed effects dependent on resitivity and physical dimensions of the respective regions (Fig. 2.13). Emitter resistance r'_{ee} is generally negligible, owing to the high impurity density in the emitter region. Base spreading resistance r'_{bb} is intended to account for transverse voltage drop in the ohmic base material

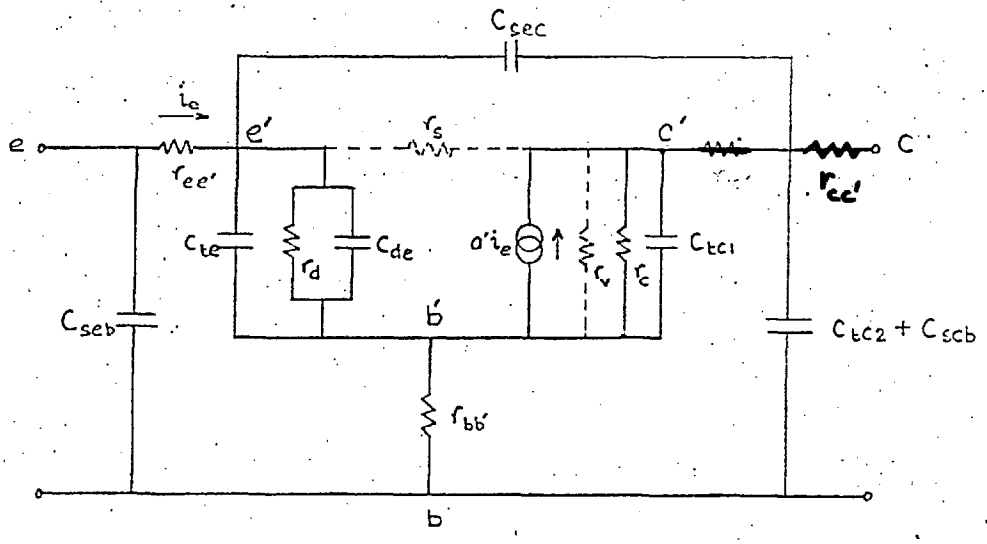


Fig. 2.12. Common-Base Equivalent Circuit for Transistor

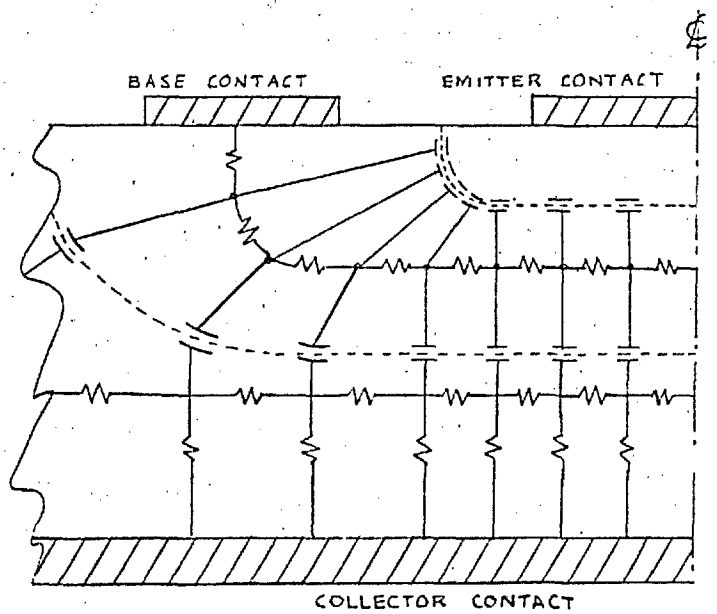


Fig. 2.13. Distributed Representation of Transition Capacitances and Base and Collector Body Resistances.

due to flow of various components of base current to the base contact. It may range in value from a few ohms in one transistor to several tens of ohms in another of different construction. The product $r'_{bb}C_{tci}$ is ofte n used as a figure of merit for transistors, a low product being preferred. (C_{tci} is discussed below.) Collector body resistance r'_{cc} is often quite significant (few tens of ohms) in double-diffused transistors, due to the low background doping used and the large dimensions of the wafer into which the transistor is diffused. Minimization is achieved by increasing N_B to its practical limit or, preferably, use of an epitaxial wafer with a low resistivity substrate.

C. Transition Capacitances. Transition capacitances have been shown to be directly proportional to junction area and inversely proportional to the width of the depletion layer (See eqn. 2.4.9). This assumes complete depletion of carriers. C_{tc1} and C_{tc2} are lumped equivalents of the components of collector transition capacitance lying under the emitter area A_e and outside this area respectively. Thus:

$$\left.\begin{aligned} C_{tc1} &= \varepsilon A_e/d_c \\ C_{tc2} &= \varepsilon (A_c-A_e)/d_c = C_{tc}-C_{tc1} \end{aligned}\right\} C_{tci}/C_{tc} = A_e/A_c \qquad 2.4.33$$

where d_c is the width of the collector depletion layer and A_c is the collector area. This lumping of distributed effects is represented in Fig. 2.13. The representation of base resistance by a single resistor, while a useful concept for predicting transistor performance in a particular application, must be used with caution when device constants are to be derived from measurement of equivalent circuit elements.

Emitter transition capacitance is given by:

$$C_{te} = \varepsilon A_e/d_e \qquad 2.4.34$$

where d_e is the width of the emitter depletion layer.

Transition capacitances are dependent on impurity profile near the junction. This dependence is reflected in the width of the depletion layer. The graded nature of junctions in double-diffused transistors results in fairly large depletion layer widths for given bias on the junction. At low reverse bias the transition capacitance may be approximated by the third power law of a linear junction ($C_t \propto V_j^{-1/3}$), while at large reverse bias the abrupt approximation may be used ($C_t \propto V_j^{-1/2}$). V_j is the junction voltage. Between these two extremes the nature of the variation of impurity density with position must be known before depletion layer width can be accurately determined. This strong dependence of transition capacitance on impurity profile suggests that measurement of transition capacitance is a very valuable source of information for determination of the impurity profiles of actual devices.

D. Intrinsic Input Admittance, Y_{ee}. Y_{ee} is defined as the input admittance of the intrinsic transistor with output shorted. It is represented by:

$$Y_{ee} = g_{ee} + j\omega C_{de} \qquad 2.4.35$$

The conductance g_{ee} is given by the incremental change in emitter (or collector) current (δI_e) with accompanying incremental change in emitter voltage (δV_{eb}). For low frequency,

$$g_{ee} = \delta I_e/\delta V_{eb} \simeq qI_e/kT \qquad 2.4.36$$

C_{de} is introduced to represent the imaginary component of Y_{ee}. It is highly dependent on impurity distribution in the base (particularly the retarding field region) and can be determined quantitatively by solving the continuity equation for the base region. This, however, is beyond the scope of the present discussion. Because V_{eb} changes only while I_e is carried substantially by diffusion, C_{de} is called the emitter diffusion capacitance. Its strong dependence on base impurity profile suggests its utilization as a source of information on this profile.

E. Base Width Modulation Effects. Base width modulation and feedback effects may be represented by two resistors r_s and r_v (shown dashed in Fig. 2.12). For simplicity they are often incorporated into one resistor (r_c) across the collector junction. Under conditions of small-signal, low frequency, low leakage and large collector reverse bias, r_c may often be considered to be infinite for all practical purposes. No detailed discussion is offered here, since r_c is of little value as a source of information on impurity distributions.

F. Current Generator. The current generator $a'i_e$ takes into account the effect of emitter transition capacitance on the intrinsic short-circuit current gain. Thus,

$$a' = a \cdot \frac{y_{ee}}{y_{ee} + j\omega C_{te}} \qquad 2.4.37$$

where a is the short-circuit gain for the intrinsic device (see Section 2.4.1). Substituting the value of a (eqn. 2.4.4) gives:

$$a'\Big|_{\omega \to o} = \frac{a_o}{1 + j\omega\tau_b} \cdot \frac{y_{ee}}{y_{ee} + j\omega C_{te}} \approx \frac{a_o}{1 + j\omega\,(\tau_b + C_{te}/g_{ee})} \qquad 2.4.38$$

The approximation applies at low frequencies. The presence of C_{te} increases the phase angle between collector and emitter currents. C_{te}/g_{ee} may therefore be considered as the emitter transit time (C_{te}/g_{ee} is the quantitative statement of emitter transit time described qualitatively in Section 2.4.1 and represented by $-\theta_e/|I_c|$ in eqn. 2.4.8).

2.4.6 Cutoff Frequency Considerations

The terminal cutoff frequency f_τ (Section 2.4.1) may now be considered in more detail with reference to the equivalent circuit. A factor which, until now, has been ignored is the average time required for carriers to cross the collector depletion region. In double-diffused transistors with wide collector depletion regions, this transit time cannot be ignored. It is usually sufficiently accurate to assume that carriers crossing the depletion layer in the presence of the strong accelerating field reach their limiting "drift"velocity for the material involved. This assumption leads to a low frequency transit time across the collector depletion region[37] of:

$$\tau_c = d_c/2v_s \qquad 2.4.39$$

where d_c is the width of the collector depletion region and v_s is the limiting 'drift' velocity. For electrons in p-type silicon v_s as given by Ryder[58] is approximately ~~8×10^6 cm./sec.~~ Eqn. 2.4.39 is likely to slightly underestimate the value of τ_c since the electric field is not constant throughout the depletion region.

Unfortunately τ_c cannot be represented as a circuit element and will not appear in any expression for current gain derived from Fig. 2.12. Considering only the elements of Fig. 2.12 short-circuit current gain is

given by:

$$\alpha = -\frac{i_c}{i_e} = \frac{a' + j\omega C_{tc_1} r'_{bb}}{(1 + j\omega C_{tc_1} r'_{bb})(1 + j\omega C_{tc_2} r'_{cc}) + j\omega C_{tc_1} r'_{cc}} \qquad 2.4.40$$

For low frequencies this becomes:

$$\alpha = \frac{a_o}{1 + j\omega\left[\tau_b + \frac{C_{te}}{g_{ee}} + r'_{cc}\,(C_{tc_1} + C_{tc_2})\right]} \qquad 2.4.41$$

When the effect of τ_c is included it is added to the delay term in the denominator of eqn. 2.4.41. Thus:

$$\alpha = \frac{a_o}{1 + j\omega[\,\tau_b + \tau_c + C_{te}/g_{ee} + r'_{cc}\,(C_{tc_1} + C_{tc_2})]}$$

$$= \frac{a_o}{1 + j\omega\tau} \qquad 2.4.42$$

where τ is the terminal transit time given by:

$$\tau = \tau_b + C_{te}/g_{ee} + d_c/2v_s + r'_{cc}\,(C_{tc_1} + C_{tc_2}) \qquad 2.4.43$$

This value of transit time determines the frequency response of the transistor and is the value normally measured in the bridge measurement of Chapter 4 (Section 4.4.3). $f_\tau = \frac{1}{2\pi\tau}$ thus defines the cutoff frequency of the transistor.

2.5 Basic Approaches to Device Characterization

For the purposes of this study characterization will be taken to mean evaluation of the detailed physical parameters of the internal transistor structure in order to understand properly the external characteristics. Included in this definition is determination of the physical

quantities of base width, junction areas, depletion layer widths, as well as those that characterize impurity density distribution.

Characterization may follow one of two basic approaches depending on the investigator's requirements. The first approach, essentially destructive and limited to those with facilities for device fabrication, will be called the Classical Distribution Approach. As the name implies, it assumes that the impurity distribution is represented by classical distributions (either double ERFC or double Gaussian for the double-diffused transistor). The physical constants of the distribution are determined from measurements of junction depths and sheet resistivities, or are approximately predicted from depletion capacitance measurements, when the boundary conditions used in the fabrication are known. Many such measurements and calculations based on these measurements have resulted in curves which may either be used for design purposes or for evaluation purposes when the above quantities are known. Section 2.6 presents a brief review of the techniques used in this approach and gives relevant curves where applicable.

When transistors are encountered in encapsulated form and detailed information on a particular transistor is required, the above approach is not practical. Assessment of the internal configuration must, necessarily, be based on terminal measurements. Interpretation of the terminal measurements requires the assumption of an equivalent circuit; hence, this assessment will be termed the Equivalent Circuit Approach. This approach may be sub-divided into two sections; (a) direct determination of the actual impurity profile from terminal measurements,

and (b) assumption of a simple, yet accurate, approximation to the actual distribution, derivation of the terminal characteristics and equivalent circuit elements in terms of this approximation and subsequent determination of the constants of the approximation from terminal measurements.

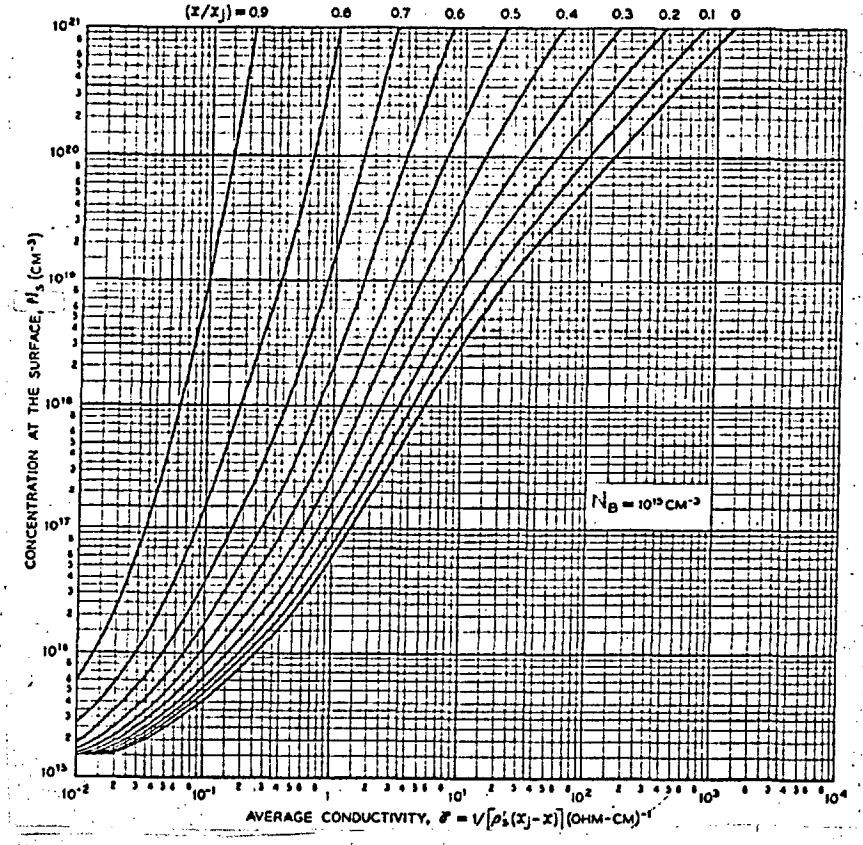
The complicated nature of the double-diffused structure generally precludes a direct determination of impurity profile from terminal measurements. Moreover, sufficient information is not available to determine accurately all the physical constants of classical distributions from terminal measurements. Under such circumstances an approximate model is justified, providing it adequately describes the physical structure of the transistor and accurately predicts electrical behaviour. Attempts to determine the impurity profile directly are discussed in Section 2.7.1, while two early models for the double-diffused structure are discussed in Sections 2.7.2 and 2.7.3.

2.6 The Classical Distribution Approach

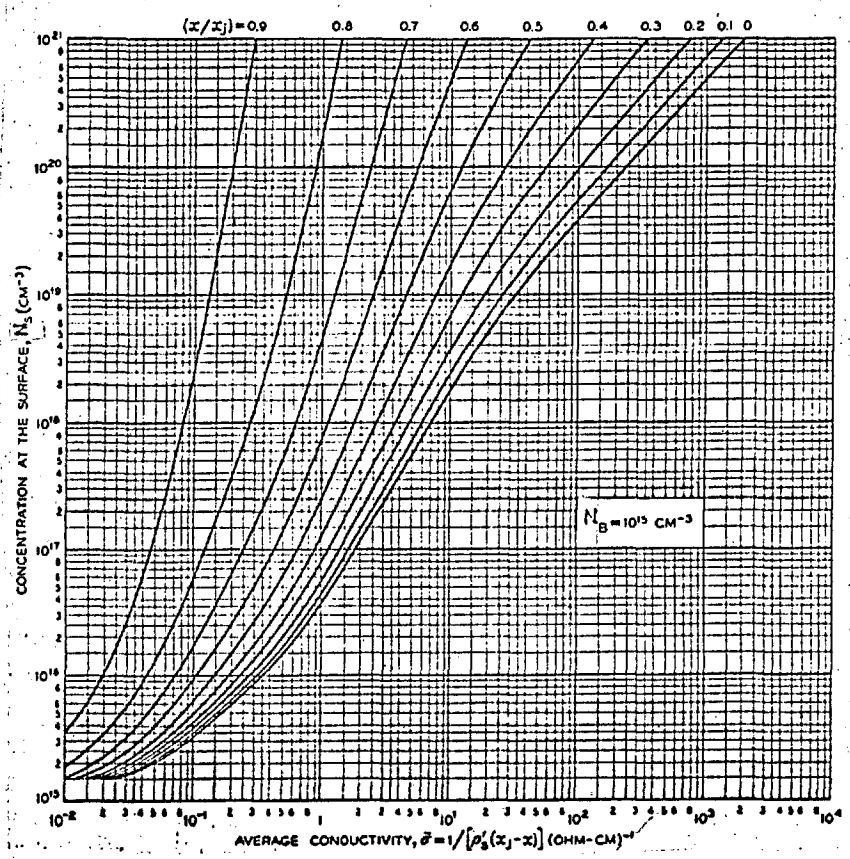
Utilization of the diffusion process to manufacture transistors was held up until the quantitative nature of the diffusion coefficient D (assumed constant) was known. Experiments by a number of investigators [9-11, 23-26], provided this information. Subtle differences in experimental techniques often led to slightly different values of D for the same element at a particular temperature. These differences were considered by Fuller[24] and Fig. 2.1 represents his assessment of the best values for a number of elements in silicon. Perhaps the most useful technique for determining D was the simultaneous diffusion of an impurity

into two wafers of different resistivities. The position of the junction was then measured, time of diffusion was known, initial resistivities were known, and D could then be determined assuming that classical distributions applied. The surface concentration N_s could also be determined. Bevelling and staining techniques allowed measurement of the junction positions, while the four-point probe technique[29] could be used to measure initial resistivities of the wafers.

Characterization of a diffused layer is possible with knowledge of four parameters; junction depth x_j, background concentration N_B, surface concentration N_s, and sheet resistivity ρ_s of the layer. Fig. 2.14 presents curves of N_s vs $1/\rho_s(x_j-x)$ with x/x_j as a parameter and a background doping N_B of 10^{15} atoms/cc. These are two of a series of curves presented by Irvin[31] for ERFC and Gaussian distributions in silicon. They represent a major correction of Backenstoss's curves[30] and their extension to enable them to be used to evaluate subsurface layers (e.g. the portion of a diffused layer remaining after the top strata has been removed to depth x) between a plane at x and the junction x_j. Utilization of these curves involves measurement of the junction position (bevelling and staining), and measurement of sheet resistance of the diffused layer. The measurement of sheet resistance involves an extension of the four-point probe technique[29,59] and relies on the fact that a slightly reverse-biased junction acts as a non-conducting bottom surface to the sheet (diffused layer). A technique for evaluating the approximate impurity density with position in the diffused layer, used originally to determine actual profiles, involves measurement of sheet resistance followed by lapping of a thin layer from the



(a)



(b)

Fig. 2.14. Average conductivity of p-type layers in silicon. (a) ERFC, (b) Gaussian. From Ref. 31.

surface followed by a further measurement of sheet resistance, etc. An alternative technique is the use of radioactive tracer elements, lapping, and count of the atoms removed to determine the impurity density distribution[32].

Applying the space-charge assumption, capacitance of a graded junction at low reverse bias is adequately represented by the linear approximation, while at high reverse bias the abrupt approximation is applicable. Between these extremes the detailed dependence on the actual distribution is important. Lawrence and Warner[33] considered this dependence in some detail, presenting curves of capacitance/unit area and depletion layer thickness versus junction voltage normalized to background doping for ERFC and Gaussian distributions. Junction depth is taken as the parameter. Several sets of curves are necessary to describe the complete range of surface concentrations likely to be encountered in diffused layers. The similar nature of ERFC and Gaussian distributions when they have fallen several decades below their initial values makes it unnecessary to present curves for both distributions. Fig. 2.15 presents a set of curves for $N_B/N_S = 10^{-3}$. Included in Fig. 2.15 is a set of curves indicating the proportion of the total depletion layer on the side of the junction nearest the surface. These curves are useful either for obtaining information on the depletion layer capacitance when the distribution is known, or for obtaining information on the distribution when transition capacitance is known. Although directly applicable to single diffused layers, these curves may be used to provide information on the base diffusion in double-diffused transistors since the emitter diffusion often has negligible influence

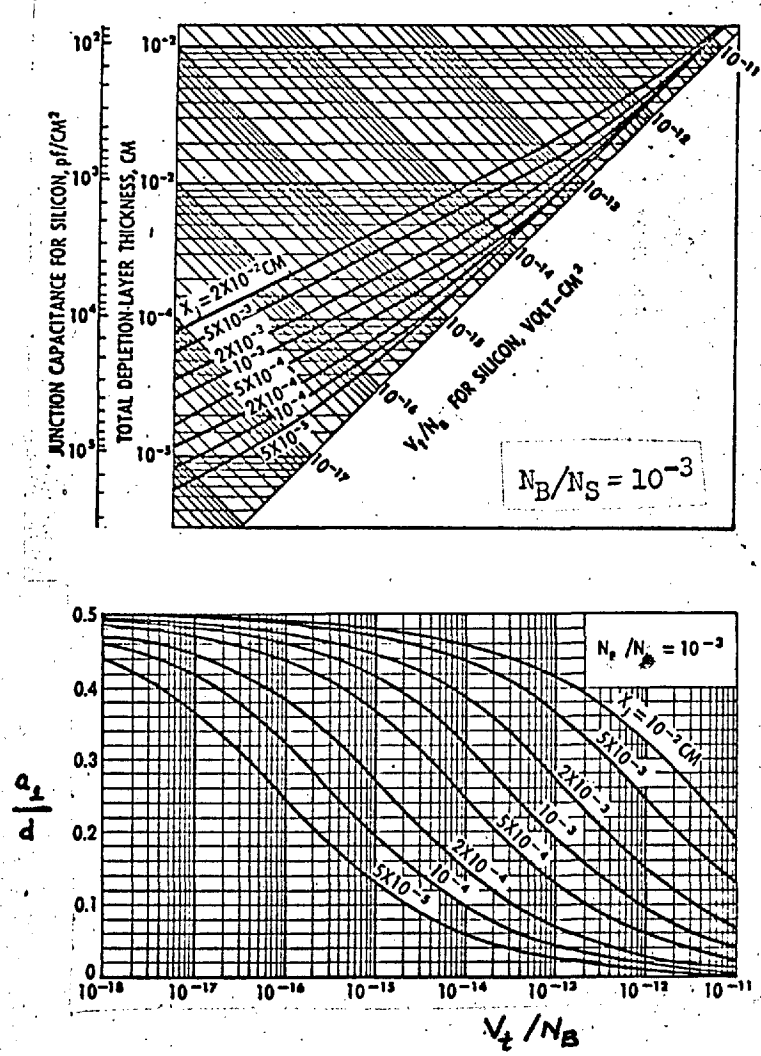


Fig. 2.15. (a) Junction capacitance per unit area and total depletion layer thickness vs junction voltage divided by background doping. Junction depth is a parameter.
(b) Fraction of depletion layer on surface side of the junction vs junction voltage divided by background doping.
Curves are applicable to either ERFC or Gaussian junctions for $3x10^{-4} \leq N_B/N_S \leq 3x10^{-3}$. After Lawrence and Warner[33]; reproduced from Ref. 78.

at the collector junction (providing that the diffusion may be represented as an ERFC or a Gaussian).

The double-diffused transistor has been treated as having for its impurity distribution the difference of two ERFCs or two Gaussians (eqns. 2.3.1 and 2.3.2). The normal techniques of sheet resistivity measurement and lapping (or radioactive tracing and lapping) have been used to verify that actual distributions approach these classical distributions. The accuracy of these techniques is limited by the minimum thickness of layer that can be removed by lapping, so determination of impurity distributions in narrow emitter and base transistors can be quite inaccurate by such techniques.

No general graphical solution for physical and electrical properties of double-diffused transistors is practical since the number of independent variables is so large. Much reliance must, therefore, be placed on the assumption of classical distributions or approximation by such distributions and on the information available for single diffused layers. As mentioned above, Lawrence and Warner's curves[33] can be used to interpret capacitance data for the collector junction. Over a limited range of voltage these curves are also applicable to the emitter junction. Although presentation of a general graphical solution is impractical, two sets of design curves as proposed by Tanenbaum & Thomas[21] would appear to be useful. These are curves of the ratio of surface concentrations (N_{S1}/N_{S2}) vs reduced emitter layer thickness ($x_e/\sqrt{4D_1 t_1}$) with ratio of diffusion lengths ($\sqrt{4D_1 t_1}/\sqrt{4D_2 t_2}$) as a parameter for given N_{S2}/N_B, and curves of N_{S2}/N_B vs reduced collector junction depth ($x_c/\sqrt{4D_1 t_1}$) with ratio of diffusion lengths as a parameter.

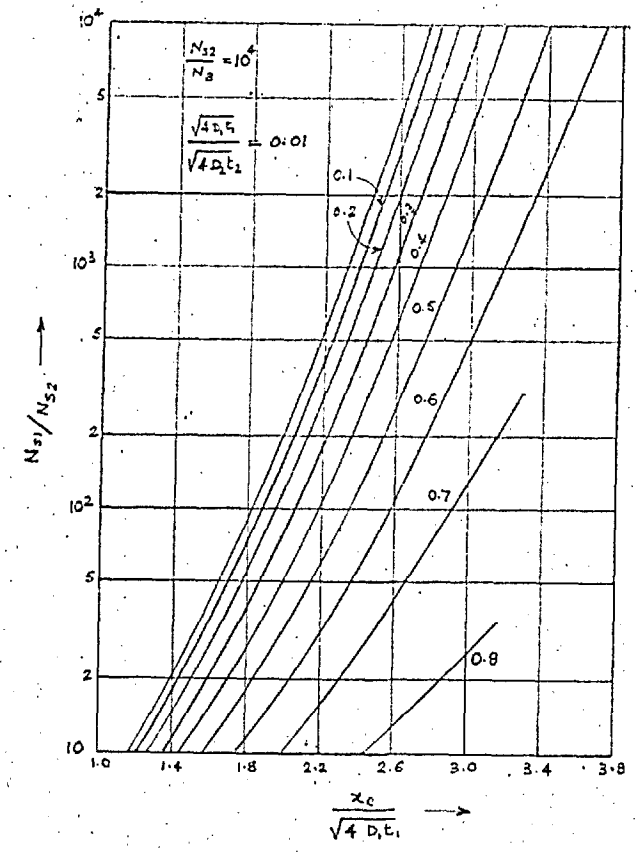
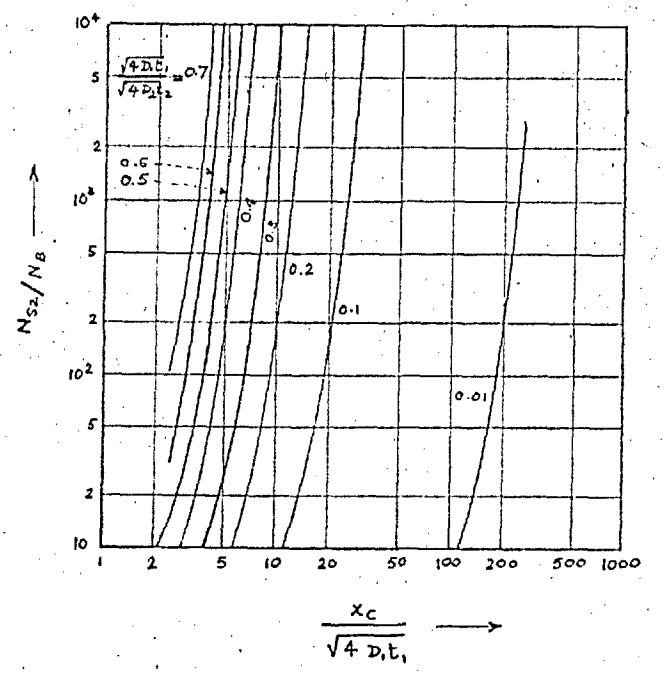


Fig. 2.16. Taken from Ref. 21.

(a)

Emitter Junction depth as a function of ratio of surface concentrations. Ratio of diffusion length is a parameter.



(b)

Collector Junction depth as a function of base diffusion.

All terms are as defined in Section 2.3. Fig. 2.16 indicates the nature of these curves for the double ERFC distribution with $N_{S2}/N_B = 10^4$. A possible alternative set of curves defining the base region for specific design parameters is a plot of N_{S1}/N_{S2} vs physical base width W_b with ratio of diffusion lengths as a parameter[60]. Such a set of curves is not general enough to justify inclusion here. Much work has been done on the design of double-diffused transistors, but this has generally been semi-empirical in nature and has been limited to the presentation of design techniques, and the study of particular examples. Although design techniques have been well developed and measurement of junction position can verify the success of the design, the study of individual transistors involving classical distributions necessarily implies numerical techniques and the destruction of the actual device. The deviation of actual distributions from the classical often makes such rigorous treatment unjustified.

2.7 Equivalent Circuit Approach

2.7.1 Direct Derivation of Actual Distributions from Terminal Measurement

Most circuit elements have either second order dependence or such an involved dependence on impurity distributions that they cannot be used directly to determine impurity distribution. Moreover, terminal measurements generally involve several elements, so unless these elements can be separated by a simple operation, the inaccuracies in the individual elements may be so great that they can not be used with any confidence to determine impurity distribution. Only the variation

of transition capacitance with reverse bias offers any possibility of success in such an evaluation.

Giacoletto[34] suggested a method for utilizing capacitance data to determine impurity distribution on one side of a highly asymetrical junction. The impurity profile of a double-diffused transistor is such that over much of the emitter, impurity density is much greater than in the base. If, near the junction itself the impurity gradient were much steeper than that on the base side of the junction, most of the depletion layer would appear on the base side of the junction. Emitter capacitance would then be governed largely by impurity profile in the base region, and capacitance data could be used to yield information on impurity distribution in the base. The collector junction is much less abrupt, so capacitance data depends in a complicated way on impurity profile on both sides of the junction. It is not possible, therefore, to locate the position of the depletion layer edge unless the distribution is already known.

For an asymetrical emitter junction (Fig. 2.17) the following expression is essentially that used by Giacoletto:

$$N_A - N_D\Big|_x = \frac{\varepsilon}{q} \cdot \frac{dv_{eb}/d(a_{2e})}{x}\Bigg|_{a_{2e} = x} \qquad 2.7.1$$

where a_{2e} is the width of depletion region in the base ($\approx$ total depletion region width). Substituting $C_{te} = \varepsilon A_e/a_{2e}$ in eqn. 2.7.1 yields:

$$N_A - N_D\Big|_{x = a_{2e}} = \frac{1}{q\varepsilon A_e^2} C_{te} \cdot \frac{dv_{eb}}{d(\frac{1}{C_{te}})}\Bigg|_{x = a_{2e}} \qquad 2.7.2$$

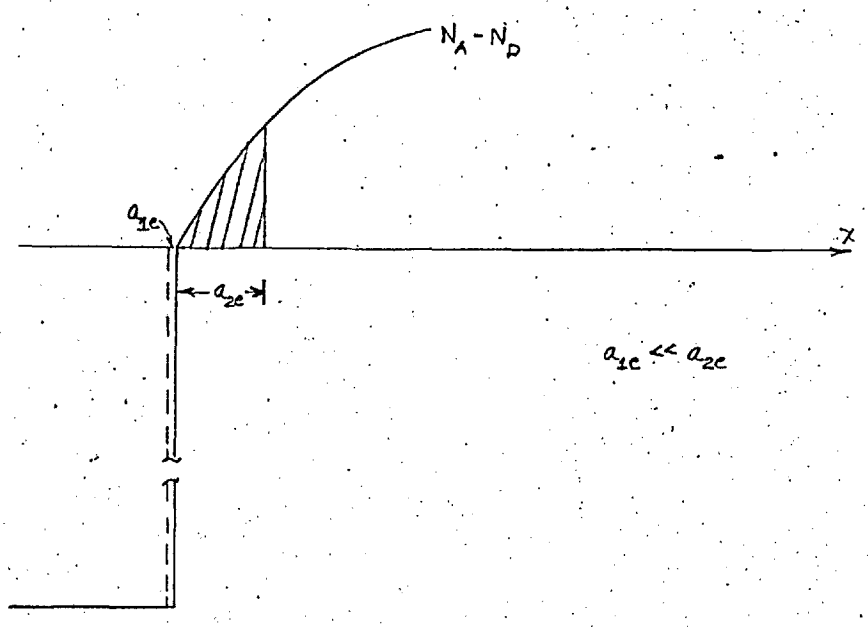


FIG. 2.17. ASYMETRICAL EMITTER JUNCTION

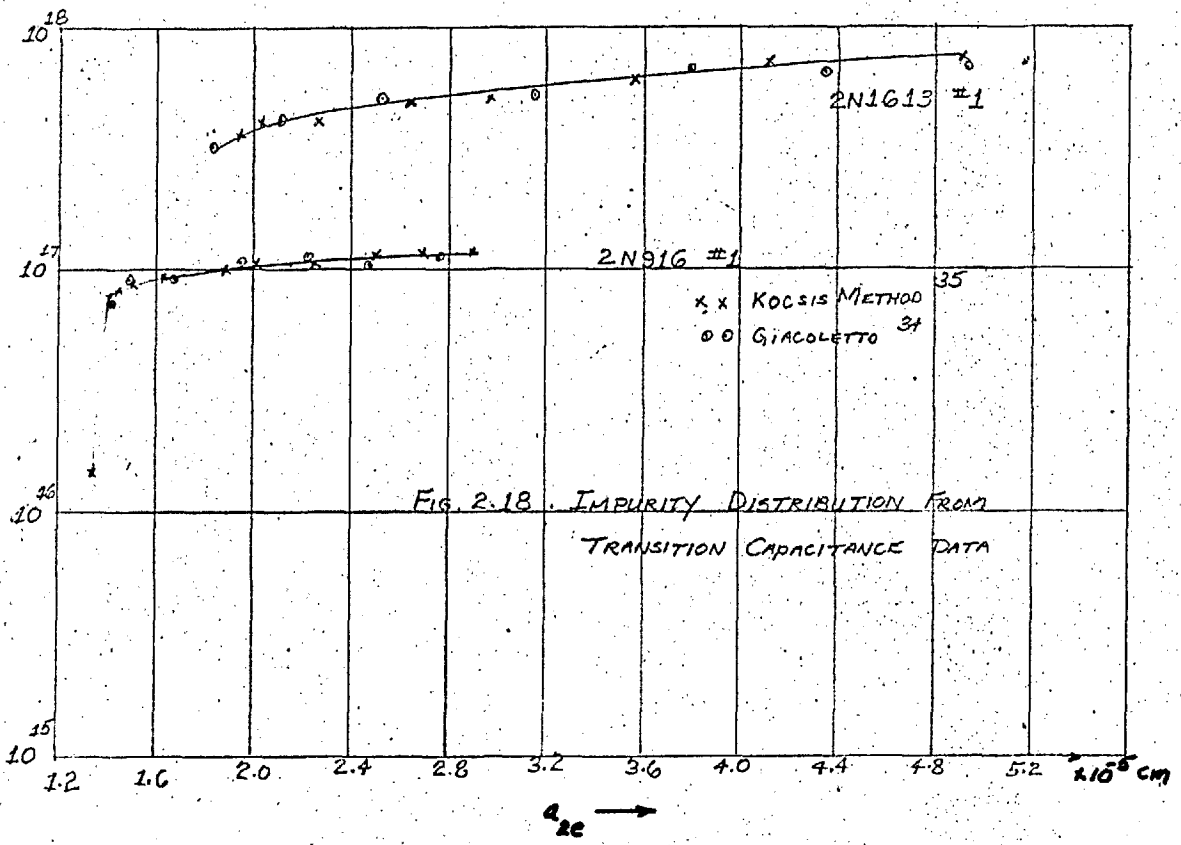


FIG. 2.18. IMPURITY DISTRIBUTION FROM TRANSITION CAPACITANCE DATA

Eqn. 2.7.2 allows determination of impurity density at $x = a_{2e}$ when A_e and the slope of the V_{eb} vs $1/c_{te}$ curve is known for a particular voltage. The inaccuracies involved in determining the slope of the inverse capacitance curve at any point from a tangent drawn at that point make the incremental method suggested by Kocsis[35] more attractive. If transition capacitance is measured by two voltages in close proximity, the assumption of a linear increment of capacitance between the two values of voltage allows determination of the impurity density at the mid-point from:

$$N_A - N_D \Big|_{a_{2e}} = \frac{V_1 - V_2}{2q\varepsilon A_e^2} \cdot \frac{C_1 C_2 (C_1 + C_2)}{C_2 - C_1} \qquad 2.7.3$$

where C_1 and C_2 are the transition capacitances at voltages V_1 and V_2 respectively. Position in the base is given by:

$$a_{2e} = \frac{x_1 + x_2}{2} = \frac{2\varepsilon A_e}{C_1 + C_2} \qquad 2.7.4$$

x_1 and x_2 are the positions of the depletion layer edge at the respective voltages. Fig. 2.18 presents curves of impurity distribution for two transistors determined by the above techniques. Transition capacitances were measured by the technique outlined in Chapter 4 (Section 4.2.3) and emitter area by optical means (Section 4.2.4).

The procedures outlined above are both tedious and inaccurate. A measurement technique presented recently by Gray and Adler[61] gives an immediate straight line plot of incremental charge q_j vs elastance ($1/C_{te}$) if the asymetrical assumption holds. The slope of this line yields $N_A - N_D$:

$$N_A - N_D \Big|_{x = a_{2e}} = \frac{1}{q\varepsilon A_e^2} \cdot \frac{dq_j}{dS_j} \qquad 2.7.5$$

where q_j is the space charge on one side of the dipole layer and S_j is the elastance. This equation is identical with eqn. 2.7.2 when the values of q_j and S_j are inserted.

The approximate nature of the highly asymetrical assumption limits the usefulness of capacitance data to an estimate of impurity density near the junction. Moreover, breakdown of the emitter junction by avalanche processes invariably occurs before the peak in base doping is reached by the edge of the depletion region. Thus only a portion of the retarding field region is represented in Fig. 2.18, insufficient for determining a mathematical distribution for the base region.

Gummel's[62] suggestion that measurement of collector current as a function of emitter-to-base voltage to yield total number of impurities in the base region is complicated by the presence of an average diffusion coefficient which is unknown. Further, base width is unknown, so this measurement is of little use in determining base distribution directly. An estimate of collector body doping (N_B) is possible from a measurement of breakdown voltage and utilization of data presented by Miller[63]. In planar transistors this estimate is likely to be too large, since breakdown normally occurs first at the periphery of the junction[64].

From these considerations it is evident that a direct determination of impurity distribution for double-diffused transistors is not practical.*

---

* Lawrence' and Warner's curves (Fig. 2.15) can yield information on the collector junction, if classical distributions apply. (See Section 2.6)

2.7.2 Single Exponential Model for Base Region

Early in the history of double-diffused transistors it was felt that the tendency would be to fabricate devices with narrow retarding field regions in the base, to allow minimum base transit time for a given base width. The present high degree of process control, making the reduction of base width the more important consideration in minimization of transit time time, was not foreseen. Thus early models for the base region either neglected the retarding field region or assumed it was extremely narrow.

The first practical model completely neglected the retarding field region and assumed a single exponential distribution throughout the base[36], in fact, an extension of the theory of drift and alloy-diffused transistors. The impurity distribution, represented in Fig. 2.19, is stated mathematically by:

$$N(x) = N_o e^{-x/L} - N_B \qquad 2.7.6$$

where N_o is the impurity density at the edge of the emitter depletion region ($x = 0$), L is the characteristic length of the exponential (distance in which it falls to 1/e of its initial value) and N_B is the background doping (in collector body). Determination of the physical constants of base width, areas, and of the distribution of Fig. 2.19 is possible by interpretation of the following measurements:

1. Base transit time τ_b and $\Delta\tau_b = \tau_{b_1} - \tau_{b_2}$, where the subscripts refer to measurements at two collector voltages, V_1 and V_2,

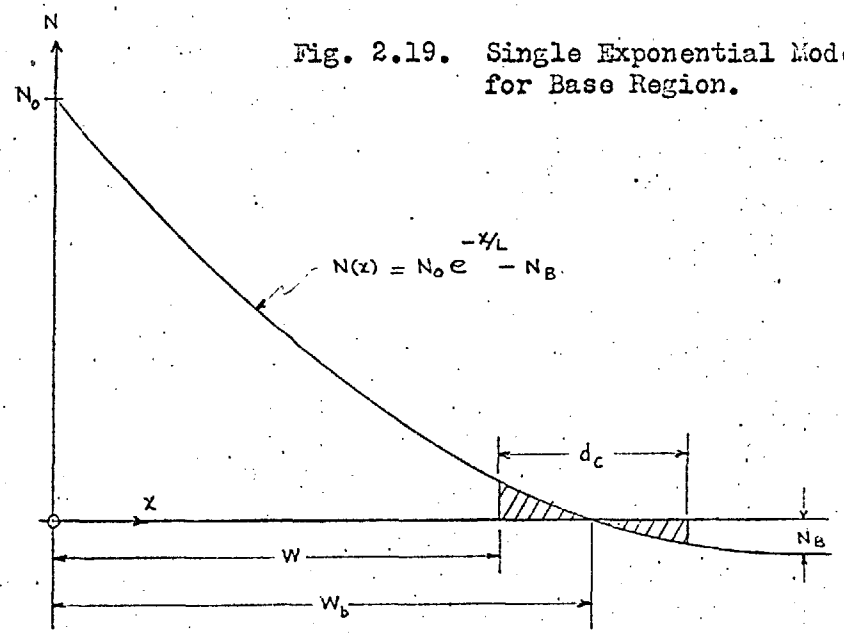


Fig. 2.19. Single Exponential Model for Base Region.

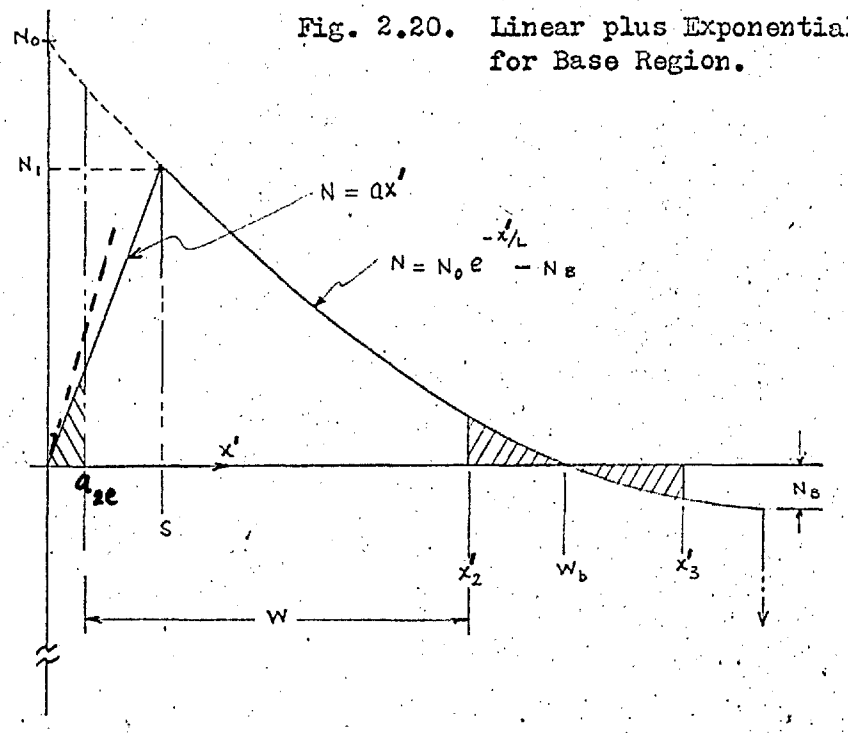


Fig. 2.20. Linear plus Exponential Model for Base Region.

2. Collector Capacitance ratio C_{c1}/C_{c2} for the two voltages,

3. Emitter transition capacitance C_{te},

4. Collector current I_c vs emitter-base voltage V_{eb} characteristics,

5. Extrinsic base resistance r'_{bb} and $r'_{bb}\,C_{tc1}$.

In this work, a constant diffusion coefficient D equal to the low impurity value was assumed to apply (≈ 28.5 cm^2/volt-sec for electrons in p-type silicon). The equations used to determine the physical constants are presented below in the order of their employment.

$$L = \sqrt{\frac{D\left(\frac{\Delta\tau}{b}\right)}{\ln(C_{c1}/F\,C_{c2})}} \qquad 2.7.7$$

where $$F = \frac{1 - e^{-d_2/L}}{1 - e^{-d_1/L}} \qquad 2.7.8$$

d_1 and d_2 are collector depletion layer widths at voltages V_1 and V_2 respectively.

$$m_1 = W_1/L \approx \frac{\tau_{-b_1}\eta}{L^2} + 1 \qquad 2.7.9$$

$$A_e/N_o = \frac{dI_c}{d\,e^{qV_{eb}/kT}} \cdot \frac{L}{qn_i^2 D} \qquad 2.7.10$$

where $dI_c/d\,e^{qV_{eb}/kT}$ is the slope of the diode characteristic, n_i is the intrinsic density of carriers, and W_1 is the effective base width at voltage V_1. Also

$$N_o A_e^2 = \frac{2}{q\varepsilon} \cdot \frac{d(1/C_{te}^2)}{dV_{eb}} \qquad 2.7.11$$

and

$$N_B = N_o \cdot \frac{L}{d_1}\,(1 - e^{-d_1/L})\,e^{-m_1} \qquad 2.7.12$$

To determine the physical constants of the model at bias voltage V_1, the following iterative procedure may be used. Assume F = 1 and calculate L from eqn. 2.7.7. Then determine m from eqn. 2.7.9 and separate A_e and N_o from eqns. 2.7.10 and 2.7.11. Collector area may be determined by using eqn. 2.4.33 at voltage V_1 (C_{tc1} results from measurement of r'_{bb} and $r'_{bb}C_{tc1}$). d_1 and d_2 are determined from the simple capacitance expression $C_t = \varepsilon A/d$ where C_{c1} and C_{c2} are substituted for C_t and A_c for A. F is then calculated from eqn. 2.7.8 and this value used in 2.7.7 to get an improved value of L. The other steps are repeated with this new L. Iteration is continued until a further step leads to no change in L.

The measured data is obtained by standard techniques (outlined in Chapter 4) and is presented in Table 2.1 for four transistors. Physical constants derived from this data are presented in Table 2.2. It will be shown in section 2.7.3 and in Chapter 5 that the assumption of negligible retarding field region for these transistors is substantially in error.

2.7.3 Linear Plus Exponential Model for Base Region

2.7.3.1 Equations for the Model

The model of Fig. 2.20[37,38] was proposed to describe the effects of a possible narrow retarding field region in the base. The retention of the exponential for the aiding field region; viz,

$$N(x') = N_o e^{-x'/L} - N_B \Big|_{x' \geq s} \qquad 2.7.13a$$

represents an attempt to use the equations for the single exponential

model (Section 2.7.2). The choice of the linear approximation for the retarding field region: viz,

$$N(x') = ax' \Big|_{0 \leq x' \leq s} \qquad 2.7.13b$$

represents an attempt to utilize the property of most graded junctions that a cubic law governs the behaviour of transition capacitance with voltage for low reverse bias. It was felt that for narrow retarding field regions the edge of the emitter depletion region would approach s, thus obviating the need for a very accurate representation.

Since Chapters 4 and 5 draw on the theory of the single exponential approximation at the collector junction, the approximation is treated in detail here. Poisson's equation is solved over the collector depletion layer employing the assumptions of complete depletion in the space charge region, base charge neutrality, and total charge neutrality in the depletion layer, i.e.

$$\int_{x'_2}^{x'_3} N(x') \, dx' = 0$$

The last assumption provides a relation between depletion layer semi-width $(W_b - x'_2)$ and total depletion layer width, d_c:

$$e^{-a_{1c}/L} = e^{-(W_b - x'_2)/L} = \frac{L}{d_c}(1 - e^{-d_c/L}) \qquad 2.7.14$$

where W_b is the physical base width and x'_2 is edge of the collector depletion layer in base region. The use of this relationship with the boundary condition for the electric field at $x' = x'_2$; viz, $E(x'_2) = kT/qL$, gives the familiar voltage relationship:

$$V + V_B = \frac{q}{\varepsilon} N_B L^2 \left[\tfrac{1}{2}(d_c/L)\coth(\tfrac{1}{2}d_c/L) - d_c/L \right] \qquad 2.7.15$$

where $V = -V_c$ and

$$V_B = V_o + \frac{kT}{q} \cdot \frac{d_c}{L} \approx V_o \approx \frac{kT}{q} \ln \left| \frac{N(x_2').N(x_3')}{n_i^2} \right|$$

x_3' is the edge of the depletion layer in the collector. V_o is defined as the equilibrium potential barrier across the junction.

Three alternatives are possible for the interpretation of capacitance data in the light of eqn. 2.7.15.

I. <u>A Two Capacitance Approach</u>. Since kT/qL is normally small with respect to V_o, V_B can be considered constant with collector voltage. If C_1 and C_2 are transition capacitances corresponding to $V_c = -V_1$, $-V_2$ respectively, eqn. 2.7.15 together with $C_{tc} \propto 1/d_c$ yields:

$$\frac{V_2 + V_B}{V_1 + V_B} = \frac{C_1}{C_2} \cdot \frac{\left[1 - \tfrac{1}{2}\left(\frac{C_1}{C_2} \cdot \frac{d_{c_1}}{L}\right) \coth \tfrac{1}{2}\left(\frac{C_1}{C_2} \cdot \frac{d_{c_1}}{L}\right) \right]}{\left[1 - \tfrac{1}{2}(d_{c_1}/L) \coth \tfrac{1}{2}(d_{c_1}/L) \right]} \qquad 2.7.16$$

Eqn. 2.7.16 can be used to determine d_{c_1}/L when the capacitance and voltage ratios are known. A plot of the eqn. 2.7.16[37] indicates that it becomes extremely critical for low capacitance ratios, so a less critical approach is desirable.

II. <u>General Treatment Using $1/C_{tc}^2$ vs V_c Data</u>. For any collector reverse bias voltage $V_c = -V$, differentiation of eqn. 2.7.15 with respect to d_c and substituting $C_{tc} = \varepsilon A_c/d_c$ gives the following expression for the slope γ_1 of $1/C_{tc}^2$ vs V:

$$\gamma_1 = \frac{d(1/C_{tc}^2)}{dV} = \frac{2}{A_c^2 q \varepsilon N_B} \cdot \frac{d_c/L}{\left[\frac{f(d_c/L)}{d_c/L}\right]^2 - \tfrac{1}{4}(d_c/L)^2} \qquad 2.7.17$$

where $f(d_c/L) = [1 - \frac{d_c}{2L} \coth(d_c/2L)] \cdot \frac{d_c}{L}$ 2.7.18

Multiplication of eqn. 2.7.17 by eqn. 2.7.15, and eliminating A_c^2 gives:

$$\frac{\gamma_1 C_{tc}^2 (V + V_B)}{2} = \Gamma\left(\frac{d_c}{L}\right) \qquad 2.7.19$$

where $\Gamma(d_c/L) = \dfrac{f(d_c/L)}{\left(\frac{d_c}{L}\right)^3 \left[\left\{\frac{f(d_c/L)}{(d_c/L)}\right\}^2 - \frac{1}{4}\right]}$ 2.7.20

Combining eqns. 2.7.17 and 2.7.20 yields:

$$A_c^2 N_B = \frac{2}{q \varepsilon \gamma_1} \cdot \xi_1(d_c/L) \qquad 2.7.21$$

where $\xi_1(d_c/L) = \Gamma(d_c/L) \cdot (d_c/L)^2 / f(d_c/L)$ 2.7.22

The functions $\Gamma(d_c/L)$ and $\xi_1(d_c/L)$ are plotted in Fig. 2.21. To use these curves, determine $\Gamma(d_c/L)$ from eqn. 2.7.19, read off d_c/L and $\xi_1(d_c/L)$ from Fig. 2.21 and calculate $A_c^2 N_B$ from eqn. 2.7.21. For sufficiently high voltages ($d_c/L \geq 10$), $\xi_1(d_c/L)$ approaches unity and the step approximation may be used.

III. General Treatment Using $1/C_{tc}^3$ vs V_c Data. Relationships similar to eqns. 2.7.17 to 2.7.22 apply when capacitance data is given in the form of $1/C_{tc}^3$ vs V_c plot. Thus,

$$\gamma_2 = \frac{d(1/C_{tc}^3)}{dV} \qquad 2.7.23$$

$$\frac{\gamma_2 C_{tc}^3 (V + V_B)}{3} = \Gamma(d_c/L) \qquad 2.7.24$$

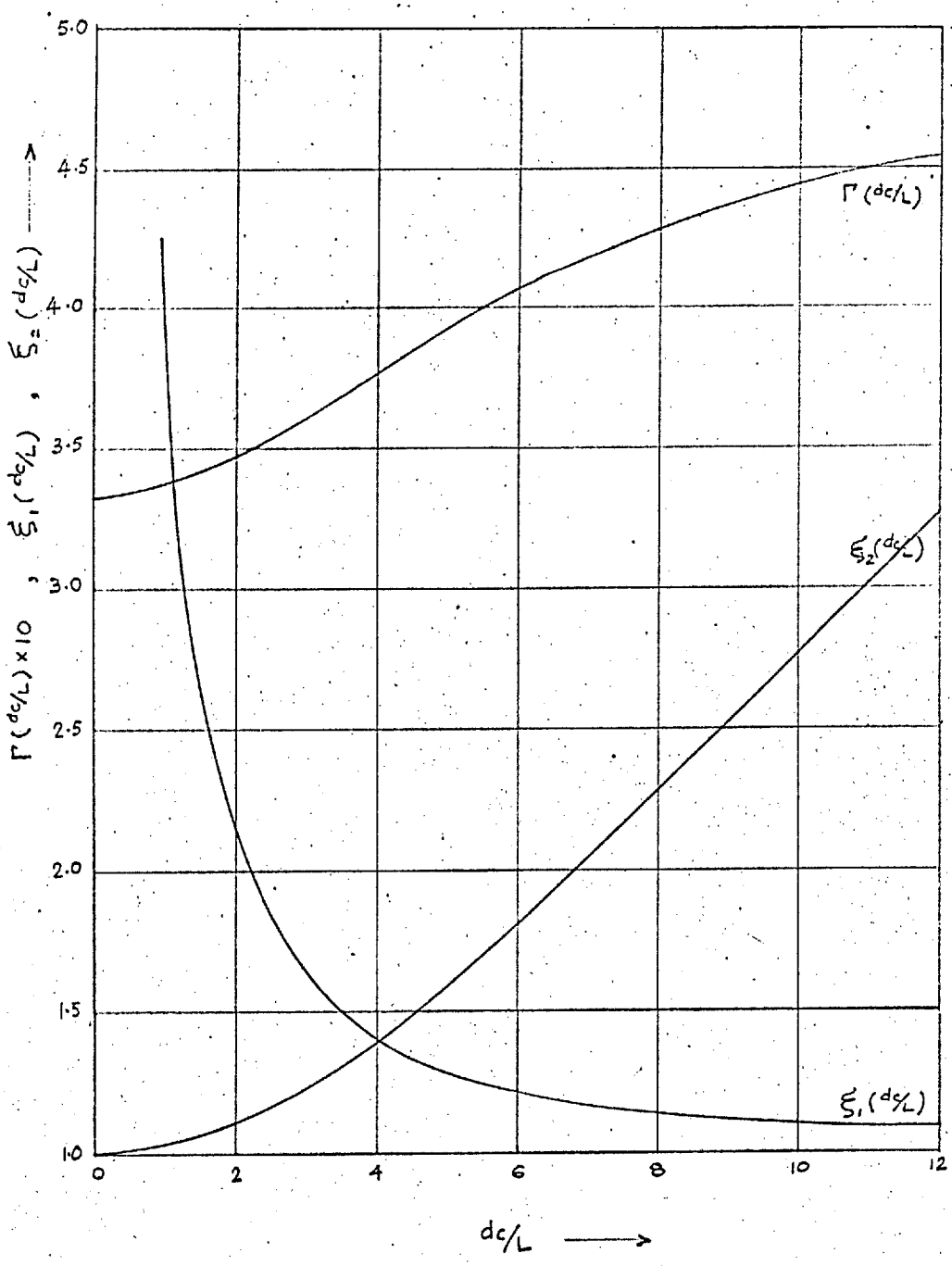


Fig. 2.21. Collector Depletion Region Functions.

$$\text{and} \quad \frac{A_c^3 N_B}{L} = \frac{12}{q \varepsilon^2 \gamma_2} \cdot \xi_2(d_c/L) \qquad 2.7.25$$

$$\text{where} \quad \xi_2(d_c/L) = \Gamma(d_c/L) \cdot (d_c/L)^3 / 4f(d_c/L) \qquad 2.7.26$$

The relationship of eqn. 2.7.26 is plotted in Fig. 2.21, and may be used in a similar manner to $\xi_1(d_c/L)$. For low voltages ($d_c/L \leq 1$), $\xi_2(d_c/L) \approx 1$ and the linear approximation to the junction may be used with little error. In general, for low voltage it is preferable to use $1/C_{tc}^3$ data and determine $A_c^3 N_B/L$ for use in further calculations.

The preferred method of utilizing collector capacitance data is to determine $A_c^3 N_B/L$ from low voltage measurements where the curve of $1/C_{tc}^3$ vs V_c approximates a straight line. This value of $A_c^3 N_B/L$ may then be used in all further calculations regardless of whether or not these other calculations use information obtained at the same bias level. In addition to ease of determining γ_2 at low bias, two other factors support the preference for using low voltage data to determine $A_c^3 N_B/L$. (1) The single exponential approximation is more accurate the nearer the edge of the collector depletion layer is to the actual junction. (2) Collector capacitance is larger for low bias and less subject to errors of measurement - important when the low values of capacitance encountered in double-diffused transistors are considered.

Collector capacitance data may be used with emitter capacitance measurements, transit time, increment of transit time with collector voltage, emitter diode equation, and r'_{bb} and $r'_{bb}C_{tc}$ data in an iterative approach for the determination of the physical constants of the model. The additional equations and the iterative techniques are outlined in Appendix A.1.

Table 2.1 - Measured data for "Single Exponential Model"

Device Number		C_{c1} PF	C_{c2} PF	$\tau_b + \tau_c$ nsec	$A_e^2 N_o$ x 10^{10} cm	$\frac{A_e}{N_o L}$ x 10^{-17} cm^4	$\frac{A_e}{A_c}$	$\Delta\tau_b$ nsec
2N696	1*	13.6	9.0	1.64	8.64	8.70	.312	0.18
2N1613	1*	14.9	9.7	1.42	7.42	8.53	.18	0.14
2N1613	3	18.2	12.1	1.17	8.86	7.66	.24	0.095
2N1711	2	16.3	10.8	0.96	5.40	11.4	.254	0.11

V_1 = 10 volts, V_2 = 30 volts. * Devices analysed by Trofimenkoff[37,38]

Table 2.2 - Calculated Parameters of "Single Exponential Model"

Device Number		A_e x 10^{-4} cm^2	A_c x 10^{-4} cm^2	N_o x 10^{17} cm^{-3}	N_B x 10^{15} cm^{-3}	L microns	m_2	W_2 microns	τ_b nsec
2N696	1	9.15	28.8	1.03	0.14	1.02	5.3	5.4	1.62
2N1613	1	8.41	46.7	1.05	0.11	0.94	5.5	5.2	1.39
2N1613	3	8.01	33.1	1.38	0.042	0.76	6.8	5.1	1.16
2N1711	2	7.96	31.3	0.85	0.19	0.81	5.0	4.1	0.94

N_B is an order of magnitude low (see Table 4.4), largely due to use of D^B= 28.5, which bears no relation to actual doping in base of model. $\Delta\tau_b$ can also be inaccurate (Sections 4.4.3 and 5.2.4). Use of lower D as in Ref. 38 recommended.

Table 2.3 - Additional measured data for "Linear-exponential model"

Device Number		$A_c^3 N_B/L$ x 10^{12} cm^2	$A_e^3 a$ x 10^{12} cm^5	$\frac{d_1}{L}$	$\frac{d_2}{L}$	Δm	$\frac{I_c}{qn_i^2 e^{qV_e/kT}}$ x 10^{-15} cm^6/sec
2N696	1	2.17	2.97	3.8	5.7	.43	2.48
2N1613	1	2.79	2.54	4.6	7.0	.44	2.43
2N1613	3	4.85	3.18	3.8	5.8	.39	2.18
2N1711	2	3.42	1.72	3.6	5.4	.44	3.26

Table 2.4 - Calculated Parameters of "Linear-exponential model"

Device Number		D $\frac{cm^2}{volt\text{-}sec}$	N x 10^{16} cm^{-3}	N_B x 10^{15} cm	A_e x 10^{-4} cm^2	A_c x 10^{-4} cm^2	m_2	L microns	$\frac{s}{L}$	$\frac{a_{2c}}{L}$	W_2 microns	Calc. τ_b nsec
2N696	1	14.6	8.8	2.3	13.8	44.3	2.29	.93	.84	.116	2.8	3.43
2N1613	1	15.9	7.3	1.7	9.4	52.4	2.26	.85	.28	.087	2.1	1.72
2N1613	3	14.0	9.7	5.4	9.1	37.7	1.53	.60	.39	.105	1.1	1.01
2N1711	2	16.2	6.6	4.9	9.2	36.1	1.30	.67	.45	.119	1.1	1.11

2.7.3.2 Results and Criticisms

The last of the three alternatives suggested in Section 2.7.3.1, to evaluate collector capacitance data, was adopted. Table 2.3 presents measured data for several transistors, while Table 2.4 lists the derived constants for these transistors. Two of the actual transistors studies by Trofimenkoff[37] are included. Measurements on these transistors were repeated, with improved accuracy in certain cases, and the physical constants re-calculated.

In addition to considerations which limit the applicability of the assumed model, certain discrepancies appeared in the results presented by Trofimenkoff. Most notable was the lack of agreement between emitter transition capacitance calculated from the resultant values of A_e and a_{ae} and the measured C_{te}. This is inexplicable since a_{ae} purports to be determined from measured C_{te}. Another discrepancy was the unintentional inclusion of stray capacitances, C_{sec} and C_{scb}, in the values of C_{tc1} and C_{tc2} used in the calculations. These discrepancies are eliminated in the transitors of Tables 2.3 and 2.4.

As initally proposed, the model of Fig. 2.20 assumed a very narrow retarding field region in the base, an emitter sufficiently abrupt that, even for forward bias on the junction, most of the depletion layer would appear in the base region, and that the exponential was a good approximation over most of the aiding field region. The linear region was tacitly assumed to have the same slope as the actual distribution at the emitter junction. The evaluation of physical

constants was based on collector capacitance data which determined the slope of the linear region and the position of the edge of the emitter depletion layer in the base. The assumption of narrow retarding field region meant that maximum doping in the base (where the straight line and exponential intersect) would not be excessively greater in the model than in the actual distribution.

From Table 2.4 it can be seen that the retarding field region occupies an appreciable portion of the base for the transistors considered. This violates the initial assumption of narrow retarding field region and should lead to a much higher value of maximum doping in the model than in the actual device. However, an unforeseen effect tends to reduce this error. Studies of classical distributions in Chapter 3, and of the emitter junction of practical devices in Chapter 4 indicates that for small reverse bias the emitter junction is better approximated by a symmetrical-linear model than by an abrupt-linear model. For the symmetrical-linear junction, the interpretation of emitter capacitance data for low voltage is as follows:

$$A_e^3 a = \frac{12}{q\,\varepsilon^2} \frac{dV_{eb}}{d\left(\frac{1}{C_{tc}^3}\right)} = A_e^3 \frac{N_1}{L} \qquad 2.7.27$$

where a is the slope of the impurity distribution at $x' = 0$. All other terms are as previously defined.

Comparison of eqn. 2.7.27 with eqn. A.1.5 of Appendix A•1 indicates a factor of 4 difference between $A_e^3 \frac{N_1}{L}$ from the two equations. Thus the slope of the linear region determined from the abrupt-linear

approximation is less than the actual slope at the junction. This is represented in Fig. 2.20 by the dashed line. Since L is fixed the value of N_1 must be reduced to account for the reduction in the slope, and is, therefore, moved down towards the actual peak in doping. Although the region near the emitter junction is less accurately represented, and the position of maximum doping may be moved too far to the right in Fig. 2.20, the total number of impurities in the base for the model and for the actual distribution may be approximately equal. Thus under conditions which do not depart seriously from the initial assumptions the model can give quite accurate results.

Other sources of error in the derived model stem from:

(1) using total emitter depletion layer width in the base;

(2) utilizing the emitter diode equation in the form of eqn. A.1.3 which assumes that the edge of the emitter depletion reaches the position of maximum doping in the base. (This relied on the very narrow retarding field region assumption which has been shown to be inaccurate for the transistors evaluated);

(3) reliance on incremental transit time $\Delta\tau_b$ which reflects changes in the collector voltage in the aiding field region only, and in the presence of an appreciable retarding field region is relatively insensitive to voltage changes:

(4) determination of the ratio A_e/A_c from C_{tc_1}/C_{tc} where C_{tc_1} was determined from measurements of r'_{bb} and

$r'_{bb}C_{tc}$. As pointed out in Section 2.4.5, while r'_{bb} is a useful concept for prediction of transistor performance in situ, it must be used with care when working back from measured data to determine physical constants of the device. The measurement procedures are such as to yield only approximate values of r'_{bb} (See Chapter 4).

The above considerations show that, while the linear plus exponential model has limited applicability (i.e. devices with narrow retarding field regions) a more accurate model applicable generally to double-diffused devices is necessary. Such a model is proposed in Chapter 3 and applied to practical devices in Chapters 4 and 5.

2.7.4 Intrinsic Input Admittance Y_{ee}

Measurement of most of the circuit elements in the equivalent circuit of Fig. 2.12 may be carried out by well-known techniques (Chapter 4). It was pointed out in Section 2.7.1 that such measurements could not be interpreted directly to yield the complete impurity distribution. One particular parameter Y_{ee} has not been fully discussed; yet this is particularly dependent on impurity distribution, and if it could be determined, then valuable deductions could be made about impurity profile from it - particularly about the retarding field region. Unfortunately, it is inaccessible to direct measurement, being masked by other elements, such as C_{te}; the actual terminals of Y_{ee} can not be reached for measurement.

Because of its strong dependence on base profile an attempt was

made early in the project to determine Y_{ee} directly, with an aim to use it as a source of information on the physical constants of the assumed distribution or as a check on the constants determined by other means.

One technique, considered theoretically, suggested the possibility of an accurate determination of Y_{ee} masked by a minimum of other circuit elements. This involved a bridge measurement of input admittance using a General Radio Admittance Bridge or a Rohde and Schwarz Diagraph with the variable termination set to balance out the effect of $C_{tc'} + C_{scb}$ (see Appendix A·2). Under this condition the input impedance Z_{ib} is given by:

$$Z_{ib} = 1/Y_{ib} \approx r'_{bb} + 1/(Y_{ee} + j\omega C_{te}) \qquad 2.7.28$$

where Y_{ib} is the input admittance. r'_{bb} and C_{te} can be measured by standard techniques and Y_{ee} determined from eqn. 2.7.28.

The success of this approach depended upon an accurate setting of the terminating line to balance out completely $C_{tc'} + C_{scb}$. For practical reasons, which are discussed in Appendix A·2, this approach was unsuccessful. It was therefore concluded that impurity distribution must be determined from measurements of other elements and Y_{ee} derived from the known distribution.

3. TREATMENT OF CLASSICAL DISTRIBUTIONS AND APPROXIMATION BY DOUBLE EXPONENTIAL MODEL

3.1 Introduction

Chapter 2 indicated the need for a simple, yet accurate, model for the double-diffused transistor - simple enough to be determined from terminal measurements, yet accurate enough to describe adequately physical and electrical properties of the device. The basis for choice of the model is, preferably, the form of the actual distribution. Although, in practice, actual diffusion profiles may depart from classical distributions, in device characterization it is commonly assumed that classical distributions apply-in double-diffused transistors these are double ERFCs or double Gaussians (See Chapter 2). This treatment is justified both by the non-universality of factors effecting deviations from the ideal in diffusions and by the similarity of most solid-state diffusion distributions when they have fallen substantially below their initial values (See Fig. 2.2). Classical distributions will, therefore, be tacitly assumed throughout this chapter as being representative of actual double-diffused transistors.

To fully justify any impurity model, its effect on junction characteristics and base region properties (the quantities most affected by impurity distribution) must be shown to approximate that of the classical distribution it represents. To provide a basis for justification of the double exponential model assumed later in the chapter, double ERFC and double Gaussian distributions are treated in turn. Poisson's equation is solved over the depletion regions to provide

equations governing electric field and junction voltage. This treatment is felt to be more general than that normally presented for double-diffused transistors, where Poisson's equation is solved by numerical means only. Equations are also presented for minority carrier density and base transit time. The complicated nature of the various expressions suggests a graphical presentation, yet the large number of independent variables precludes any general graphical representation. Accordingly, it has been found convenient to present such information in the form of a representative example.

The introduction in a planar epitaxial transistor of a diffused substrate interface characterized by the classical distributions of Chapter 2 (Section 2.3.4) considerably complicates the equations defining collector junction properties, although seldom seriously affecting the base region and emitter junction properties. Collector junction equations are extended to include the substrate interface, with the extensions being presented graphically for a substrate layer added to the double-diffused example considered earlier.

A double exponential model is chosen to represent impurity profiles formed by two classical distributions. The model is assumed to apply throughout the base and collector region, and to extend for a short distance into the emitter region. The two commonly used approximations for the emitter junction, viz., an abrupt transition at the junction or a linear region near the jun ction applicable for small reverse bias only, are considered. Equations are derived for junction characteristics and base transport properties. These quantities

are computed for the model applied to the earlier classical examples and are shown to closely approximate those for the classical distributions. The model is extended to the epitaxial transistor by assuming an abrupt interface at the substrate.

A final section is devoted to presentation of the numerical techniques involved in computing the base transport and junction properties for both the classical distributions and the double-exponential model.

3.2 The Double ERFC Distribution

3.2.1 Form of Impurity Distribution

It was shown in Chapter 2 (Section 2.3.2) that the double-diffusion process where each diffusion proceeds ideally from a source of constant surface impurity concentration results in a double ERFC distribution. This distribution is defined mathematically by eqn. 2.3.1 , repeated here for convenience:

$$N(x) = N_A - N_D = -N_{s1}\,\mathrm{erfc}\,\frac{x}{\sqrt{4D_1 t_1}} + N_{s2}\,\mathrm{erfc}\,\frac{x}{\sqrt{4D_2 t_2}} - N_B \qquad 3.2.1$$

The subscripts "1" and "2" refer to the shallower and deeper diffusions (usually called emitter and base diffusions) respectively. D_1 and D_2 are diffusion coefficients; t_1 and t_2 are diffusion times; N_B is background doping and N_{s1} and N_{s2} are surface concentrations. The convention adopted here of representing base diffusion as being positive will be continued throughout this chapter.

In deriving equations governing base transport and junction properties, certain operations must be performed on the complimentary error

functions. The following identities should facilitate performance of these operations:

I. $$\operatorname{erfc}\left(\frac{x}{\sqrt{4Dt}}\right) = 1 - \operatorname{erf}\left(\frac{x}{\sqrt{4Dt}}\right) = 1 - \frac{2}{\sqrt{\pi}}\int_0^{x/\sqrt{4Dt}} e^{-\lambda^2}\, d\lambda$$

where λ is an integration variable.

II. $$\frac{d}{dx}\operatorname{erfc}\left(\frac{x}{\sqrt{4Dt}}\right) = \frac{-1}{\sqrt{\pi Dt}}\, e^{-x^2/4Dt}$$

III. $$\frac{d}{dx}\left(\operatorname{erf}\ (x/\sqrt{4Dt})\right) = \frac{1}{\sqrt{\pi Dt}}\, e^{-x^2/4Dt}$$

IV. $$\int_a^b \operatorname{erf}\left(\frac{x}{\sqrt{4Dt}}\right) dx = \left[x \operatorname{erf}\frac{x}{\sqrt{4Dt}} + \frac{\sqrt{4Dt}}{\sqrt{\pi}}\, e^{-x^2/4Dt}\right]_a^b$$

V. $$\int_a^b \operatorname{erfc}\frac{x}{\sqrt{4Dt}}\, dx = \left[x \operatorname{erfc}\frac{x}{\sqrt{4Dt}} - \frac{\sqrt{4Dt}}{\sqrt{\pi}}\, e^{-x^2/4Dt}\right]_a^b$$

where a and b are limits of integration.

VI. $$\int x \operatorname{erf}\frac{x}{\sqrt{4Dt}} = \frac{x^2}{2}\operatorname{erf}\frac{x}{\sqrt{4Dt}} + \frac{\sqrt{Dt}}{\sqrt{\pi}}\, xe^{-x^2/4Dt} - \tfrac{1}{2}\frac{\sqrt{4Dt}}{\sqrt{\pi}}\int e^{-x^2/4Dt} dx$$

and

VII. $$\frac{\sqrt{Dt}}{\sqrt{\pi}}\int e^{-x^2/4Dt}\, dx = -Dt \operatorname{erfc}\frac{x}{\sqrt{4Dt}}$$

These identities are employed in the determination of electric field and junction voltage in the following section and will also be used in a similar treatment involving the double Gaussian distribution.

3.2.2 Depletion Region Equations

A general treatment applicable to either the emitter or the collector junction is presented here. Figure 3.1 represents the double-diffused transistor for any arbitrary impurity distribution N(x). The

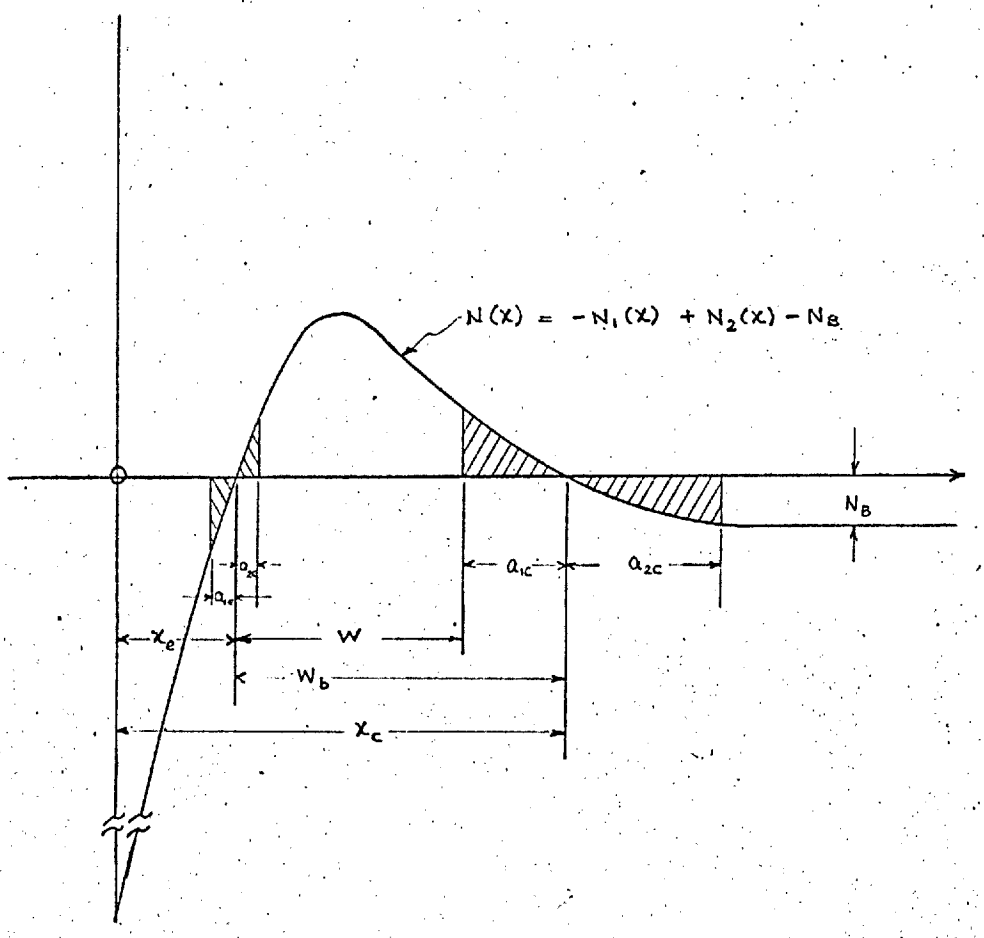


Fig. 3.1. General Representation of Impurity Profile in a Double-Diffused Transistor.

space-charge approximation of complete carrier depletion is assumed throughout the transition, or depletion, layer, together with complete ionization of donors and acceptors. In the figure, junctions are represented as occurring at x_e and x_c and depletion layer semi-widths (portion of charge dipole on either side of the junction) are represented by a_1 and a_2 with additional subscripts "e" or "c" to indicate either emitter or collector junction respectively.

With the above assumptions the net charge density in the depletion region is given by: $\rho = q\,[N(x)]$ 3.2.2

where q is the electrostatic charge.

Poisson's equation can be written as

$$\frac{d^2V}{dx^2} = -\frac{q\,N(x)}{\varepsilon} \qquad 3.2.3$$

The electric field distribution on either side of a junction can be found by integrating Poisson's equation between the appropriate limits. Thus

$$E_1(x) = -\int_{x_j - a_1}^{x} \frac{d^2V}{dx^2}\,dx = \frac{q}{\varepsilon}\int_{x_j - a_1}^{x} N(x)dx \qquad 3.2.4$$

and

$$E_2(x) = -\int_{x_j + a_2}^{x} \frac{d^2V}{dx^2}\,dx = \frac{q}{\varepsilon}\int_{x_j + a_2}^{x} N(x)dx \qquad 3.2.5$$

where $E_1(x)$ and $E_2(x)$ are the electric fields to the left and right of the junctions of Fig. 3.1 respectively. x_j is used to refer to either junction.

A relationship relating a_1 and a_2 implicitly may be derived by

utilizing the property of electric field continuity at the junction ($x = x_j$). Thus:

$$E_1(x_j) = E_2(x_j) \qquad 3.2.6$$

Which upon substitution of $E_1(x_j)$ and $E_2(x_j)$ from eqns. 3.2.4 and 3.2.5 becomes:

$$\int_{x_j - a_1}^{x_j} N(x)dx = \int_{x_j + a_2}^{x_j} N(x)dx \qquad 3.2.7$$

It should be pointed out that the electric field at the junction is at its maximum value.

Voltage across the junction is found by integrating $E_1(x)$ and $E_2(x)$ over a_1 and a_2 respectively and adding the two voltages. Thus:

$$V_1 = -\int_{x_j - a_1}^{x_j} E_1(x)dx \qquad 3.2.8(a)$$

$$V_2 = -\int_{xj}^{x_j + a_2} E_2(x)dx \qquad 3.2.8(b)$$

$$V_t = V_1 + V_2 \qquad 3.2.8(c)$$

where V_1 and V_2 are the voltages across the depletion layer to the left and to the right of the junction respectively. V_t is the total voltage across the junction. The preceding equations may be used with any impurity distribution.

The procedure of eqns. 3.2.2 to 3.2.8 will now be applied to the double ERFC distribution where N(x) is given by eqn. 3.2.1.

Poisson's equation becomes:

$$\frac{d^2V}{dx^2} = -\frac{q}{\varepsilon} N_{S2}\left[-\frac{N_{S1}}{N_{S2}}\,\mathrm{erfc}\,(x/\sqrt{4D_1t_1}) + \mathrm{erfc}\,(x/\sqrt{4D_2t_2}) - \frac{N_B}{N_{S2}}\right] \qquad 3.2.9$$

Substituting equation 3.2.9 for d^2V/dx^2 in equation 3.2.4 and performing the integration with the aid of the identities of Section 3.2.1 yields:

$$E_1(x) = \frac{q}{\varepsilon} N_{S2}\left[F_1(x,x_j - a_1,D_2t_2) - \frac{N_{S1}}{N_{S2}} F_1(x,x_j - a_1, D_1t_1) - \frac{N_B}{N_{S2}}\,(x - (x_j - a_1))\right] \qquad 3.2.10$$

where $F_1(\upsilon,\phi,\zeta) = \upsilon\,\mathrm{erfc}\,\frac{\upsilon}{\sqrt{4\zeta}} - \phi\,\mathrm{erfc}\,\frac{\phi}{\sqrt{4\zeta}} - \sqrt{\frac{4\zeta}{\pi}}\,(e^{-\frac{\upsilon^2}{4\zeta}} - e^{-\frac{\phi^2}{4\zeta}})$ 3.2.11

where υ, ϕ, and ζ are arbitrary variables; in eqn. 3.2.10 they are x, $x_j - a_1$, and Dt respectively. A similar expression applies for the electric field to the right of the junction:

$$E_2(x) = \frac{q}{\varepsilon} N_{S2}\left[F_1(x,x_j + a_2, D_2t_2) - \frac{N_{S1}}{N_{S2}} F_1(x,x_j + a_2,D_1t_1) - \frac{N_B}{N_{S2}}\,(x - (x_j + a_2))\right] \qquad 3.2.12$$

Substituting the values of eqns. 3.2.10 and 3.2.12 into eqn. 3.2.7 when $x = x_j$ and rearranging gives a relationship between a_1 and a_2:

$$\left\{F_1(x_j,x_j + a_2,D_2t_2) - F_1(x_j,x_j - a_1,D_2t_2)\right\} - \frac{N_{S1}}{N_{S2}}\left\{F_1(x_j,x_j + a_2,D_1t_1) - F_1(x_j,x_j - a_1,D_1t_1)\right\} + \frac{N_B}{N_{S2}}\,(a_1 + a_2) = 0 \qquad 3.2.13$$

When eqn. 3.2.11 is used with the variables of eqn. 3.2.13 to find the appropriate values of F_1, the "$x_j \operatorname{erfc} \frac{x_j}{\sqrt{4Dt}}$" terms cancel. Fortuitously, the resultant expression is such that it can be expressed by E_1 with $x_j - a_1$ substituted for υ and $x_j + a_2$ for ϕ. Thus:

$$F_1(x_j - a_1, x_j + a_2, D_2 t_2) - \frac{N_{S1}}{N_{S2}} (x_j - a_1, x_j + a_2, D_1 t_1) + \frac{N_B}{N_{S2}} (a_1 + a_2) = 0 \qquad 3.2.14$$

Voltages on either side of the junction may be found by performing the integrations in eqn. 3.2.8 (a) and (b) where the values of $E_1(x)$ and $E_2(x)$ from eqns. 3.2.10 and 3.2.12 are substituted. Thus:

$$V_1 = -\frac{q}{\varepsilon} N_{S2} \left[F_2(x_j, D_2 t_2, x_j - a_1) - \frac{N_{S1}}{N_{S2}} F_2(x_j, D_1 t_1, x_j - a_1) - \frac{N_B}{N_{S2}} \frac{a_1^2}{2} \right] \qquad 3.2.15$$

Where the function F_2 is defined by:

$$F_2(\upsilon, \zeta, \phi) = \left(\zeta + \frac{\upsilon^2}{2}\right) \operatorname{erfc} \frac{\upsilon}{\sqrt{4\zeta}} - \left(\zeta + \frac{\upsilon^2}{2} - \frac{(\upsilon - \phi)^2}{2}\right) \operatorname{erfc} \frac{\phi}{\sqrt{4\zeta}} - \sqrt{\frac{\zeta}{\pi}}\, \upsilon e^{-\frac{\upsilon^2}{4\zeta}} + \sqrt{\frac{\zeta}{\pi}} (2\upsilon - \phi) e^{-\frac{\phi^2}{4\zeta}} \qquad 3.2.16$$

The variables υ, ζ and ϕ in F_2 may assume different values. This function also appears in the expression for voltage to the right of the junction.

$$V_2 = \frac{q}{\varepsilon} N_{S2} \left[F_2(x_j, D_2 t_2, x_j + a_2) - \frac{N_{S1}}{N_{S2}} F_2(x_j, D_1 t_1, x_j + a_2) - \frac{N_B}{N_{S2}} \frac{a_2^2}{2} \right] \qquad 3.2.17$$

where $x_j + a_2$ is substituted for ϕ.

$$V_t = \frac{q}{\varepsilon} N_{S2} \left[\{F_2(x_j, D_2 t_2, x_j + a_2) - F_2(x_j, D_2 t_2, x_j - a_1)\} - \frac{N_{S1}}{N_{S2}} \right.$$
$$\left. \{F_2(x_j, D_1 t_1, x_j + a_2) - F_2(x_j, D_1 t_1, x_j - a_1)\} - \frac{N_B}{N_{S2}} \left(\frac{a_2^2}{2} - \frac{a_1^2}{2}\right) \right] \qquad 3.2.18$$

In eqn. 3.2.18 the terms in x_j only are eliminated when the subtraction of $F_2(x_j, Dt, x_j + a_2) - F_2(x_j, Dt, x_j - a_1)$ is carried out. It is convenient to define another function to represent repeated terms in the voltage expression. Thus,

$$V_t = \frac{q}{\varepsilon} N_{S2} \left[F_3(x_j, D_2 t_2, a_1, a_2) - \frac{N_{S1}}{N_{S2}} F_3(x_j, D_1 t_1, a_1, a_2) \right.$$
$$\left. - \frac{N_B}{N_{S2}} \tfrac{1}{2} (a_2^2 - a_1^2) \right] \qquad 3.2.19$$

where F_3 is defined by:

$$F_3(\upsilon, \zeta, \phi, \Psi) = \left\{ \left(\zeta + \frac{\upsilon^2}{2} - \frac{\phi^2}{2}\right) \operatorname{erfc} \frac{\upsilon - \phi}{2\sqrt{4\zeta}} - \left(\zeta + \frac{\upsilon^2}{2} - \frac{\Psi^2}{2}\right) \operatorname{erfc} \right.$$
$$\left. \left(\frac{\upsilon + \Psi}{\sqrt{4\zeta}}\right) + (\upsilon - \Psi)\sqrt{\frac{4\zeta}{\pi}}\, e^{-\frac{(\upsilon + \Psi)^2}{4\zeta}} - (\upsilon + \phi)\sqrt{\frac{4\zeta}{\pi}}\, e^{-\frac{(\upsilon - \phi)^2}{4\zeta}} \right\} \qquad 3.2.20$$

where υ, ζ, ϕ, and Ψ are any variables.

Eqn. 3.2.19 may be used to find voltage across the junction when a_1 and a_2 are known. To provide curves of a_1 and a_2 vs voltage, assume a_2, calculate a_1 from eqn. 3.2.14, and voltage from 3.2.19.

An equilibrium barrier potential exists across a junction in the absence of external bias. This barrier potential V_o was defined in Section 2.7.3 as follows:

$$V_o \approx \frac{kT}{q} \ln \left| \frac{N(a_1) \cdot N(a_2)}{n_i^2} \right| \qquad 3.2.21$$

where k is Boltzmann's constant, T is absolute temperature, q is

electrostatic charge, n_i is the intrinsic carrier density, and $N(a_1)$ and $N(a_2)$ are impurity densities at either edge of the depletion layer. For the double ERFC distribution, equation 3.2.21 becomes:

$$V_o = \frac{kT}{q} \ln \left| \frac{N_{s2}^2}{n_i^2} \left\{ \left(\operatorname{erfc} \frac{x_j - a_1}{\sqrt{4D_2 t_2}} - \frac{N_{s1}}{N_{s2}} \operatorname{erfc} \frac{x_j - a_1}{\sqrt{4D_1 t_1}} - \frac{N_B}{N_{s2}} \right) \times \left(\operatorname{erfc} \frac{x_j + a_2}{\sqrt{4D_2 t_2}} - \frac{N_{s1}}{N_{s2}} \operatorname{erfc} \frac{x_j + a_2}{\sqrt{4D_1 t_1}} - \frac{N_B}{N_{s2}} \right) \right\} \right| \qquad 3.2.22$$

Eqn. 3.2.19 includes both the external bias voltage as well as the equilibrium barrier potential. When external bias is zero, eqn. 3.2.19 may also be used to determine V_o when a_1 and a_2 known at V_o. A suggested procedure to determine a_1, a_2, and V_o when all three are unknown is to subtract eqn. 3.2.19 from 3.2.22 and equate to zero. This provides a relationship between a_1 and a_2 which may be solved simultaneously with eqn. 3.2.14 to yield a_1 and a_2. V_o may then be found from either eqn. 3.2.19 or 3.2.22.

The rapid fall-off of emitter diffusion means that it can normally be neglected at the collector junction. The equations governing electric field and junction voltage then reduce to the single diffused case (all the N_{s1}/N_{s2} terms vanish). To indicate the accuracy of this approximation, a comparison is initiated in Section 3.2.5, for the collector junction of the representative example, between the single and double diffused cases. Depletion layer semi-widths and capacitance data are compared over a range of voltage and found to be in excellent agreement.

3.2.3 Base Region Properties

In a double-diffused transistor, minority carrier distribution exhibits a marked increase in concentration in the retarding-field region

near the emitter. Carriers are stored here in sufficiency to overcome the retarding field before they can move across the base to the collector. The presence of the retarding field, therefore, considerably influences minority carrier distribution and base transit time. Minority carrier density was described by eqn. 2.4.18, repeated here for convenience:

$$n = -\frac{J_n}{q} \cdot \frac{1}{N_A - N_D} \int_{x}^{x_e+W} \frac{N_A - N_D}{D_n(N_A;N_D)}\, dx \Bigg|_{x>x_e} \qquad 3.2.23$$

where J_n is current density, $N_A - N_D$ is the uncompensated impurity distribution (acceptors - donors) and $D_n(N_A;N_D)$ is the variable diffusion coefficient dependent on both donors and acceptors.

When the double ERFC distribution is substituted in eqn. 3.2.23, it becomes:

$$n = -\frac{J_n}{q} \cdot \frac{1}{\operatorname{erfc}\frac{x}{\sqrt{4D_2t_2}} - \frac{N_{s1}}{N_{s2}}\operatorname{erfc}\frac{x}{\sqrt{4D_1t_1}} - \frac{N_B}{N_{s2}}} \int_{x}^{x_e+W} \frac{\left(\operatorname{erfc}\frac{x}{\sqrt{4D_2t_2}} - \frac{N_{s1}}{N_{s2}}\operatorname{erfc}\frac{x}{\sqrt{4D_1t_1}} - \frac{N_B}{N_{s2}}\right)dx}{D_n\left(N_{s2}\operatorname{erfc}\frac{x}{\sqrt{4D_2t_2}} + N_{s1}\operatorname{erfc}\frac{x}{\sqrt{4D_1t_1}} + N_B\right)} \Bigg|_{x>x_e} \qquad 3.2.24$$

The origin of x is taken to be the surface emitter, W is the distance to the edge of the collector depletion layer, embracing both effective base width and the width of the emitter depletion layer on the base side of the emitter junction (a_{2e}). The non-constant nature of the diffusion coefficient prevents an analytical solution of eqn. 3.2.24, so solution must be by numerical means for a specific case.

Base transit time in the absence of recombination may be determined from the charge control definition (see eqn. 2.4.24):

$$\tau_b = \frac{qA_e \int_{x_e+a_{2e}}^{x_e+W} n\,dx}{|I_c|} \qquad 3.2.25$$

where A_e is the emitter area and $|I_c|$ is the magnitude of the collector current. Substituting the value of n from eqn. 3.2.24 gives:

$$\tau_b = \int_{x_e+a_{2e}}^{x_e+W} \frac{1}{\left(\operatorname{erfc}\frac{x}{\sqrt{4D_2t_2}} - \frac{N_{S1}}{N_{S2}}\operatorname{erfc}\frac{x}{\sqrt{4D_1t_1}} - \frac{N_{S1}}{N_{S2}}\right)}$$

$$\int_{x}^{x_e+W} \frac{\left(\operatorname{erfc}\frac{x}{\sqrt{4D_2t_2}} - \frac{N_{S1}}{N_{S2}}\operatorname{erfc}\frac{x}{\sqrt{4D_1t_1}} - \frac{N_{S1}}{N_{S2}}\right)}{D_n\left(N_{S2}\operatorname{erfc}\frac{x}{\sqrt{4D_2t_2}} + N_{S1}\operatorname{erfc}\frac{x}{\sqrt{4D_1t_1}} + N_B\right)}\,dx^2 \qquad 3.2.26$$

$x > x_e$

Eqn. 3.2.26 can be solved only be numerical means for a specific case.

Eqns. 3.2.24 and 3.2.26 are used in Section 3.2.5 to calculate minority carrier density and base transit time for a representative example. From Figs. 3.6 and 3.7, the build-up of charge in the retarding field region and the increase in base transit time due to the retarding field are evident.

3.2.4 Emitter Doping

Over most of the emitter depletion region the impurity density is dominated by the shallower diffusion. Near the metallurgical junction, the two diffusants are of comparable magnitude and tend to compensate each other. At the junction itself complete compensation of donors and acceptors occurs, and if background doping is sufficiently low (as it is in most practical cases) little error is introduced by assuming the

junction occurs where the two diffusants are of equal magnitude. Compensation near the junction imparts a relatively steep gradient in the emitter.

For simplicity, it has often been found convenient to approximate the emitter region by a constant average impurity density N_E, with an abrupt transition to the base region at the metallurgical junction ($x = x_e$). This approximation was adopted in the models of Chapter 2, Section 2.7. Determination of N_E involves integration of the impurity distribution over the emitter thickness and dividing by x_e to average this result. For the double ERFC distribution,

$$N_E = \frac{1}{x_e} \int_0^{x_e} \left(N_{s_2} \operatorname{erfc} \left(\frac{x}{\sqrt{4D_2 t_2}}\right) - N_{s_1} \operatorname{erfc} \frac{x}{\sqrt{4D_1 t_1}} - N_B\right) dx \qquad 3.2.27$$

giving:

$$N_E = N_{s_2}\left\{\operatorname{erfc} \frac{x_e}{\sqrt{4D_2 t_2}} - \frac{1}{x_e}\sqrt{\frac{4D_2 t_2}{\pi}}\left(e^{-\frac{x_e^2}{4D_2 t_2}} - 1\right)\right\} - N_{s_1}\left\{\operatorname{erfc} \frac{x_e}{\sqrt{4D_1 t_1}} - \frac{1}{x_e}\sqrt{\frac{4D_1 t_1}{\pi}}\left(e^{-\frac{x_e^2}{4D_1 t_1}} - 1\right)\right\} - N_B \qquad 3.2.28$$

The convention of positive doping in the base region results in a negative value of N_E from eqn. 3.2.28.

In Fig. 3.3 depletion layer semi-widths are plotted against voltage for the specific example to be adopted in the next section. For the emitter junction, the values of a_{1e} and a_{2e} can be seen to be comparable for low reverse voltage. This indicates that the abrupt approximation discussed above is inaccurate when applied to double-diffused transistor. Further evidence will be offered in Chapter 4 to

support this conclusion. A symmetrical-linear approximation for low reverse voltages is suggested to be more applicable. The slope of this straight line approximation is determined by the gradient of the classical distribution at $x = x_e$. For the double ERFC distribution this gradient is:

$$S_1 = \frac{dN}{dx}\bigg|_{x=x_e} = \frac{N_{S_1}}{\sqrt{\pi D_1 t_1}} e^{-x_e^2/4D_1 t_1} - \frac{N_{S_2}}{\sqrt{\pi D_2 t_2}} e^{-x_e^2/4D_2 t_2} \qquad 3.2.29$$

Emitter doping is given by:

$$N(x)\bigg|_{x \leq x_e} = \left(\frac{N_{S_1}}{\sqrt{\pi D_1 t_1}} e^{-x_e^2/4D_1 t_1} - \frac{N_{S_2}}{\sqrt{\pi D_2 t_2}} e^{-x_e^2/4D_2 t_2}\right)(x - x_e) \qquad 3.2.30$$

Both the abrupt and the linear approximation will be considered in Section 3.5 with the double-exponential model for the base, the equations of this section being used to determine the parameters of the approximation when the original distribution is a double ERFC.

3.2.5 Representative Example

To illustrate the form of the equations presented in Sections 3.2.2 and 3.2.3, and to provide a standard against which the accuracy of the double-exponential model of Section 3.5 is compared, the following representative example was chosen. Design information is:

$N_{S_1} = 1 \times 10^{21}$ atoms/cc $\qquad x_e = 1.5 \times 10^{-4}$ cm.

$N_{S_2} = 5 \times 10^{18}$ atoms/cc $\qquad x_c = 4.5 \times 10^{-4}$ cm.

$N_B = 5 \times 10^{15}$ atoms/cc $\qquad D_1 = D_2 = 3.4 \times 10^{-13}$ volt-cm^{2X}

$n_i^2 = 9.415 \times 10^{19}$/cm^6 (@ T = 296°K.*) $\qquad$ T = 1100°C (Diffusion Temp.)

X Determined from Fuller's curves[24] at T = 1100°C (See Fig.2.1)

* Determined from $n_i^2 = 1.5 \times 10^{33} T_e^3 - 1.21q/kT$; T in °K. 3.2.31

Although other parameters such as diffusion times could equally well have been chosen as design information, it was felt that fixing the junction position would best serve the purposes of this study. On this basis a computer program was written with the above parameters as input data and t_1, t_2, impurity distribution N(x), junction voltage, depletion layer semi-widths, transition capacitance/area, minority carrier density, and base transit time as output information. It was not felt necessary to compute electric field in the depletion region, since this would contribute little to the comparison of the classical distribution and the double-exponential model.

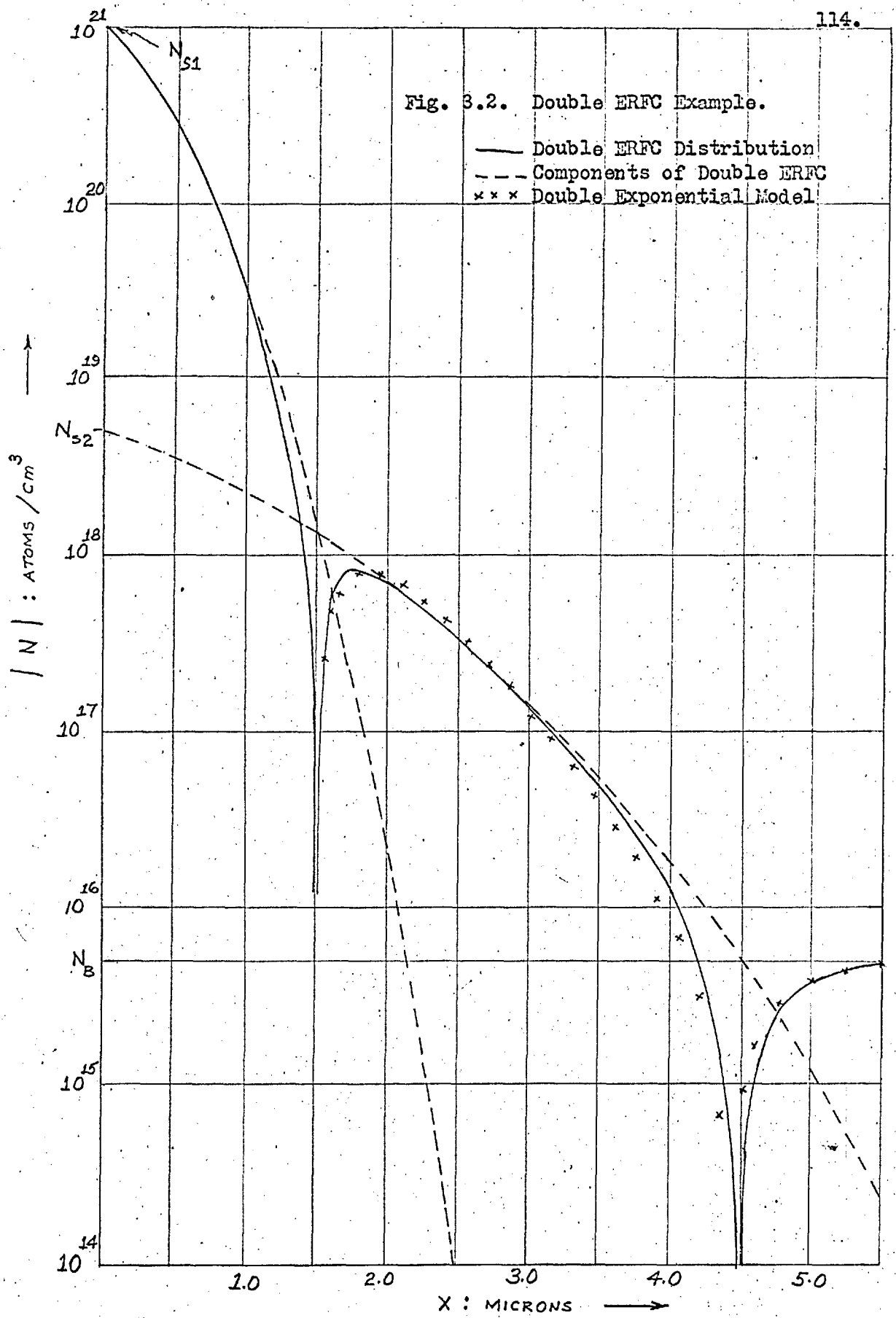
Diffusion times for this example were found to be:

t_1 = 54 min.; t_2 = 7 hr. 38 min.

The resultant impurity distribution is given by:

$$N(x) = 5 \times 10^{18} \operatorname{erfc}\left(\frac{x}{1.934 \times 10^{-4}}\right) - 10^{21} \operatorname{erfc}\left(\frac{x}{6.622 \times 10^{-5}}\right) - 5 \times 10^{15} \qquad 3.2.32$$

The distribution of eqn. 3.2.32 is plotted in Fig. 3.2 on log-linear paper. Only the magnitudes are shown. From this plot it can be seen that the emitter diffusion is negligible near the collector junction. Depletion layer semi-widths and total depletion layer width are plotted in Fig. 3.3 for both junctions. For the emitter junction, a_{ae} can be seen to be approximately equal to a_{2e} for low values of reverse bias. The linear approximation is thus preferable to the abrupt approximation for this example. At the collector junction, curves for depletion layer semi-widths when emitter diffusion is completely neglected are indistinguishable from those derived when both


Fig. 3.2. Double ERFC Example.
Double ERFC Distribution
Components of Double ERFC
Double Exponential Model
10^{21}
10^{20}
10^{19}
10^{18}
10^{17}
10^{16}
10^{15}
10^{14}
N_{S1}
N_{S2}
N_B
| N | : ATOMS / cm^3
1.0
2.0
3.0
4.0
5.0
X : MICRONS

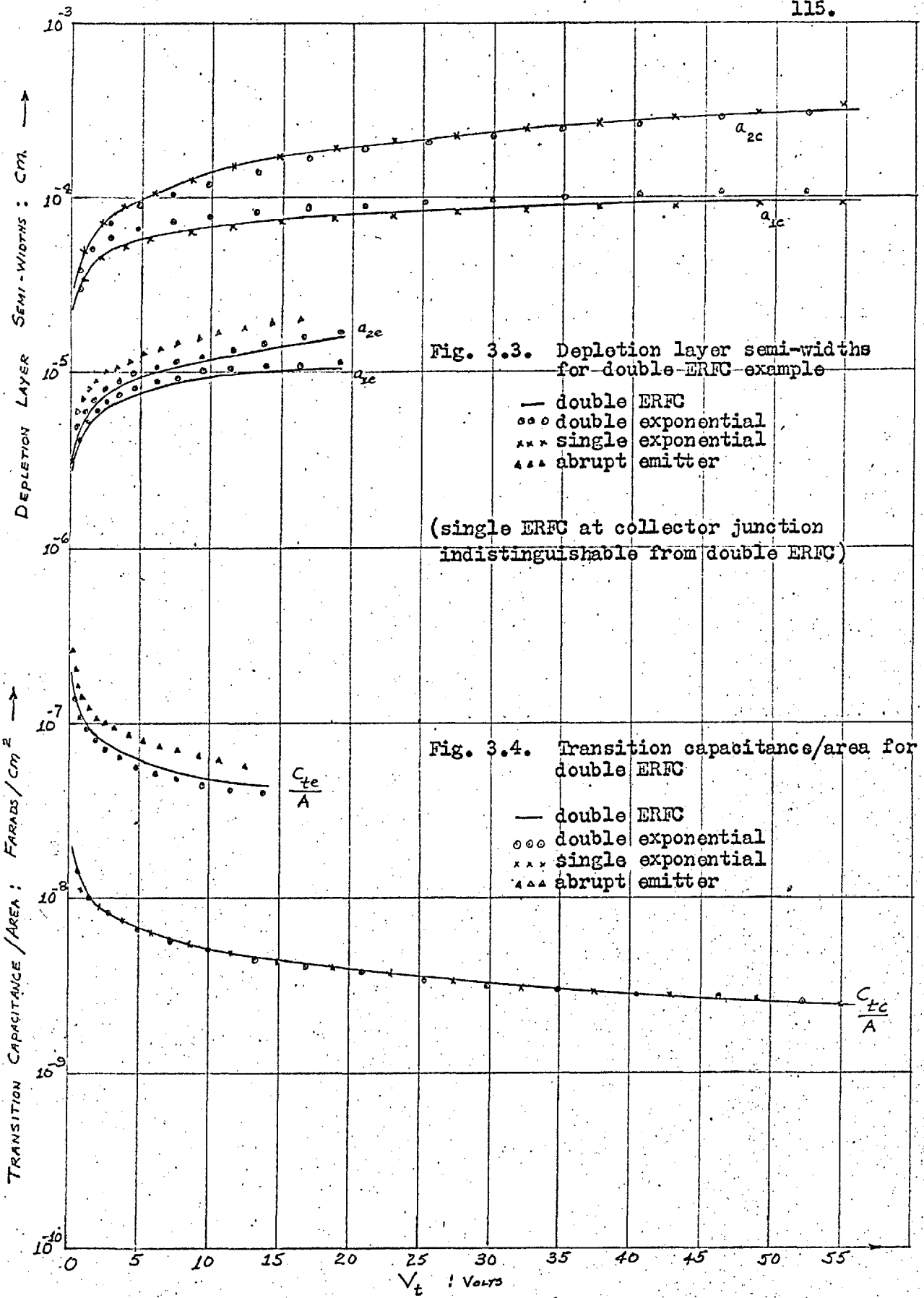


Fig. 3.3. Depletion layer semi-widths for double-ERFC example

— double ERFC
ooo double exponential
xxx single exponential
ΔΔΔ abrupt emitter

(single ERFC at collector junction indistinguishable from double ERFC)

Fig. 3.4. Transition capacitance/area for double ERFC

— double ERFC
ooo double exponential
xxx single exponential
ΔΔΔ abrupt emitter

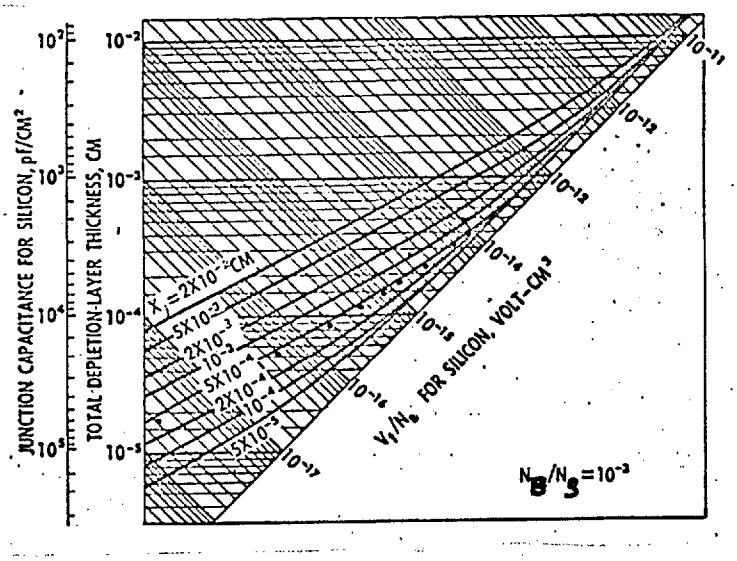


Fig. 3.5(a). Capacitance for double ERFC example superimposed on curves after Lawrence and Warner[33].

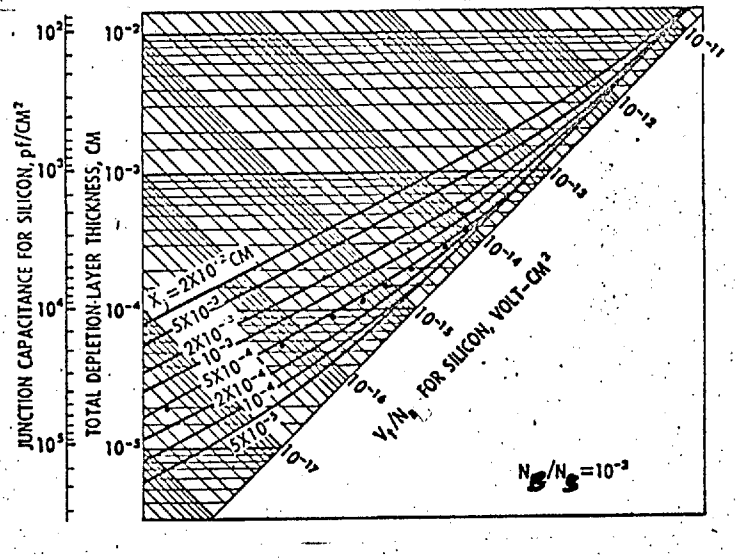


Fig. 3.5(b) Collector capacitance for double Gaussian superimposed on curves after Lawrence and Warner[33].

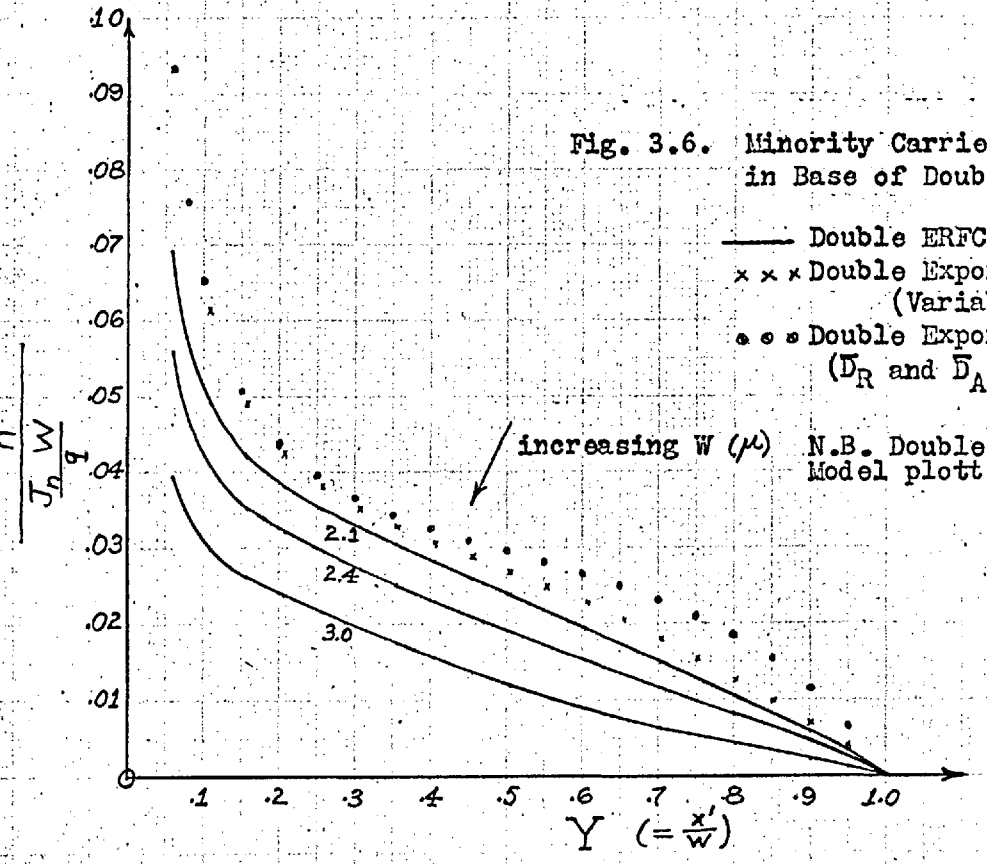


Fig. 3.6. Minority Carrier Distribution in Base of Double ERFC Example.

——— Double ERFC Distribution
× × × Double Exponential Model (Variable D_n)
• • • Double Exponential Model ($\bar{D}_R$ and $\bar{D}_A$ Approximation)

N.B. Double Exponential Model plotted for W = 2.1 μ

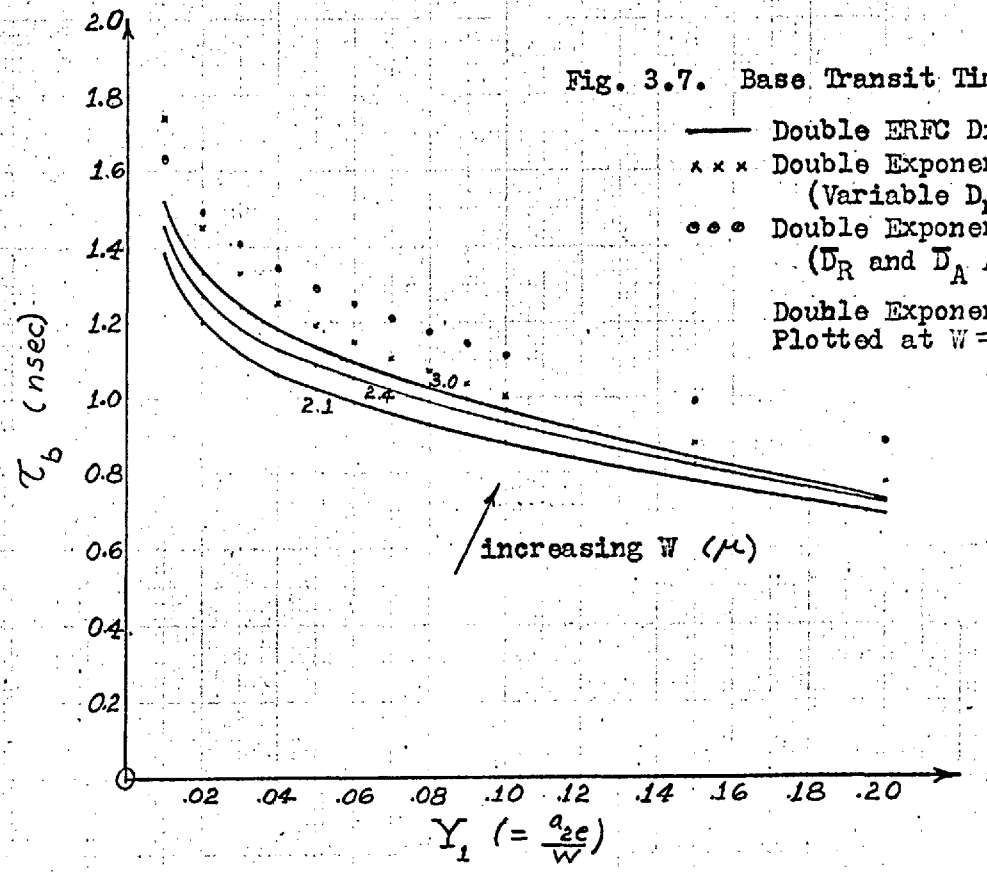


Fig. 3.7. Base Transit Time.

——— Double ERFC Distribution
× × × Double Exponential Model (Variable D_n)
• • • Double Exponential Model ($\bar{D}_R$ and $\bar{D}_A$ Approximation)

Double Exponential Model Plotted at W = 2.1 μ

diffusions are considered.

Fig. 3.4 presents curves of transition capacitance vs junction voltage for both junctions, while in Fig. 3.5 the collector curve is superimposed on a chart of the type presented by Lawrence and Warner[33]. This further indicates that the emitter diffusion is negligible at the collector junction, and suggests the use of such charts to estimate collector depth below the wafer surface. The dependence of emitter capacitance on both diffusions precludes at this stage a similar conclusion for the emitter junction (see Chapter 5, Section 5.2.3).

Minority carrier densities and base transit times are plotted in Figs. 3.6 and 3.7 respectively for a range of collector and emitter voltages. The bias information is presented in the form of variation of a_{ae} and W. The buildup of minority carriers in the retarding field region and the strong dependence of transit time on the extent of this region are evident from these curves.

3.3 Double Gaussian Distribution

.3.1 Impurity Distribution

A diffusion which has proceeded ideally from a planar source results in a Gaussian distribution (See Section 2.2.3). The basic difference between a Gaussian and an ERFC distribution is that at the semiconductor surface the former exhibits zero slope, while the latter exhibits negative slope. For a given diffusion length $(=\sqrt{4Dt})$ the Gaussian falls off less rapidly than the ERFC; or, conversely, for a given diffusion depth, diffusion length is smaller for a Gaussian than for the equivalent ERFC (See Fig. 2.2).

When both diffusions used in the fabrication of double-diffused transistors proceed from planar sources, (pre-deposition and drive-in), the combined impurity distribution is the difference of two Gaussians, viz.:

$$N(x) = -N_{s_1} e^{-x^2/4D_1 t_1} + N_{s_2} e^{-x^2/4D_2 t_2} - N_B \qquad 3.3.1$$

where all the constants are as defined for the double ERFC (Section 3.2.1). Eqn. 3.3.1 is used as the basis for the derivation of junction characteristics and base transport properties of the following sections. The identities of Section 3.2.1 find considerable application in the derivation of the equations of Section 3.3.2.

3.3.2 Depletion Region Equations

The double Gaussian junction is described completely by employing in proper sequence eqns. 3.2.2 to 3.2.8 with the value of N(x) from eqn. 3.3.1. During the course of this treatment several functions are defined which simplify presentation of the various equations. Since the sequence of operations is the same as that for the double ERFC distribution, only the final equations are presented.

Electric fields in the depletion regions are given by:

$$E_1(x) = \frac{q}{\varepsilon} N_{s_2} \left[\Sigma_1 (x, x_j - a_1, D_2 t_2) - \frac{N_{s_1}}{N_{s_2}} \Sigma_1 (x, x_j - a_1, D_1 t_1) - \frac{N_B}{N_{s_2}} (x - (x_j - a_1)) \right] \qquad 3.3.2$$

and

$$E_2(x) = \frac{q}{\varepsilon} N_{s_2} \left[\Sigma_1 (x, x_j + a_2, D_2 t_2) - \frac{N_{s_1}}{N_{s_2}} \Sigma_1 (x, x_j + a_2, D_2 t_2) - \frac{N_B}{N_{s_2}} (x - (x_j + a_2)) \right] \qquad 3.3.3$$

where $\Sigma_1(v,\phi,\zeta) = \sqrt{\pi\zeta}\,(\operatorname{erfc}\frac{\phi}{\sqrt{4\zeta}} - \operatorname{erfc}\frac{v}{\sqrt{4\zeta}})$ 3.3.4

The substitution of the appropriate values of v, ϕ, and ζ in eqn. 3.3.4 indicates which junction is being treated and which side of the junction is involved.

An expression relating a_1 and a_2 is derived by equating eqns. 3.3.2 and 3.3.3 when $x = x_j$. Thus,

$$\Sigma_1(x_j + a_2, x_j - a_1, D_2 t_2) - \frac{N_{S1}}{N_{S2}}\,\Sigma_1(x_j + a_2, x_j - a_1, D_1 t_1) - \frac{N_B}{N_{S2}}(a_1 + a_2) = 0 \qquad 3.3.5$$

When either a_1 or a_2 is known, eqn. 3.3.5 may be used to determine the other.

Integration of eqn. 3.3.2 over a_1 as in eqn. 3.2.8 determines voltage across the depletion region to the left of the junction, while a similar operation on eqn. 3.3.3 determines voltage to the right of the junction. This results in:

$$V_1 = -\frac{q}{\varepsilon} N_{S2}\left[\Sigma_2(x_j, x_j - a_1, D_2 t_2) - \frac{N_{S1}}{N_{S2}}\,\Sigma_2(x_j, x_j - a_1, D_1 t_1) - \frac{N_B}{N_{S2}}\,\frac{a_1^2}{2}\right] \qquad 3.3.6$$

and,

$$V_2 = \frac{q}{\varepsilon} N_{S2}\left[\Sigma_2(x_j, x_j + a_2, D_2 t_2) - \frac{N_{S1}}{N_{S2}}\,\Sigma_2(x_j, x_j + a_2, D_1 t_1) - \frac{N_B}{N_{S2}} \cdot \frac{a_2^2}{2}\right] \qquad 3.3.7$$

where the function Σ_2 is defined by:

$$\Sigma_2(\upsilon,\phi,\zeta) = \sqrt{\pi\zeta}\left(\operatorname{erfc}\frac{\phi}{\sqrt{4\zeta}} - \operatorname{erfc}\frac{\upsilon}{\sqrt{4\zeta}}\right) + 2\zeta\left(e^{-\frac{\upsilon^2}{4\zeta}} - e^{-\frac{\phi^2}{4\zeta}}\right) \qquad 3.3.8$$

Eqn. 3.3.8 may be stated in terms of Σ_1 as:

$$\Sigma_2(\upsilon,\phi,\zeta) = \upsilon\,\Sigma_1(\upsilon,\phi,\zeta) + 2\zeta\left(e^{-\frac{\upsilon^2}{4\zeta}} - e^{-\frac{\phi^2}{4\zeta}}\right) \qquad 3.3.8a$$

Substitution of the appropriate values of υ, ϕ and ζ in the function defined in eqn. 3.3.8 allows treatment of either junction or of either side of the junction.

Total voltage across the junction is found by adding V_1 and V_2. Introducing a new function Σ_3 this may be stated as:

$$V_t = \frac{q}{\varepsilon} N_{S2}\left[\Sigma_3(x_j - a_1, x_j + a_2, D_2 t_2) - \frac{N_{S1}}{N_{S2}}\Sigma_3(x_j - a_1, x_j + a_2, D_1 t_1) - \frac{N_B}{N_{S2}}\left(\frac{a_2^2 - a_1^2}{2}\right)\right] \qquad 3.3.9$$

where:

$$\Sigma_3(\upsilon,\phi,\zeta) = \sqrt{\pi\zeta}\,(\phi - a_2)\left(\operatorname{erfc}\frac{\phi}{\sqrt{4\zeta}} - \operatorname{erfc}\frac{\upsilon}{\sqrt{4\zeta}}\right) - 2\zeta\left(e^{-\frac{\phi^2}{4\zeta}} - e^{-\frac{\upsilon^2}{4\zeta}}\right) \qquad 3.3.10$$

Equilibrium barrier potential when a_1 and a_2 are known may be determined from either eqn. 3.3.9 or the following:

$$V_o = \frac{kT}{q}\ln\left|\frac{N_{S2}^2}{n_i^2}\left\{e^{-\frac{(x_j - a_1)^2}{4D_2t_2}} - \frac{N_{S1}}{N_{S2}}e^{-\frac{(x_j - a_1)^2}{4D_1t_1}} - \frac{N_B}{N_{S2}}\right\}\left\{e^{-\frac{(x_j + a_2)^2}{4D_2t_2}} - \frac{N_{S1}}{N_{S2}}e^{-\frac{(x_j + a_2)^2}{4D_1t_1}} - \frac{N_B}{N_{S2}}\right\}\right| \qquad 3.3.11$$

where n_i is the intrinsic carrier density. If a_1 and a_2 are unknown they may be determined by the simultaneous solution of eqn. 3.3.5 and an equation formed by equating 3.3.9 and 3.3.11. V_o is then found

from either eqn. 3.3.9 or 3.3.11.

The equations of this section reduce to those for a single diffused junction at the collector if emitter diffusion is negligible at this junction.

3.3.3 Base Region Properties

Equations similar to those of Section 3.2.3 with the double ERFC being replaced by the double Gaussian describe minority carrier density and base transit time. Minority carrier density is given by:

$$n = -\frac{J_n}{q} \cdot \frac{\int_{x_e+W}^{x} \frac{\left(e^{-x^2/4D_2t_2} - \frac{N_{s1}}{N_{s2}} e^{-x^2/4D_1t_1} - N_B/N_{s2}\right)dx}{D_n\left(N_{s2}e^{-x^2/4D_2t_2} + N_{s1}e^{-x^2/4D_1t_1} + N_B\right)}}{e^{-x^2/4D_2t_2} - \frac{N_{s1}}{N_{s2}} e^{-x^2/4D_1t_1} - N_B/N_{s2}} \Bigg|_{x>x_e} \qquad 3.3.12$$

and base transit time is given by

$$\tau_b = -\frac{q}{J_n} \int_{x_e+a_{2e}}^{x_e+W} n\, dx \qquad 3.3.13$$

where n is given in eqn. 3.3.12.

Again these equations can be solved only by numerical means for a specific case, unless an equivalent constant value of diffusion coefficient can be assumed, resulting in an analytical solution for n. This is not justified here, however, since classical distributions are presented in this Chapter as a basis for choice of a simple model, and must therefore provide information which can be used as criteria of accuracy for the simple approximation. Eqns. 3.3.12 and 3.3.13 are used in Section 3.3.5 to calculate n and τ_b for the representative example used earlier for the double ERFC distribution.

3.3.4 Emitter Region

The considerations of Section 3.2.4 apply equally to the emitter of a transistor with a double Gaussian impurity distribution. Thus, if the abrupt approximation is to be applied,

$$N_E = \frac{1}{x_e} \int_0^{x_e} (N_{s2}\, e^{-x^2/4D_2t_2} - N_{s1}\, e^{-x^2/4D_1t_1} - N_B)\, dx$$

$$N_E = \frac{N_{s2}}{x_e} \left[\sqrt{\pi D_2 t_2}\, \left(1 - \operatorname{erfc} \frac{x_e}{\sqrt{4D_2t_2}}\right) - \frac{N_{s1}}{N_{s2}} \sqrt{\pi D_1 t_1}\, \left(1 - \operatorname{erfc} \frac{x_e}{\sqrt{4D_1t_1}}\right) - \frac{N_B}{N_{s2}}\, x_e \right] \qquad 3.3.14$$

If the symmetrical-linear approximation is to be applied near the junction, the impurity gradient at the junction ($x = x_e$) is given by:

$$S_1 = \left.\frac{dN}{dx}\right|_{x=x_e} = \frac{N_{s1}x_e}{2D_1t_1}\, e^{-x_e^2/4D_1t_1} - \frac{N_{s2}x_e}{2D_2t_2}\, e^{-x_e^2/4D_2t_2} \qquad 3.3.15$$

and doping near the emitter is given by:

$$N(x)\Big|_{x<x_e} = \left\{ \frac{N_{s1}x_e}{2D_1t_1}\, e^{-x_e^2/4D_1t_1} - \frac{N_{s2}x_e}{2D_2t_2}\, e^{-x_e^2/4D_2t_2} \right\} (x - x_e) \qquad 3.3.16$$

Both these approximations will be applied in Section 3.5 for the double exponential model for the transistor.

3.3.5 Representative Example

To facilitate comparison of the double Gaussian with the double ERFC, the design parameters of Section 3.2.5 were also chosen to define

surface concentrations and junction positions for the double Gaussian distribution. On the basis of these design parameters, diffusion times were computed. Thus:

t_1 = 45 min. 30 sec., and t_2 = 5 hr. 59 min.

Impurity distributions may then be stated specifically by:

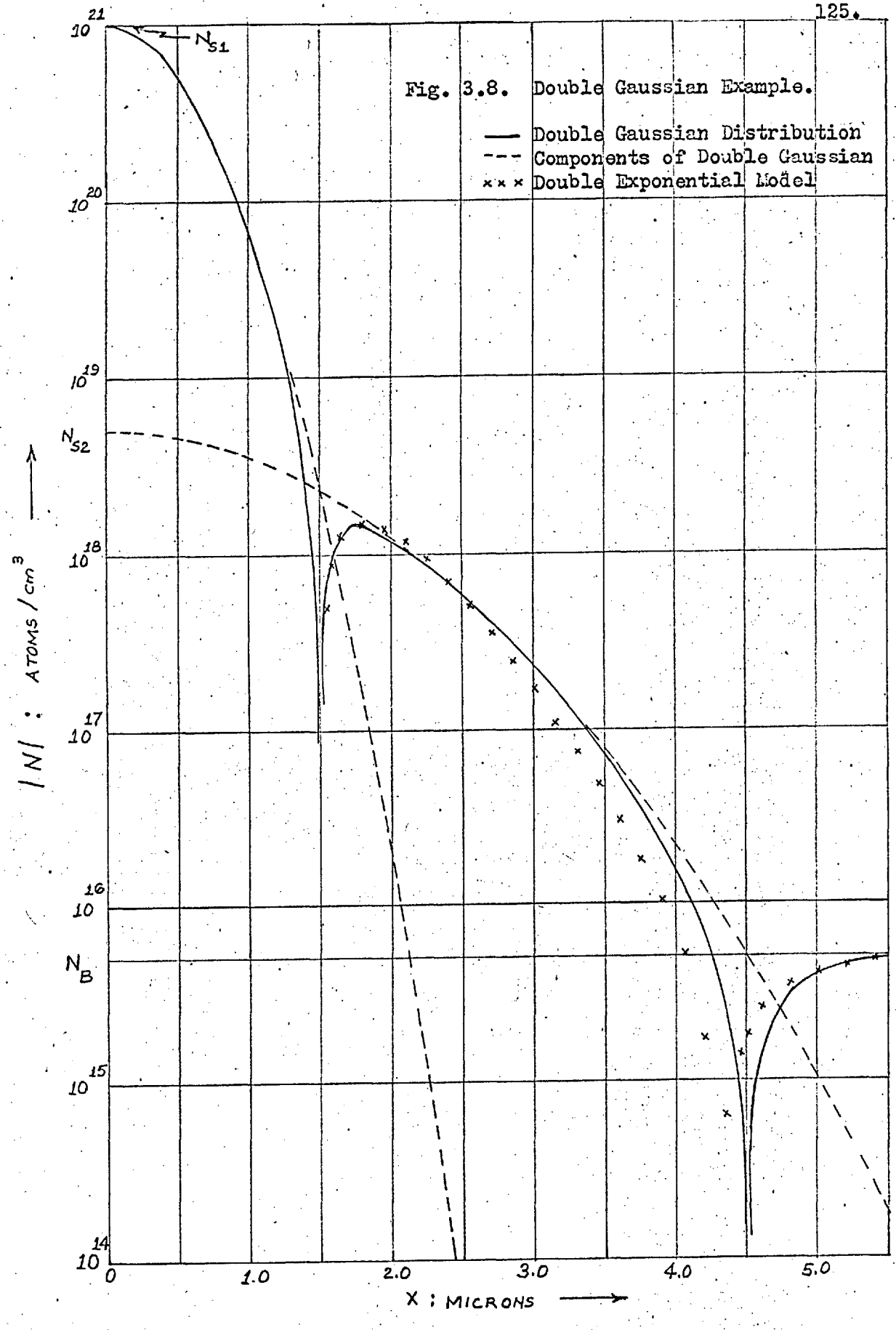
$$N(x) = 5 \times 10^{18} e^{-\frac{x^2}{2.934 \times 10^{-8}}} - 10^{21} e^{-\frac{x^2}{3.908 \times 10^{-9}}} - 5 \times 10^{15} \quad 3.3.17$$

A plot of this distribution is given in Fig. 3.8.

Fig. 3.9 is a plot of depletion layer semi-widths (a_1 and a_2) vs junction voltage for both junctions. At the emitter junction a_{1e} and a_{2e} can be seen to be comparable for low reverse bias, thus indicating that as for the ERFC case the linear approximation is more accurate than the abrupt approximation for this example. At the collector junction the single Gaussian approximation is compared with the double Gaussian and shown to be accurate over a wide range of voltages. Inclusion of the equivalent quantities for the double exponential model (see section 3.5.6) indicates the adequacy of the model in describing junction properties.

Capacitance/area is plotted in Fig. 3.10, and collector capacitance is also plotted in Fig. 3.5. This curve follows the general form of the chart curves, indicating the applicability of such charts to both ERFCs and Gaussians.

Minority carrier densities and base transit time are plotted in Fig. 3.11 and 3.12 respectively, for a range of collector and emitter voltages. The effect of the retarding field region is again obvious.


Fig. 3.8. Double Gaussian Example.
Double Gaussian Distribution
Components of Double Gaussian
Double Exponential Model
N_{S1}
N_{S2}
N_B
10^{21}
10^{20}
10^{19}
10^{18}
10^{17}
10^{16}
10^{15}
10^{14}
|N| : ATOMS / cm^3
0
1.0
2.0
3.0
4.0
5.0
X : MICRONS

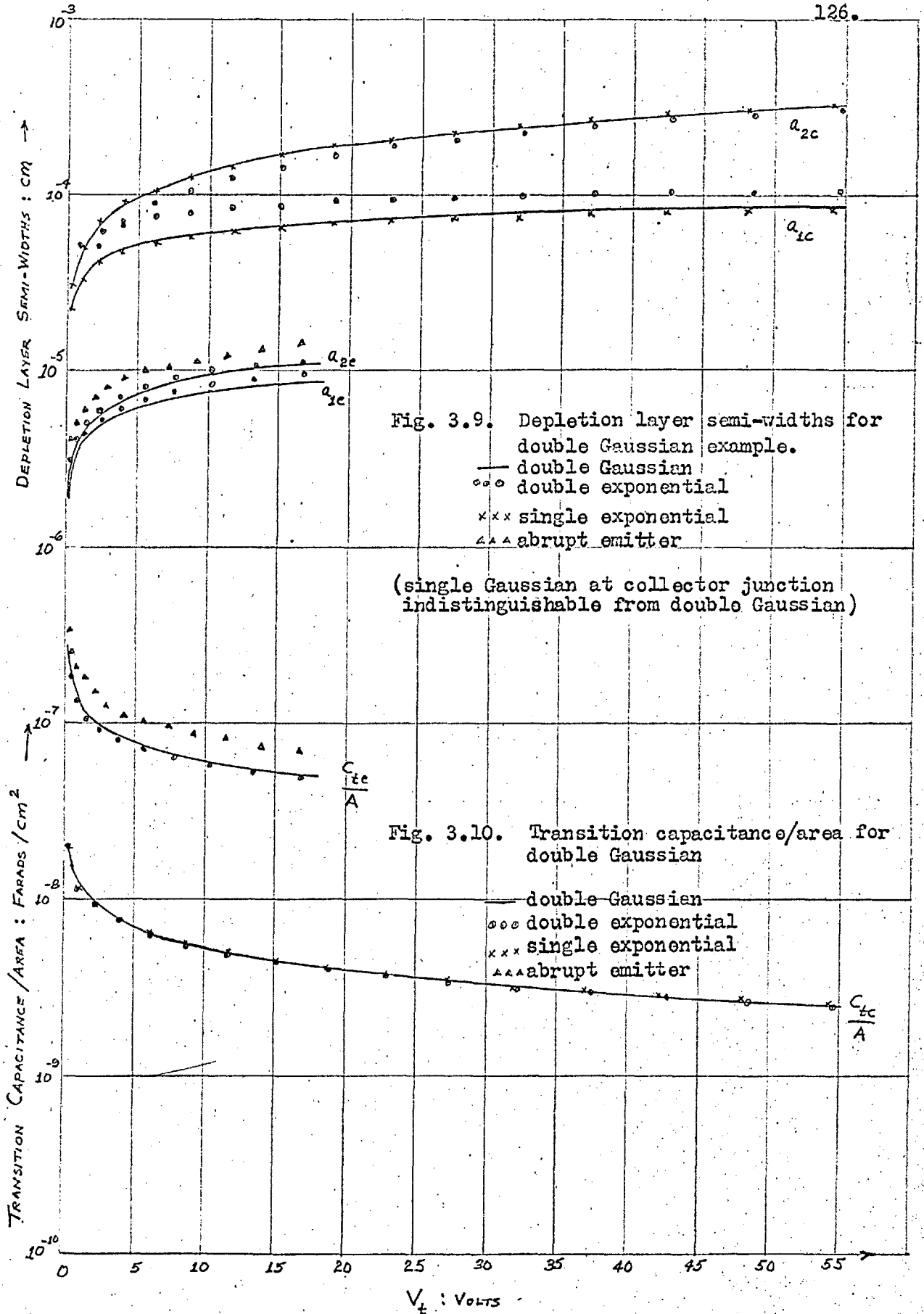


Fig. 3.9. Depletion layer semi-widths for double Gaussian example.
— double Gaussian
ooo double exponential
xxx single exponential
△△△ abrupt emitter

(single Gaussian at collector junction indistinguishable from double Gaussian)

Fig. 3.10. Transition capacitance/area for double Gaussian
— double Gaussian
ooo double exponential
xxx single exponential
△△△ abrupt emitter

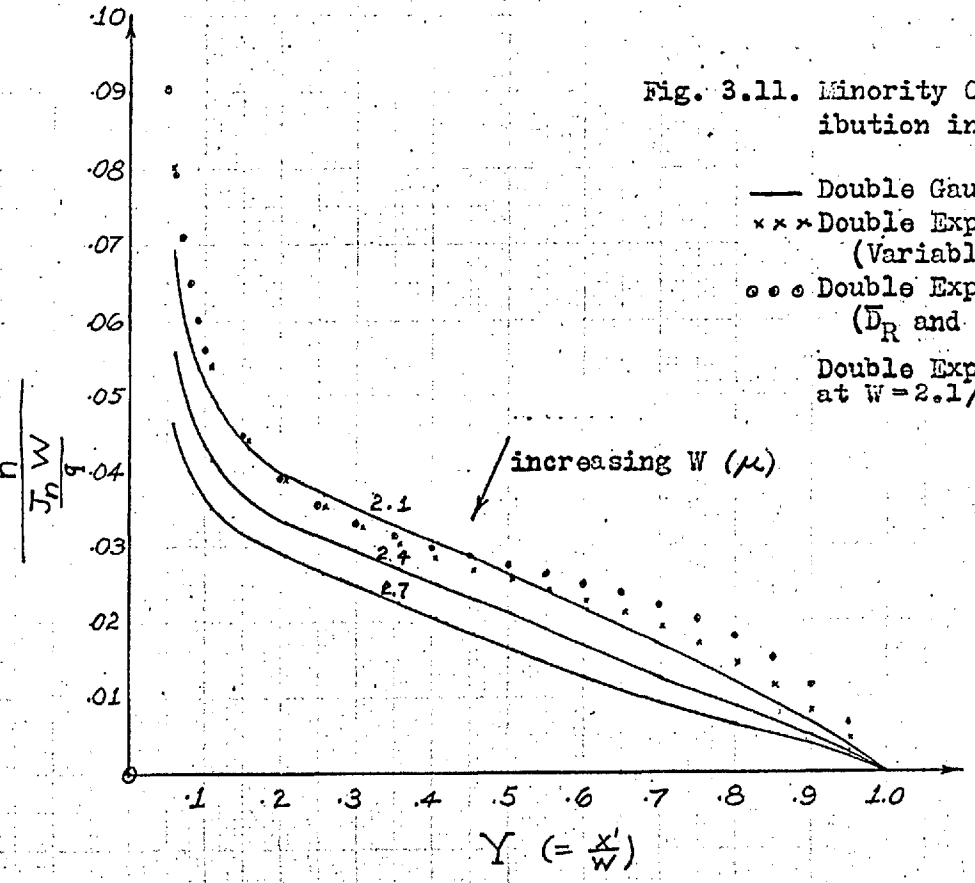


Fig. 3.11. Minority Carrier Distribution in Base.

—— Double Gaussian
× × × Double Exponential (Variable D_n)
o o o Double Exponential ($\bar{D}_R$ and $\bar{D}_A$ Approximation)

Double Exponential Plotted at W = 2.1 μ

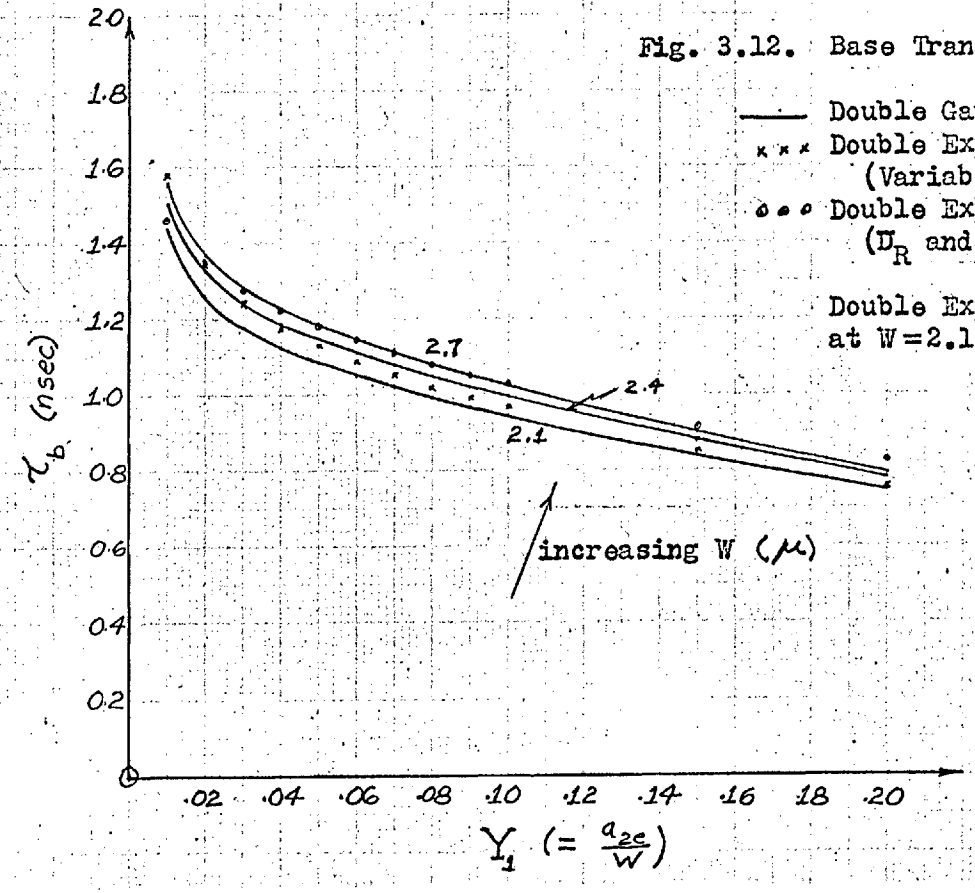


Fig. 3.12. Base Transit Time.

—— Double Gaussian
× × × Double Exponential (Variable D_n)
o o o Double Exponential ($\bar{D}_R$ and $\bar{D}_A$ Approximation)

Double Exponential Plotted at W = 2.1 μ

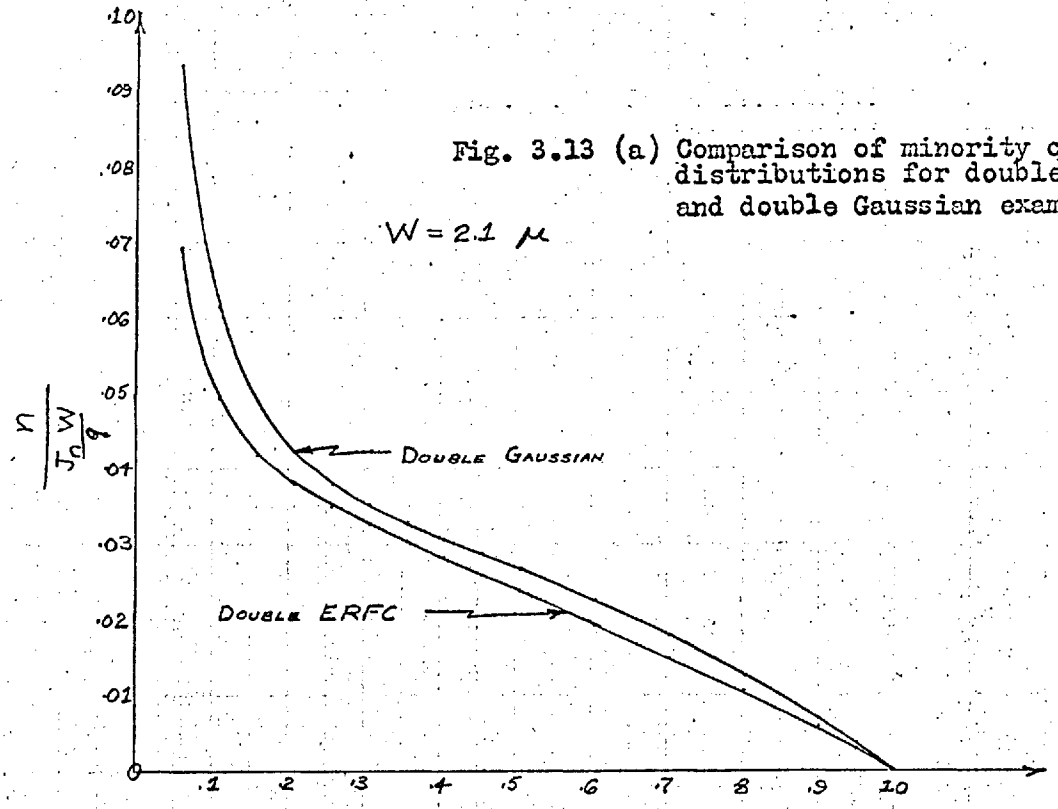


Fig. 3.13 (a) Comparison of minority carrier distributions for double ERFC and double Gaussian examples.

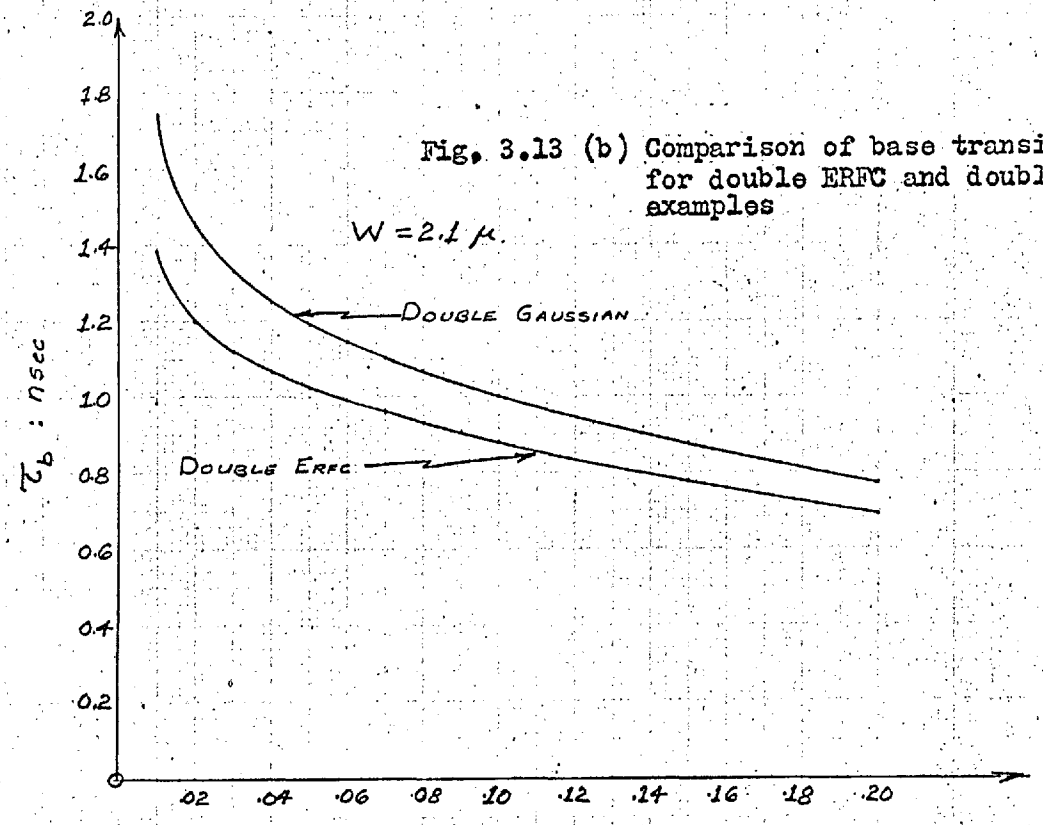


Fig. 3.13 (b) Comparison of base transit times for double ERFC and double Gaussian examples

Fig. 3.13 shows a comparison of minority carrier densities and base transit times respectively for the double ERFC and double Gaussian distributions at one value of collector voltage.

3.4 Planar Epitaxial Transistor

3.4.1 Collector Substrate

When a high resistivity epitaxial layer is grown on a low resistivity substrate, diffusion occurs from the substrate into the epitaxial layer. Further diffusion occurs when the planar process is used to form a transitor in the epitaxial layer. The initially sharp transition at the substrate interface becomes a gradual transistion in the completed device. The distributions representing this interface were presented in Chapter 2 (Section 2.3.4). In addition to the diffused nature of the substrate interface doping in the epitaxial layer decreases gradually from the interface. This decrease was shown in Section 2.3.4 to be exponential in nature. Since, however, this variation in doping in the body of the epitaxial layer is so gradual it will be neglected here and the epitaxial layer assumed to have a background concentration N_B, upon which is superimposed the two surface diffusions and the substrate diffusion.

The epitaxial transistor is represented in Fig. 3.14 (specific case). The position of the initial substrate interface ($x = x_s$) imparts a discontinuity in the impurity distribution N(x). Thus, up to the interface ($0 \leq x \leq x_s$):

$$N(x) = - N_1(x) + N_2(x) - N_B - \tfrac{1}{2} N_C \operatorname{erfc} \frac{x_s - x}{\sqrt{4 D_3 t_3}} \qquad 3.4.1$$

where $N_1(x)$ and $N_2(x)$ are emitter and base diffusion respectively (either ERFC or Gaussian), N_C is the initial substrate doping, D_s is the diffusion coefficient of the substrate impurity and t_s is the diffusion time for this impurity.*

When $x > x_S$ impurity distribution is given by:

$$N(x) \approx - N_B - \frac{N_C}{2} \left(1 + \text{erf} \frac{x - x_S}{\sqrt{4D_s t_s}}\right) \qquad 3.4.2(a)$$

where the error function was defined in Section 3.2.1. Eqn. 3.4.2(a) may also be stated as:

$$N(x) = - N_B - \frac{N_C}{2} \left(2 - \text{erfc} \frac{x - x_S}{\sqrt{4D_s t_s}}\right) \qquad 3.4.2(b)$$

Depending upon the element used as the substrate impurity, D_s may be equal to either D_1 or D_2, or entirely different, and t_s is usually greater than t_2. If, however, epitaxial growth is carried out for a limited time at a substantially lower temperature than that used in the planar diffusion process, t_s may be approximately equal to t_2. This condition will be assumed for the representative example of Section 3.4.4. From eqn. 3.4.2 it can be seen that $N(x) \approx N_C$ deep into the substrate (theoretically at $x = \infty$) since $N_C \gg N_B$.

3.4.2 Extensions to Junction Equations

The presence of diffusion from the substrate considerably complicates the impurity distribution in the epitaxial layer. For the

---

* Strictly, N_C in the expressions of this Section should be replaced by $N_C - N_B$ but, since $N_C \gg N_B$, N_B has been neglected with respect to N_C throughout the treatment of the epitaxial transistor.

simplest case where $x_s \gg x_c$, this diffusion should have negligible effect on the transistor region of the wafer. At the other extreme, $x_c \approx x_s$, and collector junction position is determined by the substrate diffusion, i.e. $N_a(x_c) = N_s(x_c)$ where $N_s(x_c)$ represents the value of substrate diffusion at the collector junction. If the base width is large, substrate diffusion is likely to have negligible effect at the emitter junction and over most of the base region. The average case would seem to be where x_s is sufficiently greater than x_c for substrate diffusion to play a large, though not necessarily the whole, part in defining the position of the collector juntion and to have minor effect at the emitter junction and throughout the effective base width.

For completeness the effect of the substrate diffusion must be included at the emitter junction (if it can be neglected the equations of Sections 3.2.2 and 3.3.2 completely define the emitter junction characteristics). The following treatment will be, however, limited to the collector junction, but may be extended to the emitter junction by substituting x_e for x_c in Case A.

The discontinuity at the substrate interface necessitates solution of Poisson's equation in three stages to the right of the junction.

A. when $x_c + a_{ac} \leq x_s$,

B. when $x_c + a_{ac} > x_s$ and $x_s < x \leq x_c + a_{ac}$,

C. when $x < x_s < x_c + a_{ac}$.

Case A only can apply to the emitter junction.

To the left of the junction (base side) impurity distribution is

given by eqn. 3.4.1. The first three terms of this equation have been considered in detail in sections 3.2.2 and 3.3.2 for the double ERFC and double Gaussian distributions respectively, so only the final term need be considered here. Thus

$$E_1(x)\Big|_{N(x)\,=\,N_3(x)} = \frac{q}{\varepsilon}\,\frac{N_c}{2}\,[F_1(x_s - x, x_s - (x_c - a_{1c}), D_3 t_3] \qquad 3.4.3$$

where the function F_1 was defined in eqn. 3.2.11. For the purposes of eqn. 3.4.3, v and ϕ of the original function are replaced by $x_s - x$ and $x_s - (x_c - a_{1c})$ respectively and ζ by $D_3 t_3$. Eqn. 3.4.3 applies irrespective of the position of $x_c + a_{2c}$. Voltage to the left of the junction is determined by integrating $E_1(x)$ as in eqn. 3.2.8(a). Thus

$$V_1\Big|_{N(x)\,=\,N_3(x)} = \frac{q}{\varepsilon}\,\frac{N_c}{2}\,[F_2\,(x_s - x_c, D_3 t_3, x_s - (x_c - a_{1c})] \qquad 3.4.4$$

where F_2 was defined in eqn. 3.2.17. Eqn. 3.4.4 is added to either eqn. 3.2.15 or 3.3.6 to determine total voltage to the left of the junction for the double ERFC or double Gaussian respectively.

CASE A. $(x_c + a_{2c} \leq x_s)$. For this case, the impurity distribution to the right of the junction is given by eqn.3.4.1. Thus the additions to $E_2(x)$ and V_2 of Sections 3.2.2 and 3.3.2 are symmetrical with eqns. 3.4.3 and 3.4.4. Thus:

$$E_2(x)\Big|_{N(x)\,=\,N_3(x)} = \frac{q}{\varepsilon}\,\frac{N_c}{2}\,[F_1(x_s - x, x_s - (x_c + a_{2c}), D_3 t_3)] \qquad 3.4.5$$

and

$$V_2\Big|_{N(x) = N_3(x)} = -\frac{q}{\varepsilon}\,\frac{N_C}{2}\,F_2(x_S - x, D_3t_3, x_S - (x_C + a_{2C})) \qquad 3.4.6$$

Eqns. 3.4.5 and 3.4.6 are added to the expressions for $E_2(x)$ and V_2 in either Section 3.2.2 or 3.3.2 to get the total values of $E_1(x)$ and V_1.

As in Section 3.2.2 and 3.3.2 an expression may be found relating a_{1C} and a_{2C} by equating $E_1(x_C)$ and $E_2(x_C)$. The additional terms introduced by the substrate diffusion are found by subtracting eqn. 3.4.3 from 3.4.5. Thus, the following expression is added to the left side of either eqn. 3.2.14 or 3.3.5:

$$\frac{N_C}{2N_{S2}}\left[F_1(x_S - x_C, x_S - (x_C + a_{2C}), D_3t_3) - F_1(x_S - x_C, x_S - (x_C - a_{1C}), D_3t_3)\right]$$

which on performing the subtraction becomes:

$$\frac{N_C}{2N_{S2}}\left[F_1(x_S - (x_C - a_{1C}), x_S - (x_C + a_{2C}), D_3t_3)\right]$$

The additional term to be added to the total voltage across the junction is found by adding eqns. 3.4.4 and 3.4.5. Thus, the part of V_t due to the substrate diffusion is:

$$V_t\Big|_{N(x) = N_3(x)} = -\frac{q}{\varepsilon}\,\frac{N_C}{2}\left[F_2(x_S - x_C, D_3t_3, x_S - (x_C + a_{2C})) - F_2(x_S - x_C, D_3t_3, x_S - (x_C - a_{1C}))\right]$$

$$= -\frac{q}{\varepsilon}\,\frac{N_C}{2}\left[F_3(x_S - x_C, D_3t_3, -a_{1C}, -a_{2C})\right] \qquad 3.4.7$$

This expression is added to the right hand side of either eqn. 3.2.19 or 3.3.9 if the planar structure is double ERFC or double Gaussian

respectively. It can also be used at the emitter junction with x_e being substituted for x_c.

CASE B. $x_c + a_{2c} > x_s$; $x_s \leq x \leq x_c + a_{2c}$. This case is certainly applicable only to the collector junction. Over the region of interest, impurity density is given by eqn. 3.4.2. The electric field in this region is given by:

$$E_2(x)\Big|_{x>x_s} = \frac{q}{\varepsilon}\left[-(N_B + N_C)\left\{x - (x_c + a_{2c})\right\} + \frac{N_c}{2}F_1(x - x_s, x_c + a_{2c} - x_s, D_3t_3)\right] \qquad 3.4.8$$

where F_1 is defined in eqn. 3.2.11.

Voltage across this region is found by integrating eqn. 3.4.8 between x_s and $x_c + a_{2c}$. Thus

$$V_2\Big|_{\substack{\text{Beyond}\\ \text{Interface}}} = \frac{q}{\varepsilon}\left[-\frac{(N_B + N_C)}{2}(x_c + a_{2c} - x_s)^2 - \frac{N_c}{2}\left\{(D_3t_3 - \frac{(x_c + a_{2c} - x_s)^2}{2})\right.\right.$$
$$\left.\left.\operatorname{erfc}\frac{x_c + a_{2c} - x_s}{\sqrt{4D_3t_3}} - D_3t_3 + \sqrt{\frac{D_3t_3}{\pi}}(x_c + a_{2c} - x_s)e^{-\frac{(x_c + a_{2c} - x_s)^2}{4D_3t_3}}\right\}\right] \qquad 3.4.9$$

Total voltage across the collector junction will include this effect in Case C.

CASE C. $x < x_s < x_c + a_{2c}$. $E_1(x)$ and V_1 are determined as for eqns. 3.4.3 and 3.4.4. $E_2(x)$ now includes the total value of E_2 as determined from eqn. 3.4.8 when $x = x_s$ plus the value from eqn. 3.4.5 in addition to the expressions of either Section 3.2.2 or 3.3.2. Since N_B applies over the whole transistor it was included in these sections and does not constitute an addition. Thus the total addition due to the presence of the substrate is:

$$E_2(x)\Big|_{subs} = \frac{q}{\varepsilon}\,\frac{N_C}{2}\left[F_1(x_S - x, x_S - x_S, D_3 t_3) + F_1(x_S - x_S, x_C + a_{2C} - x_S, D_3 t_3) - 2(x_S - (x_C + a_{2C}))\right] \qquad 3.4.10$$

where x_S has been substituted for $x_C + a_{2C}$ in eqn. 3.4.5 and $x = x_S$ in 3.4.10. Substituting the values of F_1 and simplifying yields

$$E_2(x)\Big|_{subs} = \frac{q}{\varepsilon}\left[-N_C(x_S - (x_C + a_{2C})) + \frac{N_C}{2}\{F_1(x_S - x, x_C + a_{2C} - x_S, D_3 t_3)\}\right] \qquad 3.4.11$$

The total value of $E_2(x)$ is found by adding eqn. 3.4.11 to either eqn. 3.2.12 or 3.3.3 depending on whether base and emitter diffusions are ERFCs or Gaussians.

A relationship between a_{1C} and a_{2C} may be determined by adding the effect at $x = x_C$ of the substrate diffusion terms to either eqn. 3.2.14 or 3.3.5. The addition thus becomes:

$$-\frac{N_C}{N_{S2}}(x_S - (x_C + a_{2C})) + \frac{N_C}{2N_{S2}}\{F_1(x_S - x_C, x_C + a_{2C} - x_S, D_3 t_3) - F_1(x_S - x_C, x_S - (x_C - a_{1C}), D_3 t_3)\}$$

When cancellation of equivalent terms is carried out, the expression becomes:

$$-\frac{N_C}{N_{S2}}(x_S - (x_C + a_{2C})) + \frac{N_C}{2N_{S2}}F_1(x_S - (x_C - a_{1C}), x_C + a_{2C} - x_S, D_3 t_3)$$

This is added to the left side of either eqn. 3.2.14 or 3.3.5 to give the total relationship between a_{1C} and a_{2C}. N_{S2} appears in the above expression to correspond with the factoring out of N_{S2} from the total equation and removal of $\frac{q}{\varepsilon}\,N_{S2}$. (See eqns. 3.2.14 and 3.3.5).

Voltage to the right of the collector junction for Case C is equal to that of either eqn. 3.2.11 or 3.3.7 plus the addition of 3.4.9 and 3.4.6 ($x_c + a_{c} = x_s$). Thus the addition due to 3.4.9 and 3.4.6 is:

$$V_2\Big|_{subs} = \frac{q}{\varepsilon}\left[-\frac{N_c}{2}(x_c + a_{2c} - x_s)^2 - \frac{N_c}{2}\left\{F_2(x_s - x_c, D_3 t_3, x_s - x_s)\right.\right.$$
$$+ (D_3 t_3 - \frac{(x_c + a_{2c} - x_s)^2}{2})\,\mathrm{erfc}\,\frac{x_c + a_{2c} - x_s}{\sqrt{4D_3 t_3}} - D_3 t_3 + \sqrt{\frac{D_3 t_3}{\pi}}$$
$$\left.\left.(x_c + a_{2c} - x_s)e^{-\frac{(x_c + a_{2c} - x_s)^2}{4D_3 t_3}}\right\}\right] \qquad 3.4.12$$

No simple expression based on the functions defined earlier is applicable to eqn. 3.4.12.

The total additions as a result of the substrate to the equation giving junction voltage is:

$$V_{t3}\Big|_{subs} = \frac{q}{\varepsilon}\,\frac{N_c}{2}\left[-(x_c + a_{2c} - x_s)^2 - \left\{F_2(x_s - x_c, D_3 t_3, x_s - x_s) F_2(x_s - x_c, D_3 t_3, x_s - (x_c - a_{1c}))\right.\right.$$
$$+ (D_3 t_3 - \frac{(x_c + a_{2c} - x_s)^2}{2})\,\mathrm{erfc}\,\frac{x_c + a_{2c} - x_s}{\sqrt{4D_3 t_3}} - D_3 t_3$$
$$\left.\left. + \sqrt{\frac{D_3 t_3}{\pi}}\,(x_c + a_{2c} - x_s)\,e^{-\frac{(x_c + a_{2c} - x_s)^2}{4D_3 t_3}}\right\}\right] \qquad 3.4.13$$

With the values of F_2 substituted, the equation becomes

$$V_{t_3}\Big|_{subs} = \frac{q}{\varepsilon}\frac{N_c}{2}\left[-(x_c + a_{2c} - x_s)^2 - \left\{(D_3t_3 + \frac{(x_s - x_c)^2}{2} - \frac{a_{1c}^2}{2})\,\mathrm{erfc}\,\frac{(x_s - x_c) + a_{1c}}{\sqrt{4D_3t_3}} - 2D_3t_3 + (D_3t_3 - \frac{(x_c + a_{2c} - x_s)^2}{2})\mathrm{erfc}\,\frac{x_c + a_{2c} - x_s}{\sqrt{4D_3t_3}}\right.\right.$$
$$\left.\left. + \sqrt{\frac{D_3t_3}{\pi}}\left(2(x_s - x_c) + (x_c + a_{2c} - x_s)\,e^{-\frac{(x_c + a_{2c} - x_s)^2}{4D_3t_3}} - (x_s - x_c - a_{1c})\right.\right.\right.$$
$$\left.\left.\left. e^{-\frac{(x_s - (x_c - a_{1c})^2}{4D_3t_3}}\right)\right\}\right] \qquad 3.4.13a$$

Unfortunately, none of the functions defined earlier fits this expression.

The previous equations are used in conjunction with the equation for either the double ERFC distribution or the double Gaussian distribution.

3.4.3 Base Region Properties: Normally it should be possible to neglect the effect of the substrate on minority carrier density and base transit time. However, if x_s is only marginally greater than x_c, the substrate diffusion may have considerable effect on these quantities. Minority carrier density would be given by:

$$n = -\frac{J_n}{q}\,\frac{1}{\left\{-N_1(x) + N_2(x) - N_B - \frac{N_c}{2}\,\mathrm{erfc}\,\frac{x_s - x}{\sqrt{4D_3t_3}}\right\}}$$
$$\int_x^{x_e=W} \frac{\left\{(-N_1(x) + N_2(x) - N_B - \frac{N_c}{2}\,\mathrm{erfc}\,\frac{x_s - x}{\sqrt{4D_3t_3}}\right\}dx}{D_n\,(N_1(x) + N_2(x) + N_B + \frac{N_c}{2}\,\mathrm{erfc}\,\frac{x_s - x}{\sqrt{4D_3t_3}})}\Bigg|_{x>x_e} \qquad 3.4.14$$

and base transit time results from:

$$\tau_b = \int_{x_e + a_{2e}}^{x_e + W} \frac{1}{-N_1(x) + N_2(x) - N_B - \frac{N_C}{2}\,\mathrm{erfc}\,\frac{x_s - x}{\sqrt{4D_3 t_3}}} \int_{x}^{x_e + W} \frac{\left(-N_1(x) + N_2(x) - N_B - \frac{N_C}{2}\,\mathrm{erfc}\,\frac{x_s - x}{\sqrt{4D_3 t_3}}\right)}{D_n\left(N_1(x) + N_2(x) + N_B + \frac{N_C}{2}\,\mathrm{erfc}\,\frac{x_s - x}{\sqrt{4D_3 t_3}}\right)}\,dx^2 \Bigg|_{x > x_e} \qquad 3.4.15$$

$N_1(x)$ and $N_2(x)$ may be either ERFC or Gaussian distributions.

3.4.4 Representative Example

The major purpose of a highly-doped substrate layer in a planar epitaxial transistor is to reduce the collector body resistance r'_{cc}. To achieve this most effectively the substrate interface should be positioned so that the edge of the collector depletion region penetrates into the substrate region, or at least into the substrate diffusion, at normal values of collector reverse voltage. However, the substrate diffusion should exert little influence at the actual collector junction, which is ideally formed at the position where the concentration of the base diffusion is equal to the background impurity concentration. Such conditions will allow for a wide collector depletion layer at low voltage, hence low transition capacitance and low $r'_{cc}\,C_{tc}$ time constant. The choice of the substrate impurity is most important. It is obvious that a rapidly diffusing element such as phosphorus can not be used since, for x_s only slightly greater than x_c and $N_C \gg N_B$, sufficient diffusion would

occur for the collector junction to be formed where the concentrations of base and substrate diffusions are equal ($\gg N_B$ at x_c). Although this would result in low r'_{cc}, C_{tc} would be large since the collector depletion layer would be narrow. Therefore an impurity element with a low diffusion coefficient must be used in the substrate. Arsenic was chosen in the following example.

To the examples used earlier in Sections 3.2.5 and 3.3.5 a substrate layer was added at 8 microns. The physical constants of the device are:

$N_{S1} = 1 \times 10^{21}$ atoms/cc. $\quad D_1 = D_2 = 3.4 \times 10^{-13}$ cm^2/sec.

$N_{S2} = 5 \times 10^{18}$ atoms/cc. $\quad D_3 = 3.1 \times 10^{-14}$ cm^2/sec.

$N_B = 5 \times 10^{15}$ atoms/cc. $\quad x_e = 1.5$ microns

$N_C = 5 \times 10^{18}$ atoms/cc. $\quad x_c = 4.5$ microns

Temperature = 1100°C $\quad x_s = 8.0$ microns

Assuming $t_3 = t_2$, a recalculation of t_1 and t_2 indicated that for this example the substrate diffusion had negligible effect at the collector junction when the emitter and base diffusions were (a) double ERFCs or (b) double Gaussians. Thus:

(a) for the <u>double ERFC case</u>: $t_1 = 54$ mins.

$t_2 = t_3 = 7$ hr. 38 mins.

$$N(x)\Big|_{x<x_s} = 5 \times 10^{18}\,\mathrm{erfc}\,\frac{x}{1.934 \times 10^{-4}} - 10^{21}\,\mathrm{erfc}\,\frac{x}{6.62 \times 10^{-5}}$$

$$- 5 \times 10^{15} - 2.5 \times 10^{18}\,\mathrm{erfc}\,\frac{8 \times 10^{-4} - x}{5.84 \times 10^{-5}} \qquad 3.4.16$$

and

$$N(x)\Big|_{x > x_s} \approx -5 \times 10^{15} - 2.5 \times 10^{18}\ \text{erfc}\ \frac{x - 8 \times 10^{-4}}{5.84 \times 10^{-5}} \qquad 3.4.17$$

(b) while for the double Gaussian case: $t_1 =$ 45 min. 30 sec.

$t_2 = t_3 =$ 5 hr. 59 min.

$$N(x)\Big|_{x < x_s} = 5 \times 10^{18} e^{-\frac{x^2}{2.934 \times 10^{-8}}} - 10^{21} e^{-\frac{x^2}{3.91 \times 10^{-9}}} - 5 \times 10^{15} - 2.5 \times 10^{18}\ \text{erfc}\ \frac{8 \times 10^{-4} - x}{6.35 \times 10^{-5}} \qquad 3.4.18$$

and

$$N(x)\Big|_{x > x_s} \approx -5 \times 10^{15} - 2.5 \times 10^{18}\ \text{erfc}\ \frac{x - 8 \times 10^{-4}}{6.35 \times 10^{-5}} \qquad 3.4.19$$

(x is in cm.)

The impurity distributions of eqns. 3.4.16 and 3.4.17 are plotted in Fig. 3.14, while those of eqns. 3.4.18 and 3.4.19 are plotted in Fig. 3.15. From these figures it is evident that the substrate diffusion has negligible effect until $x \simeq 6.5$ microns. Also shown is the double exponential model adopted later to represent the base region (Section 3.4) with an abrupt interface indicated at $x_s = 8$ microns. To indicate the effect of using phosphorous as the substrate impurity ($D_1 = D_2 = D_3$), the broken curves of both figures were computed. It is obvious from these curves that unless $x_s \gg x_c$ the desired degree of abruptness can not be obtained at the substrate interface when a rapidly diffusing element such as phosphorous is used in the substrate.

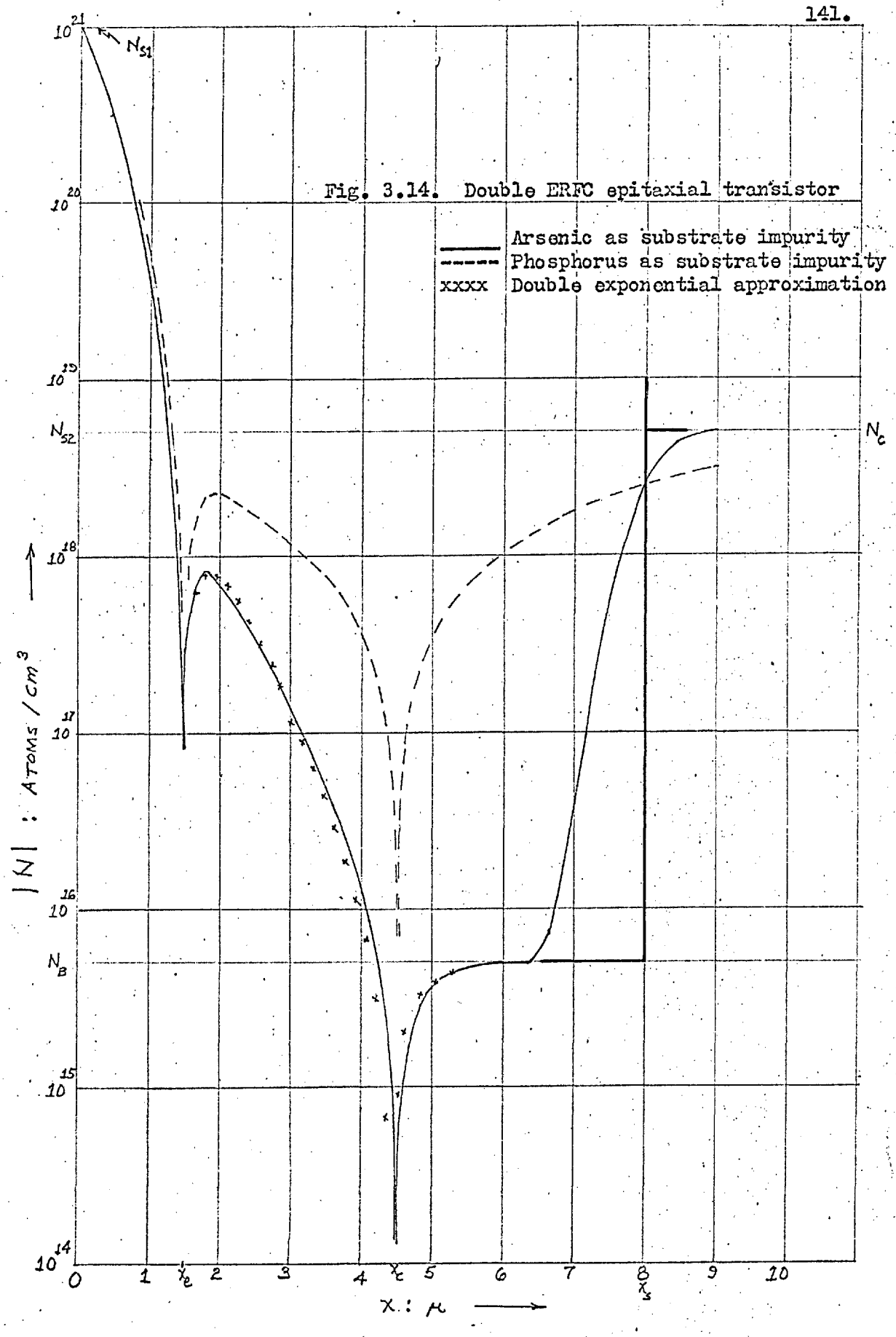


Fig. 3.14. Double ERFC epitaxial transistor

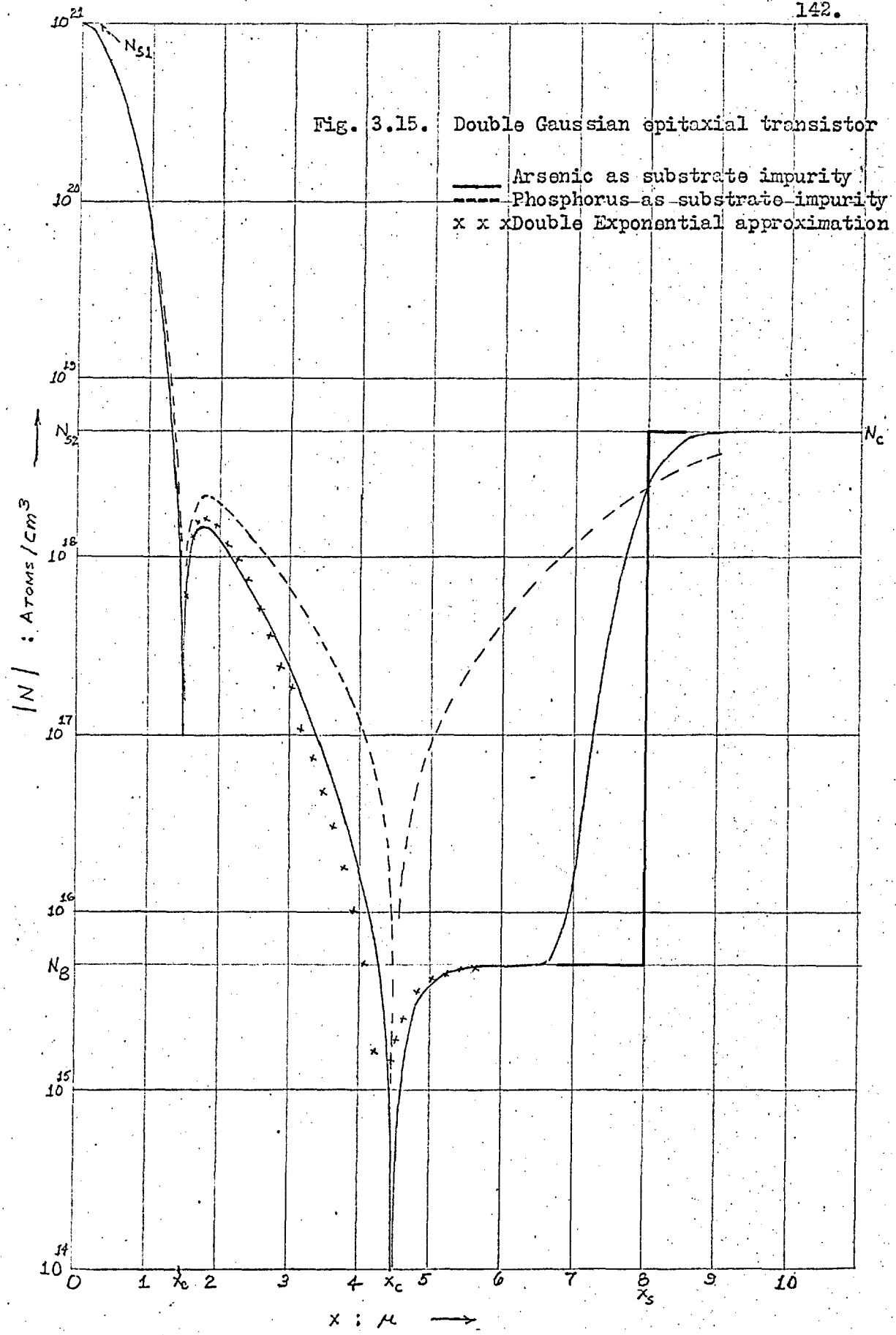


Fig. 3.15. Double Gaussian epitaxial transistor

——— Arsenic as substrate impurity
– – – – Phosphorus as substrate impurity
x x x Double Exponential approximation

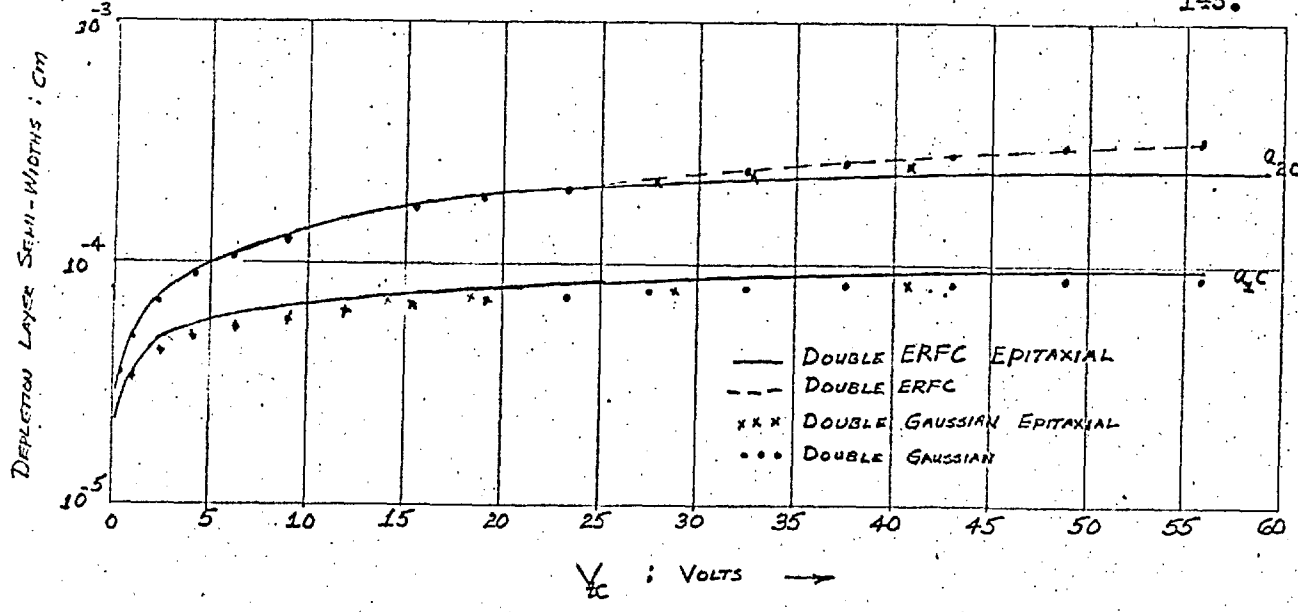


Fig. 3.16. Collector depletion layer semi-widths for epitaxial examples.

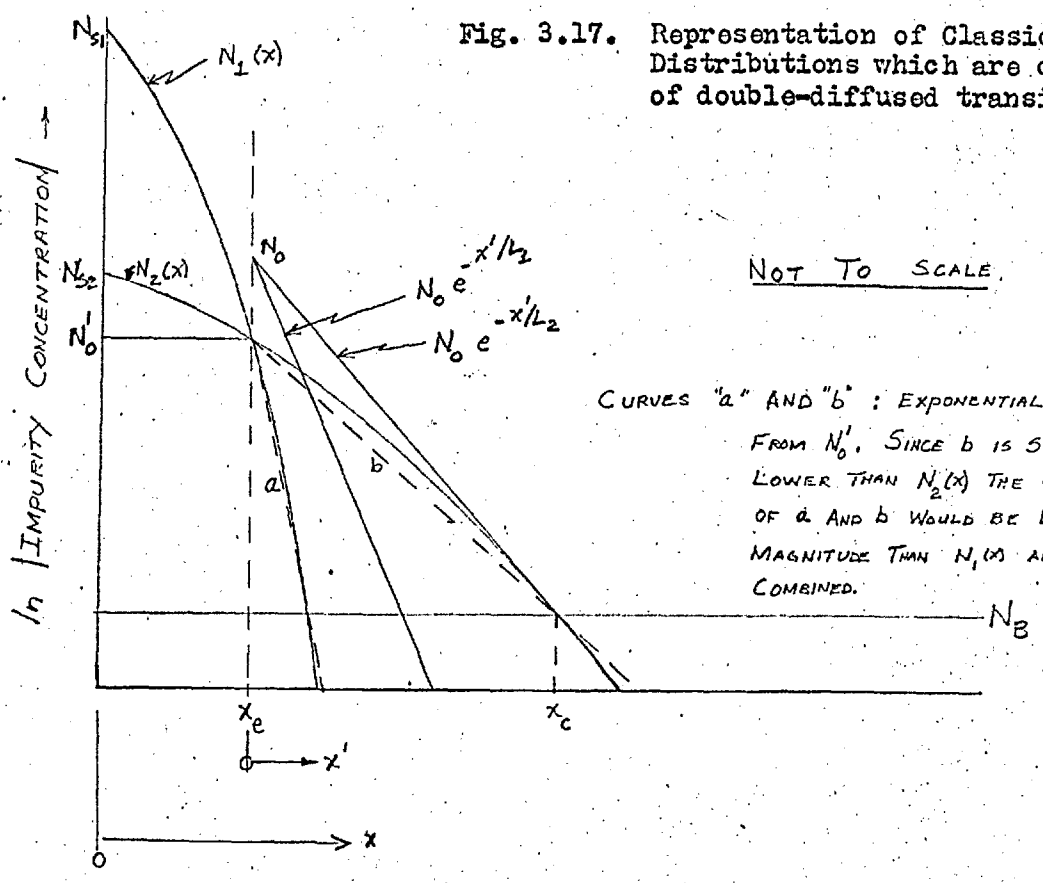


Fig. 3.17. Representation of Classical Distributions which are components of double-diffused transistor.

Not To Scale.

Curves "a" and "b" : Exponentials falling from N_0'. Since b is substantially lower than $N_2(x)$ the combination of a and b would be lower in magnitude than $N_1(x)$ and $N_2(x)$ combined.

Depletion layer semi-widths for the collector junction are plotted in Fig. 3.16 for both the ERFC and Gaussian examples. Comparison with the equivalent curves in the absence of a substrate layer (also plotted in Fig. 3.16) indicates that the effect of the substrate layer is not felt until the collector depletion layer is quite wide (reverse voltage is high). The effect then is to cause a reduction in the semi-width (a_{2C}) on the collector side of the junction at a given voltage, and a reduction in the total depletion layer width. Collector transition capacitance ($C_{tc} = \frac{\varepsilon A_c}{a_{1C} + a_{2C}}$) is somewhat increased, but this is not serious since the effect does not occur until $V_c > 20$ volts.

Since the substrate diffusion has negligible effect in the base region and at the emitter junction, it is unnecessary to include curves of emitter depletion layer semi-widths or minority carrier density and base transit time. These are already given in Sections 3.2.5 and 3.3.5.

3.5 Double Exponential Model to Approximate Base

3.5.1 Justification of the Model and Choice of Exponentials

In Chapter 2, Sections 2.2.2 and 2.2.3 it was shown that a classical distribution such as an ERFC or a Gaussian, which has fallen below 10^{-3} of its initial value may be closely approximated by an exponential. Since the 'uncompensated' base impurity profile of a double-diffused transistor is theoretically the difference of two ERFCs or Gaussians which have fallen substantially below their surface values, this suggests a representative model which is the difference of two exponentials.

The two classical distributions which form a double-diffused transistor are representated in Fig. 3.17. If N_B is low it is usually possible to represent the emitter junction as occuring at the point where $N_1(x_e) = N_2(x_e)$, where the subscripts "1" and "2" refer to the emitter and base diffusions respectively. Comparison of this value, called N_O' in Fig. 3.17, with the surface concentrations of the two diffusions leads to the following conclusions:

(1) N_O' should be sufficiently lower than N_{S_1} for an exponential to be an accurate representation of $N_1(x)$ beyond x_e;

(2) N_O' is generally not sufficiently less than N_{S_2} for an exponential falling from N_O' to be a particularly accurate representation for $N_2(x)$ beyond x_e [$N_2(x)$ falls gradually from surface concentration N_{S_2}];

(3) $N_2(x)$ should have fallen sufficiently for an exponential to be a good representative in the vicinity of the collector junction.

The choice of the exponentials which make up the model may be based on various considerations, with the guiding precept being that the resultant profile should be an accurate representation of the actual profile. The second of the considerations above precludes the choice of an exponential falling from N_O' at x_e to N_B at x_c to represent the base diffusion (unless base width is small). From Fig. 3.17 it can be seen that such a representation would result in a model in which the number of uncompensated impurities contained in the base would be substantially lower than the actual number. Some other basis for choice of the exponentials must be used.

An important consideration, which can be used as a check on the applicability of the assumed model, is that base region properties such

as transit time, and junction properties predicted by the model closely approximate those for the classical distribution. In Chapters 4 and 5, where an actual model is to be derived for practical devices, the above properties are used in the derivation. One of the most easily measured and most reliable quantities is capacitance vs voltage at the collector junction. As can be seen from Fig. 3.17, $N_1(x)$ should be negligible at the collector junction and $N_2(x)$ should have fallen sufficiently for an exponential to be a good approximation in the vicinity of the collector junction. Such an exponential can be derived from collector capacitance measurements in practical devices. Extending this exponential back to the emitter junction fixes an impurity concentration N_o at x_e which can be taken as the initial value of the exponential. N_o may exceed N_{sz}, but this is unimportant since it is to be cancelled out by an equal initial value for the other exponential to be assumed. The other exponential will be chosen to yield a distribution for which the number of "uncompensated" impurities in the base of the model is equal to the number in the base for the classical device in this chapter or the actual device in Chapter 4. Such an exponential, beginning at an initial value higher than N'_o can not be a direct representation of the emitter diffusion, which in any case can never be measured directly in a practical device.

Calling the characteristic lengths of the two exponentials L_1 and L_2 (where $L_1 < L_2$), the model becomes (See Fig. 3.17):

$$N(x') = N_o \left(e^{-x'/L_2} - e^{-x'/L_1}\right) - N_B \qquad 3.5.1$$

where the origin of the model is the emitter junction ($x' = x - x_e$) and the convention of positive doping in the base is adopted. N_B is the background doping as usual. Defining $\gamma = L_2/L_1$ eqn. 3.5.1 becomes:

$$N(Y) = N_o \left(e^{-m_2 Y} - e^{-\gamma m_2 Y} - \eta\right) \qquad 3.5.2$$

where $\eta = N_B/N_o$, $m_2 = W/L_2$ and $Y = x'/W$. (W is the distance from the emitter junction to the edge of the collector depletion layer).

Assuming $N_1(x_c)$ negligible and $\gamma \geq 2.5$, the slope of the base diffusion $N_2(x)$ may be used at the collector junction to determine L_2 by equating the slope of the exponential to the slope of the classical diffusion. For the exponential the slope is given by:

$$\left.\frac{dN(x')}{dx'}\right|_{x' = x'_c} \approx -\frac{N_o}{L_2} e^{-x'_c/L_2} \qquad 3.5.3$$

$$x'_c = x_c - x_e$$

For the double ERFC distribution;

$$\left.\frac{dN(x)}{dx}\right|_{x = x_c} \approx -N_{s2} \frac{1}{\sqrt{\pi D_2 t_2}} e^{-x_c^2/4D_2 t_2} \qquad 3.5.4$$

Equating eqns.3.5.3 and 3.5.4 and rearranging with N_o replaced by its value in terms of N_B from eqn. 3.5.1 with $e^{-x'_c/L_1}$ neglected:

$$L_2 = \frac{N_B}{N_{s2}} \sqrt{\pi D_2 t_2}\; e^{x_c^2/4D_2 t_2} \qquad 3.5.5$$

The initial value of the exponential N_o can be found from:

$$N_o = N_B e^{x'_c/L_2} \qquad 3.5.6$$

To determine L_1, the areas under the base profiles are equated

for model and for the double ERFC. Integrating eqn. 3.5.1 over the total base width $(x_c - x_e)$ yields the total number of uncompensated impurities contained under the model:

$$N_{tot.}\Big|_{Exp} = N_o \left\{ L_2(1 - e^{-x'_c/L_2}) - L_1(1 - e^{-x'_c/L_1}) - \eta\, x'_c \right\} \qquad 3.5.7$$

The total number of uncompensated impurities contained in the base of a transistor described by a double ERFC profile is given by:

$$N_{tot.}\Big|_{ERFC} = - N_{s1} \left\{ x_c \operatorname{erfc} \frac{x_c}{\sqrt{4D_1 t_1}} - x_e \operatorname{erfc} \frac{x_e}{\sqrt{4D_1 t_1}} - \sqrt{\frac{4D_1 t_1}{\pi}} \left(e^{-x_c^2/4D_1 t_1} - e^{-x_e^2/4D_1 t_1} \right) \right\}$$

$$+ N_{s2} \left\{ x_c \operatorname{erfc} \frac{x_c}{\sqrt{4D_2 t_2}} - x_e \operatorname{erfc} \frac{x_e}{\sqrt{4D_2 t_2}} - \sqrt{\frac{4D_2 t_2}{\pi}} \left(e^{-x_c^2/4D_2 t_2} - e^{-x_e^2/4D_2 t_2} \right) \right\} - N_B (x_c - x_e) \qquad 3.5.8$$

Equating eqns. 3.5.7 and 3.5.8 gives an expression which may be used to determine L_1:

$$N_o L_1 (1 - e^{-x_c'/L_1}) = N_o L_2 (1 - e^{-x_c'/L_2}) + N_{s1} \left\{ x_c \operatorname{erfc} \frac{x_c}{\sqrt{4D_1 t_1}} - x_e \operatorname{erfc} \frac{x_e}{\sqrt{4D_1 t_1}} - \sqrt{\frac{4D_1 t_1}{\pi}} \left(e^{-x_c^2/4D_1 t_1} - e^{-x_e^2/4D_1 t_1} \right) \right\}$$

$$- N_{s2} \left\{ x_c \operatorname{erfc} \frac{x_c}{\sqrt{4D_2 t_2}} - x_e \operatorname{erfc} \frac{x_e}{\sqrt{4D_2 t_2}} - \sqrt{\frac{4D_2 t_2}{\pi}} \left(e^{-x_c^2/4D_2 t_2} - e^{-x_e^2/4D_2 t_2} \right) \right\} \qquad 3.5.9$$

Unfortunately eqn. 3.5.9 can not be solved explicitly for L_1, so an iterative approach must be used.

Similarly, for the double Gaussian:

$$L_2 = \frac{N_B}{N_{S2}} \frac{2D_2t_2}{x_c} e^{x_c^2/4D_2t_2} \qquad 3.5.10$$

N_O may be found from eqn. 3.5.6 and L_1 from:

$$N_OL_1(1 - e^{-x_c'/L_1}) = N_OL_2(1 - e^{-x_c'/L_2}) + N_{S1}\sqrt{\pi D_1t_1}(\text{erfc}\frac{x_e}{\sqrt{4D_1t_1}} - \text{erfc}\frac{x_c}{\sqrt{4D_1t_1}}) - N_{S2}\sqrt{\pi D_2t_2}(\text{erfc}\frac{x_e}{\sqrt{4D_2t_2}} - \text{erfc}\frac{x_c}{\sqrt{4D_2t_2}}) \qquad 3.5.11$$

The above equations apply when $\Upsilon(=L_2/L_1)$ is ≥ 2.5. If this condition does not apply, the effect of L_1 at the collector junction must be included in the determination of L_2. The equations for this case are presented in Appendix A.3. Eqns. 3.5.5 to 3.5.11 were used in Section 3.5.6 to determine the constants of the model to represent the double ERFC and double Gaussian examples of Sections 3.2.5 and 3.3.5 respectively. The double exponentials thus determined were plotted in Figs.3.2 and 3.8.

3.5.2 Collector Junction

Study of the collector junction follows the steps outlined in eqns. 3.2.2 to 3.2.8 with the value of $N(\mathbf{X})$ from eqn. 3.5.2. The relationships derived here are used later (Chapters 4 and 5) as the start of the procedure to derive model parameters for actual devices. Thus:

$$E_{1C}(Y) = \frac{q}{\varepsilon} N_O L_2 \left[(e^{-m_2} - e^{-m_2 Y}) - \frac{1}{\gamma} (e^{-\gamma m_2} - e^{-\gamma m_2 Y}) - \eta m_2 (Y - 1) \right] \quad 3.5.12$$

where $m_2 = W/L_2$, $\gamma = L_2/L_1$, $Y = x'/W$, and $\eta = N_B/N_O$. Similarly,

$$E_{2C}(Y) = \frac{q}{\varepsilon} N_O L_2 \left[(e^{-(m_2 + d_C/L_2)} - e^{-m_2 Y}) - \frac{1}{\gamma} (e^{-(m_2 + d_C/L_2)} - e^{-\gamma m_2 Y}) \right.$$

$$\left. - \eta (m_2 (Y - 1) - d_C/L_2) \right] \quad 3.5.13$$

where $d_C = a_{1C} + a_{2C}$ = total collector depletion layer width.

Although the continuity of field at the junction may be used to get an expression to determine either d_C as a function of W, or a_{1C} as a function of a_{2C}, a similar relationship may be derived by assuming complete charge neutrality over the whole depletion layer, thus:

$$\int_1^{1 + \frac{d_C}{W}} N_O (e^{-m_2 Y} - e^{-\gamma m_2 Y} - \eta) \, dY = 0 \quad 3.5.14$$

Performing this integration and rearranging terms yields:

$$(1 - e^{-d_C/L_2}) - \frac{1}{\gamma} e^{-m_2 (\gamma - 1)} (1 - e^{-\gamma d_C/L_2}) - \eta \frac{d_C}{L_2} e^{m_2} = 0 \quad 3.5.15$$

The voltage across the portion of the depletion layer in the base region is found by integrating eqn. 3.5.12 over a_{1C}. Integrating and rearranging gives:

$$V_{1C} = - \frac{q}{\varepsilon} N_O L_2^2 \left[e^{-m_2} (e^{-a_{1C}/L_2} + \frac{a_{1C}}{L_2} - 1) - \frac{1}{\gamma^2} e^{-\gamma m_2} (e^{-\gamma a_{1C}/L_2} + \gamma \frac{a_{1C}}{L_2} - 1) \right.$$

$$\left. - \tfrac{1}{2} \eta \left(\frac{a_{1C}}{L_2}\right)^2 \right] \quad 3.5.16$$

Similarly, V_{2C} is obtained by integrating eqn. 3.5.13 over a_{2C}:

$$V_{2C} = -\frac{q}{\varepsilon} N_o L_2^2 \left[e^{-m_2} \left\{ \frac{a_{2C}}{L_2} e^{-d_C/L_2} + e^{-d_C/L_2} - e^{-a_{1C}/L_2} \right\} - \frac{e^{-\gamma m_2}}{\gamma^2} \right.$$

$$\left. \left\{ \gamma \frac{a_{2C}}{L_2} e^{-\gamma d_C/L_2} + e^{-\gamma d_C/L_2} - e^{-\gamma a_{1C}/L_2} \right\} + \tfrac{1}{2} \eta \left(\frac{a_{2C}}{L_2} \right)^2 \right] \qquad 3.5.17$$

Total voltage across the junction is given by:

$$V_{tC} = V_{1C} + V_{2C} = -\frac{q}{\varepsilon} N_o L_2^2 \left[e^{-m_2} \left\{ e^{-d_C/L_2} \left(\frac{d_C}{L_2} - \frac{a_{1C}}{L_2} + 1 \right) + \frac{a_{1C}}{L_2} - 1 \right\} \right.$$

$$- \frac{e^{-\gamma m_2}}{\gamma^2} \left\{ e^{-\gamma d_C/L_2} \left(\gamma \frac{d_C}{L_2} - \gamma \frac{a_{1C}}{L_2} + 1 \right) + \gamma \frac{a_{1C}}{L_2} - 1 \right\} + \tfrac{1}{2} \eta \left(\frac{d_C}{L_2} \right)^2$$

$$\left. - \eta \frac{d_C a_{1C}}{L_2^2} \right] \qquad 3.5.18$$

In using the above equations to compute the indicated quantities, the following procedure is suggested: assume d_C/L_2, calculate m_2 from eqn. 3.5.15, a_{1C}/L_2 from $W_b/L_2 - m_2$, hence electric fields and voltage from the pertinent equations (W_b is the physical base width between junctions, $= x'_C = x_C - x_e$). This procedure was adopted in Section 3.5.6 when computing collector properties for the model as applied to the earlier classical examples.

If $\gamma \geq 2.5$ the shallower exponential may be neglected at the collector junction, which then reduces to the familiar single exponential case where:

$$N(Y) = N_o e^{-m_2 Y} - N_B = N_B \left(e^{\frac{W_b}{L_2} - m_2 Y} - 1 \right) \qquad 3.5.19$$

This case was treated in some detail in Chapter 2, Section 2.7.3, for the linear plus exponential model for the base region. The equivalent

expression to eqn. 3.5.15 is:

$$e^{-a_{1C}/L_2} = e^{-\left(\frac{W_b}{L_2} - m_2\right)} = \frac{L_2}{d_C}\left(1 - e^{-d_C/L_2}\right) \qquad 3.5.20$$

This equation may be used to determine a_{1C}/L when d_C/L_2 is known. Electric fields on either side of the junction are given by:

$$E_{1C}(Y) = \frac{q}{\varepsilon} N_B L_2 \left[e^{a_{1C}/L_2}\left(1 - e^{-m_2(Y-1)}\right) - m_2(Y-1)\right] \qquad 3.5.21$$

and

$$E_{2C}(Y) = \frac{q}{\varepsilon} N_B L_2 \left[e^{-a_{2C}/L_2}\left(1 - e^{-\{m_2(1-Y) + d_C/L_2\}}\right) + m_2(1-Y) + \frac{d_C}{L_2}\right] \qquad 3.5.22$$

Voltage across the junction is given by:

$$V_{tc} = -\frac{q}{\varepsilon} N_B L^2 \left[\tfrac{1}{2}\left(\frac{d_C}{L_2}\right) \coth\left(\tfrac{1}{2}\frac{d_C}{L_2}\right) - d_C/L_2\right] \qquad 3.5.23$$

Eqn. 3.5.23 corresponds to eqn. 2.7.15 of Chapter 2.

Expressions are thus available to describe fully the collector depletion layer properties either when both exponentials apply or when one exponential can be neglected near the collector junction.

3.5.3 Emitter Junction

In choosing the model in Section 3.5.1, no attempt was made to equate the gradient of the profile for the model to that of the classical distribution at the emitter junction. Considering that emitter capacitance data can be used in practical devices (see Chapter 4) to determine the impurity gradient at the emitter junction, this might seem to be an oversight. However, when considering the information available for determining the constants of the model in Chapter 4:

viz, collector and emitter capacitances, emitter diode characteristics and base transit time, it will become clear* that when collector capacitance data is used to define the second exponential, only one of the constraints introduced by reliance on either emitter capacitance data or the combination of emitter diode characteristics and base transit time can be adopted. The other constraint must be relaxed. Since the combination of diode characteristics and base transit time yields information on the whole base region, while the emitter capacitance is dependent only on a limited region, it is felt that the former must take precedence. (The constraint introduced by collector capacitance data could equally have been relaxed; however, as classical and actual distributions are close to the assumed exponential form near the collector, leading to the most direct interpretation of measured data in the form of distribution parameters, such data is preferred over emitter capacitance data.)

Relaxing the constraint which would be imposed by reliance on reverse biased emitter transition capacitance data allows the base model to assume a gradient (s_2) appreciably different from that of the classical profile (s_1) at this point - indicated as less steep in Fig. 3.18. Under such conditions the junction properties are somewhat changed; the equilibrium barrier potential for the model takes on a new value, while at a given voltage, the depletion layer semi-width a_{2e} becomes larger (a'_{2e}). Obviously on the emmiter side of the junction, the model must

---

* See also Section 5.3.2.

accommodate this change in a_{2e} by a change in a_{1e}, otherwise the total depletion layer width will change sufficiently that emitter capacitance data for the model will not agree with that for the classical (or actual) distribution. In Fig. 3.18, since $s_2 < s_1$, then the model must rise more steeply in the emitter region than in the base region to allow for a reduction in a_{1e} while still retaining a space charge equal to that on the base side of the junction.

To avoid unnecessary complication of the model by introducing a discontinuity at the emitter junction, the double-exponential will be assumed to apply for an appreciable distance into the emitter region (Fig. 3.18)*. The exponential has the unique property that it can be represented by the same equation for any position of the origin, and both positive and negative values of the position variable. Moreover, since an exponential rises more rapidly than an ERFC or a Gaussian, then with greater distance into the emitter region from the junction, the double-exponential model will increase in magnitude more rapidly than the classical profile, imparting a greater degree of abruptness than was present for the classical profile (which as was concluded from Figs. 3.3 and 3.9 could be represented by a symmetrical-linear junction of gradient s_1 for low reverse bias). This increase in gradient will allow for a reduction of a_{1e} to a'_{1e} for the model in the direction to

---

* Introducing a discontinuity as indicated by the straight line of slope s_3 in Fig. 3.18 has little effect in any case for practical transistors which are operated in forward bias conditions so that a_{1e} and a_{2e} are very small (see Chapter 4, Section 4.2.2).

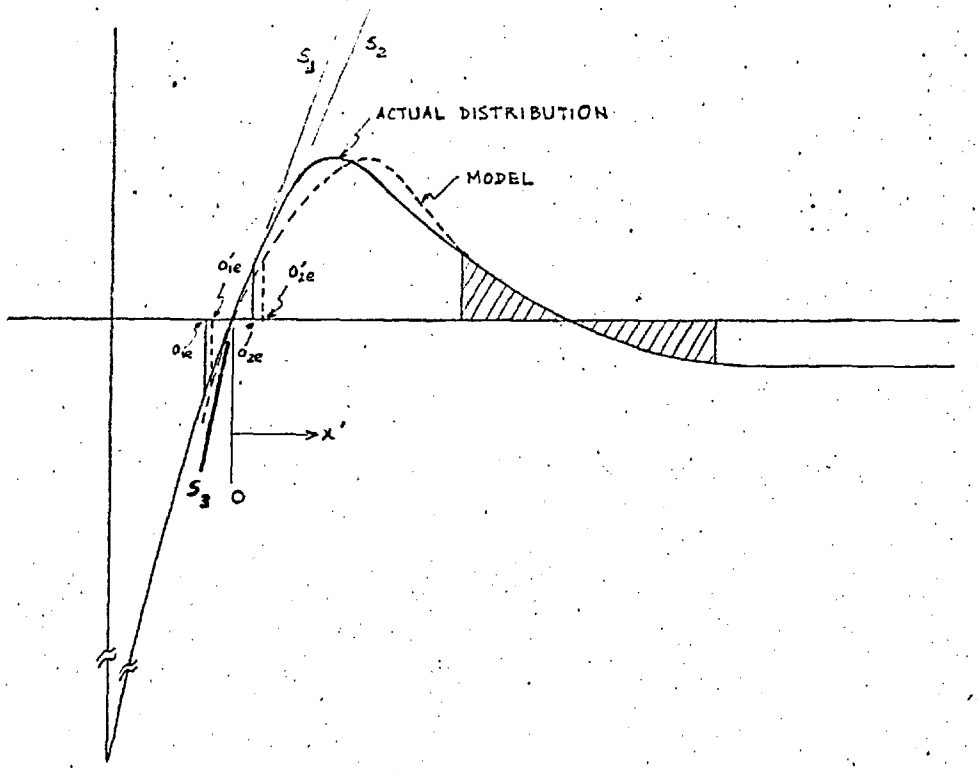


Fig. 3.18. Double Exponential Model for Double-Diffused Transistors.

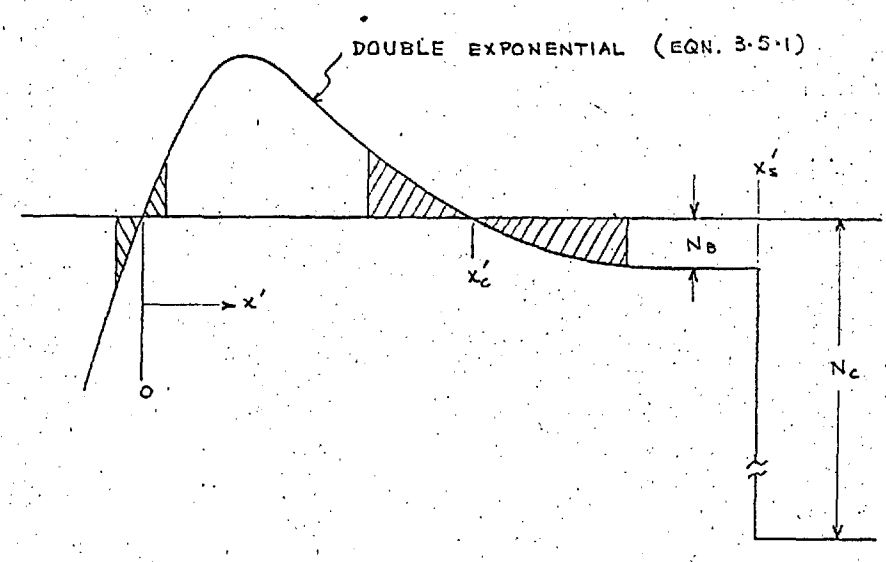


Fig. 3.19. Extension of Model to Planar Epitaxial Transistors.

compensate for the increase in a_{2e} to a'_{2e}. The total depletion layer width should not then change appreciably from that for the classical (or actual) distribution.

The equations describing the electric field and voltage properties for the model are based on a solution of Poisson's equation. Electric field on the emitter side of the junction is found by integrating the impurity distribution once from $-a'_{1e}$ to x' (as in eqn. 3.2.4). Thus

$$E_{1e}(Y) = \frac{q}{\varepsilon} N_O L_2 \left[(e^{m_2 Y_O} - e^{-m_2 Y}) - \frac{1}{\gamma} (e^{\gamma m_2 Y_O} - e^{-\gamma m_2 Y}) - \eta m_2 (Y + Y_O) \right] \qquad 3.5.24$$

where $Y_O = \frac{a'_{1e}}{W}$ and $Y = \frac{x'}{W}$. All other terms are as previously defined. Voltage across the depletion layer semi-width in the emitter is found by integrating eqn. 3.5.24 from $-Y_O$ to 0:

$$V_{1e} = -\frac{q}{\varepsilon} N_O L_2^2 \left[(m_2 Y_O - 1) e^{m_2 Y_O} - (\gamma m_2 Y_O - 1) \frac{e^{\gamma m_2 Y_O}}{\gamma^2} + (1 - \frac{1}{\gamma^2}) - \frac{\eta}{2} (m_2 Y_O)^2 \right] \qquad 3.5.25$$

Similarly on the base side of the junction,

$$E_{2e}(Y) = \frac{q}{\varepsilon} N_O L_2 \left[(e^{-m_2 Y_1} - e^{-m_2 Y}) - \frac{1}{\gamma} (e^{-\gamma m_2 Y_1} - e^{-\gamma m_2 Y}) - \eta m_2 (Y - Y_1) \right] \qquad 3.5.26$$

where $Y_1 = a'_{2e}/W$. V_{2e} is given by:

$$V_{2e} = -\frac{q}{\varepsilon} N_O L_2^2 \left[(1 + m_2 Y_1) e^{-m_2 Y_1} - (1 + \gamma m_2 Y_1) e^{-\gamma m_2 Y_1} - (1 - \frac{1}{\gamma^2}) + \frac{\eta}{2} (m_2 Y_1)^2 \right] \qquad 3.5.27$$

Total voltage across the junction is found by adding eqns. 3.5.25 and 3.5.27. Thus:

$$V_{te} = -\frac{q}{\varepsilon} N_O L_2^2 \left[(m_2 Y_O - 1)\, e^{m_2 Y_O} - (\gamma m_2 Y_O - 1)\, \frac{e^{\gamma m_2 Y_O}}{\gamma^2} + (1 + m_2 Y_1) \cdot e^{-m_2 Y_1} - (1 + \gamma m_2 Y_1)\, \frac{e^{-\gamma m_2 Y_1}}{\gamma^2} + \frac{\eta m_2^2}{2} (Y_1^2 - Y_O^2) \right] \qquad 3.5.28$$

A relationship between Y_O and Y_1 is found by equating eqns. 3.5.24 and 3.5.26 when $Y = 0$. Thus:

$$(e^{m_2 Y_O} - e^{-m_2 Y_1}) - \frac{1}{\gamma} (e^{\gamma m_2 Y_O} - e^{-\gamma m_2 Y_1}) - \eta m_2 (Y_O + Y_1) = 0 \qquad 3.5.29$$

In computations involving the above equations, Y_1 is assumed, Y_O is derived from eqn. 3.5.29, and these results are substituted in eqns. 3.5.24, 3.5.26 and 3.5.28 to determine electric field distribution and junction voltage. This approach is used in Section 3.5.6 to derive the information presented to approximate the classical examples of Sections 3.2.5 and 3.3.5.

For completeness, although it has been shown to be inapplicable for double-diffused transistors, the equations describing an abrupt transition at the emitter junction to the double exponential model are presented below. In these equations N_E is the average doping in the emitter as determined from either eqn. 3.2.28 or 3.3.14. Thus:

$$E_{1e}(x') \Big|_{Abr.} = \frac{q}{\varepsilon} N_E (x' + a'_{1e}) \qquad 3.5.30$$

and

$$V_{1e} \Big|_{Abr.} = \frac{q}{\varepsilon} N_E \frac{a'^2_{1e}}{2} \qquad 3.5.31$$

Total voltage across the junction may be found by adding eqns. 3.5.31 and 3.5.27. Also,

$$a'_{1e}\Big|_{Abr.} = \frac{N_o L_2}{N_E}\left[(e^{-m_2 Y_1} - 1) - \frac{1}{\gamma}(e^{-\gamma m_2 Y_1} - 1) + \eta m_2 Y_1\right] \qquad 3.5.32$$

In most cases N_E should be large enough that a'_{1e} can be neglected and most of the junction voltage assumed to appear across the depletion region on the base side of the junction. This is particularly true when this model is applied to the classical examples in Section 3.5.6, although the abrupt junction itself is inadequate in describing the emitter junctions of these examples.

3.5.4 Minority Carrier Density in the Base Region

The general expression for minority carrier density in the base region was given by eqn. 2.4.19. With the impurity distribution given by eqn. 3.5.21, this may be expressed as:

$$n = -\frac{J_n W}{q}\frac{1}{e^{-m_2 Y} - e^{-\gamma m_2 Y} - \eta}\int_Y^1 \frac{e^{-m_2 Y} - e^{-\gamma m_2 Y} - \eta}{D_n(N_o(e^{-m_2 Y} + e^{-\gamma m_2 Y} + \eta))}\,dY \qquad 3.5.33$$

The presence of a diffusion coefficient which varies with position in the base prevents evaluation of the integral by other than numerical means. This is carried out in Section 3.5.6 to provide a comparison of n for the model with n for the classical examples.

Eqn. 3.5.33 is simplified if the two diffusion coefficient approximation suggested in Section 2.4.3 is adopted. For such an approximation equivalent diffusion coefficients, $\overline{D}_R$ and $\overline{D}_A$, are assumed

to apply to the retarding and aiding field regions respectively. One possible choice for $\overline{D}_R$ and $\overline{D}_A$ could be the average diffusion coefficient applying in each of these regions. For such a choice $\overline{D}_R$ would be given by:

$$\overline{D}_R = \frac{1}{Y_m} \int_0^{Y_m} D_n(N_o\ (e^{-m_2 Y} + e^{-\gamma m_2 Y} + \eta))\ dY \qquad 3.5.34$$

where D_n is a function of $N_o\ (e^{-m_2 Y} + e^{-\gamma m_2 Y} + \eta)$, and that for the aiding field region $\overline{D}_A$ would be given by:

$$\overline{D}_A = \frac{1}{1 - Y_m} \int_{Y_m}^{1} D_n\ (N_o\ (e^{-m_2 Y} + e^{-\gamma m_2 Y} + \eta))\ dY \qquad 3.5.35$$

where $Y_m = x_m'/W$ is the position of maximim uncompensated doping in the base. Y_m is determined by differentiating the impurity distribution and equating to zero. Thus,

$$\left.\frac{dN(Y)}{dY}\right|_{Y = Y_m} = N_o\ (-\ m_2 e^{-m_2 Y_m} + \gamma m_2 e^{-\gamma m_2 Y_m}) = 0$$

and $$Y_m = \frac{\ln \gamma}{m_2(\gamma - 1)} \qquad 3.5.36$$

The curves of D_n vs N in Fig. 2.11 were derived experimentally and can not be represented accurately over the whole range of impurities by a simple theoretical expression. (An approximation such as eqn. 2.4.14 may, however, be used over a limited range). To avoid the use of such an approximation, it was decided to define $\overline{D}_R$ and $\overline{D}_A$ as the diffusion coefficients at the average doping in the respective regions. Average total doping in the retarding field region $\overline{N}_R$ is given by:

$$\bar{N}_R = \frac{1}{Y_m} \int_0^{Y_m} N_o \left(e^{-m_2 Y} + e^{-\gamma m_2 Y} + \eta\right) dY \qquad 3.5.37$$

Integrating gives:

$$\bar{N}_R = \frac{N_o}{m_2 Y_m} \left[(1 - e^{-m_2 Y_m}) + \frac{1}{\gamma} (1 - e^{-\gamma m_2 Y_m}) + \eta m_2 Y_m \right] \qquad 3.5.38$$

Average doping in the aiding field revion $\bar{N}_A$ is given by:

$$\bar{N}_A = \frac{N_o}{m_2(1 - Y_m)} \left[(e^{-m_2 Y_m} - e^{-m_2}) + \frac{1}{\gamma} (e^{-\gamma m_2 Y_m} - e^{-\gamma m_2}) + \eta m_2 (1 - Y_m) \right] \qquad 3.5.39$$

The values of $\bar{N}_R$ and $\bar{N}_A$ are used with Fig. 2.11 to determine $\bar{D}_R$ and $\bar{D}_A$. With less accuracy, $\bar{N}_R$ and $\bar{N}_A$ may be used in eqn. 2.4.14 to estimate $\bar{D}_R$ and $\bar{D}_A$ respectively.

Minority carrier density in the aiding field region may be determined by utilizing eqn. 2.4.23 with the value of impurity density from eqn. 3.5.2. Thus:

$$n = -\frac{J_n W}{q\bar{D}_A} \frac{1}{e^{-m_2 Y} - e^{-\gamma m_2 Y} - \eta} \int_Y^1 \left(e^{-m_2 Y} - e^{-\gamma m_2 Y} - \eta\right) dY \qquad 3.5.40$$

$$Y_m \leq Y \leq 1$$

J_n is the current density. All other terms are as previously defined. Evaluating the integral gives:

$$n = -\frac{J_n W}{q\bar{D}_A} \frac{1}{e^{-m_2 Y} - e^{-\gamma m_2 Y} - \eta} \left[\left(\frac{e^{-\gamma m_2}}{\gamma m_2} - \frac{e^{-m_2}}{m_2} - \eta\right) - \left(\frac{e^{-\gamma m_2 Y}}{\gamma m_2} - \frac{e^{-m_2 Y}}{m_2} - \eta Y\right) \right] \qquad 3.5.41$$

$$Y_m \leq Y \leq 1$$

Minority carrier density in the retarding field region is determined from eqn. 2.4.22 with N(Y) from eqn. 3.5.2. Thus

$$n = -\frac{J_n W}{q\bar{D}_R}\frac{1}{(e^{-m_2 Y} - e^{-\gamma m_2 Y} - \eta)}\left[\int_Y^{Y_m}(e^{-m_2 Y} - e^{-\gamma m_2 Y} - \eta)dY + \frac{\bar{D}_R}{\bar{D}_A}\int_{Y_m}^{1}(e^{-m_2 Y} - e^{-\gamma m_2 Y} - \eta)\,dY\right] \qquad 3.5.42$$

$$Y_1 \leq Y \leq Y_m$$

Performing the integrations gives:

$$n = -\frac{J_n W}{q\bar{D}_R}\frac{1}{(e^{-m_2 Y} - e^{-\gamma m_2 Y} - \eta)}\left[(1 - \frac{\bar{D}_R}{\bar{D}_A})(\frac{e^{-\gamma m_2 Y_m}}{\gamma m_2} - \frac{e^{-m_2 Y_m}}{m_2} - \eta Y_m) + \frac{\bar{D}_R}{\bar{D}_A}(\frac{e^{-\gamma m_2}}{\gamma m_2} - \frac{e^{-m_2}}{m_2} - \eta) - (\frac{e^{-\gamma m_2 Y}}{\gamma m_2} - \frac{e^{-m_2 Y}}{m_2} - \eta Y)\right] \qquad 3.5.43$$

$$Y_1 \leq Y \leq Y_m$$

When $Y = Y_m$, eqn. 3.5.43 reduces to 3.5.41. These equations form the basis for deriving expressions for the emitter diode law and base transit time which will be used in Chapters 4 and 5 to determine physical constants of practical devices. In Section 3.5.5 they are used to compute minority carrier densities which are then compared with those computed from eqn. 3.5.33 to establish the validity of the approximation.

3.5.5 Base Transit Time

Substituting n from eqn. 3.5.33 into eqn. 3.2.30 gives base transit time for the double exponential model: viz,

$$\tau_b = W^2\int_{Y_1}^{1}\frac{1}{(e^{-m_2 Y} - e^{-\gamma m_2 Y} - \eta)}\int_Y^1 \frac{(e^{-m_2 Y} - e^{-\gamma m_2 Y} - \eta)}{(D_n(N_o(e^{-m_2 Y} + e^{-\gamma m_2 Y} + \eta))}\,dY^2 \qquad 3.5.44$$

Eqn. 3.5.44 can be evaluated only by numerical means.

A considerable simplification is introduced by applying the two diffusion coefficient approximation. Transit time for the aiding field region becomes:

$$\tau_A = \frac{W^2}{\bar{D}_A} \int_{Y_m}^{1} \frac{\left\{ \left(\frac{e^{-\gamma m_2}}{\gamma m_2} - \frac{e^{-m_2}}{m_2} - \eta \right) - \left(\frac{e^{-\gamma m_2 Y}}{\gamma m_2} - \frac{e^{-m_2 Y}}{m_2} - \eta Y \right) \right\}}{e^{-m_2 Y} - e^{-\gamma m_2 Y} - \eta} dY \qquad 3.5.45$$

while for the retarding field region transit time is given by:

$$\tau_R = \frac{W^2}{\bar{D}_R} \int_{Y_1}^{Y_m} \frac{\left\{ (1 - \frac{\bar{D}_R}{\bar{D}_A}) (\frac{e^{-\gamma m_2 Y_m}}{\gamma m_2} - \frac{e^{-m_2 Y_m}}{m_2} - \eta Y_m) + \frac{\bar{D}_R}{\bar{D}_A} (\frac{e^{-\gamma m_2}}{\gamma m_2} - \frac{e^{-m_2}}{m_2} - \eta) + (\frac{e^{-\gamma m_2 Y}}{\gamma m_2} - \frac{e^{-m_2 Y}}{m_2} - \eta Y) \right\}}{e^{-m_2 Y} - e^{-\gamma m_2 Y} - \eta} dY$$

3.5.46

Total base transit time τ_b is equal to the sum of τ_R and τ_A,

$$\tau_b = \tau_R + \tau_A \qquad 3.5.47$$

Eqn. 3.5.44 allows for comparison of base transit time for the double exponential model with transit time for the classical distributions of Sections 3.2.5 and 3.3.5 respectively (See Section 3.5.6). In Section 3.5.6 transit time computed from eqn. 3.5.47 is seen to compare favourably with that computed from eqn. 3.5.44, so the two diffusion coefficient approximation will be used in Chapters 4 and 5 as defining transit time for practical devices.

3.5.6 Model Applied to Representative Double ERFC and Double Gaussian Examples

Using the procedure outlined in Section 3.5.1, a double exponential model was derived for the representative examples treated in Sections 3.2.5 and 3.3.5. Differences between the double ERFC and the double Gaussian distributions are reflected in different values of the physical constants of the model (i.e. N_o, L_1, L_2) for the two distributions.

For the double ERFC the model is:

$$N(x') = 1.22 \times 10^{19} \left(e^{\frac{-x'}{3.85 \times 10^{-5}}} - e^{\frac{-x'}{3.21 \times 10^{-5}}} - 4.1 \times 10^{-4}\right) \quad 3.5.48$$

For the double Gaussian the model is:

$$N(x') = 5 \times 10^{19} \left(e^{\frac{-x'}{3.26 \times 10^{-5}}} - e^{\frac{-x'}{2.98 \times 10^{-5}}} - 1 \times 10^{-4}\right) \quad 3.5.49$$

In determining the values of L_1, L_2 and N_o in the above equations, the procedure of Section 3.5.1 was used with $\Upsilon \left(= \frac{L_2}{L_1}\right)$ assumed ≥ 2.5. It is obvious from eqns. 3.5.48 and 3.5.49 that this condition is violated in the examples studied. Although the above model constants are therefore not strictly accurate (the equations of Appendix A.3 should have been used), the method of Section 3.5.1 was used to correspond with that used in Chapters 4 and 5 for actual devices. The constants in eqns. 3.5.48 and 3.5.49 should represent a "worst case" and should indicate an outside limit on the accurancy of the double-exponential model.

Equations 3.5.48 and 3.5.49 were plotted in Figs. 3.2 and 3.8 respectively to facilitate visual comparison with the double ERFC and double Gaussian examples. The models can be seen to closely approximate the classical distributions in most respects, being, however,

slightly lower in magnitude in the aiding field region, and causing a displacement (to the right) of the position of maximum doping in the base for the double ERFC case (Fig. 3.2).

Depletion layer semi-widths were plotted in Figs. 3.3 and 3.9 for comparison with the corresponding double ERFC and double Gaussian values respectively. The method of choosing exponentials ensures that the collector values are in good agreement, in particular, for the case when the single exponential only is assumed at this junction. At the emitter junction the depletion layer semi-widths for the model (a'_{1e} and a'_{2e}) are, for a given voltage, respectively slightly less than and slightly more than the equivalent values (a_{1e} and a_{2e}) for the classical examples. The model is thus accurate in describing these quanitites. The emitter depletion layer semi-widths are also presented for an abrupt emitter and can be seen to be inaccurate in representing a_{1e} and a_{2e} for the classical distributions. Comparison of the curves of transition capacitance/area for the model with the equivalent curves for the classical distributions (Figs. 3.4 and 3.10) support the above observations.

Minority carrier density distribution and base transit times for the model to the double ERFC example, computed both on the basis of variable diffusion coefficient throughout the base and on the approximation using $\overline{D}_R$ in the retarding field region and $\overline{D}_A$ in the aiding field region, were plotted in Figs. 3.6 and 3.7 respectively for one value of effective base width W(= 2.1 microns). Similar curves were plotted in Figs. 3.11 and 3.12 for the model to the double Gaussian.

For the latter case all three curves can be seen to be in good agreement, supporting (a) the validity of the model to represent base transport properties for the double Gaussian distribution, and (b) the accuracy of the approximation of variable diffusion coefficient by two discreet equivalent diffusion coefficients.

For the double ERFC case the minority carrier density and base transit time curves for the model (Figs. 3.6 and 3.7) are less accurate in describing the corresponding quantities for the classical example, being generally larger in value throughout the base region. This can be attributed to two effects which result from using the equations of Section 3.5.1 instead of those of Appendix A.3 in determining L_1 and L_2 for the model. Since γ is considerably less than 2.5, the two exponentials are of comparable magnitude in the aiding field region; thus, diffusion coefficients based on the sum of the two exponentials (which is considerably greater than the sum of the two ERFCs in this region) are considerably lower than the corresponding values for the classical distribution. As diffusion coefficients appear in the denominator of the expressions for minority carrier density (eqns. 3.5.33 and 3.5.41), this causes an increase in minority carrier density in the aiding field region of the model. The displacement towards the collector of the position of maximum doping for the model has the effect of increasing the width of the retarding field region, thus allowing a more extensive build-up of minority carriers in the retarding field region, which is further enhanced by lower diffusion coefficients due to higher doping in the model.

Since base transit time is found by integrating minority carrier density over the base region, the higher values of minority carrier density for the model are magnified in the determination of base transit time. In the region of interest ($.01 \leq Y_1 \leq 0.1$) the base transit times for the model based on $\overline{D}_R$ and $\overline{D}_A$ are approximately 30% greater than those for the double ERFC case (see Fig. 3.7). As the model chosen here represents a "worst" case, the error is likely to be considerably less for a model chosen on the basis of the equations of Appendix A.3. This consideration, and the closeness of the results for the model representing the double Gaussian distribution, prompts the conclusion that the double exponential model adequately describes depletion layer and base transport properties for classical distributions.

In actual devices, for which the double exponential model is determined in Chapter 5, values of Υ are generally only slightly less than or greater than 2.5 (Table 5.1) so that neglecting the shallower exponential at the collector junction is valid. Also values of N_o are of the order of 10^{17} atoms/cc; thus, diffusion coefficients for the model should differ only slightly from those for the actual distributions. In such cases the model should introduce little error into the base transport properties.

3.5.7 Model Extended to Epitaxial Structure

In a planar epitaxial transistor in which substrate impurities have diffused far enough into the epitaxial layer to affect the transistor region, equations describing base transport and junction (especially the collector junction) properties are considerably complicated (see

Section 3.5). This extra degree of complexity reduces the possibility of determining the impurity distribution from terminal measurements. Exceptions to this are: (a) when the distance between the collector junction and the substrate interface is sufficiently large that substrate diffusion does not reach the collector junction, and (b) when the substrate interface retains most of its original abruptness. For both these cases, the equations for either the double ERFC or double Gaussian distribution should apply, and the double exponential model may be used to represent the base region.

It is difficult to provide a simple model for the case where substrate diffusion penetrates to the base region. The addition of three independent variables (N_C, $\sqrt{4D_s t_s}$, x_S) for this diffusion, unaccompanied by an increase in data available from terminal measurements virtually precludes their derivation from measured data. It appears that only in the two exceptional cases mentioned above does the possibility exist for determination of most of the physical constants of the device. In these cases, the model of Fig. 3.19 will be assumed to apply. Eqn. 3.5.1 (or 3.5.2) defines the impurity distribution up to an abrupt transition at x'_S ($= x_S - x_e$) to a constant doping ($-N_C$ atoms/cc) in the substrate layer. For such a model the equations of Sections 3.5.2, 3.5.3 and 3.5.4 define base and depletion region properties (so long as V_{tc} is low enough that the collector depletion layer does not extend into the substrate layer). The exponential can be determined as in Section 3.5.1 and the equations of Section 3.5.2 - 3.5.4 used to compute base region and depletion layer properties. It should also be possible to

derive the base impurity model for actual devices by the techniques used for ordinary double-diffused transistors (Chapters 4 and 5), with the stipulation that low collector bias is used.

When the collector depletion layer extends beyond x_s the following equations apply:

$$E_2(Y)\Big|_{Y>Y_s} = \frac{q}{\varepsilon} N_C W \left(1 - \frac{d_c}{W} - Y\right) \qquad 3.5.50$$

where d_c = width of collector depletion layer and

$Y_s = x'_s/W$.

When $x < x_s$, $(Y < Y_s)$:

$$E_2(Y) = \frac{q}{\varepsilon} N_O L_2 \left[\left(e^{-m_2 Y_s} - e^{-m_2 Y}\right) - \frac{1}{\gamma}\left(e^{-\gamma m_2 Y_s} - e^{-\gamma m_2 Y}\right) - \eta m_2 (Y - Y_s) + \frac{N_C}{N_O}\left(m_2(1 - Y) + \frac{d_c}{L_2}\right)\right] \qquad 3.5.51$$

where all terms are as previously defined.

Voltage to the right of the collector junction is given by:

$$V_{2c} = -\frac{q}{\varepsilon} N_O L_2^2 \left[\left\{1 + m_2 (Y_s - Y_c)\right\} e^{-m_2 Y_s} - e^{-m_2 Y_c} - \frac{1}{\gamma^2}\left\{1 + m_2 (Y_s - Y_c)\right\} e^{-m_2 Y_s} - \frac{e^{-\gamma m_2 Y_c}}{\gamma^2} + \frac{1}{2}\eta m_2^2 (Y_s - Y_c)^2 + \frac{N_C m_2^2}{N_O}\left(Y_c + \frac{a_{2c}}{m_2 L_2} - Y_s\right)^2\right] \qquad 3.5.52$$

where $Y_c = \frac{x'_c}{W}$

Total voltage across the collector junction is given by:

$$V_{tc} = -\frac{q}{\varepsilon} N_O L_2^2 \left[\left(\frac{a_{1c}}{L_2} - 1\right) e^{-m_2} - \frac{1}{\gamma^2}\left(\gamma \frac{a_{1c}}{L_2} - 1\right) e^{-\gamma m_2} + \left\{1 + m_2 (Y_s - Y_c)\right\} e^{-m_2 Y_s} - \frac{1}{\gamma^2}\left\{1 + m_2 (Y_s - Y_c)\right\} e^{-\gamma m_2 Y_s} + \frac{1}{2}\eta\left\{m_2^2 Y_s \left(Y_s - 1 - \frac{2 a_{1c}}{m_2 L_2}\right)\right\} + \frac{N_C}{N_O} m_2^2 \left(Y_c + \frac{a_{2c}}{m_2 L_2} - Y_s\right)\right] \qquad 3.5.53$$

Equating $E_{1C}(Y_C)$ to $E_{2C}(Y_C)$, m_2 and d_C are related by:

$$(e^{-m_2 Y_S} - e^{-m_2}) - \frac{1}{\gamma}(e^{-\gamma m_2 Y_S} - e^{-\gamma m_2}) - \eta m_2(1 - Y_S) + \frac{N_C}{N_O}$$

$$\{m_2(1 - Y_C) - \frac{d_C}{L_2}\} = 0 \qquad 3.5.54$$

This equation may be used to find d_C/L_2 once m_2, Y_S, and Y_C are known. d_C may be readily separated into its components, since total base width x'_C is known and W can be set.

Figs. 3.14 and 3.15 include the double exponential models and the abrupt interface representation for the planar epitaxial examples of Section 3.4.3. Although in the region of the original interface (8 microns), the abrupt representation is not particularly good, the effect of substrate diffusion is not felt in the base and over much of the collector region . It is, therefore, unnecessary to present base transport and depletion layer properties for the model.

3.6 Numerical Techniques

The complicated nature of the classical distributions and the equations describing base transport and depletion layer properties requires evaluation by numerical techniques. Computer programs were written in Extended Mercury Autocode (EMA) language for running on the Ferranti Atlas of London University. To avoid complicating the programs unduly, individual programs were written to compute the above quantities for the double ERFC distribution (Appendix A.4), the double Gaussian (Appendix A.5) and for the double Exponential approximation to each of these (Appendix A.6). The construction of the programs for the

classical distributions is similar, with individual routines differing to account for differences in equations defining similar properties for the two cases (Section 3.2 and 3.3). In the programs of Appendices A.4 and A.5, certain modifications are necessary to account for the presence of a substrate interface. Such modifications are not, however, included in these Appendices. The program determining the double exponential approximation and base transport and depletion layer properties for this approximation (Appendix A.6) is the same for both the double ERFC and double Gaussian cases (with only minor modifications as indicated). The choice of variables in this program is such that it could be used as Chapter 1 of the programs of either Appendix A.4 or A.5.

The flow diagramsfor the programs are given in the appropriate appendices. Briefly, the sequence of operations is:

1. Set variable and read in information;
2. Compute t_1 and t_2 for the classical functions;
3. Set a_{2C} in steps, compute a_{1C} and V_{tc} for both the single diffused and double diffused collector junctions;
4. Set a_{2e} and repeat the same operations for the emitter junction ;
5. Compute minority carrier density distribution and base transit time for different effective base width and variation of transit time with position of edge of emitter depletion layer.

The sequence of operations in the program for the double

exponential model is the same, except that the second operation is replaced by the computation of L_1 and L_2, while at the emitter junction both the abrupt and double-exponential model for the emitter side of the junction are treated. The $\overline{D}_R$ and $\overline{D}_A$ approximation was also computed for minority carrier density and base transit time.

Certain simplifications were used to facilitate the computations of the programs:

(1) In the computation of t_1 and t_2, the emitter diffusion was neglected at the collector junction. This allowed a direct determination of t_2 at the collector junction. If this condition were violated, t_1 and t_2 could be determined from two simultaneous transcendental equations at the emitter and collector junctions by the Newton-Raphson technique as coutlined in Appendix A.3.

(2) Electric fields were not computed on the basis that they were superfluous to the establishment of the validity of the double exponential model.

(3) For the planar epitaxial transistor, the program was originally restricted to the case where $\sqrt{4D_3 t_3} = \sqrt{4D_2 t_2}$. Minor modifications have made the program applicable to the general case where $\sqrt{4D_3 t_3}$ can bear any relation to $\sqrt{4D_2 t_2}$ and $\sqrt{4D_1 t_1}$.

One routine which is common to all the programs is Routine 770. This is a routine devised by Apaydin[79] to evaluate the ERFC to five significant figures. It is essential to either include D6 in the data

or compute its value in the program before the routine is to be used - the value of D6 = $2/\sqrt{\pi}$. The routine evaluated the ERFC of the number contained in the variable DO. Routine 1 is a bisection routine which may be used to find the root of an equation when the root lies between certain limits which are included in the data fed into the computer. This routine may be used to find the roots of different equations at different points in the program, hence the reference to different subroutines. One other routine is common (Routine 50) and needs comment. This routine is used to determine diffusion coefficients during minority carrier density and base transit time calculations. Points on the curve are read into the program in the form of a table and Routine 50 extrapolates to find diffusion coefficients from this table when impurity density is known.

4. TERMINAL CHARACTERISTICS AND CIRCUIT ELEMENTS OF ACTUAL TRANSISTORS BASED ON THE DOUBLE EXPONENTIAL MODEL

4.1 Introduction

In this Chapter the double exponential impurity model, proposed in Chapter 3, is further developed with special reference to actual devices. Background information and measurement techniques are presented to provide experimental data for use in the determination of the physical constants of the model in Chapter 5.

The essence of characterization by a physical model is that the constants of the model (base width, depletion layer width, and those that define impurity distribution) may be determined from non-destructive measurements on the device. Only the following measurements are useful in this respect:

(1) collector transition capacitance,
(2) emitter transition capacitance,
(3) emitter diode law (I_C vs V_{eb}),
(4) base transit time,
(5) collector avalanche breakdown voltage,
(6) r'_{bb} and $r'_{bb}C_{tc1}$ measurements,
(7) r'_{cc} measurement (collector body resistance),
(8) emitter and collector areas.

Each of the measurements listed above is discussed in terms of the possible information which may be derived from it. Where necessary, additional equations are derived in terms of the physical model, otherwise the appropriate equations in Chapter 3 are referred to. Approximations are introduced where permissible to simplify treatment. Measurement techniques are presented and used to provide experimental data for use in Chapter 5. The reliability of such data is discussed. Presentation of information roughly follows the order in which it is used in Chapter 5.

4.2 Collector and Emitter Junctions

4.2.1 Collector Depletion Region

The double exponential model for the base region of double-diffused transistors, represented graphically in Fig. 3.17 reproduced here as Fig. 4.1, was defined by eqn. 3.5.2. For convenience this is repeated here as eqn. 4.2.1:

$$N = N_p \left(e^{-m_2 Y} - e^{-\gamma m_2 Y} - \eta\right) \qquad 4.2.1$$

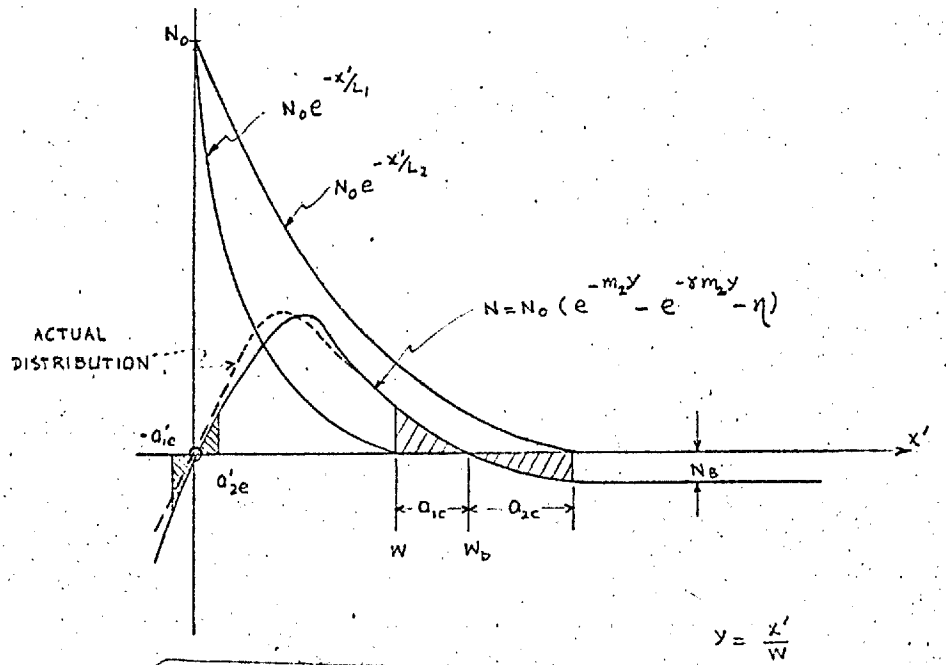


Fig. 4.1. Double Exponential Model

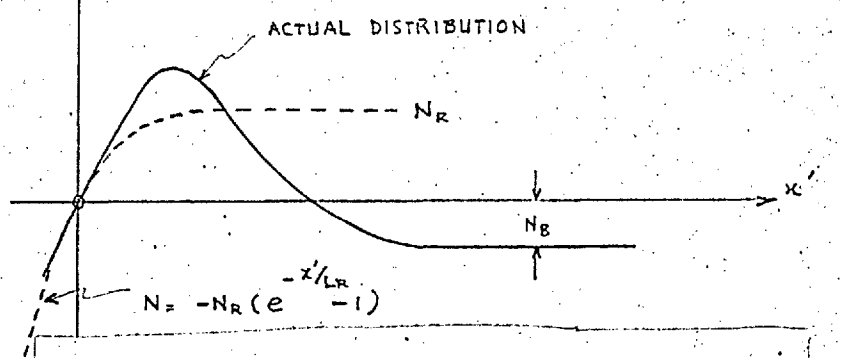


Fig. 4.2. Pseudo-Exponential Model for Emitter Junction

where $m_2 = W/L_2$, $Y = x'/W$, $\gamma = L_2/L_1$, and $\eta = N_B/N_o$. The origin of x is at the emitter metallurgical junction. All the constants which effectively define the physical model for the transistor (with the exception of [illegible] junction areas) are contained in eqn. 4.2.1. Beginning with the collector depletion region, the basis for determination of these constants will be established in this Chapter.

Eqn. 4.2.1 was used as the starting point in the derivation of electric field and voltage equations for the collector junction in Chapter 3, Section 3.5.3. Ignoring equations which contribute nothing to the determination of constants of practical transistors, collector depletion layer properties are described by:

(a) an expression for junction voltage V_c, (eqn. 3.5.18)*,

(b) an expression relating d_c/L_2 and m_2 (eqn. 3.5.15), where d_c is width of collector depletion layer and L_2 is the characteristic length of the more gradual exponential.

Eqns. 3.5.15 and 3.5.18 are complicated, containing a total of six independent variables, and do not, therefore, lend themselves to a simple treatment of the collector junction. The number of variables reduces to three when $Y \geq 2.5$, i.e. $e^{-\gamma m_2 Y}$ may be neglected at the collector junction. For this simplified case, the junction is essentially single-exponential as defined by eqn. 3.5.19. Eqns. 3.5.20 and 3.5.23 replace eqns. 3.5.15 and 3.5.18 respectively.

---

* In this and Chapter 5, the subscript "t" will be dropped from collector and emitter voltages, since only the total voltage is referred to in these Chapters.

Trofimenkoff[37] treated the single exponential collector junction in detail for the linear plus exponential model for the base region of double-diffused transistors (see Chapter 2, Section 2.7.3), presenting several techniques for utilizing transition capacitance data to yield information on the physical constants of the impurity profile. In particular, a technique based on the slope of $1/C_{tc}^3$ vs V_c curve for low reverse bias on the collector-base junction was recommended for reasons of simplicity and accuracy. The essence of this technique is as follows:

(1) determine the slope γ_2 from:

$$\gamma_2 = \left. \frac{d(1/C_{tc}^3)}{dV_c} \right|_{\text{low } V_c} \qquad 4.2.2$$

(2) for a particular value of reverse bias, use γ_2 and C_{tc} to determine the function $\Gamma(d_c/L_2)$, defined in eqn. 2.7.24 as:*

$$\frac{\gamma_2 C_{tc}^3 (V + V_B)}{3} = \Gamma(d_c/L_2) \qquad 4.2.3$$

(3) Using the value of $\Gamma(d_c/L_2)$ determined from eqn. 4.2.3 read off d_c/L_2 and $\xi_2(d_c/L_2)$ from Fig. 2.21. $\xi_2(d_c/L_2)$ is a function defined by:

$$\xi_2(d_c/L_2) = \Gamma(d_c/L_2) \cdot (d_c/L_2)^2/4 \left[1 - \frac{d_c}{2L_2} \coth (d_c/2L_2)\right] \qquad 4.2.4$$

---

* The subscript '2' did not appear in eqn. 2.7.24, but is included here since the exponential is only part of a double exponential model.

(4) from the values of γ_2 and $\xi_2 (d_c/L_2)$ determine a quantity dependent only on certain physical constants of the model:

$$\frac{A_c^3 N_B}{L_2} = \frac{12}{q \varepsilon^2 \gamma_2} \cdot \xi_2 (d_c/L_2) \qquad 4.2.5$$

In eqn. 4.2.3, $V = -V_c$ and $V_B = V_{oc} + \frac{kT}{q} \cdot \frac{d_c}{L_2}$ where V_{oc} is the collector "equilibrium barrier potential", k is Boltzmann's constant, T is absolute temperature (^oK), and q is electrostatic charge. In eqn. 4.2.5 ε is the permittivity of the material.

If, as suggested in Section 2.7.3, low collector bias is used in this determination, then d_c/L_2 is low (≤ 1), and $\frac{kT}{q} \cdot \frac{d_c}{L_2}$ ($\leq .026$ volt) may be neglected. V_B is then replaced by V_{oc} in eqn. 4.2.3. V_{oc} can be determined by a technique outlined in Section 4.2.3.

The value of $A_c^3 N_B/L_2$ can be determined at any bias voltage so long as the single exponential assumption holds. Low bias is preferred because of the ease in determining the value of γ_2 where the curve of $1/C_{tc}^3$ vs V_c assumes a straight-line relationship. Once $A_c^3 N_B/L_2$ is known, separation of the three constants can be carried out at the same low collector bias or at a higher value of bias to conform with the normal operating condition.

If A_c is known from an optical measurement (Section 4.2.4) separation of the three constants may be simply accomplished. N_B/L_2 immediately results by dividing $A_c^3 N_B/L_2$ by A_c^3. Depletion layer width d_c may be determined from:

$$d_c = \frac{\varepsilon A_c}{C_{tc}} \qquad 4.2.6$$

where C_{tc} is the value of transition capacitance at the particular value of voltage used in the determination of $\Gamma(d_c/L_2)$ (eqn. 4.2.3). Since d_c/L_2 is known from Fig. 2.21, then L_2 can be calculated, hence N_B. However, the choice of low V_c for determination of $A_c^3 N_B/L_2$ results in a calculation of $\Gamma(d_c/L_2)$ in a region where this function is approximately constant (See Fig. 2.21). Thus the value of d_c/L_2 can be quite inaccurate. This does not influence the value of $A_c^3 N_B/L_2$ since $\xi_2(d_c/L_2) \approx 1$ in this region; thus only γ_2 exerts a major influence in eqn. 4.2.5, but can lead to a very inaccurate determination of N_B and L_2. A more accurate separation is preferred and will be presented in Chapter 5, Section 5.2. The technique presented in this Section is used in Section 4.2.3 to compute $A_c^3 N_B/L_2$ (Table 4.3) from measured values of γ_2.

4.2.2 Emitter Depletion Region

In extending the double-exponential model at the emitter junction (Section 3.5.3), it was assumed that the actual impurity distribution varied approximately linearly over the depletion layer, provided that reverse bias on the junction was low enough so that the edges of the depletion layer did not penetrate far from the junction. This assumption was supported by the plots of a_{1e} and a_{2e} (depletion layer semi-widths) vs V_{te} for the classical examples studied (Figs. 3.3 and 3.9), a_{1e} and a_{2e} being approximately equal at low voltages.

In actual devices information on the emitter junction may be derived from transition capacitances measurements (Section 4.2.3), which is interperted in terms of the physical impurity configuration.*

---

* For the assumed model emitter capacitance data is used only to fix the position of the edge of the depletion layer on the base side of the junction under forward bias conditions. The discussion of this section is aimed at establishing the configuration of the actual junction.

The two most common interpretations of capacitance data rely either on the symmetrical-linear or the abrupt-linear approximation to the junction, with the slope of the linear region assumed equal to the gradient of the actual impurity distribution at the junction. Calling this gradient S_1, then

$$S_1 = \frac{dN}{dx'}\Bigg|_{x' = 0} \qquad 4.2.7$$

If this gradient applies over a limited distance from the junction (both sides as for the symmetrical junction or one side only as for the abrupt-linear junction), a plot of $1/C_{te}^3$ vs V_{eb} (C_{te} is emitter transition capacitance and V_{eb} is emitter base voltage) follows a straight-line relationship for low reverse voltage (see curves of Section 4.2.3). Using the slope of this linear region ($d(1/C_{te}^3)/dV_{eb}$), the following may be determined:

$$A_e^3 S_1 = \frac{12}{q\varepsilon^2} \cdot \frac{1}{d(\frac{1}{C_{te}^3})/dV_{eb}}\Bigg|_{V_{eb} \to 0} \qquad 4.2.8$$

if the junction is <u>symmetrical-linear</u>, or,

$$A_e^3 S_1 = \frac{3}{q\varepsilon^2} \cdot \frac{1}{d(\frac{1}{C_{te}^3})/dV_{eb}}\Bigg|_{V_{eb} \to 0} \qquad 4.2.9$$

if the junction is <u>abrupt-linear</u>. A_e is the emitter area.

A factor of 4 separates the products determined from eqns. 4.2.8 and 4.2.9. To establish which of the above approximations is more

realistic at the emitter junction of actual devices, the pseudo-exponential junction of Fig. 4.2 is postulated. The quantitative statement of the "impurity" distribution for this junction is:

$$N(x') = - N_R(e^{-x'/L_R} - 1) \qquad 4.2.10$$

where N_R and L_R have no basis in fact, but are merely a representative doping in the base and the characteristic length of the exponential respectively.

At the metallurgical emitter junction ($x' = 0$), the gradient of the pseudo-exponential junction should be the same as that for the actual junction, viz,

$$S_1 = \frac{N_R}{L_R} \qquad 4.2.11$$

For this "single exponential" junction a treatment similar to that outlined in Section 4.2.1 (based on Trofimenkoff[37]) may be used to determine $A_e^3 N_R/L_R$ at low voltages. A direct comparison of $A_e^3 N_R/L_R$ with the values of $A_e^3 S_1$ determined from eqns. 4.2.8 and 4.2.9 should establish which of the two approximations (symmertrical-linear or abrupt-linear) is more applicable to the emitter junction of the actual double-diffused transistors. Such a comparison is presented in Section 4.2.3, Table 43. This comparison strongly supports the symmetrical-linear approximation, indicating the gradual nature of the emitter junction in double-diffused transistors.

The choice of the parameters of the double exponential model, based on collector junction data and the total number of uncompensated impurities in the base region for classical distributions (Section 3.5.1),

will likewise be based on collector capacitance data and measurements thought to yield information on the total number of uncompensated impurities in the base region for actual devices (i.e. emitter diode law and base transit time - Sections 4.3, 4.4, and Chapter 5, Section 5.2). As pointed out in Section 3.5.3 no attempt is made to tie the impurity gradient of the model to that of the actual distribution at the emitter junction; thus the gradient of the model may be quite different from that of the actual distribution at this point. This effect will be felt in the emitter diode law and base transit time equation (Sections 4.3 and 4.4), in the value of Y_1 which appears in both equations. Y_1 ($= \frac{a'_{2e}}{W}$) represents the base edge of the emitter depletion layer for the model (i.e. the injection point).

Both the emitter diode characteristic and base transit time are measured under forward bias conditions. For such conditions, the space-charge approximation breaks down and numerical techniques must be used to describe the voltage dependence of emitter transition capacitance[65]. In the interests of simplicity, however, in the model of Fig. 4.1 when the transistor is operated at normal forward bias, the space-charge approximation will be assumed to apply. A method is suggested in Section 4.4.5 to measure forward biased emitter transition capacitance ($C_{te}|_{fwd}$). As shown above, for low reverse bias, the symmetrical-linear approximation is applicable to the emitter junction of actual double-diffused transistors; thus, using the space-charge approximation, total depletion layer width may be found

from $d_e = A_e/C_{tc}\,|_{fwd}$, and depletion layer semi-widths a_{1e} and a_{2e} are each equal to $\frac{1}{2}d_e$.

In the model, depletion layer semi-widths a'_{1e} and a'_{2e} are not necessarily equal (see Section 3.5.3). Moreover, for a given total depletion layer width, voltage at the emitter junction of the model may be somewhat different from that of the actual distribution. The measurement of $C_{te}\,|_{fwd}$ assumes that changes in current (brought about by small changes in emitter voltage) do not affect the width of the emitter depletion layer, which remains approximately constant. Thus, for the model, it is pointless to worry about the small changes in emitter voltage due to the different distribution at the junction. It is more important to maintain agreement between $C_{te}\,|_{fwd}$ for the model and for the actual distribution. It is, therefore, necessary to maintain total depletion layer width d_e constant, and, using d_e as a starting point, a'_{2e} for the model can be determined by employing the property of electric field continuity at the emitter junction. Thus:

$$\frac{q}{\varepsilon}\int_{-(\frac{d_e}{W}-Y_1)}^{0} N_o(e^{-m_2Y} - e^{-\gamma m_2 Y} - \eta)\,dY = \frac{q}{\varepsilon}\int_{Y_1}^{0} N_o(e^{-m_2Y} - e^{-\gamma m_2 Y} - \eta)dY$$

giving:

$$e^{-m_2Y_1}(e^{m_2\frac{d_e}{W}} - 1) - \frac{1}{\gamma}\,e^{-\gamma m_2 Y_1}(e^{\gamma m_2\frac{d_e}{W}} - 1) - \eta m_2\frac{d_e}{W} = 0 \qquad 4.2.12$$

where $Y_1 = a'_{2e}/W$, and all other terms are as previously defined. Eqn. 4.2.12 may be solved to determine Y_1 for the model.

4.2.3 Measurement of Transition Capacitances

Three small-signal low frequency measurements on an admittance bridge (such as the Wayne-Kerr B601) are sufficient to determine reverse-biased transition and stray capacitances (i.e. C_{tc}, C_{te}, C_{seb}, C_{sec}, C_{scb}, in Fig. 2.12). These measurements are:

(a) common-base input admittance with output shorted,

(b) common-emitter input admittance with output shorted,

(c) common-base output admittance with input shorted.

In all three cases both junctions are reverse biased, so negligible current flows, C_{de} disappears from Fig. 2.12, as does the current generator. For the three measurements the equivalent circuit reduces to Fig. 4.3(a), (b) and (c) respectively.

Measurements on the Wayne-Kerr B601 are given as parallel R and C, so using the equivalent circuits of Fig. 4.3, measured quantities will also be expressed in this form. Considering the magnitude of the components of these circuits and the frequency of measurement (500KHz to 5MHz) it is possible to make certain simplifications. The detailed equations are presented in Appendix A.7 for the three cases; only the simplified equations which may be readily used in calculations are presented here.

Case A. Common base input admittance. Subject to the assumptions that $\omega^2 C_{tc1}^2 r_c^2 \gg 1$ and that $1/r_c + \omega^2 C_{tc1}^2 r'_{cc} \ll 1/r'_{bb}$, the parallel resistance component is equal to:

$$R_{ib} \approx r'_{bb} + \frac{1}{\omega^2 C_{te}^2 r'_{bb}} \qquad 4.2.13$$

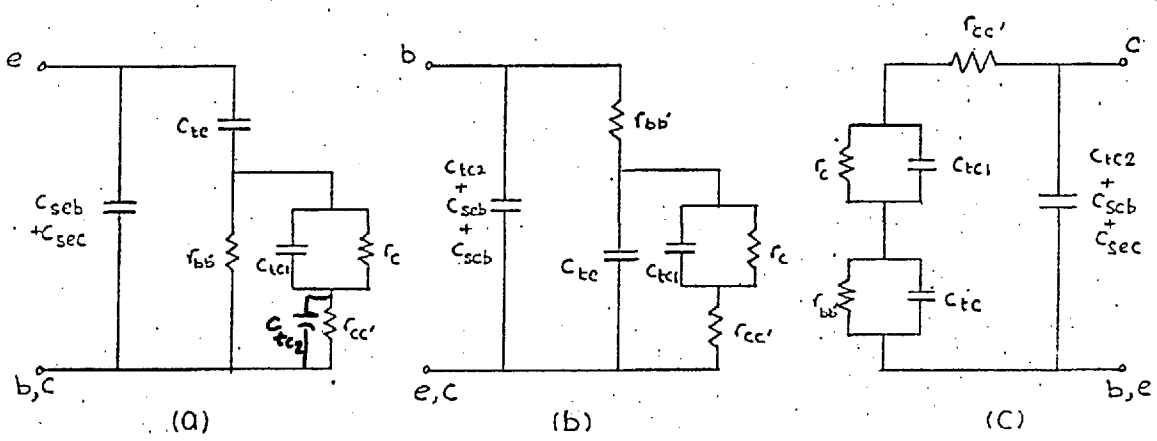


Fig. 4.3. (a) Common-base Equivalent Circuit with Output Shorted.
(b) Common-emitter Equivalent Circuit with Output Shorted.
(c) Common-base Equivalent Circuit with Input Shorted.
(Both junctions reverse biased all cases.)

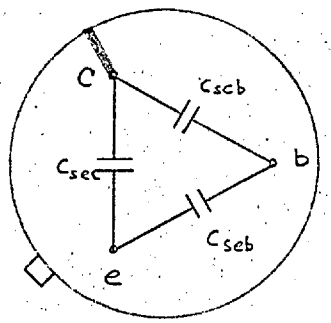


Fig. 4.4. Lead Capacitances in Transistor Header.

and the parallel capacitance is equal to:

$$C_{ib} \approx C_{seb} + C_{sec} + C_{te} \qquad 4.2.14$$

The measured value of C_{ib} may be used in the determination of C_{te}, while R_{ib} may be used to provide a quick estimate of r'_{bb}.

Case B. Common emitter input admittance. Using the circuit of Fig. 4.3(b) subject to the same simplifying assumptions,

$$R_{ie} \approx r'_{bb} + r_c + \frac{\omega^2 r_c^2 (C_{te} + C_{tc1})^2}{r'_{bb} + r_c} \qquad 4.2.15$$

and

$$C_{ie} \approx C_{seb} + C_{scb} + C_{te} + C_{tc1} + C_{tc2} \qquad 4.2.16$$

where R_{ie} and C_{ie} are parallel R and C as measured on the admittance bridge.

Case C. Common base output admittance. The circuit of Fig. 4.3(c) reduces to parallel R_{ob} and C_{ob} which, when permissible simplifications are made, may be expressed as:

$$R_{ob} \approx r'_{cc} + r'_{bb} + \frac{1}{\omega^2 C_{tc1}^2 r_c} + \frac{1}{\omega C_{tc1}\left[r'_{bb} + r'_{cc} + \frac{1}{\omega^2 C_{tc1}^2 r_c}\right]} \qquad 4.2.17$$

and $$C_{ob} \approx C_{tc1} + C_{tc2} + C_{seb} + C_{sec} \qquad 4.2.18$$

In eqns. 4.2.14, 4.2.16 and 4.2.18, the unknowns are C_{te}, C_{tc1}, C_{tc2}, C_{seb}, C_{sec} and C_{scb}. Unless other information is available, there are too many unknowns to be separated from these

equations. Fortunately, in most planar transistors the collector is normally tied to the "header" so that most of the strays between the base lead and the collector, and between the emitter lead and the collector are caused by the header and its "can". Thus $C_{scb} \approx C_{sec}$, which eliminates one unknown from the equations. Thus,

$$C_{sec} = C_{scb} = \frac{C_{ob} + C_{ib} - C_{ie}}{2} \qquad 4.2.19$$

$$\text{and } C_{tc} = C_{tc_1} + C_{tc_2} = C_{ie} - C_{ib} \qquad 4.2.20$$

Emitter-base strays may either be neglected or equated to the value measured for a transistor 'header'. Thus, C_{seb} = .02pF (TO-5); = .04pF (TO-18). 4.2.21

$$C_{te} = C_{ib} - C_{seb} - C_{sec} \qquad 4.2.22$$

It must be stressed that in these calculations reverse bias voltages used in the measurements of C_{ib}, C_{ie} and C_{ob} are identical. Table 4.1 presents capacitance values for various transistors computed by this method. A frequency of 500 KHz was used to measure values of C_{ib}, C_{ob}, and C_{ie}. From eqn. 4.2.13 it is possible to get a quick estimate of r'_{bb} once C_{te} is known. Values of r'_{bb} determined from this equation at zero reverse bias on the emitter junction are presented in Table 4.1. Although this value of r'_{bb} may differ slightly from the value under forward biased conditions, the approximate nature of the concept of a single lumped base resistor does not justify a more rigorous determination.

As a check on the stray capacitances in Table 4.1, header strays (including can but no transistor) were measured. Fig. 4.4, represents the strays existing between the three leads. A two-terminal measurement

Device Number		V_c (volts)	C_{tc} (PF)	C_{te}* (PF)	$C_{scb}=C_{sec}$ (PF)	C_{seb} (PF)	r'_{bb} (Ω)
2N696	1	30	9.00	65.0	.60	.02	90
2N1613	1	30	9.70	62.4	.55	.02	90
	2	30	12.2	67.4	.64	.02	57
	3	5	23.0	67.7	.55	.02	83
	3	10	18.2	67.7	.55	.02	84
	3	20	14.1	67.7	.55	.02	87
	3	30	12.1	67.7	.55	.02	88
	12	30	11.5	74.8	.65	.02	57
2N1711	1	30	11.5	62.4	.60	.02	108
	2	30	10.8	55.3	.65	.02	-
	3	10	19.4	54.3	.65	.02	165
2N910	1	10	11.5	56.5	.63	.04	107
	2	10	12.1	55.2	.63	.04	112
	3	10	11.3	59.7	.65	.04	100
2N916	1	10	2.03	6.34	.65	.04	119
	2	5	3.10	7.10	.69	.04	119
	2	10	2.44	7.10	.69	.04	126
	3	10	3.03	7.20	.62	.04	145
2N706A	1	0.6	3.78	4.43	.69	.04	-
	2	0.6	4.09	5.24	.69	.04	-

* C_{te} determined for zero external bias on emitter Measurements at frequency of 500 KHz.

Table 4.1 - Transition and Stray Capacitances

includes the effect of the strays associated with the third terminal, so a method was employed in which two of the leads were shorted and strays between these shorted leads and the third lead were measured. The measured quantities are thus:

$$\begin{aligned} C_{(ec-b)} &= C_{seb} + C_{sec} \\ C_{(be-c)} &= C_{scb} + C_{seb} \\ C_{(cb-e)} &= C_{scb} + C_{sec} \end{aligned} \qquad 4.2.23$$

On the left hand side of the equation, the first two subscripts represent measurement terminals while the third subscript represents the terminal shorted to the terminal included as the second subscript (e.g. $C_{(ec-b)}$ means e and c are measurement terminals, while b is shorted to c). To separate the strays in eqn. 4.2.23, the following procedure may be used:

$$\left.\begin{aligned} C_{seb} &= \frac{C_{(ec-b)} + C_{(be-c)} - C_{(cb-e)}}{2} \\ C_{scb} &= C_{(be-c)} - C_{seb} \\ C_{sec} &= C_{(ec-b)} - C_{seb} \end{aligned}\right\} \qquad 4.2.24$$

Strays determined by this means are presented in Table 4.2. Comparison with the stray capacitances of Table 4.1 indicates that internal leads used to make connections between the header leads and the actual transistor contribute little to stray capacitances.

Header	Measurement Terminals	Shorted Terminals	Measured Capacitance	Name of Stray	Calculated Stray
TO-5	c & b	b-e	1.12 pF	C_{sec}	0.56 pF
TO-5	b & e	e-c	0.57	C_{scb}	0.56
TO-5	e & c	c-b	0.58	C_{seb}	0.02
TO-18	c & b	b-e	1.36	C_{sec}	0.68
TO-18	b & e	e-c	0.72	C_{scb}	0.68
TO-18	e & c	c-b	0.72	C_{seb}	0.04

Table 4.2 Measurement of Header Strays

Fig. 4.5 is a plot of $1/C_{te}^3$ and $1/C_{tc}^3$ vs reverse voltage for a typical transistor. From this and similar curves γ_2 $\left[= \frac{d(1/C_{tc}^3)}{dV} \right]$ and $\frac{d(1/C_{te}^3)}{dV_{eb}}$ were determined from the linear portions of the curves at low voltages. Values for these slopes are presented in Table 4.3 for various transistors. For the collector junction, γ_2 was used in the technique outlined in Section 4.2.1 to determine $A_c^3 N_B/L_2$ (see Table 4.3). For the emitter capacitance data $d(1/C_{te}^3)/dV_{eb}$ was used in both eqns. 4.2.8 and 4.2.9 to determine $A_e^3 S_1$ where S_1 is the slope of the impurity distribution at the junction. These values are also presented in Table 4.3. The values of $d(1/C_{te}^3)/dV_{eb}$ were also used (as in Section 4.2.2) to compute the value of $A_e^3 N_R/L_R$ for the pseudo-exponential emitter junction. Comparison in Table 4.3 of $A_e^3 N_R/L_R$ with $A_e^3 S_1$ computed from eqns. 4.2.8 and 4.2.9 respectively indicates close agreement with the values computed for the former case. It therefore appears that the emitter junction of actual double-diffused transistors may be accurately represented by a symmetrical-linear approximation for low bias voltages.

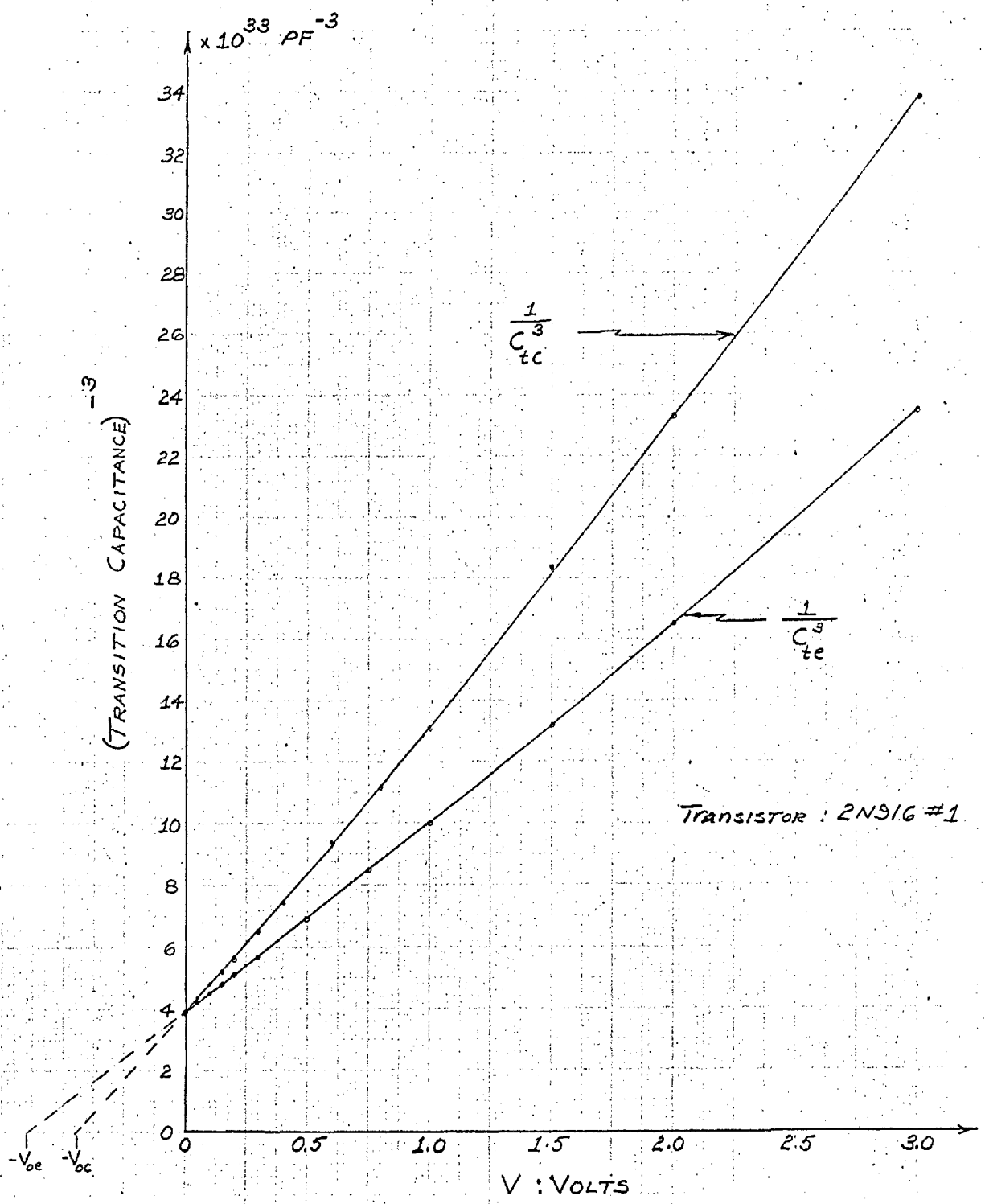


Fig. 4.5. Plot of Transition Capacitance Data.

Device Number		γ_2 (Farad^3/volt)	$A_c^3 N_I / L_2$ cm^2	$d(\frac{1}{C_{te}^3})/dV$ Farad^3/volt)	$A_e^3 S_1$ (Sym.-Lin) cm^2	$A_e^3 S_1$ (Abr.-lin) cm^2	$A_e^3 \frac{N_R}{L_R}$ cm^2	V_{oc} (Volt)	V_{oe} (Volt)
2N696	1	3.06×10^{31}	2.17×10^{12}	5.58×10^{30}	11.9×10^{12}	2.97×10^{12}	12.2×10^{12}	0.48	0.66
2N1613	1	2.37	2.79	6.53	10.2	2.54	10.2	0.46	0.62
	2	1.40	4.75	5.09	13.0	3.26	13.0	0.43	0.64
	3	1.37	4.85	5.21	12.7	3.18	12.7	0.47	0.61
	12	1.62	4.11	3.76	17.6	4.41	17.9	0.47	0.64
2N1711	1	1.61	4.13	6.48	10.2	2.56	10.2	0.48	0.63
	2	1.96	3.42	9.39	6.86	1.71	7.06	0.47	0.61
	3	1.16	5.70	10.4	6.40	1.60	6.59	0.52	0.61
2N910	1	4.44	1.52	8.52	7.78	1.95	7.78	0.46	0.65
	2	3.90	1.70	9.28	7.15	1.79	7.15	0.44	0.63
	3	4.58	1.47	7.43	8.93	2.23	8.93	0.43	0.62
2N916	1	9.23×10^{33}	0.72×10^{10}	6.09×10^{33}	10.9×10^{9}	2.72×10^{9}	10.9×10^{9}	0.42	0.65
	2	5.52	1.20	4.36	15.2	3.80	15.2	0.43	0.65
	3	2.97	2.23	4.12	16.1	4.03	16.1	0.52	0.65
2N706A	1	14.2	4.68×10^{9}	17.1	3.88	0.97	3.98	0.68	0.68
	2	10,9	6.06	9.91	6.70	1.67	6.69	0.69	0.70

Table 4.3 - Interpretation of Transition Capacitance data

The extrapolation of the curves of $1/C_{tc}^3$ and $1/C_{te}^3$ vs V in Fig. 4.5 until they intersect the voltage axis determines the equilibrium barrier potentials V_{oc} and V_{oe} respectively. The equilibrium barrier potentials are set up by the depletion of carriers near the junction in the absence of an external voltage to prevent the flow of carriers across the junction. Assuming complete depletion, an appreciable depletion layer exists at either junction due to the potential barrier. Theoretically, if sufficient forward bias were applied to the junction, the width of the depletion layer could be reduced to zero, at which point transition capacitance would be infinite and the $1/C_t^3$ vs V curve would intersect the voltage axis at this value of forward bias. (Practical considerations, not necessary to this argument, prevent the complete elimination of the depletion layer). If the junction were linear, then for forward bias (if complete depletion still held) the plot of $1/C_t^3$ vs V would be an extension to the linear portion of the reverse biased curves (see Fig. 4.5). Thus, although transition capacitances can not be readily measured for forward bias, barrier potentials can be estimated by extrapolating curves similar to those of Fig. 4.5 until they intersect the voltage axis. The values of V_{oc} and V_{oe} listed in Table 4.3 were determined by this method.

4.2.4 Emitter and Collector Areas

Emitter and collector areas appear in the constants determined from transition capacitance data (Table 4.3). These areas must be known if the constants of the assumed model (Fig. 4.1) are to be separated from the measured data. Two possibilities exist for their determination:

(a) an optical measurement when the protective "can" is removed, and (b) evaluation during the course of parameter determination from terminal measurements when the ratio A_e/A_c is known.

Although some transverse diffusion occurs during fabrication of the planar transistor, emitter and collector areas are approximately equal to the areas of the "windows" opened in the protective oxide layer by masking techniques. Thus knowledge of the masking areas is sufficient to yield junction areas. This information may be obtained from the manufacturer of the transistor, or, taking advantage of the fact that the same masks are used for all devices of a particular type by a particular manufacturer, may be determined from an optical measurement through a microscope of masking areas for one sample of the type to be studied from which the protective can has been removed. Light refraction by the different thicknesses of oxide for the different regions causes the regions to appear to be coloured differently under the microscope. The photograph in Fig. 4.6 is of a 2N916 magnified 250X, with the scale presented below the photograph. Areas determined by optical means are presented in Table 4.4. These areas will be used in the calculations of Chapter 5. This optical determination of areas is felt to be justified since it is non-destructive of the actual transistor (only the outer can is removed), and the areas so determined can be applied to other transistors of the same type, providing a valid starting point in the evaluation of the internal configuration of the transistor.

To provide a basis for determination of A_e and A_c solely from terminal measurements, the ratio A_e/A_c may be determined as follows:

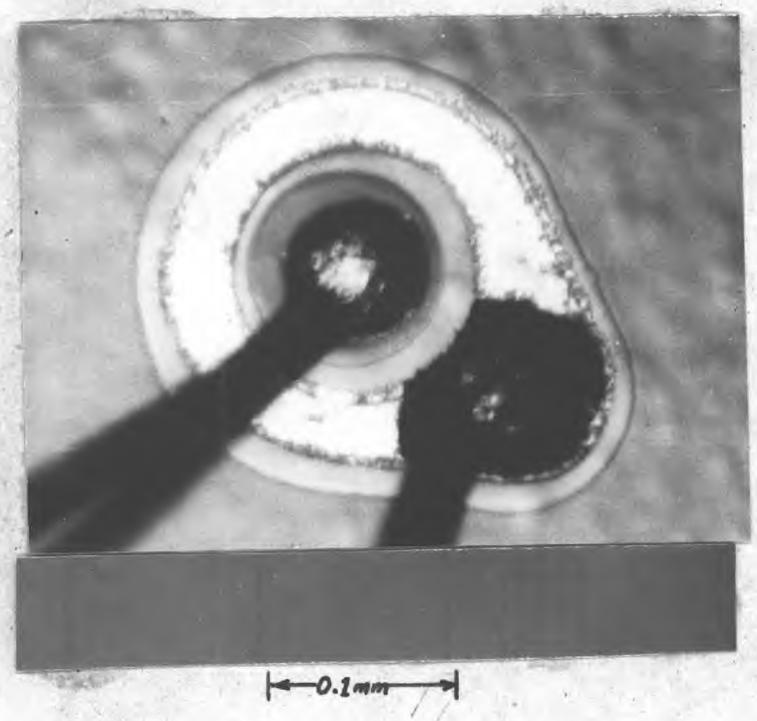


Fig. 4.6. Photograph of Planar Transistor (2N916#1)

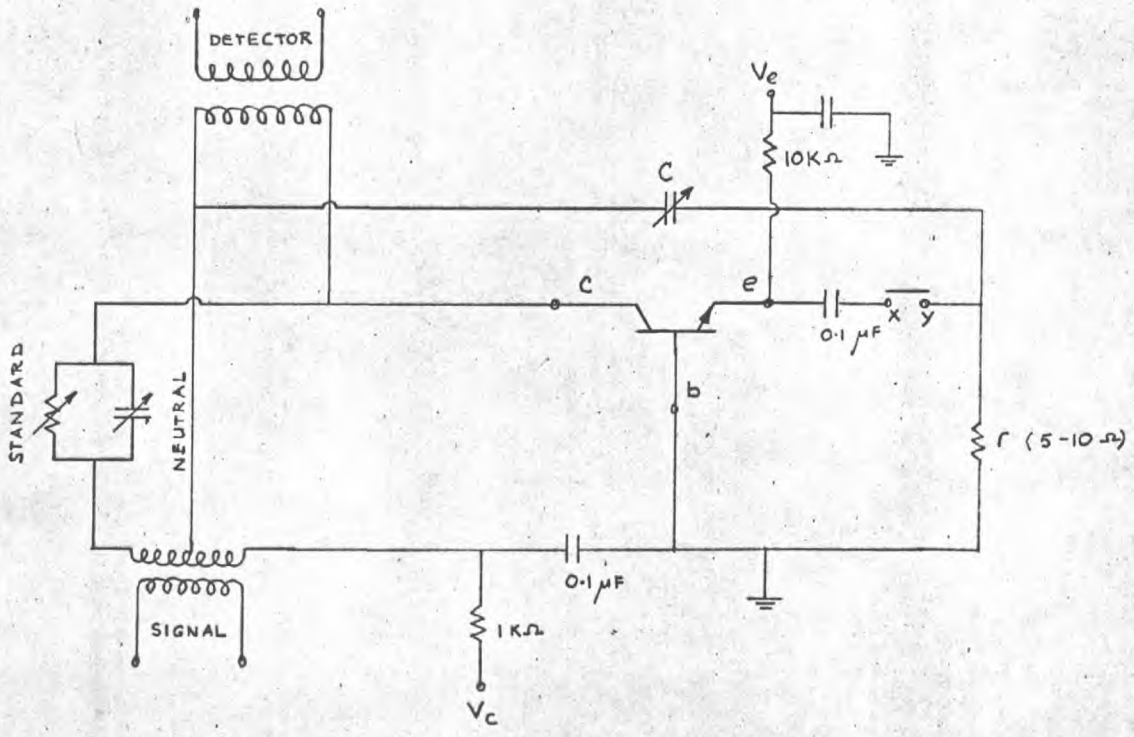


Fig. 4.7. Bridge for Measuring $r'_{bb}C_{tcl}$.

Table 4.4 - Junction Areas and Background Doping

Device Number		A_e x $10^{-4}cm^2$	A_c x $10^{-4}cm^2$	r'_{bb} C_{tc1} PF ~	C_{tc1} PF	C_{tc} ## PF	C_{sec} ## PF	$\frac{A_e}{A_e}$ *	$\frac{A_e}{A_c}$ **	N_B / x 10^{15} cm^{-3}	N_B ## x 10^{15} cm^{-3}
2N636	1	13.2	48.6	253	2.81	-	-	.312	.272	3.2	2.1
2N1613	1	11.0	52.5	157	1.74	-	-	.180	.210	3.7	2.3
	2	11.0	52.2	153	2.68	-	-	.219	.211	4.3	2.6
	3	11.0	52.2	474	5.72	23.8	0.49	.248	.211	4.5	2.7
	3	11.0	52.2	366	4.36	18.6	0.53	.239	.211	4.5	2.7
	3	11.0	52.2	293	3.37	14.3	0.57	.239	.211	4.5	2.7
	3	11.0	52.2	257	2.92	12.2	0.58	.242	.211	4.5	2.7
	12	11.2	52.2	167	2.92	11.7	0.52	.254	.215	4.2	2.4
2N1711	1	11.3	52.0	264	2.44	-	-	.213	.212	4.0	2.4
	2	11.3	52.0	399	3.25	13.1	0.60	.254	.212	5.2	3.9
	3	11.3	52.0	-	-	-	-	-	.212	4.8	2.6
2N910	1	11.2	49.3	310	2.90	11.5	0.57	.252	.227	0.95	1.6
	2	11.2	49.3	321	2.87	12.1	0.60	.237	.227	0.92	1.3
	3	11.2	49.3	267	2.67	11.3	0.61	.236	.227	0.97	1.8
2N916	1	.785	4.76	55	0.46	1.91	0.70	.227	.165	6.3	3.8
	2	.785	4.76	93	0.78	2.82	0.73	.250	.165	13.2	9.4
	2	.785	4.76	75	0.60	2.32	0.69	.250	.165	13.2	9,4
	3	.785	4.76	108	0.75	2.78	0.64	.250	.165	-	-
2N706A	1	.43	2.38	-	-	-	-	-	.18	-	-
	2	.43	2.38	-	-	-	-	-	.18	-	-

* From C_{tc1}/C_{tc}. ** From optical measurements ## From curves similar to Fig. 4.8
/ N_B from Miller's data. ## N_B corrected from Figs. 2.15 and 4.11 (see also Table 5.4) + Measured at 1 MHz.

$$\frac{C_{tc_1}}{C_{tc}} = \frac{\varepsilon A_e/d_c}{\varepsilon A_c/d_c} = \frac{A_e}{A_c} \qquad 4.2.25$$

where C_{tc_1} is the component of collector capacitance under the emitter area and C_{tc} is the total collector capacitance. No direct measurement of C_{tc_1} is possible. However, C_{tc_1} can be calculated once r'_{bb} and $r'_{bb}C_{tc_1}$ are known. The most satisfactory measurement of $r'_{bb}C_{tc_1}$ is by means of the Turner bridge[66], but in the absence of such a bridge the Wayne-Kerr B601 admittance bridge may be employed in the arrangement of Fig. 4.7[36] to determine this product. The step-by-step procedure is:

(1) With transistor removed balance the bridge for a null with the main dials at the "Set Zero" position;

(2) With points xy unconnected but with transistor in and properly biased, use the main dials to obtain a null. The reading of the capacitance dial is the common base output capacitance C_{ob} $(= C_{tc} + C_{scb})$.

(3) Connect points xy and rebalance with C_x for a new null.

Inductive effects may cause a change in the R-balance of the bridge, but do not significantly affect the capacitance measurement.

The balancing condition for Step 3 is:

$$\frac{j\omega C_x R_x}{1 + j\omega C_x R_x} = \frac{j\omega \left(\frac{C_{sec}}{Y_{ee}} + r'_{bb}C_{tc_1}\right) + \sigma}{1 + j\omega \left(\frac{C_{sec}}{Y_{ee}} + r'_{bb}C_{tc_1}\right) + \sigma} \qquad 4.2.26$$

where $\sigma = \frac{j\omega C_{sec}}{Y_{ee}} \left[(1 - a')Y_{ee} + j\omega C_{tc_1}\right] r'_{bb}$

The terms of σ are of second-order significance, so it can usually be neglected in eqn. 4.2.26. The balance conditionbecomes:

$$C_x R_x = C_{sec}/Y_{ee} + r'_{bb}C_{tc_1} \qquad 4.2.27$$

If the frequency of measurement is low, ($\omega \ll \omega_\tau$), then $Y_{ee} \approx g_{ee}$ $= qI_e/kT$. Eqn. 4.2.27 reduces to:

$$C_x R_x = \frac{kT}{qI_e} C_{sec} + r'_{bb}C_{tc_1} \qquad 4.2.28$$

where I_e is the emitter current.

Measurement of $C_x R_x$ over a range of emitter current (I_e) results in a straight line plot of $C_x R_x$ vs $1/I_e$ for which theslope is given by $C_{sec}.\frac{kT}{q}$ and $r'_{bb}C_{tc_1}$ by the intercept on the vertical axis (see Fig. 4.8). This projection must be of the straight line portion of the curve at low currents, since for high currents emitter diffusion capacitance C_{de} becomes significant and causes $C_x R_x$ to increase. Values of $r'_{bb}C_{tc_1}$ are listed in Table 4.4. The slope of the straight line provides an alternative method for determining C_{sec}, while the balance condition in Step 2 allows determination of C_{tc} from $C_{cb} - C_{scb}$. Values of C_{sec} and C_{tc} from this method are included in Table 4.4 and compare favourably with those determined in Section 4.2.3 and listed in Table 4.1.

Although other methods are available for determination of r'_{bb} [38,67] they are generally complicated. Since r'_{bb} is only an approximate concept, it is felt that the estimate of r'_{bb} from eqn. 4.2.13 is sufficiently accurate for most purposes. The values of r'_{bb} from Table 4.1 were therefore used with the values of $r'_{bb}C_{tc_1}$

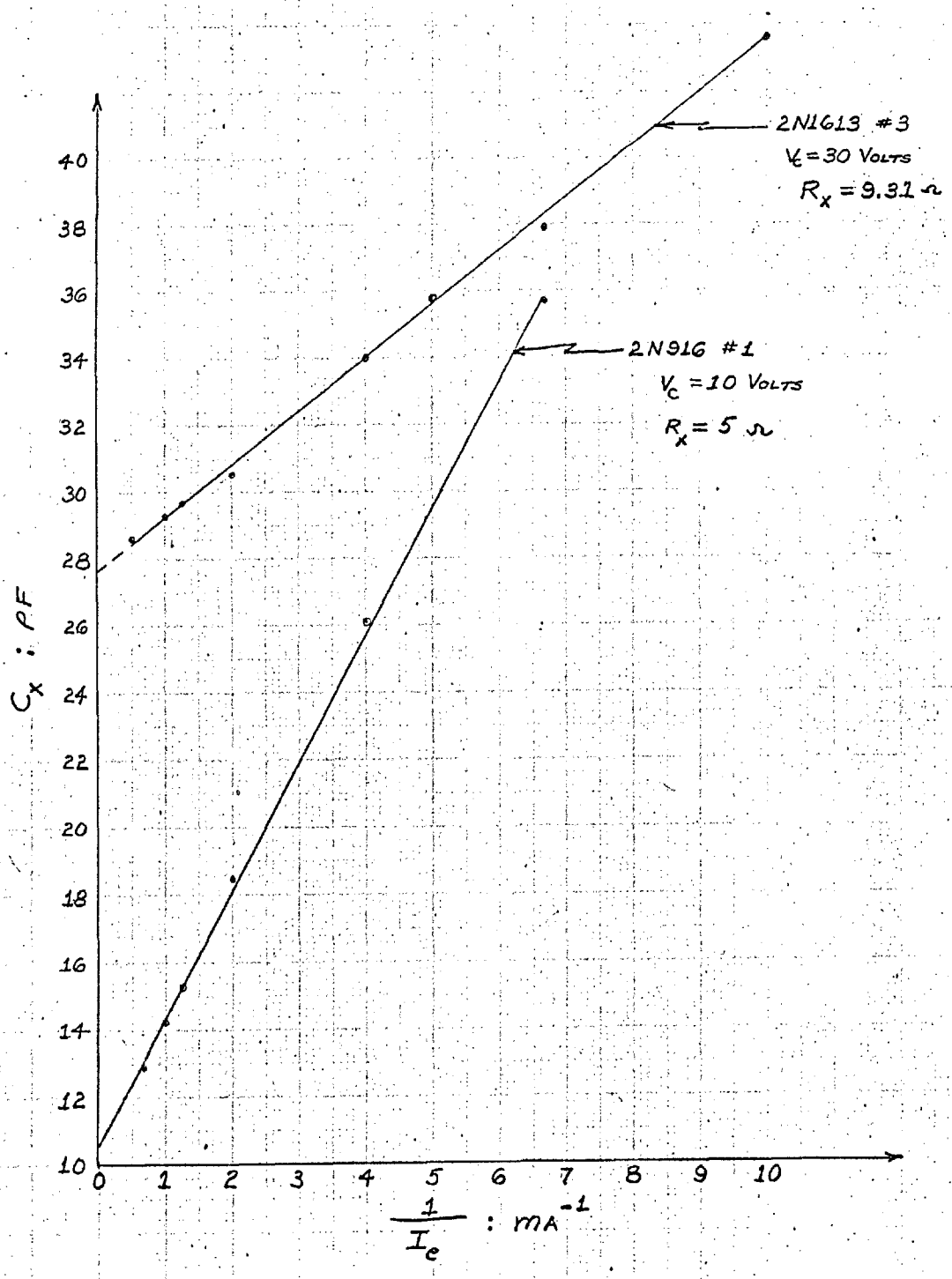


Fig. 4.8. Determination of $r'_{bb}C_{tcl}$.

(Table 4.4) to estimate C_{tc1}. Values of C_{tc1} and A_e/A_c from eqn. 4.2.25 are listed in Table 4.4. For comparison A_e/A_c as computed from the optically measured areas is also presented.

4.2.5 Estimate of N_B from Collector Breakdown

When the electric field in a reverse biased junction exceeds a critical value, the junction exhibits large reverse current increase for small increase in voltage. Such breakdown is either Zener[68] (internal field emission) or avalanche (large carrier multiplication) [63,69]. The voltage at which breakdown occurs is a function of the impurity concentration on either side of the junction. Zener breakdown normally occurs in junctions where narrow depletion layers (due to low resistivity) lead to very high electric fields, while avalanche breakdown normally occurs in high resistivity junctions with wide depletion layers. Consequently, breakdown in diffused junctions is generally by the avalanche process.

Miller[63] and McKay[69] studied avalanche breakdown for step junctions, concluding that for asymmetrical junctions (one side of the junction more highly doped than the other), since most of the depletion layer lies on the high resistivity side of the junction, avalanche voltage is a direct function of doping on this side of the junction. Veloric et al[70] treated linear approximations to graded junctions, while Root et al[71] extended the theory to include prediction of avalanche voltage in a junction with ERFC distribution:

$$N(x) = N_s \operatorname{erfc}\left(\frac{Mx}{x_j}\right) - N_B \qquad 4.2.29$$

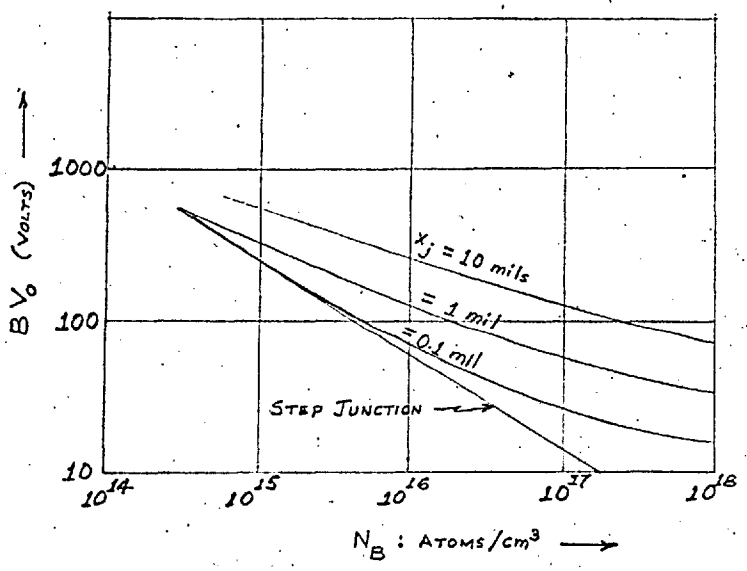


Fig. 4.9. Breakdown voltage in Diffused Junction in Silicon (from Ref. 71).

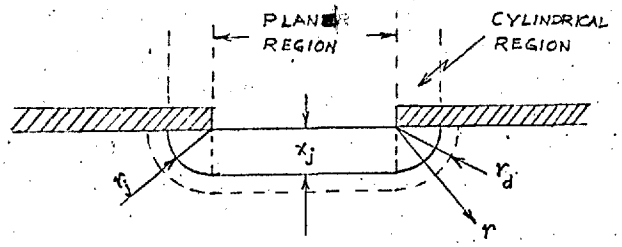


Fig. 4.10. Plane-Cylindrical Diffused Junction.

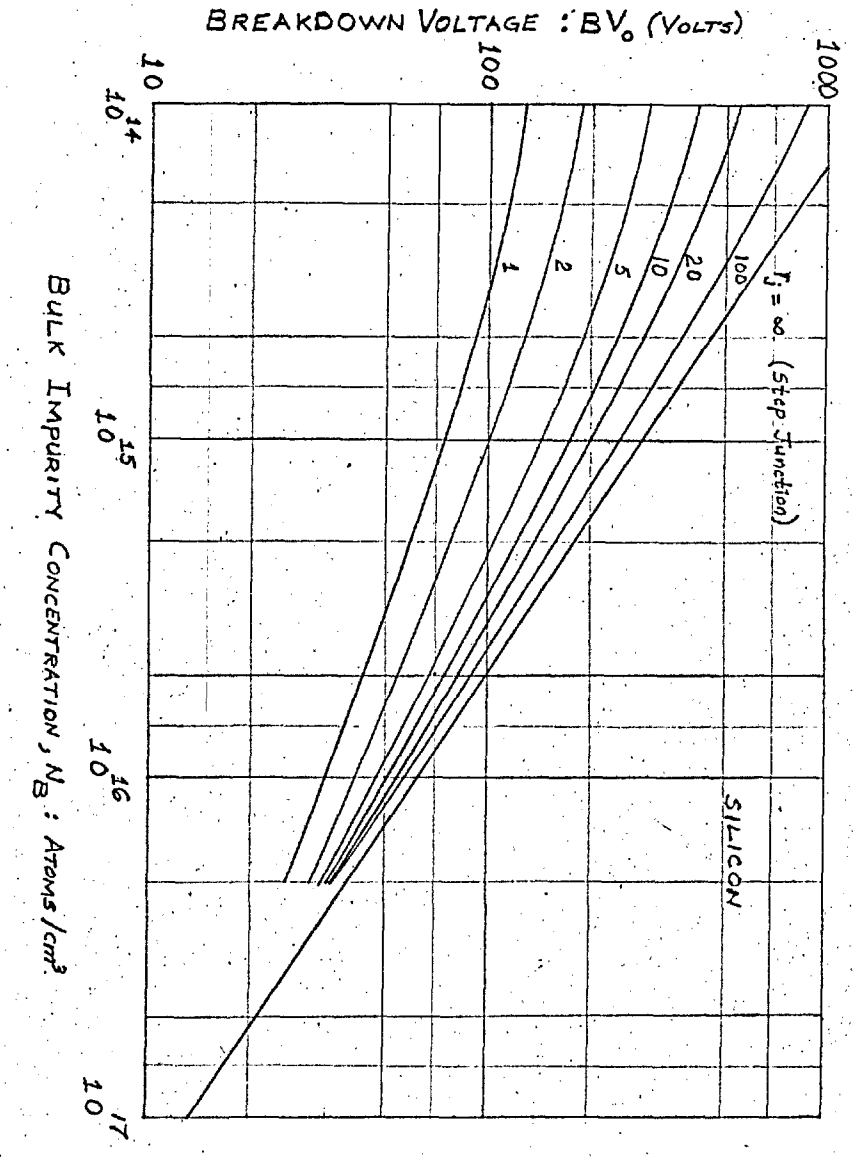


Fig. 4.11. Breakdown Voltage vs Bulk impurity concentration with junction radius as a parameter.

where N_s is surface concentration, N_B is background doping, M is defined as erfcM = N_B/N_s, and x_j is junction depth. Fig. 4.9 is a plot of breakdown voltage BV_o vs N_B with x_j as a parameter (for silicon) reproduced from Root et al[71]. The curve for a step junction (Miller [63]) is represented in the figure by the straight line. Fig. 4.9 indicates that when $x_j \leq 0.1$ mil (2.54 μ) and $N_B \leq 10^{16}$ atoms/cc, the avalanche voltage for the diffused junction closely approximates that for a step junction when $N_s \geq 10^{18}$ atoms/cc. Since the general form of any diffused junction is the same (see Fig. 2.2) when the junction is formed at a concentration considerably less than the surface concentration, Fig. 4.9 may be used equally well for any impurity grading (including an exponential) - providing the junction lies in a single plane - to determine doping on the high resistivity side of the junction.

To determine collector body doping of a planar transistor from measurement of breakdown voltage, consideration must be given to the actual shape of the junction. The actual form of the junction is an oblate spheroid which may be approximated as in Fig. 4.10 by a flat junction with cylindrical edges. The radius of the cylinder is approximately equal to the depth of penetration of the junction, x_j, and is small with respect to the junction area. Avalanche breakdown for a cylindrical junction is dependent not only on the resistivity of the material, but also on the radius of the junction and will occur at a much lower voltage than for a planer junction of the same resistivity[72,73]. Thus breakdown in the collector junction of a planar transistor will begin at the cylindrical edge, so that use of this voltage to estimate N_B

from Fig. 4.9 will lead to a value of N_B which is too high.

Gibbons and Kocsis[64] have presented equations which relate breakdown voltage to the radius of the cylindrical region. Electric field is given by

$$E = -\frac{q}{2\varepsilon} N_B \left(r - \frac{r_d^2}{r}\right) \qquad 4.2.30$$

where r is the radius in cm, and r_d is the radius of the depletion layer in the collector (see Fig. 4.10). Collector breakdown voltage is given by:

$$BV_{CBo} = \frac{q}{2\varepsilon} N_B \left\{\frac{r_d^2 - r_j^2}{2} - r_d^2 \ln \frac{r_d}{r_j}\right\} \qquad 4.2.31$$

where $r_j = x_j$ is the radius of the junction (since transverse diffusion occurs at approximately the same rate as inward diffusion during fabrication).

Avalanche breakdown occurs when

$$\int_{r_j}^{r_d} \alpha_i(E)dr = 1 \qquad 4.2.32$$

where α_i is the ionization factor. Root et al[71] used the following empirical relationships for ionization coefficients in silicon:

$$\alpha_{i_1} = 1.935 \times 10^{-24} E^5 \qquad 200Kv/cm \leq E \leq 500\ Kv/cm \qquad 4.2.33(a)$$

$$\alpha_{i_2} = 2.5 \times 10^{-7} E^2 \qquad 500Kv/cm \leq E \leq 750Kv/cm \qquad 4.2.33(b)$$

$$\alpha_{i_3} = 1.3 \times 10^5 \qquad 750K_v/cm \leq E \leq 1000Kv/cm \qquad 4.2.33(c)$$

Substituting E from eqn. 4.2.30 into eqn. 4.2.33 and employing eqn. 4.2.32 gives

$$-1.953 \times 10^{-24} \left(\frac{q}{2\varepsilon} N_B\right)^5 \int_{r_j}^{r_d} \frac{(r^2 - r_d^2)^5}{r^5} dr = 1 \qquad 4.2.34(a)$$

$$2.5 \times 10^{-7} \left(\frac{q}{2\varepsilon} N_B\right)^2 \left[-\frac{8}{3} r_d^3 - \frac{r_j^3}{3} - 2r_d^2 r_j - \frac{2r_d^4}{r_j} \right] = 1 \qquad 4.2.34(b)$$

$$1.3 \times 10^{-5} (r_d - r_j) = 1 \qquad 4.2.34(c)$$

A computer program was written to determine r_d from eqn. 4.2.34 for different values of r_j, and BV_{CBo} was determined from eqn. 4.2.31. Fig. 4.11 presents curves of BV_{CBo} vs N_B with r_j as a parameter from the above computation. These curves (for silicon) are similar to those presented for germanium by Gibbons and Kocsis[64]. When $r_j \to \infty$ in Fig. 4.11 the curve becomes that for a step junction.

The following method is suggested for determination of the value of collector body doping from Fig. 4.11. Measure BV_{CBo} for the collector junction, and estimate N_B from the curve for the step junction. With collector transition capacitance at a particular value of reverse bias and this value of N_B, estimate x_j (= r_j) from Lawrence and Warner's[33] curves (Fig. 2.15). Use this value of r_j in Fig. 4.11 to recalculate a new value of N_B, which is then used in the same way to get a new r_j. This iteration should reach convergence very quickly within the accuracy of the two sets of curves. N_B determined from this method may be used

either in parameter determination or as a check on the value determined by other means. Values of N_B from this treatment are included in Table 4.4.

In certain cases (i.e..narrow base) it may be impossible to measure BV_{CBo}, since "punch-through" occurs before the collector can break down. Increase of the collector voltage eventually causes the emitter junction to break down at its periphery whereupon collector voltage falls back to a lower value. A negative resistance is exhibited in the V-I characteristics[74].

4.3 Emitter Diode Characteristics

4.3.1 General Equations

Forward bias on the emitter junction causes minority carriers to be injected into the base region resulting in a flow of current. At any point in the base, assuming Boltzmann statistics apply, the product of minority and majority carriers is given by:

$$pn = n_i^2 \, e^{q V_e/kT} \qquad 4.3.1$$

where in an NPN transistor, p and n are the number of majority and minority carriers respectively, V_e is the emitter voltage and n_i is the intrinsic carrier density which may be determined from the empirical relationship:

$$n_i^2 = 1.5 \times 10^{33} \, T^3 \, e^{-1.21q/kT} \text{ for silicon}[75] \qquad 4.3.2$$

or

$$n_i^2 = 3.1 \times 10^{32} \, T^3 \, e^{-.785q/kT} \text{ for Germanium}[76] \qquad 4.3.3$$

Assuming non-degeneracy (complete ionization of impurities) and low level injection, the number of majority carriers at any point is approximately equal to the number of "uncompensated" impurities at that point (i.e. $p = N_A - N_D$). At the base edge of the emitter depletion region, ($Y_1 = a_{2c}/W$), eqn. 4.3.1 becomes:

$$n(Y_1) = \frac{n_i^2}{N(Y_1)} e^{qV_e/kT} \qquad 4.3.4$$

where $N(Y_1)$ is the uncompensated impurity density at this point. For the double exponential model,

$$N(Y_1) = N_o(e^{-m_2 Y_1} - e^{-\gamma m_2 Y_1} - \eta) \qquad 4.3.5$$

Minority carrier density at any point in the base was given by eqn. 3.5.38, which becomes at Y_1:

$$n(Y_1) = -\frac{J_n W}{q} \frac{1}{e^{-m_2 Y_1} - e^{-\gamma m_2 Y_1} - \eta} \int_{Y_1}^{1} \frac{e^{-m_2 Y} - e^{-m_2 Y} - \eta}{D_n(N_o(e^{-m_2 Y} + e^{-\gamma m_2 Y} + \eta))} dY \qquad 4.3.6$$

where J_n is the current density. Assuming the collector junction is reverse biased and high emitter efficiency, J_n is carried mostly by electrons injected into the base from the emitter. Thus $J_n \approx -I_c/A_e$ where I_c is the collector current. (Collector reverse saturation current can usually be neglected in silicon planar transistors). Using this relationship and substituting $n(Y_1)$ and $N(Y_1)$ into eqn. 4.3.4 gives:

$$\frac{I_c}{qn_i^2 e^{qV_e/kT}} = \frac{A_e W}{N_o} \cdot \int_{Y_1}^{1} \frac{1}{\frac{(e^{-m_2 Y} - e^{-\gamma m_2 Y} - \eta)}{D_n (N_o (e^{-m_2 Y} + e^{-\gamma m_2 Y} + \eta))}} dY \qquad 4.3.7$$

The left-hand side of eqn. 4.3.7 represents the form in which measured information is presented in Section 4.3.4. This equation applies for the general case when the diffusion coefficient varies with impurity density throughout the base.

4.3.2 $\bar{D}_R$ and $\bar{D}_A$ Approximation

No serious loss of accuracy was evident when minority carrier density and base transit time were computed for the double exponential model in Chapter 3 with the variable diffusion coefficient replaced by $\bar{D}_R$ in the retarding field region, and $\bar{D}_A$ in the aiding field region. Consequently, this two-diffusion coefficient approximation will be adopted for practical devices, and applied here in treating doide characteristics.

Under forward bias conditions at the emitter, Y_1 is invariable less than Y_m (position of maximum doping in the base). Thus minority carrier density is given by eqn. 3.5.42. Minority carrier density at Y_1 is given by:

$$n(Y_1) = \frac{I_c W}{q\bar{D}_R A_e} \left[\left(1 - \frac{\bar{D}_R}{\bar{D}_A}\right) \left(\frac{e^{-\gamma m_2 Y_m}}{\gamma m_2} - \frac{e^{-m_2 Y_m}}{m_2} - \eta Y_m \right) + \frac{\bar{D}_R}{\bar{D}_A} \left(\frac{e^{-\gamma m_2}}{\gamma m_2} - \frac{e^{-m_2}}{m_2} - \eta \right) - \left(\frac{e^{-\gamma m_2 Y_1}}{\gamma m_2} - \frac{e^{-m_2 Y_1}}{m_2} - \eta Y_1 \right) \right] \cdot \frac{1}{e^{-m_2 Y_1} - e^{-\gamma m_2 Y_1} - \eta} \qquad 4.3.8$$

where - I_c/A_e has been substituted for J_n. Substitution of $n(Y_1)$ from eqn. 4.3.8 and $N(Y_1)$ from eqn. 4.3.5 into eqn. 4.3.4 results in the following expression for the emitter diode:

$$\frac{I_c}{qn_i^2 e^{qV_e/kT}} = \frac{\bar{D}_R A_e}{N_o L_2} \left[\frac{1}{\left\{ \left(1 - \frac{\bar{D}_R}{\bar{D}_A}\right)\left(\frac{e^{-\gamma m_2 Y_m}}{\gamma} - e^{-m_2 Y_m} - \eta m_2 Y_m\right) + \frac{\bar{D}_R}{\bar{D}_A}\left(\frac{e^{-\gamma m_2}}{\gamma} - e^{-m_2} - m_2\right) - \left(\frac{e^{-\gamma m_2 Y_1}}{\gamma} - e^{-m_2 Y_1} - \eta m_2 Y_1\right)\right\}} \right] \qquad 4.3.9$$

Eqn. 4.3.9 provides the basis for employment of emitter diode characteristics in the determination of the constants of the physical model in Chapter 5. I_c, V_e and T can be measured, Y_m can be determined from eqn. 3.5.36, and $\bar{D}_R$ and $\bar{D}_A$ can be determined from Fig. 2.11 once average dopings in the retarding and aiding field regions have been found from eqns. 3.5.38 and 3.5.39 respectively. The values of γ, m_2, and Y_1 used in these equations are derived in Chapter 5 during the course of parameter determination.

4.3.3 Approximation based on $\bar{D}_R$ only.

Since the emitter diode law depends strongly on the number of minority carriers injected at the base edge of the emitter depletion layer and on the impurity density at this point (eqn. 4.3.4) it is intuitively felt that the retarding field region exerts a much greater influence on the diode law than does the aiding field region. If this were true, it should be possible to treat the diode law on the basis of

a single equivalent diffusion coefficient $\overline{D}_R$ (for the retarding field region) applying throughout the base. Eqn. 4.3.8 reduces to:

$$\frac{I_c}{qn_i^2 e^{qV_e/kT}} = \frac{\overline{D}_R A_e}{N_o L_2} \quad \frac{1}{\left(\frac{e^{-\gamma m_2}}{\gamma} - e^{-m_2 - \eta m_2}\right) - \left(\frac{e^{-\gamma m_2 Y_1}}{\gamma} - e^{-m_2 Y_1 - \eta m_2 Y}\right)} \qquad 4.3.10$$

Eqn. 4.3.10 is used in Chapter 5 in the determination of the constants of the model. Comparison of the results based on eqn. 4.3.10 with those based on eqn. 4.3.9 supports the intuitive argument.

4.3.4 Measurement of Diode Characteristic

The emitter diode characteristic can be obtained by a straightforward d.c. measurement of collector current and emitter forward bias voltages. As indicated in eqns. 4.3.7, 4.3.9 and 4.3.10, the emitter diode law is highly termperature dependent (T appears in both $e^{qV_e/kT}$ and in n_i^2 as determined from eqn. 4.3.2). Thus junction temperature must be accurately determined during the d.c. measurement. Power dissipation in the transistor during the measurement raises the temperature of the junction. This power dissipation depends largely on the reverse bias voltage on the collector junction and the size of the collector current, but owing to the close proximity of the two junctions, the temperature of both emitter and collector junctions should rise by an equal amount.

Junction temperature can not be measured directly, but can only be estimated. The method adopted in the measurements of this section was to measure the temperature of the can (held constant) by means of a thermocouple, and to use the values of junction-to-can thermal resistances

supplied by the manufacturers to estimate the temperature rise at the junction due to the power dissipated. Junction temperature was equal to the can temperature plus the temperature rise.*

The choice of the current at which to measure V_e and T to use in eqns. 4.3.9 and 4.3.10 is important. To reduce collector dissipation it is preferable to choose as low a current as possible. However at very low currents, as shown in Fig. 4.12, diode current is no longer proportional to $e^{qV_e/kT}$. In this region the component of current necessary to supply recombination in the space charge layer dominates[77]. At high currents ohmic drop due to series resistance causes the characteristics to depart from the $e^{qV_e/kT}$ law (Fig. 4.12). From curves similar to that of Fig. 4.12 which were used to establish the lower limit of the $e^{qV_e/kT}$ relationship, it was decided to use a current of 0.1 ma to determine $\frac{I_c}{qn_i^2 e^{qV_e/kT}}$ for the various transistors measured. This data is listed in Table 4.5 and is used in Chapter 5 in deriving the constants of the double-exponential model.

A brief discussion will serve to point out the attractiveness of emitter diode measurements as a source of information on the base impurity profile. Limiting the discussion to the $\overline{D}_R$ and $\overline{D}_A$ approximation of eqn. 4.3.9, it can be seen that all the parameters of the double exponential model appear in the expression. Although the

---

*It is possible to measure thermal resistance of each transistor by a method based on collector saturation current[38], but for the low power dissipated during the measurements of this section the manufacturers' values were assumed to be sufficiently accurate.

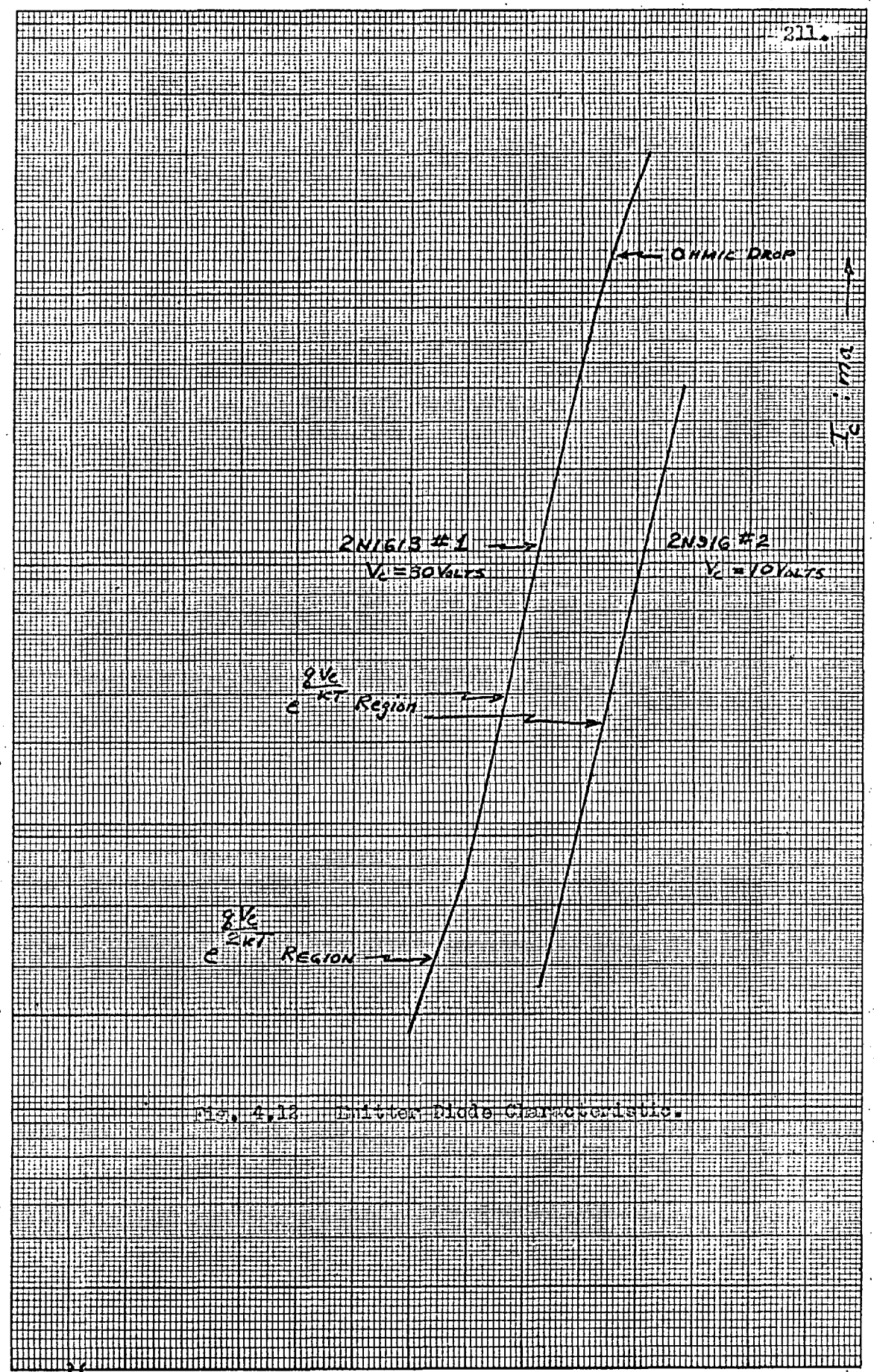


Fig. 4.12 Emitter Diode Characteristic.

expression is complicated so that the diode measurement must be used in conjunction with other measurements to separate the variables, being a d.c. quantity it is easily measured with good accuracy. Thus assuming the double-exponential model is accurate for actual devices, diode measurements are a valuable source of information on the constants of the model. Bias information appears on the right-hand side of the expression in the form of Y_1 for the emitter and $m_2 (= \frac{W}{L_2})$ for the collector. The presence of Y_1 stems from the space charge approximation at the emitter junction. For forward bias this approximation is inaccurate[65] and can be a source of error in computations involving eqn. 4.3.9. In the interests of simplicity, however, this approximation is felt to be justified. Perhaps the best justification for this is the successful determination in Chapter 5 of the constants of the model for actual transistors. The presence of m_2 in eqn. 4.3.9 means that during measurement of I_c and V_e the collector must be biased to the voltage to be used in calculations for the collector junction.

4.4 Base Transit Time

4.4.1 General Equations

Using the charge control definition of base transit time (eqn. 2.4.7), expressions were determined in Chapter 3, Section 3.5.5. for transit time across a base on which the impurity distribution is a double-exponential. The general expression in which the diffusion coefficient varies throughout the base with impurity distribution is given by eqn. 3.5.44.

As for the emitter diode, the two-diffusion coefficient

Device Number		$\frac{I_c}{qn_i^2 e^{qV_e/kT}}$ $\times 10^{-15}$ cm^{6}sec^{-1}	C_{te} fwd pF	τ' ** nsec	τ_c nsec	r'_{cc} * Ω	$r'_{cc}C_{tc}$ nsec	τ_b nsec
2N696	1	2.48	136	1.78	.036	16	.144	1.60
2N1613	1	2.43	135	1.45	.036	4	.039	1.38
	2	1.16	171	1.60	.028	5.8	.071	1.50
	3	2.09	152	1.46	.015	6.3	.145	1.30
	3	2.10	152	1.38	.019	6.3	.115	1.25
	3	2.12	152	1.29	.025	6.3	.089	1.18
	3	2.18	152	1.24	.029	6.3	.076	1.14
	12	1.27	178	1.60	.030	6.0	.069	1.50
2N1711	1	3.32	146	1.04	.030	4.0	.046	0.96
	2	3.32	121	0.80	.032	7.8	.084	0.68
	3	4.32	119	0.98	.018	4.6	.089	0.87
2N910	1	3.19	110	1.46	.028	18	.207	1.22
	2	3.27	111	1.36	.027	13.5	.163	1.17
	3	2.77	119	1.56	.029	14	.158	1.37
2N916	1	0.27	15.5	.352	.016	10	.020	.316
	2	0.37	15.9	.432	.010	10	.031	.391
	2	0.39	15.8	.412	.013	10	.024	.375
	3	0.42	15.5	.337	.010	28	.084	.243
2N706A	1	0.155	9.7	.337	.004	5	.019	.314
	2	0.784	12.0	.452	.004	4	.016	.432

* For zero bias on collector junction.

** Measured at 1MHz. Collector bias corresponds to values in Table 4.1.

Table 4.5 - Emitter Diode and Transit Time data.

approximation will be used in computations involving transit time for actual double-diffused transistors. Adding the retarding field and aiding field region components as indicated in eqn. 3.5.47 gives:

$$\tau_b = \frac{W^2}{\overline{D}_R}\left[\int_{Y_1}^{Y_m} \frac{(1-\frac{\overline{D}_R}{\overline{D}_A})(\frac{e^{-\gamma m_2 Y_m}}{\gamma m_2} - \frac{e^{-m_2 Y_m}}{m_2} - \eta Y_m) + \frac{\overline{D}_R}{\overline{D}_A}(\frac{e^{-\gamma m_2}}{\gamma m_2} - \frac{e^{-m_2}}{m_2} - \eta) + (\frac{e^{-\gamma m_2 Y}}{\gamma m_2} - \frac{e^{-m_2 Y}}{m_2} - \eta Y}{e^{-m_2 Y} - e^{-\gamma m_2 Y} - \eta} dY\right.$$

$$\left. + \frac{\overline{D}_R}{\overline{D}_A}\int_{Y_m}^{1} \frac{(\frac{e^{-\gamma m_2}}{\gamma m_2} - \frac{e^{-m_2}}{m_2} - \eta) - (\frac{e^{-\gamma m_2 Y}}{\gamma m_2} - \frac{e^{-m_2 Y}}{m_2} - \eta Y)}{e^{-m_2 Y} - e^{-\gamma m_2 Y} - \eta} dY\right] \quad 4.4.1$$

Unfortunately, the presence of the double exponential in the denominator of the integrands precludes analytical evaluation of the integrals so eqn. 4.4.1 must be evaluated by numerical means.

Base transit time is directly dependent on the minority carrier density, which is found by integrating the impurity density from the base edge of the collector depletion layer, where the gradient of minority carrier density is defined, as a boundary condition, by the current. The aiding field region, adjacent to the collector boundary, is critical in defining the minority carrier density throughout the base, for not only does the impurity grading in this region directly control the carrier density there, but also the extent of the build-up of carrier density in the retarding field region. This is evident by reference to Fig. 4.13. The solid curve (I) represents minority carrier density in a uniform base transistor. Adding a retarding field region up to Y_m superimposes a build-up of minority carriers in this region on the original curve

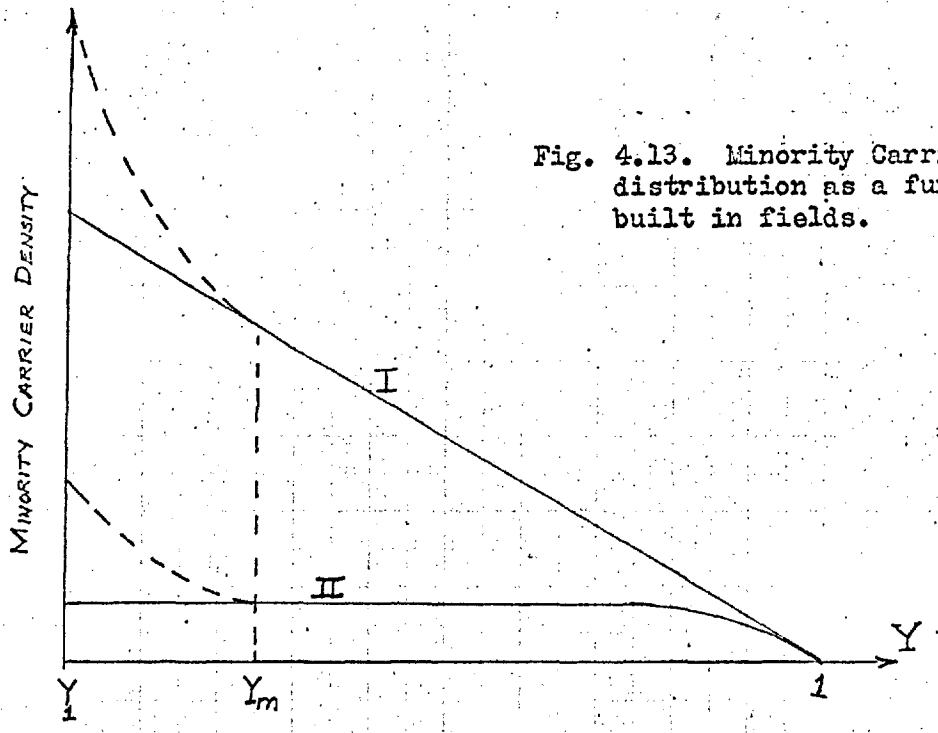


Fig. 4.13. Minority Carrier distribution as a function of built in fields.

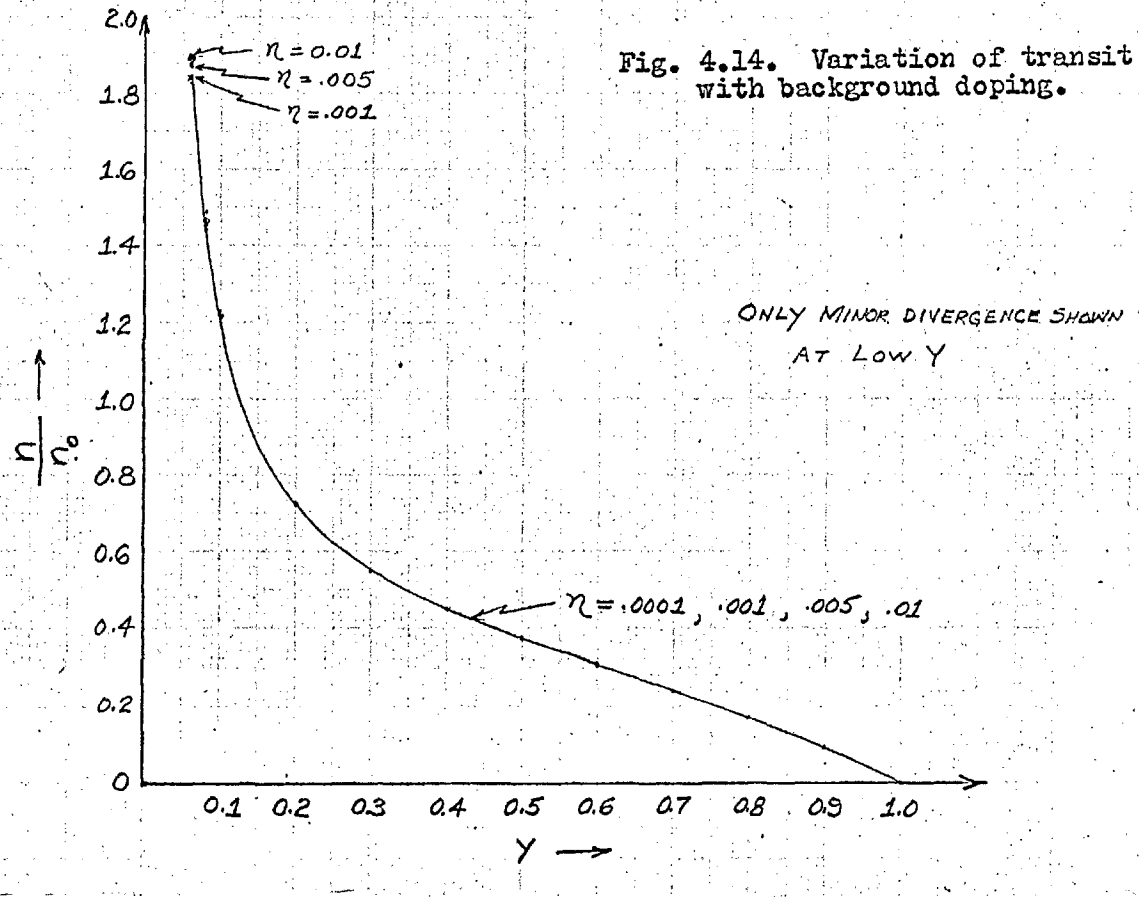


Fig. 4.14. Variation of transit time with background doping.

(broken extension of I). Curve II represents minority carrier density in a base with a built-in aiding field throughout, and indicates a large reduction in minority carrier density from the uniform base. The broken extension of II indicates the effect of a retarding field region up to Y_m. This build-up of minority carriers is superimposed on a much lower density than for the uniform base case - the lower density being caused by the presence of the aiding field. The greater the extent of the aiding field region the less is the build-up of minority carriers in the retarding field region. If the aiding field region occupies the major portion of the base (as in most transistors studied) and has a fairly high field strength, then minority carrier density is largely dependent on the impurity grading in this region. Under such conditions it should be possible, while integrating minority carrier density over the whole base region, to apply a single equivalent diffusion coefficient throughout the base to the transit time expression - dependent approximately on the average doping in the aiding field region. For such an approximation:

$$\tau_b \frac{W^2}{\overline{D}_A} \int_{Y_1}^{1} \frac{\left(\frac{e^{-\gamma m_2}}{\gamma m_2} - \frac{e^{-m_2}}{m_2} - \eta\right) - \left(\frac{e^{-\gamma m_2 Y}}{\gamma m_2} - \frac{e^{-m_2 Y}}{m_2} - \eta Y\right)}{e^{-m_2 Y} - e^{-\gamma m_2 Y} - \eta} dY \qquad 4.4.2$$

where $\overline{D}_A$ is determined at the average doping $\overline{N}_A$ given by eqn. 3.5.39.

Use of this approximation in Chapter 5 results in the determination of γ, m_2, η and W which are only slightly different from those determined on the basis of the $\overline{D}_R$ and $\overline{D}_A$ approximations. Such

quantitative information supports the above intuitive argument.

4.4.2 Simplification when N_B is Negligible in the Base

The expression for base transit time (eqns. 4.4.1 and 4.4.2) are complicated by the presence of an integral which can not be evaluated analytically. When, as is often possible, N_B (background doping) can be neglected in the neutral base region with respect to the uncompensated impurity density, the disappearance of all terms containing $\eta (= N_B/N_o)$ in the above equations considerably simplifies their soltuion. Neglecting η in eqn. 4.4.1 and rearranging into a more readily integrable form gives:

$$\tau_b \simeq \frac{W^2}{\overline{D}_R}\left[\int_{Y_1}^{Y_m}\left\{\frac{1}{\gamma m_2(1 - e^{(\gamma-1)m_2Y})} + \frac{1}{m_2(1 - e^{-(\gamma-1)m_2Y})}\right\}dY\right.$$

$$+ \frac{\overline{D}_R}{\overline{D}_A}\int_{Y_m}^{1}\left\{\frac{1}{\gamma m_2(1 - e^{(\gamma-1)m_2Y}} + \frac{1}{m_2(1 - e^{-(\gamma-1)\ m_2Y})}\right\}dY$$

$$+ \left(1 - \frac{\overline{D}_R}{\overline{D}_A}\right)\left(\frac{e^{-\gamma m_2 Y_m}}{\gamma m_2} - \frac{e^{-m_2 Y_m}}{m_2}\right)\int_{Y_1}^{Y_m}\frac{1}{e^{-m_2Y} - e^{-\gamma m_2 Y}}\,dY$$

$$\left. + \frac{\overline{D}_R}{\overline{D}_A}\left(\frac{e^{-\gamma m_2}}{\gamma m_2} - \frac{e^{-m_2}}{m_2}\right)\int_{Y_1}^{1}\frac{1}{e^{-m_2Y} - e^{-\gamma m_2 Y}}\,dY\right] \qquad 4.4.3$$

The first two integrals may be evaluated by use of the integration formula:

$$\int \frac{dx}{1 - e^{-bx}} = \frac{1}{b} \ln(e^{bx} - 1) + C$$

where b is any constant and C is the integration constant. Applying this formula to eqn. 4.4.3 and rearranging, transit time becomes

$$\tau_b \approx \frac{W^2}{\bar{D}_R} \left[\frac{1}{m_2^2(\gamma - 1)} \ln \left| \frac{e^{(\gamma-1)m_2 Y_m} (e^{-(\gamma-1)m_2 Y_m} - 1)^{1 - \frac{1}{\gamma}}}{e^{(\gamma-1)m_2 Y_1} (e^{-(\gamma-1)m_2 Y_1} - 1)^{1 - \frac{1}{\gamma}}} \right| \right.$$

$$- \frac{\bar{D}_R}{\bar{D}_A} \left\{ \frac{1}{m_2^2(\gamma - 1)} \ln \left| \frac{e^{(\gamma-1)m_2 Y_m} (e^{-(\gamma-1)m_2 Y_m} - 1)^{1 - \frac{1}{\gamma}}}{e^{(\gamma-1)m_2 Y_1} (e^{-(\gamma-1)m_2 Y_1} - 1)^{1 - \frac{1}{\gamma}}} \right| \right.$$

$$+ \left(1 - \frac{\bar{D}_R}{\bar{D}_A}\right) \left(\frac{e^{-\gamma m_2 Y_m}}{\gamma m_2} - \frac{e^{-m_2}}{m_2}\right) \int_{Y_1}^{Y_m} \frac{dY}{e^{-m_2 Y} - e^{-\gamma m_2 Y}} + \frac{\bar{D}_R}{\bar{D}_A} \left(\frac{e^{-\gamma m_2}}{\gamma m_2} - \frac{e^{-m_2}}{m_2}\right)$$

$$\left. \int_{Y_1}^{1} \frac{dY}{e^{-m_2 Y} - e^{-\gamma m_2 Y}} \right] \qquad 4.4.4$$

Only the last two terms of eqn. 4.4.4 involve an integral which can not be evaluated generally for any value of γ. It can, however, be evaluated for the specific cases where γ is equal to either 2 or 3. The method of evaluation is indicated in Appendix A.8. Thus, for $\gamma = 2$:

$$\tau_b \approx \frac{W^2}{2\overline{D}_R m_2^2}\left[\ln\left|\frac{e^{m_2Y_m}(e^{m_2Y_m}-1)}{e^{m_2Y_1}(e^{m_2Y_1}-1)}\right| - \frac{\overline{D}_R}{\overline{D}_A}\ln\left|\frac{e^{m_2Y_m}(e^{m_2Y_m}-1)}{e^{m_2}(e^{m_2}-1)}\right|\right.$$

$$+ \left(1-\frac{\overline{D}_R}{\overline{D}_A}\right)(e^{-2m_2Y_m}-2e^{-m_2Y_m})\left\{(e^{m_2Y_m}-e^{m_2Y_1}) + \ln\left|\frac{e^{m_2Y_m}-1}{e^{m_2Y_1}-1}\right|\right\}$$

$$\left. + \frac{\overline{D}_R}{\overline{D}_A}(e^{-2m_2}-2e^{-m_2})\left\{(e^{m_2}-e^{m_2Y_1}) + \ln\left|\frac{e^{m_2}-1}{e^{m_2Y_1}-1}\right|\right\}\right] \qquad 4.4.5$$

For $\gamma = 3$:

$$\tau_b \approx \frac{W^2}{6\overline{D}_R m_2^2}\left[\ln\left|\frac{e^{2m_2Y_m}(e^{2m_2Y_m}-1)^2}{e^{2m_2Y_1}(e^{2m_2Y_1}-1)^2}\right| - \frac{\overline{D}_R}{\overline{D}_A}\ln\left|\frac{e^{2m_2Y_m}(e^{2m_2Y_m}-1)^2}{e^{2m_2}(e^{2m_2}-1)^2}\right|\right.$$

$$+ \left(1-\frac{\overline{D}_R}{\overline{D}_A}\right)(e^{-3m_2Y_m}-3e^{-m_2Y_m})\left\{2(e^{m_2Y_m}-e^{m_2Y_1}) + \ln\left|\frac{(e^{m_2Y_m}-1)(e^{m_2Y_1}+1)}{(e^{-m_2Y_m}+1)(e^{m_2Y_1}-1)}\right|\right\}$$

$$\left. + \frac{\overline{D}_R}{\overline{D}_A}(e^{-3m_2}-3e^{-m_2})\left\{2(e^{m_2}-e^{m_2Y_1}) + \ln\left|\frac{(e^{m_2}-1)(e^{m_2Y_1}+1)}{(e^{m_2}+1)(e^{m_2Y_1}-1)}\right|\right\}\right] \qquad 4.4.6$$

Similar considerations apply when the single diffusion coefficient approximation of eqn. 4.4.2 is to be used for transit time. Neglecting η, the general expression is:

$$\tau_b \approx \frac{W^2}{\overline{D}_A}\left[\frac{1}{m_2^2(\gamma-1)}\ln\left|\frac{e^{(\gamma-1)m_2Y_m}(e^{-(\gamma-1)m_2Y_m}-1)^{1-\frac{1}{\gamma}}}{e^{(\gamma-1)m_2Y_1}(e^{-(\gamma-1)m_2Y_1}-1)^{1-\frac{1}{\gamma}}}\right|\right.$$

$$\left. + \left(\frac{e^{-\gamma m_2}}{\gamma m_2} - \frac{e^{-m_2}}{m_2}\right)\int_{Y_1}^{1}\frac{dY}{e^{-m_2Y}-e^{-\gamma m_2 Y}}\right] \qquad 4.4.7$$

For $\gamma = 2$:

$$\tau_b \approx \frac{W^2}{2\bar{D}_A m_2^2}\left[\ln\frac{e^{m_2}(e^{m_2}-1)}{e^{m_2Y_1}(e^{m_2Y_1}-1)} + (e^{-2m_2}-2e^{-m_2})\left\{(e^{m_2}-e^{m_2Y_1}) + \ln\left|\frac{e^{m_2}-1}{e^{m_2Y_1}-1}\right|\right\}\right] \qquad 4.4.8$$

and for $\gamma = 3$,

$$\tau_b \approx \frac{W^2}{6\bar{D}_A m_2^2}\left[\ln\left|\frac{e^{2m_2}(e^{2m_2}-1)^2}{e^{2m_2Y_1}(e^{2m_2Y_1}-1)^2}\right| + (e^{-3m_2}-3e^{-m_2})\left\{2(e^{m_2}-e^{m_2Y_1}) + \ln\left|\frac{(e^{m_2}-1)(e^{m_2Y_1}+1)}{(e^{m_2}+1)(e^{m_2Y_1}-1)}\right|\right\}\right] \qquad 4.4.9$$

Neither eqn. 4.4.4 nor 4.4.7 are general enough to be applied directly to actual double diffused transistors without prior knowledge of the background doping level. However, they can be used to indicate the effect of variation of m_2, Y, and, to a lesser degree, of γ upon τ_b. For this limited purpose it is sufficient to use eqns. 4.4.8 and 4.4.9 for the specific cases when $\gamma = 2$ and 3. To indicate the effect of N_B on base transit time, eqn. 4.4.2 was used to compute transit time for η = .0001, .001, .005 and .01 respectively for $\gamma = 2$ and $m_2 = 2$. These results are plotted in Fig. 4.14 and indicate that N_B does not have a serious effect on τ_b until it becomes an appreciable fraction of N_c. The normalizing factor in this figure is $W^2/2\bar{D}_A$, so that at higher values of η the effect will also appear in $\bar{D}_A$. Figs. 4.15 and 4.16 are plots of $\tau_b/\frac{W^2}{2\bar{D}_A}$ for $1 \leq m_2 \leq 7$ for $\gamma = 2$ and 3

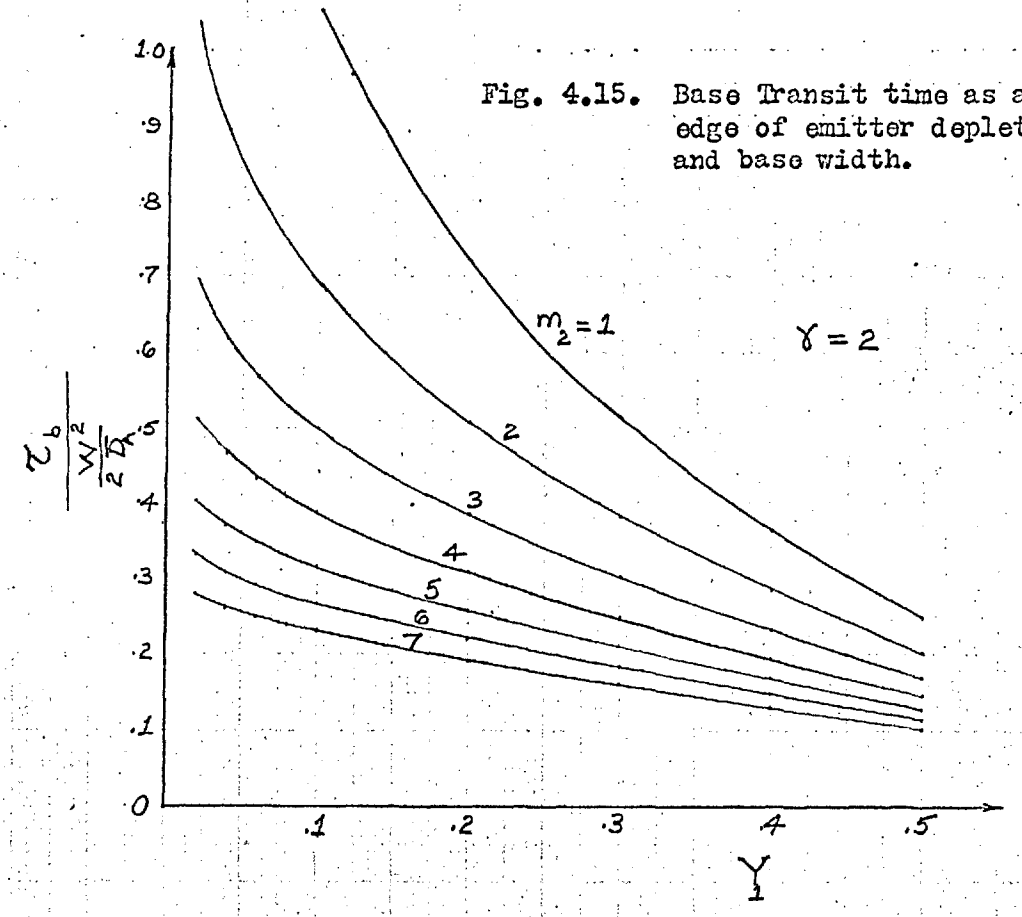


Fig. 4.15. Base Transit time as a function of edge of emitter depletion layer and base width.

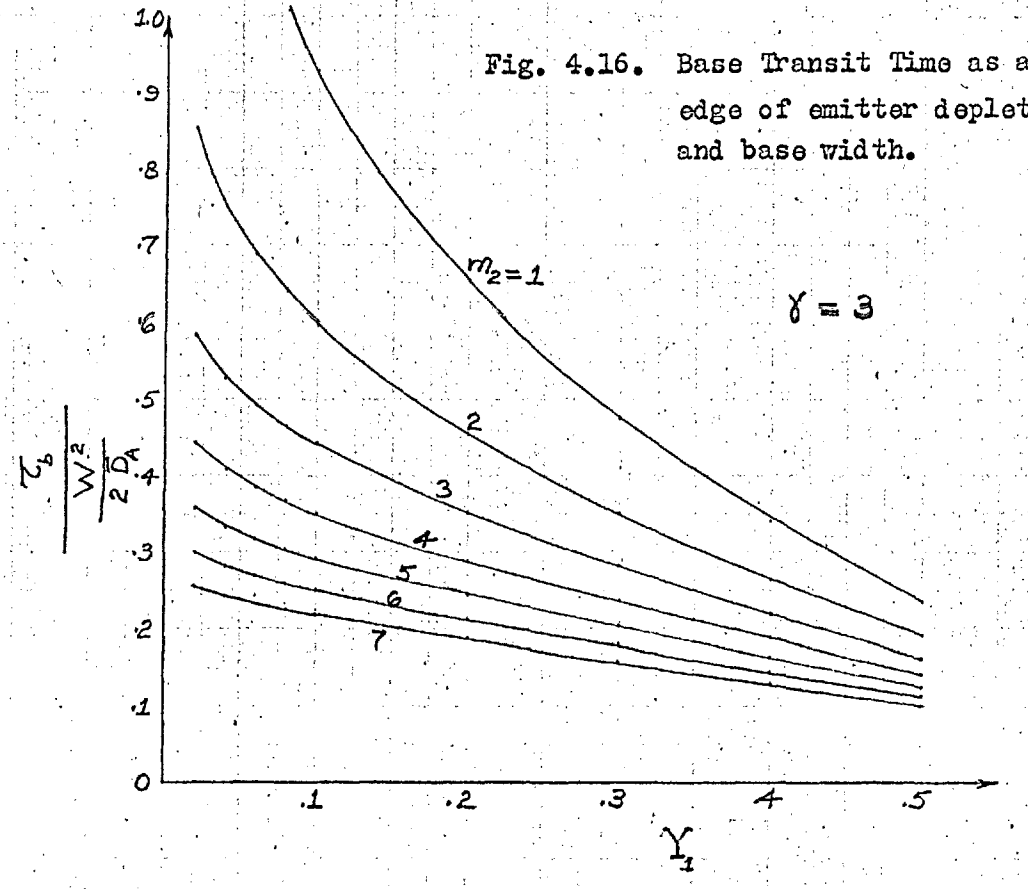


Fig. 4.16. Base Transit Time as a function of edge of emitter depletion layer and base width.

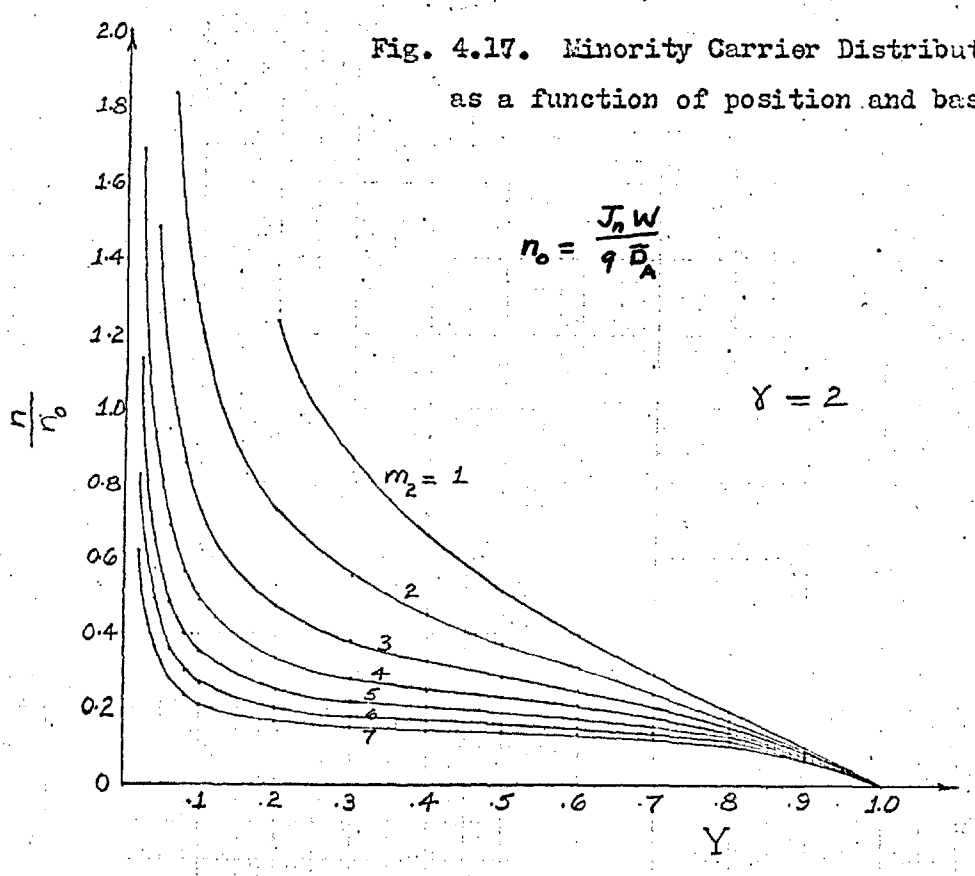
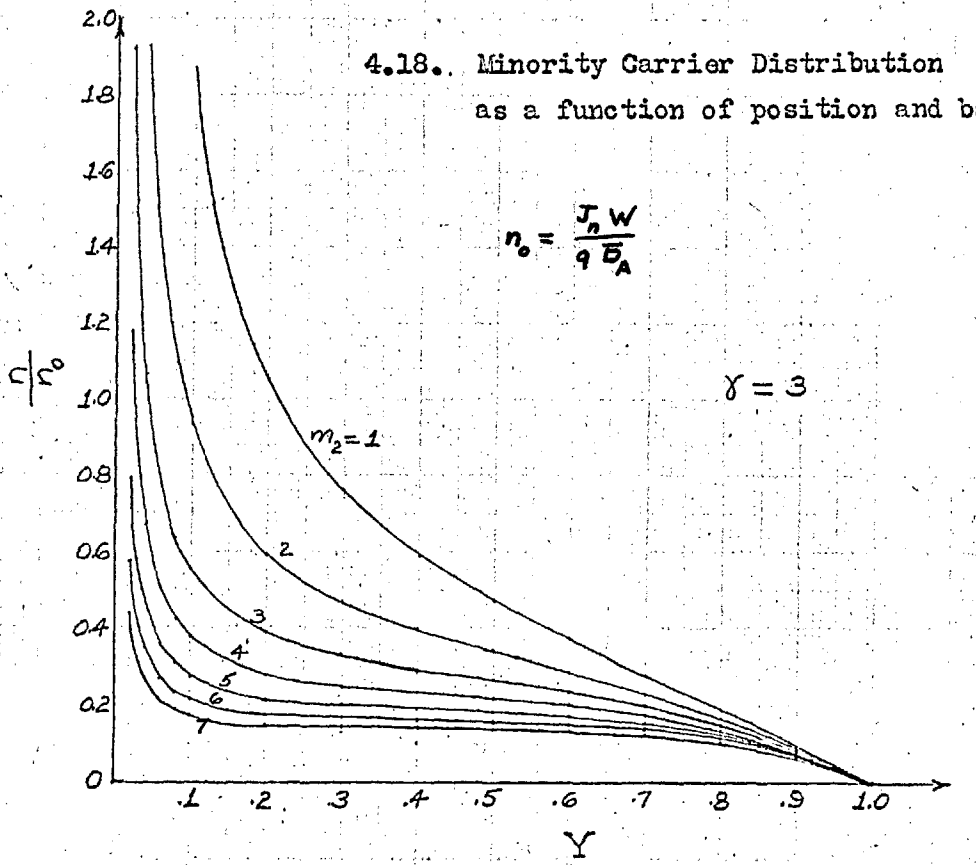


Fig. 4.17. Minority Carrier Distribution as a function of position and base width.



4.18. Minority Carrier Distribution as a function of position and base width.

respectively, while Figs, 4.17 and 4.18 are similar plots for $n/\frac{J_n W}{qD_A}$.

From these curves it is evident that the retarding field region causes a considerable build-up of minority carriers near the emitter junction, hence rapid increase in τ_b for low levels of Y_1, and increase of Υ results in a decrease of minority carrier density and base transit time due to the narrower retarding field region.

4.4.3 Transit time Measurement

The bridge arrangement shown in Fig. 4.19 can be used to measure transit time at low frequencies (i.e. $\omega\tau << 1$). This bridge arrangement effectively measures the phase angle between base current i_b and collector current i_c, which, as was shown in Chapter 2, Section 2.4.1 effectively defines the "terminal" transit time τ. As indicated by eqn. 2.4.42, emitter-to-collector current gain α is given by:

$$\alpha \Big|_{\omega \to 0} = -\frac{i_c}{i_e} \approx \frac{a_o}{1 + j\omega\tau} \qquad 4.4.10$$

where

$$\tau = \tau_b + \tau_c + \frac{C_{te}}{g_{ee}} + r'_{cc}(C_{tc_1} + C_{tc_2}) \qquad 4.4.11$$

where τ_b is base transit time, $\tau_c (= \frac{dc}{2v_s})$ is transit time across the collector depletion layer and the other terms are elements of the equivalent cirucit of Fig. 2.12. $(g_{ee} = \frac{qI_c}{kT})$.

Neglecting stray capacitance and inductances which can influence the balance condition of the bridge (i.e. when voltage across the CR combination is equal to the voltage across r so that no

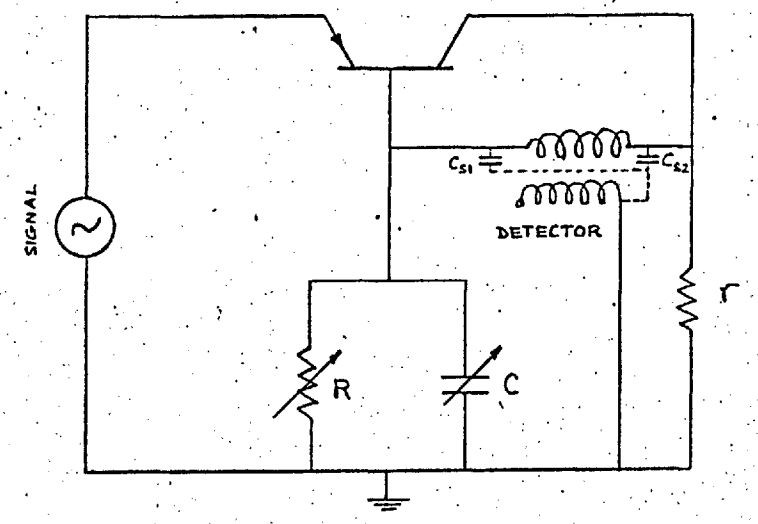


Fig. 4.19. Transit Time Bridge.

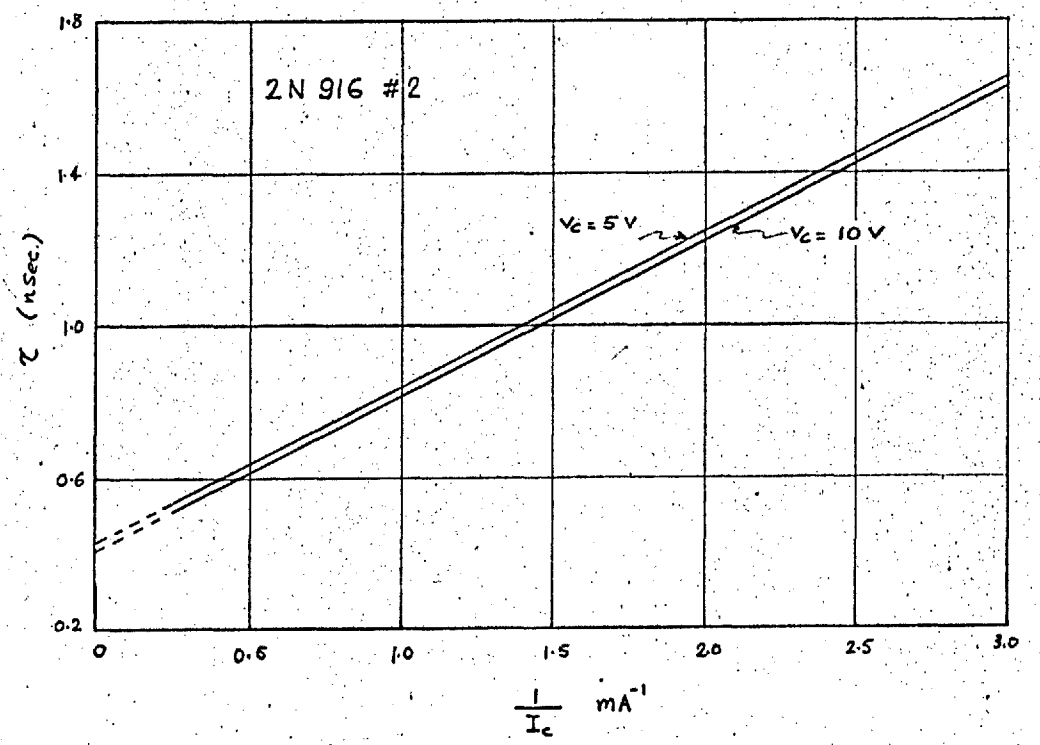


Fig. 4.20. Terminal Transit Time vs Inverse Collector Current.

current flows through the detector transformer), the balance condition is:

$$\frac{R\, i_b}{1 + j\omega CR} = - i_c\, r \qquad 4.4.12$$

Since $i_c = -\alpha\, i_e$ and $i_b = (1 - \alpha)\, i_e$, eqn. 4.4.12 becomes:

$$\frac{(1 - \alpha)R}{1 + j\omega CR} = \alpha r \qquad 4.4.13$$

Substituting the value of α from eqn. 4.4.10 gives:

$$\left(1 - \frac{a_o}{1 + j\omega\tau}\right) \frac{R}{r(1 + j\omega CR)} = \frac{a_o}{1 + j\omega\tau} \qquad 4.4.14$$

Evaluating this expression and equating real parts gives:

$$a_o = \frac{R}{R + r} \qquad 4.4.15$$

while equating imaginaries gives:

$$\tau = a_o\, Cr = \frac{CRr}{R + r} \qquad 4.4.16$$

Eqn. 4.4.16 does not take into account any stray capacitances which might be present in the bridge. Although great care was taken to eliminate strays in the bridge used in the measurements of this section, their complete elimination was not physically possible. Two strays in particular greatly affect the balance condition - stray capacitance across the CR combination (C_{s_1} in Fig. 4.19) and stray

capacitance across r (C_{s_2} in Fig. 4.19). These strays are due in large measure to the detector transformer. The primary winding of the transformer used was layered so that strays between this winding and the grounded screen between it and the secondary winding appeared unevenly over the winding. Resolving this distributed stray into two capacitances at the base and collector ends of the winding allows measurement of C_{s_1} and C_{s_2} (3 terminal measurement on Wayne-Kerr B601) and their use in subsequent calculations of transit time.

Allowing for C_{s_1} and C_{s_2} in the bridge balance equations, eqns. 4.4.15 and 4.4.16 become:

$$a_o = \frac{R}{R + r} - \frac{\omega^2 \tau C_{s_2} R r}{R + r} \qquad 4.4.17$$

and

$$\tau \approx \frac{(C + C_{s_1} + C_{s_2})\, Rr}{R + r} - C_{s_2} r \qquad 4.4.18$$

For many of the transistors studied in this Chapter the value of C_{s_2} r is an appreciable fraction of τ as determined from eqn. 4.4.18. Moreover, $C_{s_1} + C_{s_2}$ is an appreciable fraction of C; therefore, to achieve an adequate degree of accuracy in the determination of τ, C_{s_1} and C_{s_2} must be accurately known and employed in eqn. 4.4.18*. For the bridge used here:

---

*An additional error may be introduced by the presence of inductances in series with r. For the bridge used, this was not thought to be a serious problem, and was not considered in the calculation of τ.

C_{s1} = 33.5 pf, C_{s2} = 11.2 pf at 1 MHz.

Before transit time can be used in parameter determination, it must be separated into its components and τ_b be extracted (only τ_b is a useful source of information on the impurity profile). Plotting τ vs $1/I_c$ and extrapolating to the vertical axis as in the example of Fig. 4.20 yields $\tau_b + \tau_c + r'_{cc}(C_{tc1} + C_{tc2})$ as an interecept and $\frac{kT}{q} \cdot C_{te}$ as the slope.* τ_b may then be determined once τ_c and $r'_{cc}(C_{tc1} + C_{tc2})$ are known. Calling the sum of these three components τ', the values of τ' listed in Table 4.5 were determined by the above method. C_{te} from the slope of τ vs $1/I_c$ is also listed.

A quick estimate of r'_{cc} to be used to eliminate $r'_{cc}(C_{tc1} + C_{tc2})$ from τ' may be obtained from a method suggested by Kocsis[35], and based on the circuit of Fig. 4.21. V_{ec} is small in a transistor with negligible r'_{cc} when it enters saturation. Thus from Fig. 4.21:

$$V_{ex} - V_{ec} = I_s (R + r'_{cc}) \qquad 4.4.19$$

where I_s is the maximum or saturation current that can be made to flow by increasing I_e. If $V_{ex} \gg V_{ec}$, then $V_{ex} - V_{ec} \approx$ constant and a plot of $1/I_s$ vs R for constant V_{ex} will give r'_{cc} as an intercept. Fig. 4.22 presents curves for two transistors based on this method. These curves were obtained from the Tetronix Type 575 Transistor-Curve Tracer by

---

* For forward bias conditions, I_c changes rapidly with small change in V_e so that the depletion layer width (assuming complete depletion) remains relatively constant giving a value of C_{te} ($= \epsilon A_e/d_e$) which is approximately constant. This then is a method for estimating forward biased C_{te}.

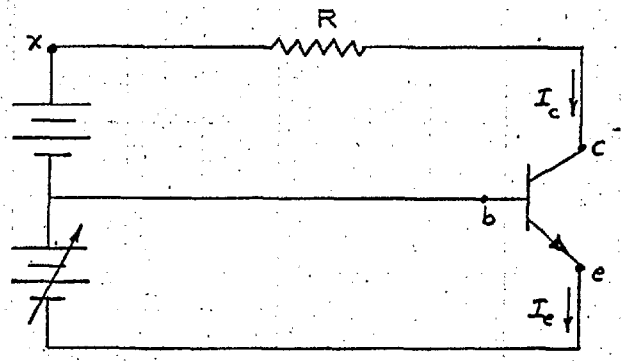


Fig. 4.21. Circuit for estimating r_{cc}'.

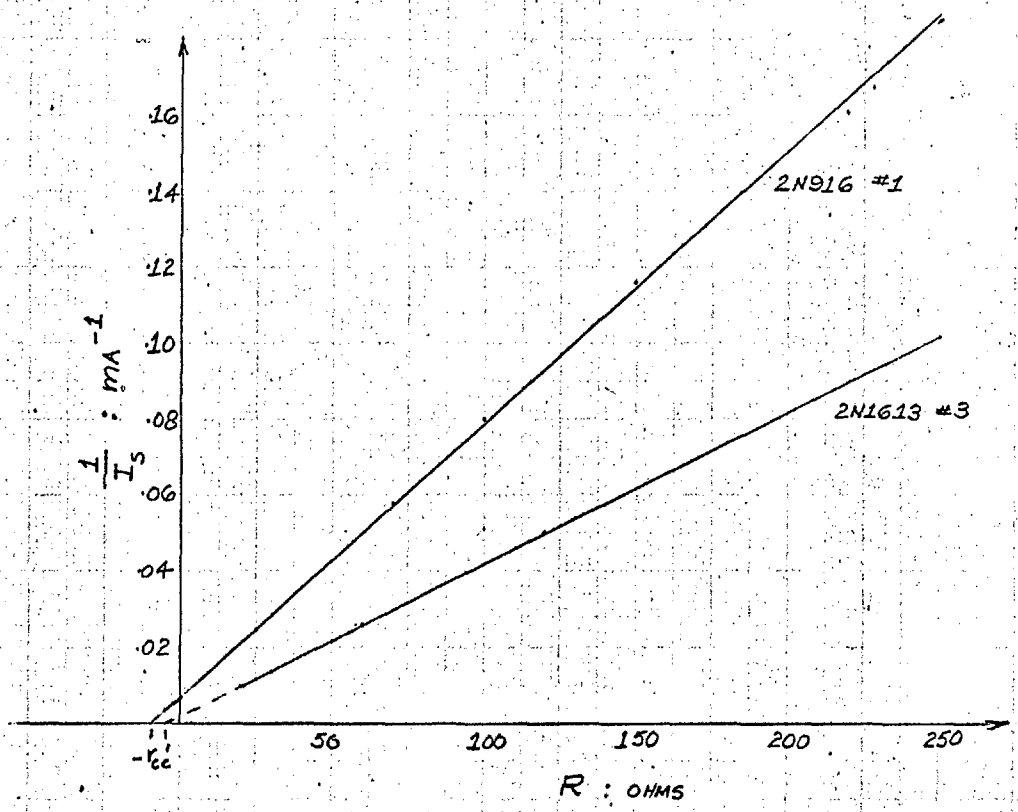


Fig. 4.22. Estimate of r_{cc}'.

varying the combined value of the "Current Sampling Resistance" and the "Dissipation-Limiting Resistor" and measuring I_s. Values of r'_{cc} by this method are included in Table 4.5.

τ_c ($= \frac{d_c}{2v_s}$ where v_s is the limiting drift velocity in the collector depletion layer, $\simeq 8 \times 10^6$ cm/sec for silicon devices) may be determined once d_c is known from eqn. 4.2.6. Value of τ_c are presented in Table 4.5. Values of τ_b, once all the above effects were eliminated are listed in Table 4.5 and were used in the computations of Chapter 5.

As indicated above, care must be taken to eliminate the effects of strays in the measurement of τ. Although τ_b is strongly dependent on the base impurity profile, it is subject to errors in determining r'_{cc}, C_{tc_1}, C_{tc_2}, C_{te} and d_c. This can be critical when, for very high frequency transistors, τ_b is of the same order of magnitude as these effects. However, provided sufficient care is taken in determining τ_b, it can be a valuable source of information on the parameters of the impurity distribution. As shown in Table 4.5, where τ_b has been determined for several values of collector voltage for some transistors, large change in collector voltage results in only a small change in τ_b. This can be partially atrributed to the significant contribution of the retarding field region to τ_b, which is unaffected by changes in V_{cb}.* Thus incremental transit time (used by Trofimenkoff etc.[36-38]) can be virtually discounted as a useful source of information on transistor parameters for double-diffused devices.

---

* Significant errors in measurement of transit time by the bridge used in this thesis can also mask the increment in transit time with change in collector voltage (See also Section 5.2.4).

5. DETERMINATION OF THE PHYSICAL CONSTANTS OF THE DOUBLE EXPONENTIAL MODEL FOR ACTUAL DEVICES

5.1 Introduction

This chapter outlines the techniques used in determining the model constants from the measured data presented in Chapter 4, and discusses the derived constants with checks where available. For reasons discussed in Chapters 3 and 4 the two diffusion coefficient approximation ($\overline{D}_R$ and $\overline{D}_A$) is adopted as the standard representation of base transport properties. A step-by-step procedure is presented to evaluate the constants based on the above approximation, and results for various transistors are presented in Table 5.1. To indicate whether such a simplification is possible, the same transistors are evaluated in terms of an emitter diode law dependent on $\overline{D}_R$ only and a base transit time expression dependent on $\overline{D}_A$ only.

Both the above evaluations rely on a prior knowledge of emitter and collector areas (A_e and A_c respectively). An alternative procedure requiring knowledge of the ratio A_e/A_c (from measurements of r'_{bb} and $r'_{bb}C_{tc_1}$ in section 4.2.4) and on an estimate of collector body doping N_B (see Section 4.2.5) is presented and used to compute the constants of the model for several transistors. These constants are then compared with those evaluated earlier for the same transistors.

Where possible, checks are provided on the constants determined by the above methods and the results are discussed with special reference to the accuracy of the measurements used to provide the data from which they

were derived. Discrepancies in the results and the limitations to evaluating the model for epitaxial transistors are discussed.

In the above mentioned evaluations, reverse biased emitter capacitance data was not utilized. To indicate the effect of using such data to fix the gradient of the model at the emitter junction, several transistors were evaluated with the emitter capacitance data being interpreted on the basis of both the symme trical-linear and the abrupt-linear representations of the junction. The results from such computations are discussed in terms of their physical meaning and compared with those determined earlier.

A section is devoted to discussion of numerical techniques.

5.2 Evaluation of Constants of Model

5.2.1 Emitter and Collector Areas known

In Section 3.5.6 it was established, for representative examples of the double ERFC and double Gaussian distribution, that the double exponential model could adequately represent the above classical impurity profiles, and that approximating the impurity-dependent diffusion coefficient in the base by two discrete equivalent diffusion coefficients ($\overline{D}_R$ and $\overline{D}_A$) introduced no serious error in determining base transport properties. Chapter 4 provided measured information which can be used in the evaluation of the physical constants of the model for actual devices, and provided the basis for applying the $\overline{D}_R$ and $\overline{D}_A$ approximation to the emitter diode characteristic and the base transit time.

From Chapter 4 the following information is available for use

in the determination of the model constants:

(1) A_e and A_c,

(2) Collector data; $A_c^3 N_B/L_2$ and C_{tc} at V_c,

(3) $I_c/qn_i^2 e^{qV_e/kT}$ and C_{te} at forward bias,

(4) Base transit time: $\tau_b + \tau_c$,

(5) A_e/A_c from r'_{bb} and $r'_{bb}C_{tc}$ measurements,

(6) N_B from collector breakdown (Section 4.2.5).

In this section the data from (1) to (4) is used in an iterative approach to determine the physical constants of the model. The starting point in this technique is collector capacitance data as interpreted on the basis of a single exponential at the collector junction ($\gamma \geq 2.5$). The following step-by-step procedure is suggested:

(1) at the chosen collector bias determine $\frac{A_c}{d_c}$ from $A_c/d_c = C_{tc}/\varepsilon$; hence d_c results from knowledge of A_c. Compute $\tau_c = d_c/2v_s$ and subtract from $\tau_b + \tau_c$ to get τ_b.

(2) Divide $A_c^3 N_B/L_2$ by $(A_c/d_c)^3$ to get $N_B \frac{d_c^3}{L_2}$.

(3) Divide eqn. 2.7.15 by $N_B \frac{d_c}{L_2}$ to get:

$$\frac{V + V_B}{N_B \frac{d_c^3}{L_2}} = \frac{q}{\varepsilon} \left(\frac{L_2}{d_c}\right)^3 \left[\frac{1}{2}\left(\frac{d_c}{L_2}\right) \coth\left(\frac{1}{2}\frac{d_c}{L_2}\right) - \frac{d_c}{L_2}\right] \qquad 5.2.1$$

where $\left|V + V_B\right| = \left|V_c + V_{oc} + \frac{kT}{q}\frac{d_c}{L_2}\right|$

Use eqn. 5.2.1 to determine d_c/L_2 hence L_2. N_B results from $A_c^3 N_B/L_2$ where A_c and L_2 are now known. a_{1c} may be found from eqn. 2.7.14.

(4) From forward biased emitter transition capacitance, $C_{te}\,|_{fwd}$ determine an initial injection point from $a_{2e} = \frac{1}{2}d_e = \frac{\varepsilon A_e}{2C_{te}\,|_{fwd}}$.

(5) Assume an initial value of γ (say 2.5) and, with this value and the above injection point, determine the corresponding values of m_2, $\overline{D}_R$, $\overline{D}_A$ and N_o. This may be done as follows: Assume m_2, determine position of maximum doping Y_m from eqn. 3.5.36, compute W ($= m_2 L_2$) and $Y_1 = a_{2e}/W$, use $W + a_{1C}$ to determine N_o from $N_o = N_B e^{(W + a_{1C})/L_2}$ which may then be used in eqns. 3.5.38 and 3.5.39 to determine average doping in the retarding and aiding field regions respectively. $\overline{D}_R$ and $\overline{D}_A$ are then determined from Fig. 2.11 or eqn. 2.4.14. Substitute these values in the emitter diode law (eqn. 4.3.9) and compare the computed value of the R.H.S. of the equation with the measured value on the L.H.S. If the two do not agree assume a new value of m_2 and repeat the above steps. Iterate until agreement is reached. (A bisection routine is provided in the computer program of Appendix A.9 to perform the above iteration). Now substitute the values of γ, m_2, N_o, η ($= \frac{N_B}{N_o}$), $\overline{D}_R$, $\overline{D}_A$ and Y_m in the transit time expression (eqn. 4.4.1) and compare the computed value of transit time with the measured value. If the two do not agree, repeat the above procedure with a new value of γ and iterate until agreement is reached.

(6) Step (5) was carried out for the initial injection point determined in Step (4). Using the parameters determined in Step (5), find a new value of the injection point Y_1 from eqn. 4.2.12 and repeat the iteration process of Step (5). Continue Steps (5) and (6) until mutually consistent values of Y_1, γ, m_2, W, N_o, η, $\overline{D}_R$, $\overline{D}_A$ and Y_m

have been determined. It should be unnecessary to correct Y_1 more than twice.

The above procedure is too complicated for computation without the aid of a computer so a computer program (discussed in Section 5.4) was written, which, operating on the measured data of Chapter 4, gave the results of Table 5.1. Certain checks on these results are presented in Section 4.2.3 while the results are discussed in some detail in Section 4.2.4. A cursory examination, however, reveals, that for most of the transistors considered, the initial assumption that $\gamma \geq 2.5$ is approximately met, and that N_o is of the order of 10^{17} atoms/cc; thus diffusion coefficients $\overline{D}_R$ and $\overline{D}_A$ should be close to the values which would be determined on the basis of the actual distributions.

In Sections 4.3.3 and 4.4.1 respectively, it was argued intuitively that a single equivalent diffusion coefficient $\overline{D}_R$ (based on the retarding field region only) could be used in the emitter diode law, and that an equivalent coefficient $\overline{D}_A$ (based on the aiding field region only) could be applied to the base transit time expression. The step-by-step procedure outlined earlier was repeated with eqns. 4.3.10 and 4.4.2 being used in Step 5 for the emitter diode law and base transit time respectively. Comparison of the results presented in Table 5.2 with those of Table 5.1 supports the intuitive arguments of Chapter 4. Since d_c/L_2, L_2 and N_B are the same for both cases, only those parameters derived from the diode law and base transit time are presented in Table 5.2.

Table 5.1 - Parameters Based on Known A_e and A_c (Both $\overline{D}_R$ and $\overline{D}_A$ applied to Diode Law and Transit Time)

Device Number		V_c (volts)	$\frac{d_c}{L_2}$	L_2 (microns)	N_B ($\times 10^{15}$ $\frac{\text{atoms}}{\text{cc}}$)	γ	m_2	W (microns)	W_B (microns)	Y_1	Y_m	$\overline{D}_{R_2}$ ($\frac{\text{cm}^2}{\text{volt-sec}}$)	$\overline{D}_{A_2}$ ($\frac{\text{cm}^2}{\text{volt-sec}}$)	$N_{O_{17}}$ ($\times 10$ $\frac{\text{atoms}}{\text{cc}}$)
2N696	1	30	5.8	.98	1.9	2.53	2.58	2.54	4.26	.024	.235	10.2	14.7	1.43
2N1613	1	30	6.1	.94	1.8	2.56	2.48	2.32	4.02	.023	.243	10.4	14.9	1.32
	2	30	4.4	1.0	3.5	2.98	2.59	2.68	4.17	.016	.213	9.3	13.5	2.04
	3	5	2.2	1.1	3.7	5.37	2.46	2.65	3.65	.018	.157	10.9	15.3	1.07
	3	10	3.0	1.0	3.5	4.12	2.38	2.42	3.57	.020	.190	10.7	15.0	1.19
	3	20	4.3	.92	3.1	3.06	2.33	2.14	3.49	.023	.233	10.2	14.4	1.40
	3	30	5.0	.91	3.1	2.87	2.20	2.02	3.49	.025	.256	10.2	14.2	1.43
	12	30	4.8	1.0	2.9	3.87	2.52	2.52	4.10	.016	.187	9.7	13.9	1.76
2N1711	1	30	4.9	.97	2.9	3.30	1.92	1.88	3.43	.029	.270	11.2	15.1	.98
	2	30	4.8	1.1	2.6	4.43	1.89	2.00	3.73	.031	.230	11.7	15.7	.83
	3	10	2.8	1.0	4.2	3.59	1.85	1.91	3.00	.039	.267	11.8	15.6	.78
2N910	1	10	5.5	.83	1.0	2.45	3.00	2.51	3.93	.024	.206	10.8	16.1	1.17
	2	10	5.1	.85	1.2	2.40	2.94	2.40	3.79	.026	.212	10.7	16.0	1.18
	3	10	5.7	.81	1.0	-	-	-	-	-	-	-	-	-
2N916	1	10	3.9	.64	4.2	5.82	1.83	1.17	2.05	.029	.200	11.0	14.6	1.05
	2	5	2.6	.63	7.1	2.82	1.77	1.12	1.77	.044	.322	10.7	14.0	1.15
	2	10	3.5	.60	6.7	2.39	1.69	1.01	1.78	.050	.370	10.4	13.5	1.30
	3	10	3.0	.55	11.5	2.48	1.41	0.78	1.41	.076	.434	9.9	12.4	1.49
2N706A	1	0.6	.64	1.0	36	6.65	1.00	1.05	1.35	.083	.335	9.9	11.6	1.34
	2	0.6	.98	.65	28	3.26	1.79	1.12	1.40	.047	.293	8.6	11.1	2.65

Device Number		V_c (volts)	γ	m_2	W (microns)	W_b (microns)	Y_1	Y_m	$\bar{D}_B$	$\bar{D}_A$	N_o ($\times 10^{17}$ atoms/cc)
									cm^2/volt-sec.		
2N696	1	30	2.13	2.52	2.48	4.20	.026	.266	10.4	14.8	1.35
2N1613	1	30	2.15	2.42	2.27	3.97	.025	.275	10.6	14.9	1.25
	2	30	2,45	2.51	2.60	4.09	.019	.246	9.5	13.6	1.89
	3	5	3.96	2.36	2.55	3.55	.021	.197	11.2	15.6	0.97
	3	10	3.24	2.30	2.34	3.49	.023	.228	10.9	15.2	1.09
	3	20	2.51	2.27	2.09	3.44	.026	.268	10.4	14.5	1.32
	3	30	2.41	2.15	1.97	3.44	.028	.290	10.3	14.2	1.35
	12	30	3.03	2.43	2.43	4.01	.018	.225	9.9	14.1	1.60
2N1711	1	30	2.74	1.88	1.83	3.38	.033	.308	11.3	15.2	0.93
	2	30	3.53	1.82	1.93	3.66	.034	.274	11.9	15.8	0.77
	3	10	3.01	1.80	1.86	2.95	.044	.305	11.9	15.7	0.74
2N910	1	10	2.11	2.90	2.42	3.84	.026	.232	11.0	16.3	1.05
	2	10	2.72	2.66	2.27	3.66	.028	.218	11.5	16.7	0.88
	3	10	1.85	3.14	2.54	3.95	.023	.231	10.4	15.7	1.32
2N916	1	10	4.40	1.76	1.12	2.00	.032	.248	11.2	14.7	0.98
	2	5	2.45	1.75	1.11	1.76	.051	.353	10.7	14.0	1.13
	2	10	2.09	1.70	1.02	1.80	.056	.397	10.4	13.4	1.30
	3	10	2.21	1.43	0.79	1.42	.084	.458	9.9	12.4	1.52
2N706A	1	0.6	5.55	1.01	1.06	1.36	.097	.372	9.9	11.6	1.36
	2	0.6	2.83	1.77	1.11	1.39	.056	.321	8.6	11.1	2.61

Table 5.2 - Model Parameters for known A_e and A_c, based on $\bar{D}_B$ only for emitter diode law and $\bar{D}_A$ only for base transit time.

Device Number		V_c (volts)	A_{e_2} $cm^2 \times 10^{-4}$	A_{c_2} $cm^2 \times 10^{-4}$	$\frac{d_c}{L_2}$	L_2 (microns)	γ	m_2	W (microns)	W_b (microns)	Y_1	Y_m	$\bar{D}_{R_2}$ $\frac{cm^2}{volt\text{-}sec}$	$\bar{D}_{A_2}$ $\frac{cm^2}{volt\text{-}sec}$	$N_o \times 10^{17}$ atoms/cc
2N696	1	30	11.6	37.1	5.82	.0.75	1.40	2.82	2.12	3.44	.031	.298	8.4	12.0	3.14
2N1613	1	30	6.6	36.7	6.14	0.66	1.23	2.73	1.79	2.99	.033	.330	8.2	11.5	3.50
	2	30	10.3	46.8	4.39	0.93	2.15	2.60	2.41	3.80	.019	.256	8.8	12.6	2.58
	3	5	11.7	47.2	2.23	0.98	3.51	2.51	2.45	3.35	.023	.200	10.3	14.6	1.38
	3	10	10.9	45.8	2.99	0.89	2.62	2.42	2.16	3.18	.026	.246	9.9	14.0	1.59
	3	20	10.4	43.6	4.28	0.77	1.87	2.42	1.86	2.99	.030	.297	9.1	12.8	2.20
	3	30	10.5	43.4	5.03	0.76	1.81	2.31	1.76	2.99	.032	.318	9.1	12.5	2.29
	12	30	11.0	43.3	4.83	0.83	2.16	2.59	2.15	3.46	.021	.256	8.7	12.5	2.73
2N1711	1	30	3.0	13.9	4.95	0.26	-	-	-	-	-	-	-	-	-
	3	10	10.8	42.6	3.56	0.99	3.00	1.86	1.84	3.13	.039	.296	11.0	14.7	1.03
2N910	1	10	13.1	51.9	5.46	0.76	3.15	3.07	2.70	3.99	.026	.174	10.8	16.4	1.13
	2	10	13.4	56.5	5.08	0.88	5.93	2.94	2.87	4.31	.025	.123	11.5	17.0	0.89
	3	10	11.8	50.0	5.72	0.98	2.29	3.24	2.65	4.36	.022	.198	10.2	15.6	1.42
2N916	1	10	0.89	3.91	3.91	0.52	2.83	1.93	1.01	1.73	.042	.294	9.7	13.0	1.74
	2	5	0.87	3.48	2.57	0.46	1.51	2.16	1.00	1.47	.072	.375	8.3	11.1	3.19
	3	10	1.25	5.07	3.02	0.59	3.67	1.53	0.90	1.58	.068	.318	10.0	12.8	1.48

Table 5.3 - Model Parameters from $r'_{bb}C_{tc_1}$ and collector breakdown data.

5.2.2 A_e/A_c Known from r'_{bb} and $r'_{bb}C_{tc_1}$ Measurements

When emitter and collector areas are unknown it is still possible to derive an approximate model from terminal measurements. Additional information which makes this possible is found from measurements of r'_{bb} and $r'_{bb}C_{tc_1}$ (Section 4.2.4) and collector breakdown voltage (Section 4.2.5). From such measurements the ration A_e/A_e is determined ($= \frac{C_{tc_1}}{C_{tc}}$) and collector body doping N_B is estimated from the bottom curve of Fig. 4.9 or the top curve of Fig. 4.11. A_e/A_c is only an approximate value since it depends on the lumping of a distributed base resistance into a single discreet value r'_{bb}, and distributed capacitance into a lumped value C_{tc_1} (See Fig. 2.13). Also, N_B can be considerably in error for reasons discussed in Section 4.2.5. To obtain a more accurate value, a method of determining N_B from breakdown measurements was presented in Section 4.2.5, but it can only be applied when A_c is known. This can be used as a corrective procedure once A_c has been determined during the following procedure.

The bulk of the iterative procedure to evaluate model constants remains the same as that discussed in Section 5.2.1. The following steps replace Steps (1) to (3) of Section 5.2.1.

(1) From collector transition capacitance $\frac{A_c}{d_c} = \frac{C_{tc}}{\varepsilon}$

(2) Divide $\frac{A_c^3 N_B}{L_2}$ by $\left(\frac{A_c}{d_c}\right)^3$ to get $N_B \frac{d_c^3}{L_2}$ and divide eqn. 2.7.15 by the resulting value to get eqn. 5.2.1 from which it is possible to determine d_c/L_2.

(3) Divide $\frac{N_B d_c^3}{L_2}$ by $\frac{d_c}{L_2}$ to determine $N_B d_c^2$. Use the value of N_B from breakdown voltage to determine d_c from this product. A_c results from the value of A_c/d_c from Step (1) and L_2 from d_c/L_2. A_e is found by dividing A_c by the ratio A_e/A_c. At this point the procedure outlined in Section 4.2.5 may be used to correct N_B, and Steps 1 to 3 repeated as often as necessary to obtain mutually consistent values of A_e, A_c, N_B, d_c, N_B, L_2^*. a_{ic} may now be found from eqn. 2.7.14 and τ_c from $d_c/2v_s$ which gives the value of τ_b to be used in the rest of the computation. Steps 4, 5, and 6 are presented in Section 5.2.1.

Table 5.3 lists the parameters of the model for various transistors computed by the above procedure. Since no correction was applied to N_B, these results are somewhat in error, but indicate the sort of values to be expected in such a computation. Comparison with the values of Table 5.1 indicates that the generally higher values of N_B used in the calculation of Table 5.3 yields values of γ which are only slightly in excess of those listed in Table 5.1. However, the emitter and collector areas in Table 5.3 are generally considerably lower than those determined by optical measurement (see Table 4.4). An improvement in these values can be expected when the corrective procedure of Section 4.2.5 is used to determine a more accurate value of N_B.

---

* This procedure was not actually adopted in determining the results of Table 5.3 since it would involve either an unwarranted complication of the computer programs used in computing the various parameters, or a laborious correction by hand.

5.2.3 Checks on Parmeters Determined

The most obvious check on the parameters determined at a particular collector reverse bias voltage (V_c) is to see how the model fits for other values of V_c. Thus in Table 5.1 the model parameters are listed for four values of V_c for the 2N1613 #3 and for two values of V_c for the 2N916 # 2. The values of L_2, N_B, γ, W_b and N_o (which should be the same regardless of collector bias if the assumed conditions are fulfilled, i.e. emitter diffusion negligible near the collector junction and $\gamma \geq 2.5$) are appreciably different for the different values of V_c. The following discussion should indicate the origin of these differences.

Fig. 5.1 represents the collector junction of a double-diffused transistor. The lower curve (in the base) represents the actual impurity distribution, while the upper curve represents the single exponential defined at the collector junction if the emitter diffusion is negligible at this point. A depletion layer width d_c is shown, corresponding to a high value of V_c, for which the base edge of the depletion layer is in a region where emitter diffusion can not be neglected. For the same voltage a depletion layer width d'_c is shown which would apply if the impurity distribution followed the single exponential in this region (d_c is larger than d'_c). The value of d_c/L_2, determined from eqn. 5.2.1 at this voltage is actually d'_c/L'_2 and applies for the exponential shown in Fig. 5.1. Thus, when the value of d_c, determined from collector transition capacitance for the actual distribution, is used with d'_c/L'_2 to calculate L_2, the value of

Device Number		V_c (volts)	x_c (microns)	a_{ic} (microns)	N_R (atoms/cc x 10^{19})	x_e (microns)	W_b (microns) (a)	(b)	(c)	(d)
2N696	1	30	18	1.7	6.4	14	4	4.26	4.20	3.44
2N1613	1	30	14	1.8	6.9	10	4	4.02	3.97	2.99
	2	30	10	1.4	5.5	6	4	4.17	4.09	3.80
	3	30	10	1.5	3.3	5	5	3.49	3.44	2.99
	12	30	9	1.5	3.0	4	5	4.10	4.01	3.46
2N1711	1	30	10	1.5	5.4	7	3	3.43	3.38	-
	3	10	6	.85	.97	3	3	3.00	2.95	3.13
2N910	1	10	10	1.5	1.7	4	6	3.93	3.84	3.99
	2	10	11	1.4	2.2	6	5	3.79	3.66	4.31
	3	10	20	1.8	4.2	10	10	-	3.95	4.36
2N916	1	10	6	.82	3.7	2	4	2.05	2.00	1.73
	2	10	10	.86	6.2	3	7	1.78	1.80	1.49

Table 5.4 - Check on Physical base width W_b.

(a) $x_c - x_e$ (b) From Table 5.1 (c) From Table 5.2 (d) From Table 5.3

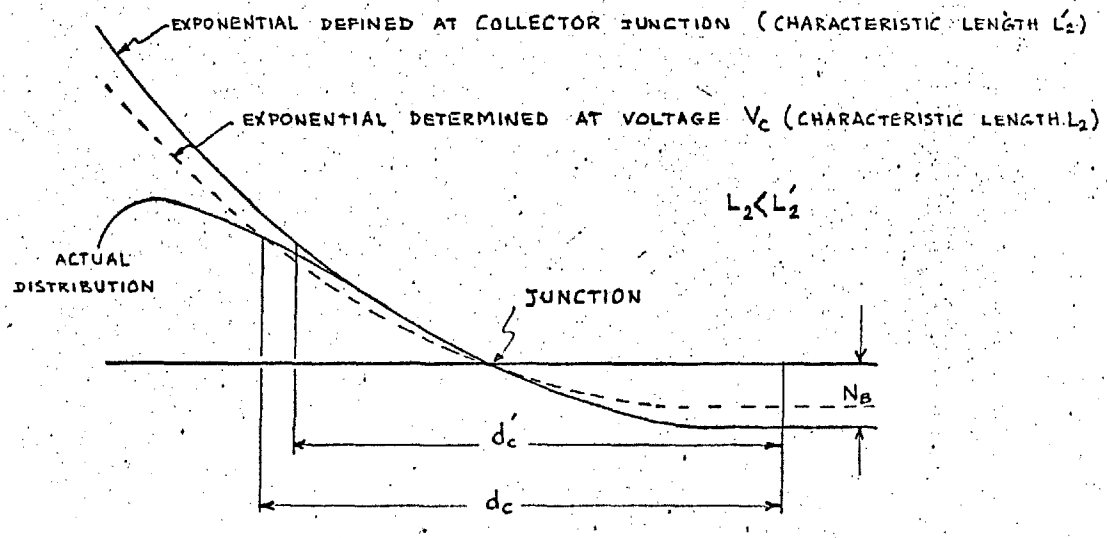


Fig. 5.1. Collector Junction showing Exponential determined at Voltage V_c where Emitter diffusion can not be neglected.

L_2 so determined must be less than the value of L'_2 for the exponential defined at the collector junction. Using this value of L_2 with $A_C^3 N_B/L_2$ results in a value of N_B which is lower than the actual value. The resulting exponential is shown in Fig. 5.1. It is obvious that, so long as the voltage used in this calculation is such that the base edge of the collector depletion layer lies in the region where the actual distribution departs from the exponential defined at the collector junction, a different exponential is determined for each value of V_C. At higher voltages (see 2N1613 #3 at 20 and 30 volts) the effect becomes less marked as the penetration of depletion layer into the base changes only slightly with voltage (i.e. depletion layer edge is in a region of high doping).

Changes in Υ, W_b and N_o with V_C are more marked since they depend on more complex measurements for their determination. Not only do they reflect the changes in L_2 and N_B discussed above, but also are affected by errors in measurement of emitter diode law and base transit time. The former measurement is quite accurate, while the latter measurement can be quite inaccurate (see Section 5.2.4). It is expected that if the base transit times used to compute the values in Table 5.1 were completely accurate, better agreement would be attained. This is supported by the results of Table 5.6, which, though based on the assumption of an abrupt emitter, do not rely on base transit time. These results show better agreement for the different voltages. It is therefore suggested that with accurate measured data, the parameters

determined for a range of collector voltages can be expected to be in reasonable agreement. For best results, however, the parameters should be determined at moderate values of collector voltage .

Few independent checks are available on the parameters determined in Tables 5.1 and 5.2, unless the actual design information used during fabrication is known (i.e. diffusion temperature, diffusion times, initial resistivity of the wafer, final sheet resistance and surface concentrations used in the diffusions). A further check would be the physical measurement of the base width by bevelling and staining techniques. As the former information was not available, and the facilities for carrying out the latter measurement were not available, such checks are not presented here.

In Section 4.2.5 a method was presented to estimate collector body doping, N_B, from breakdown measurements, taking into account the effect of the cylindrical part of the junction. Values of N_B by this method were listed in Table 4.4. Comparison of these values with those of Table 5.1 indicates good agreement in most cases. In computing the values of N_B in Section 4.2.5, Fig. 2.15(a), which is strictly applicable when the surface concentration for the base diffusion is of the order of 300 to 3000 times higher than N_B, was used. If this condition does not apply in the devices studied, the values of N_B in Table 4.4 will be somewhat in error, and a chart similar to that of Fig. 2.15(a), but applicable to the appropriate surface concentrations should be used. Lack of information on surface concentrations prompted the above-mentioned compromise.

Collector junction depth, x_c, estimated from Fig. 2.15(a) is presented in Table 5.4 along with a_{1C} from Fig. 2.15(b). Since the emitter junction is dependent on both emitter and base diffusions, the curves of Fig. 2.15 are not strictly applicable to this junction. In Section 4.2.2 a pseudo-exponential emitter junction was postulated to establish the impurity gradient at the emitter junction. From this "model" it is possible to establish a representative impurity doping N_R in base region (Table 4.4). Considering that an exponential is a good representation of a classical distribution when it has fallen below 10^{-3} of its initial value, it can be argued that this pseudo-exponential represents part of a single classical distribution which has formed a junction at the position where this distribution has fallen from its surface value to N_R. Since N_R is of the order of 10^{17} atoms/cc, while the surface concentration of the emitter diffusion is usually of the order of 10^{20} atoms/cc in double-diffused devices, it should be possible to use the chart of Fig. 2.15(a) to estimate the depth of penetration of the emitter junction. Values of x_e by this method are presented in Table 5.4 and are subtracted from x_c to estimate the physical base width W_b. Comparison with values of W_b calculated by the methods of Section 5.2.1 (also presented in Table 5.4) indicates reasonable agreement for certain devices, but points out the limited value of this check for other devices. (The small scale of Fig. 2.15(a) and the uncertainties regarding surface concentrations limits the accuracy of W_b determined by this method.)

5.2.4 Discussion of Results

As the value of N_B used to compute the parameters in Table 5.3 is

substantially in error, it is unnecessary to discuss these parameters in detail. The evidence indicates that when the corrective procedure outlined in Section 4.2.5 is applied when treating collector data, a good estimate of the model parameters is possible when A_e and A_c are initially unknown. The principle limitations to the accuracy of these parameters are the values of A_e/A_c as determined from r'_{bb} and $r'_{bb}C_{tc_1}$ measurements, and on the accuracy of the base transit time measurements (as discussed below).

The checks presented in Section 5.2.3 support the validity of the parameters presented in Table 5.1. Although independent checks are not available on all the constants presented it is felt that, coupled with the demonstration in Chapter 3 that the double exponential can adequately represent classical distributions, the fact that the model constants are derived from the terminal measurements which are most dependent on the impurity distribution, is sufficient evidence to support the validity of the model as a good physical representation for actual double-diffused transistors. Although in several cases $\gamma < 2.5$ this is not felt to introduce sufficient error at the collector junction to invalidate the results. The method of derivation of the constants ensures that the electrical characteristics can be accurately predicted from the model, so this requirement of modelling has been fulfilled.

The major limitation on the accuracy of the results given in Table 5.1 is the value of base transit time used in the computations. The measurement technique, presented in Chapter 4, Section 4.4.3, results in a value of terminal transit time τ which consists of

τ_b, $\frac{C_{te}}{g_{ee}}$, $d_c/2v_s$, and $r'_{cc}C_{tc}$, while the transit time used in computations is the value of τ_b. Obviously the determination of τ_b is subject to inaccuracies in:

(a) Measurement technique - as pointed out in Section 4.4.3, the measured value of τ is influenced by stray capacitances and stray inductances in the bridge used for the measurement. Only two stray capacitances (See Fig. 4.19) were taken into account. Inductance effects were neglected at the frequency of measurement (1MHz). In actual fact, in the bridge used the effect of inductance in series with r was observed under certain conditions (very low r) to introduce a 4% error in measured τ. For high frequency transistors (low τ), the effect of the two stray capacitances C_{s_1} and C_{s_2} in eqn. 4.4.18 can be an appreciable fraction of τ, so unless C_{s_1} and C_{s_2} are accurately known, the value of τ can be considerably in error. Obviously the higher the value of τ the more tolerable are inaccuracies in C_{s_1} and C_{s_2}. The effect of C_{s_1} and C_{s_2} is strongly felt in the 2N916s and 2N706As of Table 5.1.

(b) Separation of τ into its components - This separation is accomplishe first by means of a plot of τ vs $1/I_c$, which at its intercept yields $\tau_b + \frac{d_c}{2V_s} + r'_{cc}C_{tc}$. r'_{cc} and C_{tc} are determined from the measurements of Section 4.4.3 and 4.2.3 respectively. d_c is determined from C_{tc} when A_c is known, thus τ_b can be determined. Although C_{tc} can be measured with good accuracy the values of r'_{cc} used in these calculations were measured with no external bias on the collector junction. Thus, any effect of

collector bias on r'_{cc} (change in depletion layer width) has not been accounted for. In many cases, as is evident from Table 4.5, the value of $r'_{cc}C_{tc}$ is of the same order of magnitude as τ_b, so considerable error may be incorporated into τ_b as a result of an inaccurate determination of r'_{cc}. Although $d_c/2v_s$ is likely to be an underestimation of transit time through the collector depletion layer (since electric field is not at its maximum throughout this region), this effect is small, so does not introduce a serious error in τ_b. For the lower frequency devices of Table 5.1 (2N696, 2N1613, 2N1711, 2N910) the approximate accuracy of measured τ_b is $\pm$ 10%, while for the higher frequency devices the accuracy is approximately $\pm$ 25%.

From Table 5.1 where the model for such devices as the 2N1613 #3 has been computed for several values of collector bias, considerable difference is observable between the values of Υ at the different voltages. This was discussed in Section 5.2.3, and is partially attributable to the inaccuracy of measured τ_b. In the bridge used, it was difficult to detect changes in terminal transit time with collector voltage. In the calculation of base transit time, the same value of r'_{cc} was used to compute the $r'_{cc}C_{tc}$ product; thus, any effect of voltage change on collector body resistance was neglected, introducing a further error in the calculated value of τ_b.

An additional error in the model is attributable to reliance on $C_{te}\,|_{fwd}$ determined from the slope of the plot of τ vs $1/I_c$

(Section 4.4.3), and the use of the space charge approximation to determine an injection point (Y_1). As this was discussed in Section 4.2.2 it is unnecessary to comment further here.

A comparison of Table 5.2 with Table 5.1 indicates that, although γ may be somewhat in error, the values of m_2, W, and N_o are sufficiently in agreement for $\overline{D}_A$ to be neglected in the diode law and $\overline{D}_R$ in transit time expression, in the determination of these quantities. In fact, considering the inaccuracy of the transit time measurement, the more rigorous treatment may often be unjustified.

Certain other transistors were studied, for which data has not been presented. Included among these were several 2N706s, 2N708s and two 2N709s. The latter device was an epitaxial device, the collector junction of which was found to be highly dependent on the substrate diffusion, so a simple model could not be determined. Obviously, as discussed in Section 3.5.7, the simple model can be determined for epitaxial devices only when the substrate diffusion has negligible influence at the collector junction (see the 2N706As in Table 5.1).

For the 2N706s and 2N708s, the model could not be determined for the following reason. The collector equilibrium barrier potentials (V_{oc}) for these transistors were found to range from 0.70 to 0.80 volt (compare with 0.4 to 0.5 in Table 4.3 for most other devices considered - exception 2N706A). As these devices were not epitaxial and breakdown voltages indicated background dopings similar to those for the 2N916 (Table 4.4), the higher values of V_{oc} must be attributable to some unknown effect. Since these devices are known to be strongly gold doped,

it would appear that there is some correlation between the presence of the gold doping and the higher values of V_{oc}. No evidence is offered to support this thoery, and, to the author's knowledge, no information is available on the effect of gold doping on equilibrium barrier potentials. The effect of the higher values of V_{oc} was to yield ridiculously low values of d_c/L_2 ($\ll 1$) and, hence, extremely high L_2. These values of d_c/L_2 and L_2 would not, when used with the other measured data, yield allowable parameters.

5.3 Evaluation from Emitter Capacitance Data

5.3.1 Derivation of Parameters

In the calculations of Section 5.2 reverse biased emitter capacitance data was not used, while forward biased capacitance was used only to determine an initial injection point which was later readjusted in the model. In Section 4.2.2 it was established that, for low reverse bias, the emitter junction of double-diffused transistors could be treated as having linear grading. The slope of this linear region could be determined by interpreting reverse biased emitter capacitance data on the basis of eqn. 4.2.8. The values of $A_e^3 S_1$ for the symmetrical-linear approximation listed in Table 4.3 were determined by this method.

If the double exponential model were assumed to have the same gradient as for the actual junction, viz,

$$A_e^3 \frac{N_o}{L_2} (\gamma - 1) = A_e^3 S_1 \qquad 5.3.1$$

where the L.H.S. of eqn. 5.3.1 represents the gradient of the model at

the emitter junction, then the values of $A_e^3 S_1$ in Table 4.3 could be used to determine the constants of the model. For such an interpretation, it is unnecessary to use transit time data, since sufficient information is available to determine the constants from eqns. 5.3.1 and the diode law (eqn. 4.3.9). For such an interpretation, Steps (1) - (4) are identical with those of Section 5.2.1. Steps (5) and (6) are replaced by the following:

Assume Υ and determine N_o from eqn. 5.3.1. Since $N_o \approx N_B e^{(W + a_{1c})/L_2}$, W is now known, hence $m_2 (= W/L_2)$. Y_m results from eqn. 3.5.36 and $\bar{D}_R$ and $\bar{D}_A$ from eqns. 3.5.38 and 3.5.39 respectively in conjunction with Fig. 2.11 or eqn. 2.4.14.

$Y_1 = a_{2e}/W$.

The above values are then substituted in the R.H.S. of eqn. 4.3.9 to compute a value which is compared with the measured value on the L.H.S. of the equation. If the two do not agree assume a new value of Υ and repeat the above steps as often as necessary to yield mutually consistent values of Υ, N_o, W, m_2, Y_1, Y_m, $\bar{D}_R$ and $\bar{D}_A$.

Base transit time may be used as a check on these results.

The above procedure was employed to determine the parameters listed in Table 5.5 for several transistors. A similar procedure applies when the abrupt-linear approximation is assumed to apply at the emitter junction (as used by Trofimenkoff etc.[37,38]). The value of $A_e^3 S_1$ used in the above calculations is now that determined from eqn. 4.2.9, while the injection point is determined by assuming that the

total forward biased emitter depletion layer lies on the base side of the junction. Thus $a_{2e} = d_e$ and $a_{1e} = 0$. The values of $A_e^3 S_1$ from Table 4.3, determined from emitter transition capacitance using the abrupt-linear approximation, were used to compute the parameters of Table 5.6. As the values of d_C/L_2, N_B, and L_2 are the same as those of Table 5.1, they are not included in Tables 5.5 and 5.6.

5.3.2 Discussion of Results

Comparison of the parameters listed in Table 5.5 with those of Table 5.1 indicates that, in general, a considerably higher value of γ and lower W and N_o results when emitter capacitance data, interpreted in terms of the symmetrical-linear approximation at the emitter junction, is used to determine the parameters of the double exponential model. This may be explained with reference to Fig. 5.2.

In Fig. 5.2(a) the actual diffusions are represented as having equal concentration N_o' at the emitter junction ($x' = 0$). The resultant impurity profile is the difference of the two diffusions. Over a limited region on either side of the emitter junction the impurity gradient thus determined does not change appreciably from S_1, the gradient at the junction (see Section 4.2.2). It is this gradient which is determined from emitter capacitance data. Representing the two diffusions over this limited region by exponentials of characteristic lengths L'_1 and L'_2 then the gradient at the junction is given by:

$$S_1 = \frac{N_o'}{L'_2} (\gamma' - 1) \qquad 5.3.2$$

where $\gamma' = L'_2/L'_1$

Device Number		V_c (volts)	γ	m_2	W (microns)	W_b (microns)	Y_1	Y_m	$\bar{D}_R$	$\bar{D}_A$	N_o x 10^{17} atoms/cc	τ_b* nsec
									cm^2/volt-sec			
2N696	1	30	5.6	2.33	2.29	4.01	.022	.162	10.9	15.2	1.12	1.02
2N1613	1	30	7.9	2.18	2.04	3.74	.021	.137	11.2	15.4	0.99	0.78
	3	5	11.6	2.36	2.55	3.55	.015	.098	11.2	15.3	0.97	1.06
	3	10	10.5	2.24	2.27	3.42	.017	.111	11.1	15.1	1.02	0.91
	3	20	8.9	2.10	1.93	3.28	.020	.132	10.9	14.7	1.11	0.73
	3	30	8.9	1.94	1.78	3.25	.022	.142	10.9	14.5	1.10	0.65
2N1711	1	30	9.7	1.71	1.67	3.22	.025	.153	11.8	15.4	0.79	0.57
2N910	1	10	6.3	2.72	2.27	3.69	.024	.127	11.6	16.7	0.88	0.78
2N916	1	10	16.1	1.72	1.10	1.98	.024	.107	11.3	14.5	0.95	0.24
2N706A	2	0.6	28.9	1.45	0.91	1.19	.021	.083	9.4	11.3	1.89	0.20

* Compare with measured values in Table 4.5.

Table 5.5 - Model Parameters from symmetrical-linear interpretation of emitter capacitance data.

Device Number		V_c (volts)	γ	m_2	W (microns)	W_b (microns)	Y_1	Y_m	$\bar{D}_R$	$\bar{D}_A$	N_o x 10^{17}	τ_b* nsec
									cm^2/volt-sec			
2N1613	1	30	2.7	2.21	2.07	3.77	.042	.265	11.1	15.5	1.01	1.10
	2	30	2.5	2.37	2.45	3.94	.028	.255	9.8	13.9	1.64	1.87
	3	5	4.0	2.25	2.42	3.42	.032	.207	11.5	15.9	0.87	1.25
	3	10	3.6	2.15	2.18	3.33	.035	.229	11.3	15.5	0.94	1.13
	3	20	3.1	2.06	1.89	3.24	.040	.264	11.0	15.0	1.07	0.98
2N910	1	10	2.1	2.90	2.42	3.84	.044	.232	11.0	16.3	1.05	1.17
2N916	1	10	5.3	1.60	1.02	1.90	.053	.243	11.6	15.0	0.84	0.26
	2	5	8.3	1.24	0.79	1.44	.067	.233	12.1	14.9	0.68	.145
	2	10	7.7	1.08	0.65	1.43	.081	.282	12.0	14.6	0.70	.11
2N706A	2	0.6	10.8	1.11	0.70	0.98	.054	.219	10.0	11.9	1.35	0.15

* Compare with measured values in Table 4.5

Table 5.6 - Model Parameters from abrupt-linear interpretation of emitter capacitance data.

Device Number		V_c (volts)	$S_1 \times 10^{21}$ Sym-linear	$S_1 \times 10^{21}$ Abr-linear	Gradient of Model $\times 10^{21}$		
					(a)	(b)	(c) *
2N696	1	30	5.17	1.29	2.23	1.55	1.66
2N1613	1	30	7.30	1.82	2.20	1.54	1.21
	2	30	9.79	2.45	3.92	2.64	3.19
	3	20	9.56	2.39	3.14	2.16	2.49
2N1711	1	30	7.02	1.75	2.31	1.67	-
	3	10	4.43	1.11	1.96	1.46	-
2N910	1	10	5.60	1.40	2.03	1.34	2.76
2N916	1	10	22.5	5.62	7.97	5.23	3.23
	2	10	31.5	7.88	3.01	2.39	6.07
2N706A	2	0.6	84.2	21.0	9.53	7.58	-

(a) From models determined in Table 5.1
(b) From models determined in Table 5.2
(c) From models determined in Table 5.3

(* should in reality be compared with S_1 based on areas listed in Table 5.3)

Table 5.7 - Comparison of Gradients at emitter junction

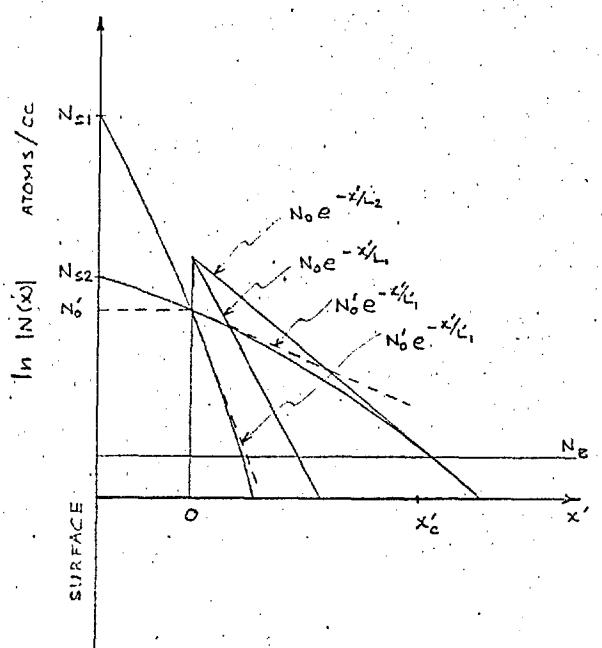


Fig. 5.2. (a) Components of Impurity Distribution showing exponentials defined by emitter and collector capacitance data.

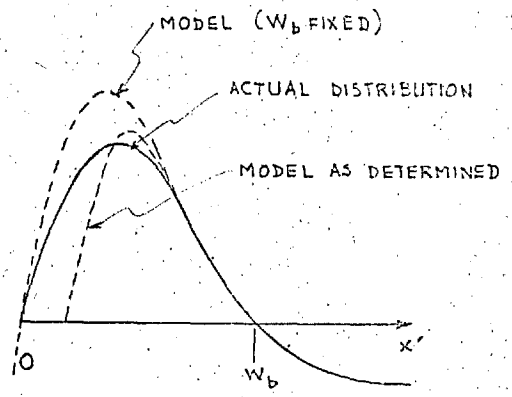


Fig. 5.2. (b) Base Region of Double-diffused Transistor showing Model resulting from reliance on emitter capacitance data.

Assuming for the moment fixed base width (the value for the model is established later), then from collector transition capacitance data (see Sections 3.5.1 and 3.5.3) an exponential of characteristic length L_2 is determined at the collector junction. Extending this exponential back to the emitter junction results in a concentration N_O which may be appreciably higher than N'_O (see Fig. 5.2(a)). Calling the characteristic length of the shallower exponential L_1, the gradient at the emitter junction is given by:

$$\left.\frac{dN}{dx'}\right|_{x' = 0} = \frac{N_O}{L_2} (\Upsilon - 1), \text{ where } \Upsilon = \frac{L_2}{L_1}$$

Equating this gradient to the actual gradient S_t gives:

$$\frac{N_O}{L_2} (\Upsilon - 1) = \frac{N'_O}{L'_2} (\Upsilon' - 1) \qquad 5.3.3$$

In the calculations resulting in Table 5.5, L'_2 was assumed to equal L_2. Thus, since $N_O > N'_O$, Υ' must be $> \Upsilon$. This indicates that emitter capacitance data tends to produce a higher ratio of L_2/L_1 than that required by collector capacitance data in order to retain the same gradient at the emitter junction.

The model thus determined from collector and emitter capacitance data (base width fixed) is represented by the top curve in Fig. 5.2(b). The gradient is shown to be equal to that of the actual profile (solid curve in Fig. 5.2(b)).

In the actual calculations of the model parameters collector capacitance data determines L_2, but emitter capacitance data is not

sufficient to determine both base width and γ. Additional information in the form of the emitter diode law is introduced to allow determination of both these parameters. During this determination the emitter diode law (which is dependent on minority carrier density at the injection point) forces a compromise where the base width of the model is reduced from the actual base width, resulting in an impurity distribution for which the combination of minority carrier density and impurity density for the injection point (eqn. 4.3.4) is the same as that for the actual distribution. The model thus determined is shown as the lower curve in Fig. 5.2(b).

The effect of the lower value base width and the higher value of γ (hence narrow retarding field region) is felt very strongly in base transit time, the calculated values in Table 5.5 being considerably lower than the measured values.

In a similar manner, applying the abrupt approximation at the emitter junction fixes the gradient S_1 for low reverse bias. However, the value of S_1 from eqn. 4.2.9 (see Table 4.1) is reduced by a factor of 4 from that for the symmetrical-linear approximation. Thus in the computation of γ and m_2 (hence W) from this slope and the emitter diode law (injection point Y_1 is twice the value used in the symmetrical-linear approximation) results in a compromise solution for which the values of γ (Table 5.6) are considerably lower than those of Table 5.5. Comparison of the values of Table 5.6 with those of Table 5.1 indicates that the values of γ, m_2, and N_0 in Table 5.1 are generally only

slightly higher than those for the abrupt junction case. This indicates that relaxing the gradient restriction at the emitter junction when determining the parameters of Table 5.1 allowed the gradient of the model to be reduced to the extent that it is only slightly more steep than that for the abrupt approximation. This is evident from the comparison initiated in Table 5.7. This explains the unexpected success of the model presented by Trofimenkoff[37,38] (Section 2.7.3) in representing the internal profile of double-diffused transistors, even though the retarding field region was an appreciable fraction of the aiding field region.

In Section 5.2.4 limitations on the accuracy of the model due to transit time measurements were discussed. In Table 5.6, where base transit time is employed only as a check on the final model, comparison of the values of γ for the 2N1613 #3 and 2N916 #2 determined at different values of collector voltage indicates that approximately the same model parameters apply over a range of operating conditions (see Section 5.2.3).

5.4 Numerical Techniques

Although several variations were written to compute the parameters of Tables 5.1 to 5.6, only the program using both $\overline{D}_R$ and $\overline{D}_A$ in the emitter diode law and base transit time expression to compute the parameters of Table 5.1 is presented in Appendix A.9. The flow diagram corresponds with the step-by-step procedure outlined in Section 5.2.1.

The program is written in the form of a main Chapter (Chapter 0)

which calls on routines as necessary. The various routines are:

Routine 1 - used in conjunction with Routine 4 to calculate d_c/L_2 from eqn. 5.2.1,

Routine 2 - operates on the emitter diode law (eqn. 4.3.9),

Routine 3 - computes base transit time (eqn. 4.4.1) and compares it with the measured value,

Routine 4 - bisection routine which calls on Routines 1, 2 and 5 to compute d_c/L_2, m_2 and Y_1, respectively,

Routine 5 - used to compute Y_1 from eqn. 4.2.12.

Included in Appendix A.9 is sample data for one transistor. Data which must be included regardless of the number of transistors is given in the first three blocks, while that for the specific transistor is given in the fourth block. Included in the former category are: (a) Coefficients (first block)and (b) Nodes (second block) for integration in fifteen intervals by Gaussian Quadrature. (c) q, k, upper and lower limits of d_c/L_2(0.05, 20.0), upper and lower limits of m_2 or γ, number of transistors, values of N_γ, D_γ, and θ for use in eqn. 2.4.14 to determine diffusion coefficients. Included in the fourth block for the specific device are:

(a) A_e
(b) A_c
(c) ε
(d) C_{te} fwd
(e) $T(^oK)$
(f) C_{tc}
(g) $A_e{}^s N_B/L_2$
(h) $V + V_{oc}$
(i) $A_e{}^s S_1$(Sym-lin)
(j) $\tau_b + \tau_c$
(k) $I_c/qn_i{}^2 e^{qV_e/kT}$
(l) $2v_s$

Output data is indicated in Chapter 0 by the "Caption" statements.

These are labelled, where possible, by the names used in the actual equations from which they are calculated. A_0 represents the value of $d_e/2$ calculated from $C_{te|fwd}$, while A_1 and A_2 represent a_{1e} and a_{2e} for the model. T_0 is the value of τ_b. All other terms are self-explanatory. The number of figures allowed in the print-out is no indication of the accuracy of the computed variables. This is obviously dependent on the accuracy of the input information.

In the computation of $\overline{D}_R$ and $\overline{D}_A$ in this program, the simple approximation of eqn. 2.4.14 was used. As can be seen from Fig. 2.11 and the values of $\overline{D}_R$ and $\overline{D}_A$ listed in Table 5.1, this should introduce little error in the region of interest. If greater accuracy is desired, Routine 50 of Appendix A.4 can be added. The required variables E_5 - E_{22} and F_5 - F_{22} have already been specified. The only changes necessary to allow for Routine 50 are the inclusion of the tabulated data for these variables (see Appendix A.4), the addition of "Read" statements to read in this information, and the substitution of:

JUMPDOWN (R50)

D10 = D↑ (or D11 = D↑)

for the 5 statements in the locations marked in Routine 2.

6. CONCLUSIONS

6.1 General Conclusions

The central aim of this study has been to establish the simplest physical model which can give an accurate representation of classical distributions and characterize actual devices over a wide range of operating conditions. In pursuit of this goal it has been necessary to thoroughly re-examine the solid-state diffusion process. Such a re-examination has been valuable both in describing the idealized impurity profiles, which are generally assumed to apply in diffused devices, and in pointing out the modifications to be expected owing to the non-linear nature of the diffusion process.

The overall effect of the double-diffused structure (i.e. graded junctions and retarding and aiding field regions in the base) has been considered in terms of a "terminal transit time" which defines the cut-off frequency of the transistor. The individual components of this transit time, associated with the base region and with emitter and collector depletion layers, were first discussed qualitatively and then quantitatively in terms of an equivalent circuit. The general conclusion from this review is that the double-diffusion process can result in transistors with upper frequency limits well in excess of that possible for transistors produced by most other fabrication processes.

While the study of diffused devices on a large physical scale by destructive techniques has been shown to be useful in predicting the physical configuration of devices on a small scale, such techniques have

been shown to be inapplicable to individual devices. Moreover, it is believed that the accuracy of the information derived by the above techniques is poor. The concept of physical modelling has been shown to be both a desirable and necessary outcome of the need for a thorough understanding of the physical and electrical properties of the transistor, since terminal measurements by themselves are inadequate to determine the actual impurity distribution. A survey of two of the earlier models[36-38] proposed to represent the base region of double-diffused transistors has pointed out their limited applicability and emphasized the need for a more general and more accurate model.

Since the idealized impurity profiles which result from the boundary conditions normally imposed on the diffusions used to fabricate double-diffused transistors are either double ERFCs or double Gaussians, both these distributions have been considered in detail. Equations are presented which thoroughly describe depletion layer and base transport properties. These equations have been used to determine depletion layer and base transport properties for a representative example which is then employed as a standard against which the double-exponential model assumed later in studies on actual devices may be compared. This comparison has demonstrated the ability of the double-exponential model to accurately represent both classical impurity profiles and the electrical properties dependent on these profiles.

The effect of diffusion from a substrate layer in a planar epitaxial transistor has been studied, and this has vividly demonstrated that an impurity element with a low diffusion coefficient must be used

in the substrate. The double-exponential model is seen to be applicable to planar epitaxial transistors so long as the substrate diffusion has little effect at the collector junction, i.e. either the substrate interface retains most of its original abruptness or the distance between the collector junction and this interface is large.

To facilitate the study of classical distributions, computer programs have been written which, presented with certain design information, can predict the expected impurity distribution as well as the base transport and depletion layer properties. It is suggested that in addition to their usefulness in the simulation of devices, they could be used as part of design procedure for manufacturing double-diffused devices. A further computer programs operates on classical distributions to produce a double-exponential model. Although, as a result of certain simplifications in the program, the best model is not determined, only minor modifications would be needed to determine the best model. If desired, this program can be simply incorporated into a larger program for the purpose of simultaneously studying classical distributions and determining the corresponding double exponential models.

To establish the basis for application of the physical model to actual devices, it has been necessary to thoroughly examine all the measurement techniques which yield information on the model, both in terms of accuracy and their interpretation in terms of the model constants. Collector transition capacitance measurements are shown to be a particularly valuable source of information when interpreted in a manner similar to that presented by Trofimenkoff[37,38]. At the

emitter junction it is forcibly demonstrated that for low reverse bias the abrupt emitter assumed in earlier models was not applicable, the symmetrical-linear representation being much more accurate.

A simple technique based on three measurements is shown to be sufficient to separate transition and stray capacitances. Comparison of strays determined by this means with "header" strays indicates that internal leads used to make connection between header leads and the transistor contribute little to stray capacitance.

Knowledge of emitter and collector areas (optical measurement) has been assumed to be a reasonable starting point in the evaluation of the constants of the model. The estimate of the ratio of emitter to collector area from terminal measurements of base resistance and the components of collector transition capacitance, used in the earlier models[36-38] has been shown to be very approximate, suggesting only limited usefulness as a source of information on the above-mentioned constants. It has further been shown that before collector breakdown voltage can be used to estimate background doping, a corrective procedure must be applied to allow for the breakdown starting at the cylindrical periphery of the planar junction.

The two major sources of information on the base region, i.e. emitter diode law and base transit time, have been discussed both in terms of two discreet diffusion coefficients, which apply for the retarding field and aiding field regions respectively. The effect of applying only the retarding field region diffusion coefficient to the

emitter diode law and the aiding field region diffusion coefficient to base transit time has been demonstrated. Measurement of the emitter diode characteristic is straightforward. A thorough examination of the transit time measurement has indicated that this measurement can be in considerable error (particularly for high frequency devices) and can thus provide the major limitation on the accuracy of the model determined from terminal measurements.

It has been demonstrated that conflicting requirements of emitter and collector capacitance data forces reliance on only one of these sources of information; the latter is preferred as being more directly dependent on the impurity distribution. In the actual determination of the model from terminal measurements, emitter capacitance data has been used only to estimate an initial injection point which is later readjusted to account for a difference of gradient between the model and the actual distribution at the emitter junction. This difference in gradient, a consequence of reliance on collector data, emitter diode law and base transit time, is unavoidable, but not a serious error. The change in gradient of the model is towards a less rapid rise in concentration in the base region, in fact, in the direction of the gradient determined by interpretation of emitter capacitance data at low reverse bias in terms of the abrupt-linear approximation. This explains why the abrupt-linear-exponential model used by Trofimenkoff[37,38], although based initially on a wrong assumption, enjoyed some measure of success in representing double-diffused transistors.

The double-exponential model is concluded to be a good representation for ordinary double-diffused transistors and for planar epitaxial transistors when the substrate diffusion has negligible effect at, or near, the collector junction.

6.2 Suggestions for Further Work

Non-one-dimensional considerations (e.g. emitter biasing-off and collector depletion width contraction at high bias current levels) have been ignored in this thesis. Such considerations are strongly dependent on the impurity distribution. Since the double exponential model determined for one-dimensional operation of the device (small-signal, low-level injection) has been shown to be a good representation of the base impurity profile, it could be used as the basis for analysis of non-one-dimensional effects in double-diffused transistors; such analysis is suggested for further study.

While the essential aims of this study are considered to have been met, the interests of simplicity and expediency have led in certain cases to a less rigorous treatment than is strictly warranted. This is particularly true in the determination of the double exponential model to represent classical distributions. As the method used determined a "worst case" approximation, it is suggested that it might be of benefit to modify the computer programs used in this determination in order to derive a more accurate model. In conjunction with this, a master program which treats different classical distributions, as well as deriving the model would be useful. The programs of Appendices A.4, A.5, and A.6 could form the basis for such a program. To render such

a program more general, provision could be made for design information other than junction position, surface concentrations, background doping, and temperature.

The major limitation of this and other attempts to determine the internal configuration of transistors has been the lack of information on the emitter region. As the primary objective of modelling is to yield information on the structure itself, as well as allowing prediction of the electrical properties, it would be of value to carry the model one step further to enable it to be used to yield information on the design parameters used in the fabrication process. A study is, therefore, suggested which, being based on the analysis of a large number of d evices for which the original design parameters are known, could be used to provide the necessary basis for working back from the model determined (for a particular device) to the design parameters. Such a study would be valuable in establishing closer correlation between the original design parameters and the device actually fabricated, as well as demonstrating the applicability of the double exponential model, which could be used in such a study.

The study of measurement techniques has indicated the large errors possible in the determination of base transit time (particularly for high frequency devices with low transit times). In the bridge used to make the measurements for this thesis, the minimum "terminal transit time" which could be measured was of the order of 0.25 nanoseconds, with, however, an accuracy of no better than $\pm$ 25%. With careful

minimization of strays etc., it is felt that it should be possible to improve this accuracy and to reduce the minimum possible measurement to the order of 0.1 nanoseconds. As the base transit time plays such an important role both in determining the internal configuration and in defining the upper frequency limit of transistors, it would be valuable to have an accurate bridge which may be used to measure transit times down to the value mentioned. A thorough study aimed at producing such a bridge is suggested. Included in this study would be an examination of any other methods which might be used to determine transit time. A commercial instrument produced on a limited scale would be welcome.

The program (Appendix A.9) used to determine the parameters of the double exponential model is quite inefficient. It is suggested that a more experienced programmer could produce a version which would minimize the number of operations required, hence the operating time.

For reasons which are unknown, but which are felt to be associated with gold doping, several transistors could not be evaluated to yield the constants of the model. To the author's knowledge, no information has previously been published which indicates the effect of gold-doping on the equilibrium barrier potential of transistors. It is therefore suggested that a study be undertaken to determine what effect, if any, gold doping has on this potential. A parallel study of devices fabricated in the same wafer, half of which are later gold doped, would be the most obvious method of ascertaining the effect of such doping on the determination of the double exponential model.

REFERENCES

1. Hoerni, J.A.: "Planar Silicon Transistors and Diodes", Technical Report, Fairchild Semiconductor Corporation, Palo Alto, California, 1961.

2. Bardeen, J. and Brattain, W.H.: "The Transistor, a Semi-Conductor Triode", Phys. Rev., Vol. 74, p.230, July, 1948.

3. Shockley, W.: "The theory of P-N Junctions in Semi-Conductors and P-N Junction Transistors", B.S.T.J., Vol. 28, pp. 435-489, July, 1949.

4. Shockley, W., Sparks and Teal: "P-N Transistors", Phys. Rev., Vol. 83, pp. 151-162, July, 1951.

5. Saby, J.S.: (a) "Recent Developments in Transistors and Related Devices," Tele-Tech., Vol. 32, p. 10, 1951.
   (b) "Fused Impurity P-N-P Junction Transistors", Proc. IRE, Vol. 40, pp. 1512-1518, Nov. 1952.

6. 'The Surface Barrier Transistor'
   - Part 1: Bradley, W.E.: "Principles of the Surface-Barrier Transistor", Proc. IRE, Vol. 41, pp. 1702-1706, Dec. 1953.
   - Part 2: Tiley, J.W. and Williams, R.A.: "Electrochemical Techniques for Fabrication of Surface-Barrier Transistors", loc. cit., pp. 1706-1708.
   - Part 3: Angell, J.B., and Keiper, F.P.: "Circuit Applications of Surface-Barrier Transistors", loc. cit., pp. 1709-1712.
   - Part 4: Kansas, R.: "On the High-Frequency Performance of Transistors", loc. cit., pp. 1712-1714.
   - Part 5: Schwarz, R.F.: "The Properties of Metal to Semiconductor Contacts", loc. cit., pp. 1715-1720.

7. Kromer, H.: "Der Drifttransistor", Naturwissenschaften, Vol. 40, pp. 578-579, Nov. 1953.

8. Kromer, H.: "Zur Theorie des Diffusions - und Des Drifttransistors' Arch. elektr. Übertragung, Vol. 8,
   Part 1: "Die Vierpolmatrix und ihr Niederfrequenzverhalten", pp. 223-228, May, 1954.

Part 2: "Frequenzabhängigkeit", pp. 363-369, Aug. 1954.
Part 3: "Dimensionierungsfragen", pp. 499-504, Nov. 1954
and
"The Drift Transistor", in Transistors I, Princeton, N.J., R.C.A. Laboratories, pp. 202-220, March 1956.

9. Dunlap, W.C., Jr.: "Diffusion of Impurities in Germanium", Phys. Rev. Vol. 94, pp. 1531-1540, June 1954.

10. Fuller, C.S.: "Diffusion of Donor and Acceptor Elements in Germanium", Phys. Rev., Vol. 86, pp. 137-138, April 1952.

11. Dunlap, W.C., Jr., Bohm, H.V., and Mahon, H.P., Jr.: "Diffusion of Impurities in Silicon", Abstract Phys. Rev., Vol. 27, pp. 544-543. May 1956.

12. Chapin, D.M., Fuller, C.S., and Pearson, G.L.: "A New Silicon P-N Junction Photocell for Converting Solar Radiation into Electrical Power", J. Appl. Phys., Vol. 25, pp. 676-677, May 1954.

13. Pearson, G.L., and Fuller, C.S.: "Silicon P-N Junction Power Rectifiers and Lightning Protectors", Proc. IRE. Vol. 42, P. 760, Apr., 1954.

14. Fick, A.: "Ueber Diffusion" Ann. Phys. Vol.94, pp. 59-86, 1855.

15. Carslaw, H.S. and Jaeger, J.C.: "Conduction of Heat in Solids", Clarendon Press, Oxford, 1947.

16. Barrer, R.M.: "Diffusion In and Through Solids", Cambridge Univ. Press, 1951.

17. Jost, W.: "Diffusion in Solids, Liquids and Gases", Academic Press, New York, 1952.

18. Seith, W.: "Diffusion in Metallen", Springer - Verlag, Berlin, 1955.

19. Crank, J.: "The Mathematics of Diffusion", Clarendon Press, Oxford, 1956.

20. Lee, C.A.: "A High-Frequency Diffused Base Germanium Transistor", B.S.T.J., Vol. 35, pp. 23-34, Jan. 1956.

21. Tanenbaum, M., and Thomas D.E.: "Diffused Emitter and Base Silicon Transistors", B.S.T.J., Vol. 35, pp. 1-34, Jan. 1956.

22. Ditrick, N.H., and Kestenbaum, A.L.: "The Design, Construction and High-Frequency Performance of Developmental Drift Transistors", 2nd Annual Meeting on Electron Devices, October 25-26, 1956, Washington (abstracted in IRE. Trans. on Electron Devices, ED-4, p. 195, April 1957).

23. Fuller, C.S. and Ditzenberber, J.A.: "Diffusion of Donor and Acceptor Elements in Silicon", J. Appl. Phys. vol. 27, pp. 544-553, May 1956.

24. Fuller, C.S.: "Formation of Junctions by Diffusion", Bell Lab. Series on Transistor Technology, Ed. Biondi Vol. 3, Chapter 3, pp. 64-89, 1958. (See p. 87 for list of publications on diffusion data for Germanium and Silicon prior to 1958).

25. Mackintosh, I.M.: "The Diffusion of Phosphorus in Silicon", J.E.C.S. Vol. 109, No. 5, pp. 392-401, May 1962.

26. Yatsko and Kesperis: "A Modified Closed Box System for the Diffusion of Boron in Silicon", J.E.C.S. Vol. 107, No. 11, pp. 911-915, Jan. 1956.

27. Theurer, H.C., Kleimack, T.J., Loar, H.H., and Christensen, H.: "Epitaxial Diffused Transistors", Proc. IRE, Corresp., Vol. 48, pp. 1642-3, September 1960.

28. Bond, W.L., and Smits, F.M.: "The Use of an Interference Microscope for Measurement of Extremely Thin Layers", B.S.T.J., Vol. 35, pp. 1209-1221, Sept. 1956.

29. Valdes, L.B.: "Resistivity Measurement on Germanium for Transistors", Proc. IRE. Vol. 42, pp. 420-427, Feb. 1954.

30. Backenstoss, G.: "Evalaution of the Surface Concentration of Diffused Layers in Silicon", B.S.T.J. Vol. 37, pp. 699 - 710, May 1958.

31. Irvin, J.C.: "Resistivity of Bulk Silicon and of Diffused Layers in Silicon", B.S.T.J., Vol. 41, pp. 387-410, March 1962.

32. Subashiev, V.K., Landsman, A.P., and Kukharskii, A.A.: "Distribution of Phosphorus Atoms during Diffusion in Silicon", Soviet Phys. - Solid State, Vol. 2, p.2406, 1961.

33. Lawrence, H., and Warner, R.M.J : "Diffused Junction Depletion Layer Calcultions", B.S.T.J., Vol. 39, pp. 389-404, March, 1960.

34. Giacoletto, L.J.: "Junction Capacitance and Related Characteristics Using Graded Impurity Semiconductors", IRE. Trans. on Electron Devices, Vol. ED-4, pp. 207-215, July 1957.

35. Kocsis, J.: "The Properties of Junction Transistors at Very High Frequencies and their Representation by Equivalent Circuits", Ph.D. Thesis, Univ. of London, pp. 112-121, 1962.

36. Boothroyd, A.R.: "Determination of the Physical Parameters of Drift Transistors having a Diffused Collector Junction", Electronics Research Laboratory, Univ. of California, Series No. 60, Issue No. 391, AF49 (638) - 1043, 1961.

37. Trofimenkoff, F.N.: "A study of the Physical Behaviour of Transistors at High Current Levels", Ph.D. thesis, Univ. of London, Aug. 1962.

38. Boothroyd, A.R. and Trofimenkoff, F.N.: "Determination of Physical Parameters of Transistors of Single and Double-Diffused Structures", IEEE Trans. on Electron Devices, Vol. ED-10, No. 3, pp. 140-163, May 1963.

39. Pritchard, R.L., Angell, J.B., Adler, R.B., Early, J.M., Webster, W.M.: "Transistor Internal Parameters for Small-Signal Representation", Proc. IRE, Vol. 49, pp. 725-738, April 1961.

40. Smits, F.M.: "Formation of Junction Structures by Solid-State Diffusion", Proc. IRE, Transistor Issue,Vol. 46, No. 6, pp. 1049-1061, June 1958.

41. Smits, F.M. and Miller, R.C.: "Rate Limitation at the Surface for Impurity Diffusion in Semiconductors", Phys. Rev., Vol. 104, pp. 1242-1245, Dec. 1956.

42. Trumbore, F.A.: "Solid Solubilities of Impurity Elements in Germanium and Silicon", B.S.T.J., Vol. 3, pp. 205-234, Jan. 1960.

43. Woking, W.: "Diffusion Concentration Profiles by Analog Computation", J.E.C.S., Dec. 1958.

44. Nomura, K.C.: "Analytic Solution of the Double Diffusion Profile", J. Appl. Phys., Vol. 32, p. 1167, June, 1961.

45. Thomas, C.O.:, Kahng, D., and Manz, R.C.: "Impurity Distribution in Epitaxial Silicon Films", J.E.C.S., pp. 1055-1061, Nov. 1962.

46. Kahng, D., Thomas, C.O., and Manz, R.C.: "Anomalous Impurity Diffusion in Epitaxial Silicon Near the Substrate", J.E.C.S., pp. 1106-1108, Nov. 1962.

47. Caughey, D.M.: "Study of Transistor Noise with Particular Reference to High Level Operation", Ph.D. Thesis, Univ. of London, 1964.

48. Shockley, W.: "Electrons and Holes in Semiconductors, with applications to Transistor Electronics", D. Van Nostrand Co. Inc., N.Y., 1950.

49. Prince, M.B.: "Drift Mobilities in Semiconductors, I. Germanium", Phys. Rev., Vol. 92, pp. 681-687. Nov. 1953.

50. Prince, M.B.: "Drift Mobilities in Semiconductors, II, Silicon", Phys. Rev., Vol. 93, pp. 1204-1206, March 1954.

51. Ludwig, G.W., and Walters, R.L.: "Drift and Conductivity Mobility in Silicon", Phys. Rev., vol. 101, pp. 1699-1701, March, 1956.

52. Backenstoss, G.: "Conductivity Mobilities of Electrons and Holes in Heavily Doped Silicon", Phys. Rev., Vol. 108, pp. 1416-1419, Dec. 1957.

53. Horn, F.H.: "Densitometric and Electrical Investigation of Boron in Silicon", Phys. Rev., Vol. 97, pp. 1521-1525, March 1956.

54. Carlson, R.O.: "Electrical Properties of Near Degenerate Boron-Doped Silicon", Phys. Rev., Vol. 100, pp. 1075-1078, Nov. 1955.

55. Conwell, E.M.: "Properties of Silicon and Germanium II", Proc. IRE, Vol. 46, pp. 1281-1300, June 1958.

56. Conwell, E.M., and Weisskopf, V.F.: "Impurity Scattering in Semiconductors", Phys. Rev., Vol. 69, p.258A, 1946. and "Theory of Impurity Scattering in Semiconductors" Vol. 77, pp. 388-390, 1950.

57. Sugano, T. and Koshiga, F.: "The Calculation of Cutoff Frequencies of Minority-Carrier Transport Factor in Drift Transistors when mobilities are not Constant". Proc. IRE, Vol. 49, pp. 1218, July, 1961.

58. Ryder, E.J.: "Mobility of Holes and Electrons in High Electric Fields", Phys. Rev., Vol. 90, pp. 766-769, 1953.

59. Uhlir, A.: "The Potentials of Infinite Systems of Sources and Numerical Solutions of Problems in Semiconductor Engineering", B.S.T.J., vol. 34, pp. 105-128, Jan. 1955.

60. Kennedy, D.P., and O'Brien, R.R.: "Depletion Layer Properties in Double-Diffused Transistors", J. of Electronics and Control, pp. 303-315, July-Dec. 1963.

61. Gray, P.E., and Adler, R.B.: "A simple Method for Determining the Impurity Distribution Near a P-N Junction", IEEE Trans. on Electron Devices, ED-12, No. 8, pp. 475-477, Aug. 1965.

62. Gummel, H.K.: "Measurement of the Number of Impurities in the Base Layer of a Transistor", Proc. IRE, Correspondence, Vol. 49, p.834, April 1961.

63. Miller, S.L.: "Ionization Rates for Holes and Electrons in Silicon", Phys. Rev., Vol. 105, pp. 1246-1299, Feb. 1957.

64. Gibbons, G., and Kocsis, J.: "Breakdown Voltage of Germanium Plane-Cylindrical Junctions", IEEE Trans. on Electron Devices, Vol. ED-12, No. 4, pp. 193-198, April 1965.

65. Morgan, S.P., and Smits, F.M.: "Potential Distribution and Capacitance of a Graded P-N Junction", B.S.T.J., Vol. 39, pp. 1573-1603, Nov. 1960.

66. Turner, R.J.: "Surface-barrier Transistor Measurements and Applications", Tele-Tech, Vol. 13, pp.78-80, August, 1954.

67. Das, M.B.: "On the Determination of the Extrinsic Equivalent Circuit Parameters of Drift Transistors", J. of Electronics and Control, Vol. 8, No. 5, pp. 351-363, May 1960.

68. Zener, C.: "Theory of Electric Breakdown of Solid Di electrics", Proc. Roy. Soc., Vol. 145, pp. 523-529, July 2, 1934.

69. McKay, K.G.: "Avalanche Breakdown in Silicon", Phys. Rev., Vol. 94, pp. 887-889, May 15, 1954.

70. Veloric, H.S., Prince, M.B., and Eder, M.J.: "Avalanche Breakdown in Silicon Diffused p-n Junctions as a function of Impurity Gradient", J. Appl. Phys., Vol. 227, pp. 895-899, August 1956.

71. Root, C.D., Lieb, D.P., and Jackson, B.: "Avalanche Breakdown Voltages of Diffused Silison and Germanium Diodes", IRE Trans. on Electron Devices, Vol. ED-7, pp. 257-262, Oct. 1960.

72. Armstrong, H.L., Metz, E.D. and Wieman, I.: "Design Theory and Experiments for Abrupt Hemispherical p-n Junction Diodes", IRE Trans. on Electron Devices, Vol. ED-3, pp. 86-92, April 1956.

73. Armstrong, H.L.: "A theory of Voltage Breakdown of Cylindrical p-n Junctions with Applications", IRE Trans. on Electron Devices, Vol. ED-4, pp. 15-16, Jan., 1957.

74. Thomas R.E., Johnston, R.H., and Boothroyd, A.R.: "Negative Resistance in a Transistor Under Punch-Through Conditions," Proc. IEEE, Correspondence, Vol. 54, No. 1, pp. 84-85, Jan. 1966.

75. Morin, F.J., and Maita, J.P.: "Conductivity and Hall Effect in the Intrinsic Range of Germanium", Phys. Rev., Vol. 94, pp. 1525-1529, June, 1954.

76. Morin, F.J., and Maita, J.P.: "Electrical Properties of Silicon Containing Arsenic and Boron", Phys. Rev., Vol. 96, pp. 28-35, Oct. 1954.

77. Gray, P.E., DeWitt, D., Boothroyd, A.R., Gibbons, J.F.: "Physical Electronics and Circuit Models of Transistors", SEEC Vol. 2, J. Wiley & Sons, Inc., 1964, See pp. 59-61.

78. "Integrated Circuits Design Principles and Fabrication". Motorola series in Solid-State Electronics, Ed. Warner, R.M., Jr., Fordemwalt, J.N., McGraw-Hill, 1965, p. 91.

79. Apaydin, B.P.: "Study of Analogue Simulation of the Dynamic Behaviour of Transistors for small signals", Ph.D. Thesis, Univ. of London, August 1964.

A.1 DETERMINATION OF PARAMETERS OF LINEAR-EXPONENTIAL MODEL

In addition to the method outlined in Chapter 2, Section 2.7.3, to utilize collector capacitance data the equations below are also necessary to use measured date to determine physical constants of the Linear plus Exponential model for the base.

$$\tau_b \approx \frac{L^2}{\overline{D}} \left[e^{-\theta m} \left(\frac{e^{\theta m}}{\theta} - 1 \right) + \frac{s^2}{L^2} \left(\frac{L}{s} + \frac{1}{2} \right) \ln \frac{s}{a_{2e}} \right] \qquad \text{A.1.1}$$

where $m = W/L$, a_{2e} is the edge of the emitter depletion layer in the base and s is the position of maximum doping (N_1) in the base. $\overline{D}$ is an average diffusion coefficient related to the diffusion coefficient D_o at $N = N_1$, by $\overline{D} = D_o (1 + \theta)$. θ is the fractional index of eqn. 2.4.14. Eqn. A.1.1 is derived by considering the aiding and retarding field regions separately and adding the results.

The variation of transit time with collector voltage is given by:

$$\frac{\Delta \tau_b}{\Delta m} \approx \frac{L^2}{\overline{D}} e^{-\theta m} (1 + \theta) \qquad \text{A.1.2}$$

The emitter diode equation, assuming negligible retarding field region, is given by:

$$I_c \approx - \frac{A_e n_i^2 q \overline{D}}{N_1 L} \frac{1}{\left[1 + \frac{1}{2} (1 + \theta) \frac{s}{L} \right]} \cdot e^{qV_e/kT} \qquad \text{A.1.3}$$

from which it is possible to determine

$$A_e/N_1 L = \frac{I_c}{q n_i^2 \overline{D} e^{qV_{eb}/kT}} \qquad \text{A.1.4}$$

From emitter capacitance data, the abrupt-linear approximation yields:

$$A_e^3 a = \frac{3}{q \varepsilon^2} \cdot \frac{dV_{eb}}{d(1/C_{te}^3)} = A_e^3 N_1/L \qquad \text{A.1.5}$$

where $dV_{eb}/d(\frac{1}{C_{te}^3})$ may be found from the slope of $1/C_{te}^3$ vs V_{eb} at low reverse bias.

α_{ae} is given by $\frac{\varepsilon A_e}{C_{te}|_{fwd}}$ for forward biased C_{te}. The ratio of A_e/A_c is determined from:

$$\frac{A_e}{A_c} = \frac{C_{tc1}}{C_{tc}} \qquad \text{A.1.6}$$

The following iterative procedure allows determination of the physical constants of the model:

1. For the appropriate ratios of $\frac{C_{tc1}}{C_{c2}}$ and $\frac{V_2 + V_{oc}}{V_1 + V_{oc}}$ determine d_{1c}/L from eqn. 2.7.16, hence $\frac{d_{2c}}{L}$ is also known.

2. Determine $\Delta m = \ln\left|\frac{C_{c1}}{C_{c2}} \cdot F\right|$ where $F = \frac{1 - e^{-d_{2c}/L}}{1 - e^{-d_{1c}/L}}$

3. Assume N_1, hence D_o. $\bar{D} = D_o (1 + \theta)$.

4. Choose an initial value of m. A first estimate of L follows from eqn. A.1.2.

5. Use $\frac{A_c^3 N_B}{L} \cdot \left[\frac{A_e}{A_c} \cdot \frac{N_1 L}{A_e}\right]^3 = N_1^4 L^2 e^{-m} \left[\frac{(1 - e^{-d_{1c}/L})}{d_c/L}\right]$

6. Determine $e^{-a_{1c}/L}$ from eqn. 2.7.14. Substituting for N_B in eqn. 2.7.15, $N_B = N_1 e^{-a_{1c}/L} \cdot e^{-m}$ allows determination of a new value of m. The process is repeated until mutually consistent values of m, L and N_1 are obtained.

7. If necessary, adjust the value of $\bar{D}$ and repeat. It should not be necessary to do this more than once.

8. Calculate A_e from A_e/N_1L, hence A_c and N_B.

9. a is then found from $A_e^3 a$ and s from $s = N_1/a$.

10. α_{ac} is found from C_{te} | fwd.

11. τ_b is used as a check.

A.2 ATTEMPT TO MEASURE Y_{ee}

In Fig. A.1(a) the transistor is represented as being terminated by the adjustable co-axial line of either the General Radio Admittance Bridge or the Rohde and Schwarz Diagraph. The simplified equivalent circuit of Fig. A.1(b) is assumed, neglecting for the moment lead inductances, C_{seb}, C_{sec}, r'_{cc} and r_c (See Fig. 2.12). If the terminating line is assumed to present only an inductive component to the transistor, then a particular line length l_s exists so that the line inductance L_s is in parallel resonance with $C_{tca} + C_{scb}$. Thus:

$$L_s = \frac{1}{\omega^2 C_{ca}} \qquad \text{A.2.1}$$

where $C_{ca} = C_{tca} + C_{scb}$.

For this conditon it may be shown from eqn. 2.7.27 that:

$$\frac{1}{(Z_{ib}/r_d) - d} = 1 + j\omega\ (C_{te} + C_{de}) \qquad \text{A.2.2}$$

If r'_{bb} is not known, then a real quantity d may be subtracted from Z_{ib}/r_d such that

$$R_e\ \left[\frac{1}{(Z_{ib}/r_d) - d}\right] = 1$$

Since $d \propto I_e$ it is possible to determine its value from measurement of Z_{ib} at low I_e to avoid the effects of high level injection on r'_{bb}. At low level injection, a reasonable assumption is

$$C_{de} \propto I_e$$
$$= I_e F_o$$

Thus

$$j\left[\frac{1}{(Z_{ib}/r_d) - d}\right] = j\left[\frac{\omega \beta C_{te}}{I_e} + \omega \beta F_o\right] = A \qquad \text{A.2.3}$$

where $\beta = \frac{kT}{q}$

Provided the assumptions are correct, a plot of A vs $1/I_e$ should give a straight line of slope ωC_{te} with intercept F_o at $1/I_e = 0$; hence C_{te}, F_o and C_{de} are known. Obviously the major problem is, therefore, to determine the line length l_s necessary to obtain the parallel resonance.

For the circuit of Fig. A.1(b) it may be shown that for any line length l:

$$Z_{ib} = r'_{bb}(1 - a'B) + \frac{j\omega C_{te}}{1 + \frac{j\omega C_{te}}{Y_{ee}}} \qquad \text{A.2.4}$$

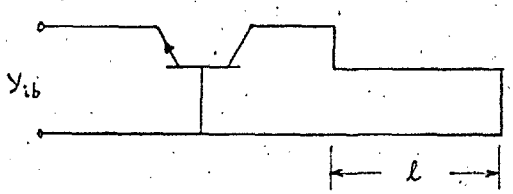


Fig. A.1(a) Measurement of Y_{ib} with variable output line.

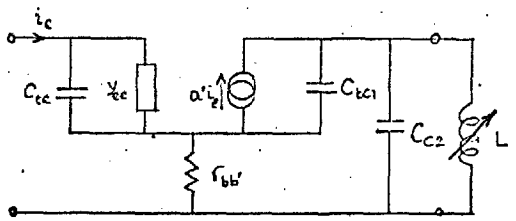


Fig. A.1(b) Equivalent circuit with Inductive Load.

where $B = \dfrac{\omega C_{c2} - \dfrac{1}{\omega L}}{\omega(C_{tc1} + C_{c2}) - 1/\omega L}$ A.2.5

When L reaches a value of L_1 such that L_1 resonates with $C_{tc1} + C_{c2}$, the value of B exhibits a rapid change between two extreme large magnitude values. Thus $C_{tc1} + C_{c2}$ may be found by adjusting l until a similar rapid change is observable in Z_{ib}.

If the assumed simplifications are applicable, the locus of Z_{ib} should follow a straight-line relationship as shown in Fig. A.2. At the points shown,

A: $L = 0, \quad l = \lambda/4$

B: $L = \infty, \quad l = \lambda/2$

C: $L = L_3$, to be determined

D: $L = L_2$, to be determined

A trial and error method may be employed to determine L_3 after $C_{tc1} + C_{c2}$ is known. From $C_{c2} = u(C_{tc1} + C_{c2})$, assume u. Calculate L_2 and L_3 from:

$$L_2 = \frac{2}{\omega^2 (C_{tc1} + 2C_{c2})} \qquad \text{A.2.6}$$

and

$$L_3 = \frac{1}{\omega^2 C_{c2}} \qquad \text{A.2.7}$$

Line lengths l_2 and l_3 may then be determined and input admittance measured for these terminations, as well as for L = 0 and L = ∞. Plotting points A, B, C, and D should satisfy the requirements:

AC = CD

BC/AC = u

if the initial choice of u is correct. If not, adjust the value of u and repeat until agreement is reached.

The above method is strictly applicable only when the terms neglected are, in fact, negligible. The general effect of the presence of r'_{cc}, r_c, strays, and a resistive component in the output line is to cause Z_{ib} to follow a circular locus, as shown in Fig. A.2(b). The method could still be applied if the radius of this circle were large. However, for all the samples studied, the radius was small. Even though it was possible to balance out the value of C_{c2} by L_s, the presence of a resistive component (largely due to the output line) meant that the value of Z_{ib} was strongly dependent on the output circuit, and the simple relationships of eqn. A.2.2 and A.2.3 could not be used to determine C_{te}, F_o and C_{de}. For this reason the approach was abandoned as being impractical.

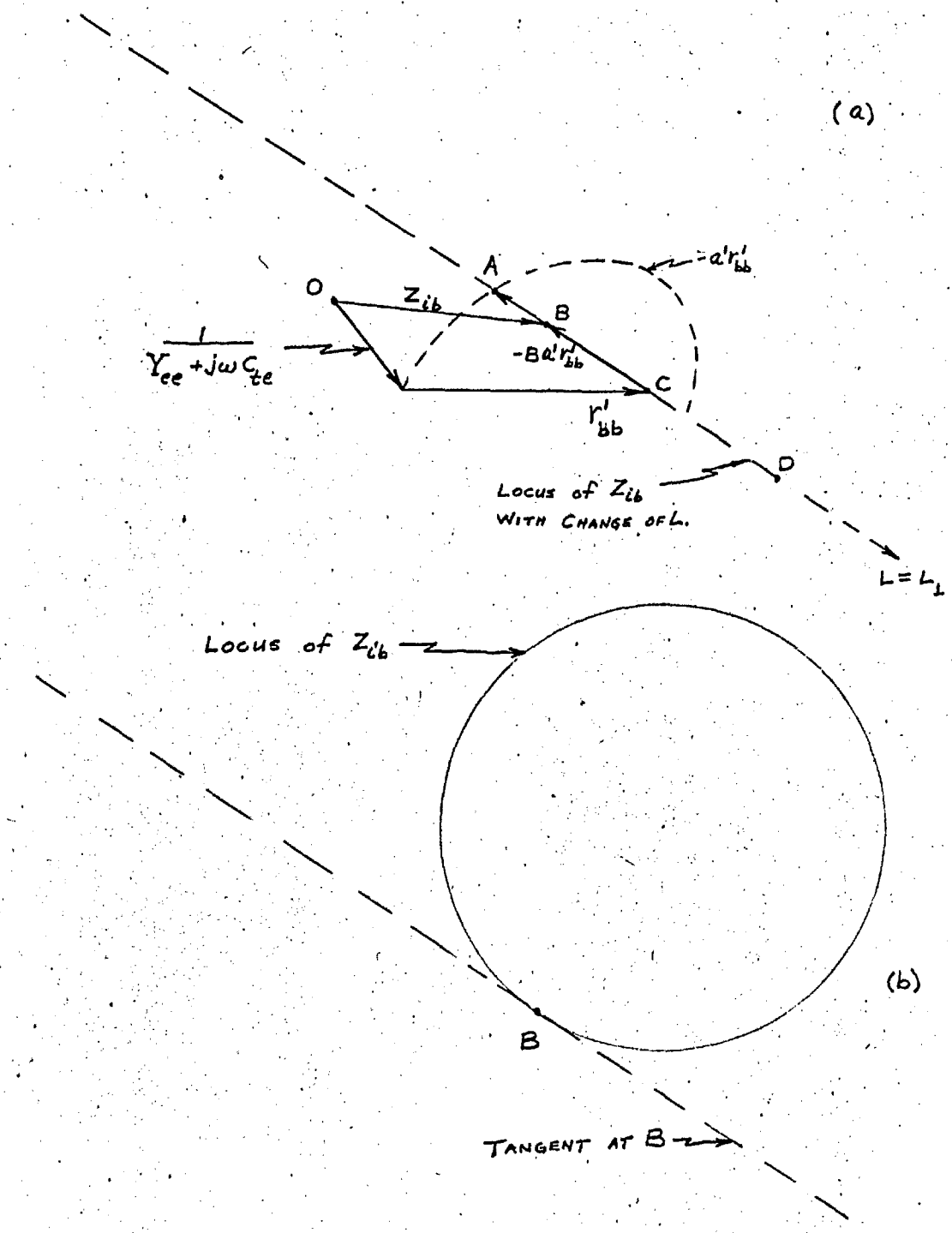


Fig. A.2. (a) Ideal Locus of Z_{ib} with variation in L.
(b) Circular Locus of Z_{ib}.

A.3 DETERMINATION OF L_1 AND L_2 WHEN BOTH EXPONENTIALS ARE SIGNIFICANT AT COLLECTOR JUNCTION

If both exponentials are significant at the collector junction, ($\Upsilon < 2.5$), then the equations of Section 3.5.1 are no longer applicable. Essentially the same basis may be used for choice of the exponentials, i.e. the slope of the classical distribution at the collector junction, and the total number of uncompensated impurities in the base of the double-diffused transistor. Although in most cases it is possible to completely neglect the emitter diffusion at the collector junction, this simplification is not made in the following equations.

For the double ERFC case:

$$\left.\frac{dN(x)}{dx}\right|_{x=x_c} = \frac{-N_{s2}}{\sqrt{\pi D_2 t_2}} e^{-x_c^2/4D_2t_2} + \frac{N_s}{\sqrt{\pi D_1 t_1}} e^{-x_c^2/4D_1t_1} \qquad \text{A.3.1}$$

while for the double exponential:

$$\left.\frac{dN(x')}{dx'}\right|_{x'=x'_c} = -\frac{N_o}{L_2} e^{-x_c'/L_2} + \frac{N_o}{L_1} e^{-x_c'/L_1} \qquad \text{A.3.2}$$

From the collector junction the following applies:

$$N_o = \frac{N_B}{e^{-x_c'/L_2} - e^{-x_c'/L_1}} \qquad \text{A.3.3}$$

Substituting this value in eqn. A.3.2 the slope becomes:

$$\left.\frac{dN(x')}{dx'}\right|_{x'=x'_c} = \frac{N_B}{(e^{-x_c'/L_2} - e^{-x_c'/L_1})}\left[\frac{e^{-x_c'/L_1}}{L_1} - \frac{e^{-x_c'/L_2}}{L_2}\right] = N_B\theta_1 \qquad \text{A.3.4}$$

Equating eqns. A.3.1 and A.3.4 gives:

$$N_B\,\theta_1 = -\frac{N_{s2}}{\sqrt{\pi D_2 t_2}}\,e^{-x_c^2/4D_2t_2} + \frac{N_{s1}}{\sqrt{\pi D_1 t_1}}\,e^{-x_c^2/4D_1t_1} \qquad \text{A.3.5}$$

Equating the areas of the double exponential (eqn. 3.5.7) and the double ERFC (eqn. 3.5.8) gives:

$$N_B\,\theta_2 = N_{s2}\left[x_c\,\mathrm{erfc}\frac{x_c}{\sqrt{4D_2t_2}} - x_e\,\mathrm{erfc}\frac{x_e}{\sqrt{4D_2t_2}} - \sqrt{\frac{4D_2t_2}{\pi}}\left(e^{-x_c^2/4D_2t_2} - e^{-x_e^2/4D_2t_2}\right)\right]$$

$$- N_{s1}\left[x_c\,\mathrm{erfc}\frac{x_c}{\sqrt{4D_1t_1}} - x_e\,\mathrm{erfc}\frac{x_e}{\sqrt{4D_1t_1}} - \sqrt{\frac{4D_1t_1}{\pi}}\left(e^{-x_c^2/4D_1t_1} - e^{-x_e^2/4D_1t_1}\right)\right] \qquad \text{A.3.6}$$

where $\theta_2 = \dfrac{L_2(1 - e^{-x_c'/L_2}) - L_1(1 - e^{-x_c'/L_1})}{e^{-x_c'/L_2} - e^{-x_c'/L_1}}$

Eqns. A.3.5 and A.3.6 may be solved simultaneously for L_1 and L_2.

For the <u>double Gaussian</u> the two equations are:

$$N_B\,\theta_1 = -\frac{N_{s2}\,x_c}{2D_2t_2}\,e^{-x_c^2/4D_2t_2} + \frac{N_{s1}\,x_c}{2D_1t_1}\,e^{-x_c^2/4D_1t_1} \qquad \text{A.3.7}$$

and

$$N_B\,\theta_2 = N_{s2}\sqrt{\pi D_2t_2}\left(\mathrm{erfc}\frac{x_e}{\sqrt{4D_2t_2}} - \mathrm{erfc}\frac{x_c}{\sqrt{4D_2t_2}}\right)$$

$$- N_{s1}\sqrt{\pi D_1t_1}\left(\mathrm{erfc}\frac{x_e}{\sqrt{4D_1t_1}} - \mathrm{erfc}\frac{x_c}{\sqrt{4D_1t_1}}\right) \qquad \text{A.3.8}$$

The Newton-Raphson technique is suggested to solve the above sets of equations simultaneously. In general terms this technique is outlined below.

Consider two general equations - 2 unknowns:

$$f(x,y) = 0$$

$$g(x,y) = 0 \qquad \text{A.3.9}$$

The initial values x_o and y_o are assumed and a correction Δx and Δy is sought so that the new values of x and y are:

$$x = x_o + \Delta x$$

$$y = y_o + \Delta y$$

for which $f(x_o + \Delta x, y_o + \Delta y) = 0$

$$g(x_o + \Delta x, y_o + \Delta y) = 0$$

The correction is found by employing the Taylor expansion and ignoring all terms of higher order than the first. Thus:

$$f'_x (x_o, y_o)\,\Delta x + f'_y (x_o,y_o)\,\Delta y = -f (x_o,y_o)$$

$$g'_x (x_o, y_o)\,\Delta x + g'_y (x_o,y_o)\,\Delta y = -g (x_o,y_o) \qquad \text{A.3.10}$$

where f'_x and f'_y and the partial derivatives of (x,y) with respect to x and y respectively, and g'_x and g'_y are the partial derivatives of g(x,y) with respect to x and y respectively. The process is repeated with $x_1 = x_o + \Delta x$ and $y_1 = y_o + \Delta y$. Eqns. A.3.10 are again evaluated for x_1 and y_1. The process is repeated until the desired degree of accuracy is attained. In eqns. A.3.5 and A.3.6 or A.3.7 and A.3.8, L_1 and L_2 are substitutedfor x and y in the above process.

A.4 Program for Double ERFC

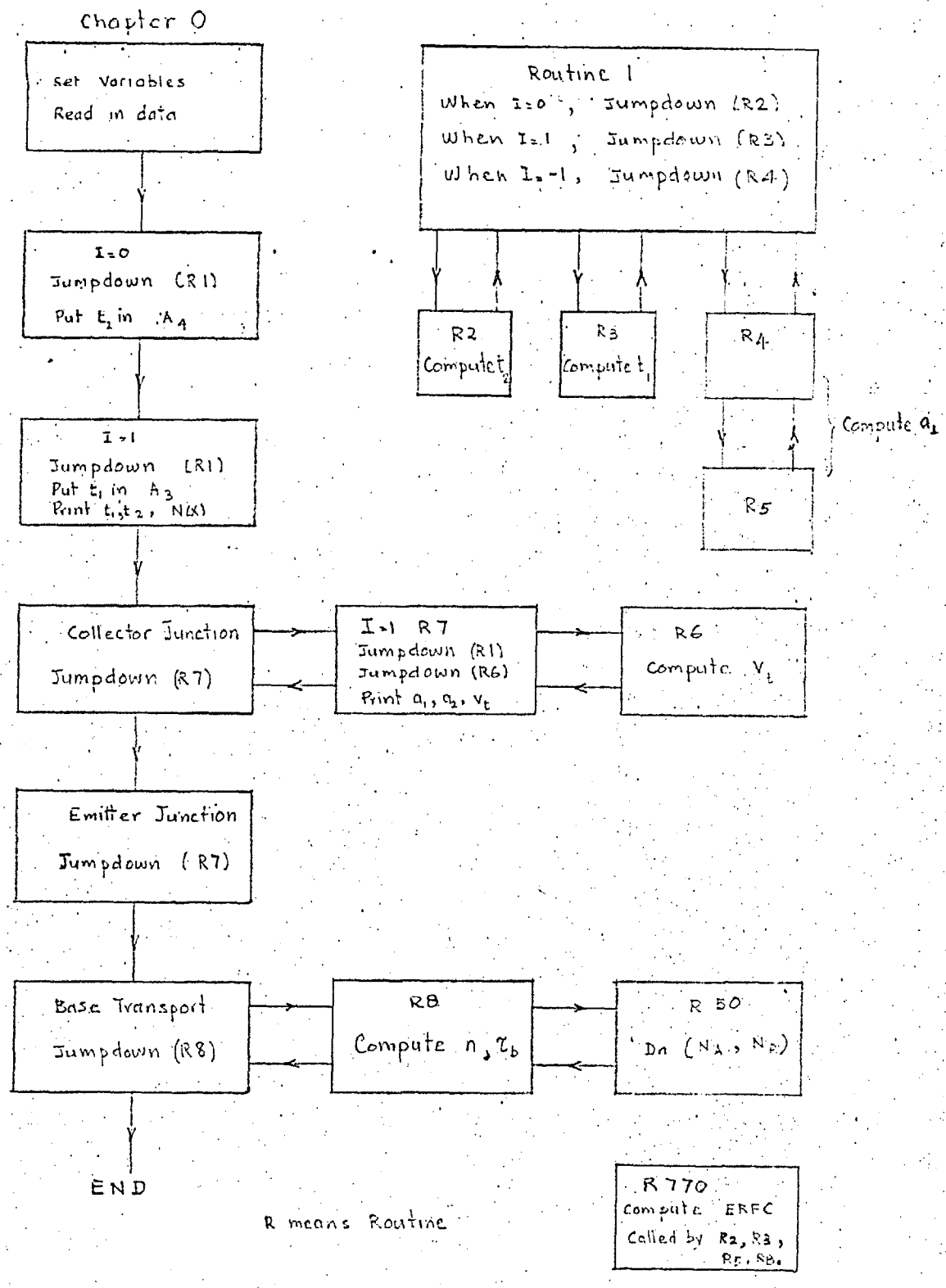


Fig. A.3 Flow Diagram for Double ERFC Program

```
JOB
LXK43PA1, THOMAS RUN70 5/5/66
COMPUTING 20000 INSTRUCTIONS
OUTPUT
0 LINE PRINTER 2000 LINES
STORE 32 BLOCKS
COMPILER EMA
MAIN→500
AUXILIARY(0,0)
DEPTH 6
DUMPS 0
TITLE
DBLE ERFC DISTN (EX) - V,T,N/No.

ROUTINE770
D1=0.3275911D0+1
D1=1/D1
D0=xEXP(-D0D0)
D2=D1D1
D3=D2D1
D4=D3D1
D5=D4D1
D1=0.225836846D1-0.252128668D2
D3=D1+1.259695D3-1.287822453D4+0.94064607D5
D2=D6D0
D1=D3D2
RETURN
xEXP
**

ROUTINE1
E1=G7
H=E1
JUMP1,0>I
JUMP2,I=0
JUMP3,I=1
1)JUMPDOWN(R4)
JUMP9
2)JUMPDOWN(R2)
JUMP9
3)JUMPDOWN(R3)
9)F1=B
E3=G8
H=E3
JUMP10,0>I
JUMP11,I=0
JUMP12,I=1
10)JUMPDOWN(R4)
JUMP18
11)JUMPDOWN(R2)
JUMP18
12)JUMPDOWN(R3)
18)F3=B
E2=50
C=F1F3
JUMP30,C>0
```

```
19)E2=0.5E1+0.5E3
H=E2
JUMP20,0>I
JUMP21,I=0
JUMP22,I=1
 20)JUMPDOWN(R4)
JUMP28
21)JUMPDOWN(R2)
JUMP28
22)JUMPDOWN(R3)
28)F2=B
C=E3-E1
C=C/E1
JUMP30,An>C
C=F1F2
JUMP29,0>C
F1=F2
E1=E2
JUMP19
29)F3=F2
E3=E2
JUMP19
30)RETURN
**

ROUTINE2
A=H
B=xSQRT(4AA2)
D0=Y1/B
JUMPDOWN(R770)
B=C2D1-C3
RETURN
**

ROUTINE3
A=H
B=xSQRT(4AA1)
D0=X/B
JUMPDOWN(R770)
C=D1C1
B=xSQRT(4A2A4)
D0=X/B
JUMPDOWN(R770)
D=D1C2
B=D-C-C3
JUMP61,In=0
NEWLINE
PRINT(X)0,4
PRINT(C)0,4
PRINT(D)0,4
PRINT(B)0,4
61)RETURN
**
```

```
ROUTINE4
A=H
A14=A6
JUMPDOWN(R5)
A26=B
JUMP51,A20=0
A14=A5
JUMPDOWN(R5)
51)B=A26-BA20/C2
RETURN
**

ROUTINE5
D0=Y3/A14
JUMPDOWN(R770)
B0=D1
A=H
B1=E4+A
B1=B0B1
B6=Y3+E4
B9=B6/A14
D0=B9
JUMPDOWN(R770)
B7=D1
B2=B6B7
B8=B9B9
B10=xEXP(-B8)
B30=A14/A15
B3=B30B10
B11=Y3-A
B12=B11/A14
D0=B12
JUMPDOWN(R770)
B13=D1
B4=B11B13
B14=B12B12
B15=xEXP(-B14)
B5=B30B15
B=B1-B2+B3+B4-B5
RETURN
**
ROUTINE6
 D=.5E0E0
E=.5E4E4
B=E-D
B16=BB0
Bn=A16+0.5Y3Y3-D
B17=BnB13
Cn=Bn+D-E
B18=CnB7
Cn=Y3+E0
B19=0.5CnB5
C=Y3-E4
B20=0.5CB3
B=B16-B17+B18+B19-B20
RETURN
**
```

```
ROUTINE7
N=R(S)T
E4=AoNA13
G7=Go
G8=G1
I=-1
A20=C1
JUMPDOWN(R1)
Eo=E2
A16=A2A4
A14=A6
JUMPDOWN(R5)
JUMPDOWN(R6)
A19=B
Vn=-A19C2Un
A14=A5
A16=A1A3
JUMPDOWN(R5)
JUMPDOWN(R6)
A19=B
V=A19C1Un
V=Vn+V
C=Eo+E4
D=A12/C
NEWLINE
NEWLINE
PRINT(Eo)o,4
PRINT(E4)o,4
PRINT(C)o,4
PRINT(V)3,5
PRINT(D)o,4
CAPTION
- DOUBLE ERFC
JUMP6o,Y3=Yo
G7=Go
G8=G1
I=-1
A20=o
JUMPDOWN(R1)
Eo=E2
A16=A2A4
H=E4
JUMPDOWN(R6)
A17=B
Vn=-A17C2Un
C=Eo+E4
D=A12/C
NEWLINE
PRINT(Eo)o,4
PRINT(E4)o,4
PRINT(C)o,4
PRINT(Vn)3,5
PRINT(D)o,4
CAPTION
- SINGLE ERFC
6o)REPEAT
RETURN
**
```

```
ROUTINE8
H6=1+H5-E4
H6=0.05H6
K=0(1)20
A=E4+KH6
Do=AW/A5
JUMPDOWN(R770)
X=D1C1
Do=AW/A6
JUMPDOWN(R770)
Y=D1C2
Cn=X+Y+C3
JUMPDOWN(R50)
 C=-X+Y-C3
UK=C/Dn
REPEAT
Vo=0
J=1(1)20
Vo=Vo+0.5UJ+0.5U(J-1)
REPEAT
Vo=H6Vo
Vo=xMOD(Vo)
L=1
70)Xn=0.5H6UL+0.5H6U(L-1)
Xn=xMOD(Xn)
VL=V(L-1)-Xn
L=L+1
JUMP70,20≥L

L=0
71)A=E4+LH6
Do=AW/A5
JUMPDOWN(R770)
X=D1C1
 Do=AW/A6
JUMPDOWN(R770)
Y=D1C2
C=-X+Y-C3
VL=VL/C
JUMP72,Jn>1
NEWLINE
Z=AW
PRINT(Z)0,5
PRINT(VL)0,5
72)L=L+1
JUMP71,20≥L
Hn=0
L=1(1)20
Hn=Hn+0.5VL+0.5V(L-1)
REPEAT
Hn=H6Hn
NEWLINE
NEWLINE
CAPTION
    X              T/WW              T
NEWLINE
```

```
Z=WE4
PRINT(Z)o,4
PRINT(Hn)o,5
V=WWHn
PRINT(V)o,5
RETURN
**

ROUTINE5o
B=Cn/C5
JUMP86,B>E21
J=5
Bn=EJ
82)JUMP84,B=Bn
JUMP83,B>Bn
V=FJ
M=J-1
U=FM
V=U-V
E22=EM
Bn=xMOD(Bn)
E22=xMOD(E22)
C=xLOG(Bn)
D=xLOG(E22)
C=C-D
F=xLOG(B)
F=F-D
C=FV/C
Dn=U-C
JUMP85
83)J=J+1
Bn=EJ
JUMP82
86)Dn=6.2o
JUMP85
84)Dn=FJ
85)RETURN
**

CHAPTERo
A→3o
B→3o
 C→15
D→2o
E→25
F→25
G→15
H→1o
Y→5
U→3o
V→3o
READ(Ao)
READ(A1)
READ(A2)
M=9(1)13
READ(AM)
REPEAT
```

```
M=1(1)5
READ(CM)
REPEAT
READ(Yo)
READ(Y1)
READ(An)
M=0(1)5
READ(GM)
REPEAT
READ(R)
READ(S)
READ(T)
READ(O)
READ(P)
READ(Q)
READ(Kn)
READ(Ln)
M=5(1)21
READ(EM)
REPEAT
M=5(1)21
READ(FM)
REPEAT
A15=xSQRT(£)
D6=2/A15
H1=C1/C2
H2=C3/C2
NEWLINE
NEWLINE
CAPTION
DBLE ERFC PROFILE
NEWLINE
NEWLINE
G7=G4
G8=G5
I=0
JUMPDOWN(R1)
A4=E2
In=0
I=1
X=Yo
JUMPDOWN(R1)
A3=E2
CAPTION
T1=
PRINT(A3)0,5
CAPTION
T2=
PRINT(A4)0,5

D7=xSQRT(£A2A4)
D8=xSQRT(£A1A3)
H=A3
In=1
A5=xSQRT(4A1A3)
A6=xSQRT(4A2A4)
```

```
CAPTION
L(ERFC)1=
PRINT(A5)0,5
CAPTION
L(ERFC)2=
PRINT(A6)0,5
NEWLINE
NEWLINE

CAPTION
       X              ERFC1              ERFC2              TOTAL

NEWLINE
M=Kn-1
N=0(1)M
X=0.1NA13
JUMPDOWN(R3)
REPEAT
M=10M+1
J=10Kn+10
N=M(1)J
X=0.01NA13
JUMPDOWN(R3)
REPEAT
M=Kn+2
J=Ln-1
N=M(1)J
X=0.1NA13
JUMPDOWN(R3)
REPEAT
M=10J+1
J=10Ln+10
N=M(1)J
X=0.01NA13
JUMPDOWN(R3)
REPEAT
M=Ln+2
J=2Ln
N=M(1)J
X=0.1NA13
JUMPDOWN(R3)
REPEAT
NEWLINE
NEWLINE
CAPTION
COLLECTOR JUNCTION
NEWLINE
NEWLINE
CAPTION
   A1                 A2                 D                  VC
CAPTION
            CTC/A
H3=A6/A5
Un=A11/A12
Y3=Y1
JUMPDOWN R
```

```
NEWLINE
NEWLINE
CAPTION
EMITTER JUNCTION
NEWLINE
NEWLINE
CAPTION
   A1              A2              D               VE
CAPTION
          CTE/A

Rn=R
Sn=S
Tn=T
R=O
S=P
T=Q
Y3=Yo
JUMPDOWN(R7)
NEWLINE
NEWLINE
NEWLINE
CAPTION
MIN. CARRIER DENSITY + TRANSIT TIME
NEWLINE
Zn=Y1-Yo
N=5o(1o)1oo
W=o.o1NZn
H4=W/A6
H5=Yo/W
NEWLINE
NEWLINE
CAPTION
W=
PRINT(W)o,4
CAPTION
W/LERFC2=
PRINT(H4)o,4
CAPTION
XE/W=
PRINT(H5)o,4
NEWLINE
NEWLINE
NEWLINE
CAPTION
     X              N/JW/Q
Jn=1(1)1o
E4=o.o1Jn+H5
JUMPDOWN(R8)
REPEAT
Jn=15(5)5o
E4=o.o1Jn+H5
JUMPDOWN(R8)
REPEAT
```

```
      END
      xEXP
      xLOG
      CLOSE

      0.01
      3.4,-13
      3.4,-13
      296
      1.38,-23
      1.6025,-19
      1.06248,-12
       1.0,-4
      1.0,21
      5.0,18
      5.0,15
      9.415,19
      1,15
*     1.5,-4
      4.5,-4
      1.0,-5
      1.0,-12
      2.0,-4
      0.001
      24
      10
     100000
      10
      20
      450
      1
     1
      20
**    15
      45

      1
      2
      4
      6
      8
      10
      20
      40
      60
      80
      100
      200
      400
      600
       1000
      4000
      8000
```

```
28.42
27.66
26.32
25.00
23.84
22.74
19.12
15.48
13.50
12.14
11.22
8.75
7.30
6.96
6.86
6.70
6.40

→
***Z
```

A.5. Program for Double Gaussian

```
TITLE
DOUBLE GAUSSIAN DISTN (EX)-V,T,N/No.

ROUTINE770
AS IN APPENDIX A.4

ROUTINE1
E1=G7
H=E1
1)JUMPDOWN(R3)
3)F1=B
E3=G8
H=E3
4)JUMPDOWN(R3)
6)F3=B
E2=50
C=F1F3
JUMP12,C>0
7)E2=0.5E1+0.5E3
H=E2
8)JUMPDOWN(R3)
10)F2=B
C=E3-E1
C=C/E1
C=xMOD(C)
JUMP12,An>C
C=F1F2
JUMP11,0>C
F1=F2
E1=E2
JUMP7
11)F3=F2
E3=E2
JUMP7
12)RETURN
**

ROUTINE2
NEWLINE
A=xDIVIDE(XX,A5A5)
A=xEXP(-A)
A=AC1
B=xDIVIDE(XX,A6A6)
B=xEXP(-B)
B=BC2
C=-A+B-C3
PRINT(X)0,4
PRINT(A)0,4
PRINT(B)0,4
PRINT(C)0,4
RETURN
**
```

```
ROUTINE3
B3=Y3-H
Do=B3/A6
JUMPDOWN(R770)
Bo=D1
B4=Y3+E4
Do=B4/A6
JUMPDOWN(R770)
B1=D1
B2=Bo-B1
D9=B2D7
B=D9-HH2-H2E4
JUMP30,In=1
Do=B3/A5
JUMPDOWN(R770)
Bo=D1
Do=B4/A5
JUMPDOWN(R770)
B1=D1
B2=Bo-B1
D10=B2D8
B=B-D10H1
30)RETURN
**

ROUTINE4
JUMP33,In=1
B=D8Y3B2
C=xEXP(-B3B3/B5)
D=xEXP(-B4B4/B5)
C=C-D
B=BH1-2CA1A3H1
33)Do=B3/A6
JUMPDOWN(R770)
Bo=D1
Do=B4/A6
JUMPDOWN(R770)
B1=D1
C=D7Y3Bo-D7Y3B1
D=xEXP(-B3B3/B6)
E=xEXP(-B4B4/B6)
D=D-E
D=C-2DA2A4
C=o.5EoEoH2-o.5E4E4H2
D=D-C
JUMP34,In=1
D=D-B
34)Vn=-DC2Un
RETURN
**
```

```
ROUTINE5
N=R(S)T
In=o
E4=NAoA13
JUMPDOWN(R1)
Eo=E2
JUMPDOWN(R4)
NEWLINE
PRINT(Eo)o,4
PRINT(E4)o,4
A=Eo+E4
PRINT(A)o,4
PRINT(Vn)3,6
A=A12/A
PRINT(A)o,4
JUMP31,Y3=Yo
CAPTION
- DOUBLE GAUSSIAN
In=1
JUMPDOWN(R1)
Eo=E2
JUMPDOWN(R4)
NEWLINE
PRINT(Eo)o,4
PRINT(E4)o,4
A=Eo+E4
 PRINT(A)o,4
PRINT(Vn)3,6
A=A12/A
PRINT(A)o,4
CAPTION
- SINGLE GAUSSIAN
NEWLINE
31)Gn=o.75Y1-o.75Yo
JUMP32,Eo>Gn
REPEAT
32)RETURN
**

ROUTINE6
 H6=1+H5-E4
 H6=o.o5H6
 K=o(1)20
 A=E4+KH6
 X=xEXP(-AAWW/B5)
 Y=xEXP(-AAWW/B6)
 Cn=XC1+YC2+C3
 JUMPDOWN(R5o)
 C=-XC1+YC2-C3
 UK=C/Dn
 REPEAT
 Vo=o
 J=1(1)20
 Vo=Vo+o.5UJ+o.5U(J-1)
 REPEAT
 Vo=H6Vo
 Vo=xMOD(Vo)
```

```
L=1
70)Xn=0.5H6UL+0.5H6U(L-1)
Xn=xMOD(Xn)
VL=V(L-1)-Xn
L=L+1
JUMP70,20≥L
L=0
71)A=E4+LH6
X=xEXP(-AAWW/B5)
Y=xEXP(-AAWW/B6)
C=-XC1+YC2-C3
VL=VL/C
JUMP72,Jn>1
NEWLINE
Z=AW
PRINT(Z)0,5
PRINT(VL)0,5
72)L=L+1
JUMP71,20≥L
Hn=0
L=1(1)20
Hn=Hn+0.5VL+0.5V(L-1)
REPEAT
Hn=H6Hn
NEWLINE
NEWLINE
CAPTION
    X              T/WW              T
NEWLINE
 Z=WE4
PRINT(Z)0,4
PRINT(Hn)0,5
V=WWHn
PRINT(V)0,5
RETURN
**

ROUTINE50
AS IN APPENDIX A4

CHAPTER0
FIRST 40 STATEMENTS AS IN APPENDIX A.4

A15=xSQRT(£)
D6=2/A15
H1=C1/C2
H2=C3/C2
NEWLINE
CAPTION
DOUBLE GAUSSIAN DISTN
NEWLINE
NEWLINE
```

```
A=xLOG.H2.
A4=xDIVIDE(-Y1Y1,4AA2)
A=xDIVIDE(YoYo,4A2A4)
A=xEXP(-A)
A=AC2/C1-C3/C1
B=xMOD(A)
B=xLOG(B)
A3=xDIVIDE(-YoYo,4BA1)
NEWLINE
CAPTION
T1=
PRINT(A3)o,5
CAPTION
T2=
PRINT(A4)o,5
A5=xSQRT(4A1A3)
A6=xSQRT(4A2A4)
B5=4A1A3
B6=4A2A4
CAPTION
LG1=
PRINT(A5)o,5
CAPTION
LG2=
PRINT(A6)o,5
NEWLINE
NEWLINE
CAPTION
      X              G1              G2              TOTAL
M=Kn-1
N=o(1)M
X=o.1NA13
JUMPDOWN(R2)
REPEAT
M=10M+1
J=10Kn+10
N=M(1)J
X=o.o1NA13
JUMPDOWN(R2)
REPEAT
M=Kn+2
J=Ln-1
N=M(1)J
X=o.1NA13
JUMPDOWN(R2)
REPEAT
M=10J+1
J=10Ln+10
N=M(1)J
X=o.o1NA13
JUMPDOWN(R2)
REPEAT
M=Ln+2
J=2Ln
N=M(1)J
X=o.1NA13
JUMPDOWN(R2)
REPEAT
NEWLINE
```

```
CAPTION
COLLECTOR JUNCTION
NEWLINE
NEWLINE
CAPTION
   A1              A2              D               VC
CAPTION
            CTC/A
NEWLINE
H3=A6/A5
Un=A11/A12
D7=xSQRT(£A2A4)
D8=xSQRT(£A1A3)
Y3=Y1
G7=G0
G8=G1
JUMPDOWN(R5)
NEWLINE
NEWLINE
NEWLINE
CAPTION
EMITTER JUNCTION
NEWLINE
NEWLINE
CAPTION
   A1              A2              D               VE
CAPTION
            CTE/A
NEWLINE
Y3=Y0
Rn=R
Sn=S
Tn=T
R=0
S=P
T=Q
JUMPDOWN(R5)

NEWLINE
NEWLINE
NEWLINE
CAPTION
CARRIER DENSITY + TRANSIT TIME
NEWLINE
Zn=Y1-Y0
N=50(10)100
W=0.01NZn
NEWLINE
NEWLINE
CAPTION
W=
PRINT(W)0,4
```

```
CAPTION
W/LG2=
H4=W/A6
PRINT(H4)2,5
H5=Yo/W
NEWLINE
NEWLINE
CAPTION
     X                N/JW/Q
Jn=1(1)10
E4=H5+0.01Jn
JUMPDOWN(R6)
REPEAT
Jn=15(5)50
E4=H5+0.01Jn
 JUMPDOWN(R6)
REPEAT
REPEAT

END
xEXP
xLOG
CLOSE

0.01
3.4,-13**
*3.4,-13
296
1.38,-23
1.6025,-19
1.0625,-12
1.0,-4
1.0,21
5.0,18
5.0,15
9.415,19
1,15
1.5,-4
4.5,-4
1.0,-4
1.0,-11
2.0,-4
0.001
25
10
20
450
1
1
20
15
45
REST OF DATA AS IN APPENDIX A.4
```

*

A.5 Double Exponential for Double ERFC

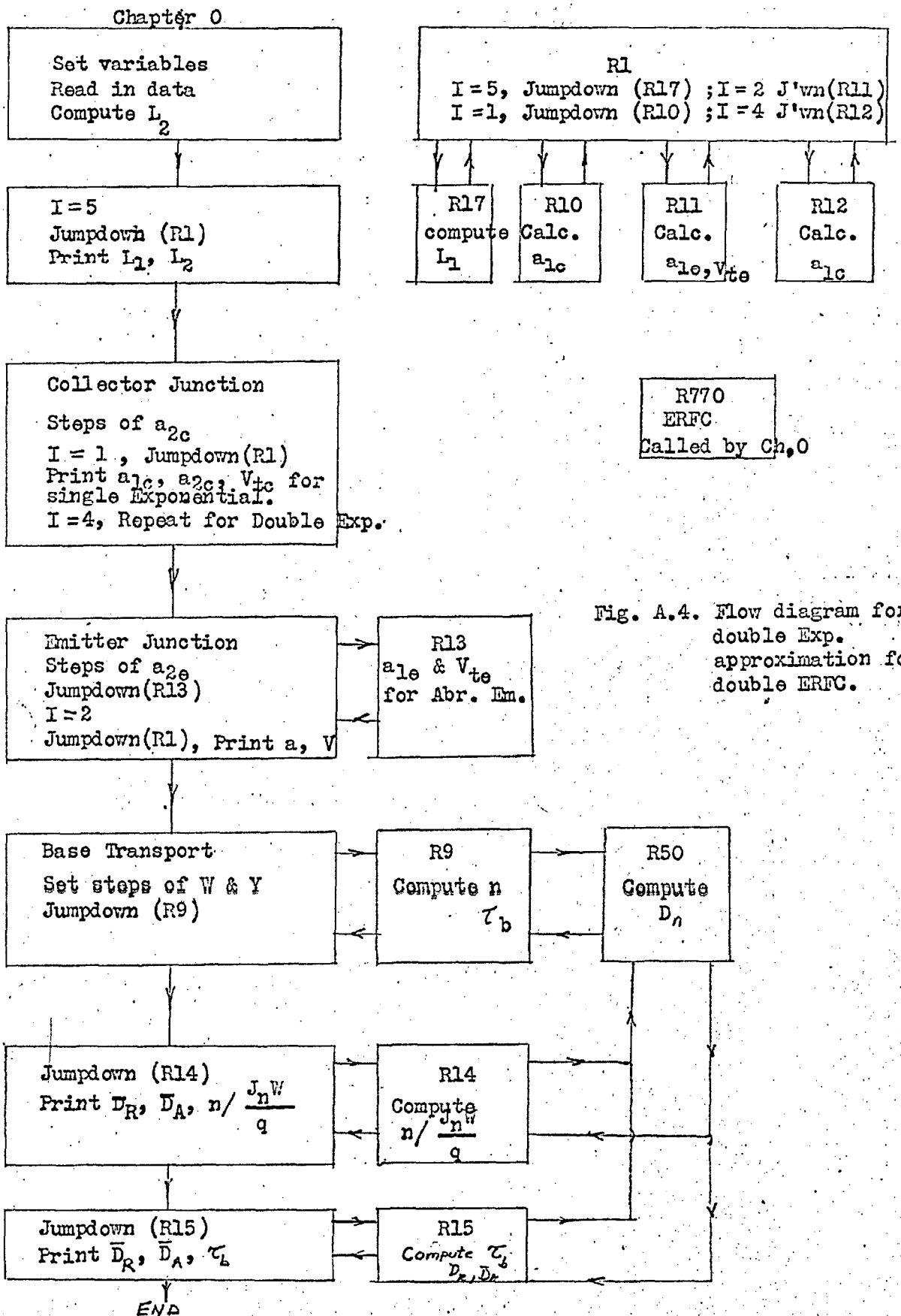


Fig. A.4. Flow diagram for double Exp. approximation for double ERFC.

```
TITLE
DBLE EXP FOR DBLE ERFC - AREAS

ROUTINE770
AS IN APPENDIX A.4

ROUTINE1
E1=G7
H=E1
JUMP2,I=1
JUMP13,I=2
JUMP4,I=4
JUMP27,I=5
2)JUMPDOWN(R10)
JUMP3
13)JUMPDOWN(R11)
JUMP3
4)JUMPDOWN(R12)
JUMP3
27)JUMPDOWN(R17)
3)F1=B
E3=G8
H=E3
JUMP5,I=1
JUMP15,I=2
JUMP8,I=4
JUMP28,I=5
5)JUMPDOWN(R10)
JUMP6
15)JUMPDOWN(R11)
JUMP6
8)JUMPDOWN(R12)
JUMP6
28)JUMPDOWN(R17)
6)F3=B
E2=50
C=F1F3
JUMP12,C>0
7)E2=0.5E1+0.5E3
H=E2
JUMP9,I=1
JUMP17,I=2
JUMP19,I=4
JUMP29,I=5
9)JUMPDOWN(R10)
JUMP10
17)JUMPDOWN(R11)
JUMP10
19)JUMPDOWN(R12)
JUMP10
29)JUMPDOWN(R17)
10)F2=B
C=E3-E1
C=C/E1
```

```
C=xMOD(C)
JUMP12,An>C
C=F1F2
JUMP11,o>C
F1=F2
E1=E2
JUMP7
11)F3=F2
E3=E2
JUMP7
12)RETURN
**

ROUTINE10
A=H
B=xEXP(A)
B=B-1
B=A/B
E=xEXP(-A25)
B=E-B
RETURN
**

ROUTINE11
B=xEXP(H/A8)
C=xEXP(-E4/A8)
B=CA8-BA8
D=xEXP(H/A7)
E=xEXP(-E4/A7)
B=B-EA7+DA7+HH8+E4H8
RETURN
**

ROUTINE12
B=xEXP(H/A8)
C=xEXP(-A25)
B=B-C
D=xEXP(-Zn/A8)
B=BDA8
C=xEXP(-E4/A7)
A=xEXP(H/A7)
C=A-C
D=xEXP(-Zn/A7)
C=CDA7
B=B-C-HH8-E4H8
RETURN
**
```

```
ROUTINE14
E=xEXP(-Ho)
F=xEXP(-HoB25)
G=FA7/W-E/Ho-H8
En=xEXP(-HoB25E4)
Fn=xEXP(-HoE4)
Gn=EnA7/W-Fn/Ho-H8E4
Hn=Fn-En-H8
Wn=xEXP(-YnHo)
Xn=xEXP(-YnHoB25)

Cn=A8-A8Wn+A7-A7Xn+WH8Yn
Cn=xDIVIDE(CnCo,WYn)
Cn=xMOD(Cn)
JUMPDOWN(R50)
D11=Dn
Cn=A8Wn-EA8+A7Xn-FA7+WH8-WH8Yn
Cn=xDIVIDE(CnCo,W-WYn)
Cn=xMOD(Cn)
JUMPDOWN(R50)
D12=Dn
D13=D11/D12

JUMP55,E4>Yn
A=XnA7/W-Wn/Ho-H8Yn
A=A-AD13+GD13-Gn
A=xDIVIDE(A,D11Hn)
JUMP56
55)X=D13G/Hn-D13Gn/Hn
X=X/D11
56)RETURN
**

ROUTINE15
E=xEXP(-Ho)
F=xEXP(-HoB25)
G=FA7/W-E/Ho-H8
Wn=xEXP(-YnHo)
Xn=xEXP(-YnHoB25)

Cn=A8-A8Wn+A7-A7Xn+WH8Yn
Cn=xDIVIDE(CnCo,WYn)
Cn=xMOD(Cn)
JUMPDOWN(R50)
D11=Dn
Cn=A8Wn-EA8+A7Xn-FA7+WH8-WH8Yn
Cn=xDIVIDE(CnCo,W-WYn)
Cn=xMOD(Cn)
JUMPDOWN(R50)
D12=Dn
D13=D11/D12
```

```
  Y5=E4
JUMP57,E4>Yn
Dn=XnA7/W-Wn/Ho-H8Yn
M=1(1)15
D=0.5XMYn-0.5XME4+0.5Yn+0.5E4
B=xEXP(-HoB25D)
C=xEXP(-DHo)
En=C-B-H8
Fn=BA7/W-C/Ho-DH8
B=Dn-DnD13+GD13-Fn
B=B/En
C=0.5Yn-0.5E4
ZM=BCWM
REPEAT
M=2(1)15
ZM=ZM+Z(M-1)
REPEAT
D14=ZM
Y5=Yn
57)M=1(1)15
D=0.5XM-0.5XMY5+0.5+0.5Y5
B=xEXP(-DHoB25)
C=xEXP(-DHo)
En=C-B-H8
Fn=G-BA7/W+C/Ho+DH8
B=Fn/En
C=0.5-0.5Y5
ZM=BCWM
REPEAT
M=2(1)15
ZM=ZM+Z(M-1)
REPEAT
D15=ZMD13
JUMP58,E4>Yn
 D15=D15+D14
58)RETURN
**

ROUTINE50
AS IN APPENDIX A.4

ROUTINE9
H6=0.05-0.05E4
K=0(1)20
A=E4+KH6
X=xEXP(-AHo)
Y=xEXP(-AHoB25)
Cn=XCo+YCo+C3
Cn=xMOD(Cn)
JUMPDOWN(R50)
C=XCo-YCo-C3
UK=C/Dn
REPEAT
```

```
Vo=o
J=1(1)2o
Vo=Vo+o.5UJ+o.5U(J-1)
REPEAT
Vo=H6Vo
Vo=xMOD(Vo)
L=1
7o)Xn=o.5H6UL+o.5H6U(L-1)
Xn=xMOD(Xn)
VL=V(L-1)-Xn
L=L+1
JUMP7o,2o≥L

L=o
71)A=E4+LH6
X=xEXP(-AHo)
Y=xEXP(-AHoB25)
C=XCo-YCo-C3
VL=VL/C
JUMP72,Jn>1
NEWLINE
PRINT(A)o,5
PRINT(VL)o,5
72)L=L+1
JUMP71,2o≥L
Hn=o
L=1(1)2o
Hn=Hn+o.5VL+o.5V(L-1)
REPEAT
Hn=H6Hn
NEWLINE
NEWLINE
CAPTION
   X              T/WW                T
NEWLINE
PRINT(E4)o,4
PRINT(Hn)o,5
V=WWHn
PRINT(V)o,5
RETURN
**

ROUTINE13
A=H
B=xEXP(-A/A8)
C=xEXP(-A/A7)
D=BA8-CA7-A8+A7+AH8
Eo=DCo/G6
D=o.5EoEoG6/Co
E=-BA8A8+A8A8+CA7A7-A7A7-ABA8+ACA7-o.5AAH8
D=DCoUn
E=ECoUn
Vn=D+E
```

```
B=B-C-H8
B=BCoG6/C4
C=xMOD(B)
C=xLOG(C)
V=CA9A10/A11
B=V-Vn
RETURN
**

ROUTINE16
B=xEXP(Eo/A8)
C=xEXP(Eo/A7)
D=xDIVIDE(CEoA7,A8A8)
E=B25B25
F=xDIVIDE(o.5H8EoEo,A8A8)
B=BEo/A8+1-B-D-1/E+C/E-F
V=-BCoA8A8Un
C=xEXP(-E4/A8)
D=xEXP(-E4/A7)
F=xDIVIDE(o.5H8E4E4,A8A8)
G=xDIVIDE(DE4,B25A8)
C=C+CE4/A8-D/E-G-1+1/E+F
Vn=-CCoA8A8Un
Vo=V+Vn
RETURN
**

ROUTINE17
B=xEXP(-Zn/H)
B=HCo-BHCo
B=B-B20
RETURN
**

CHAPTERo
A→30
B→30
C→15
D→20
E→25
F→25
G→10
H→10
Y→5
W→15
X→15
Z→15
U→30
V→30
M=1(1)15
READ(WM)
REPEAT
M=1(1)15
READ(XM)
REPEAT
```

```
M=0(1)6
READ(AM)
REPEAT
M=9(1)13
READ(AM)
REPEAT
M=1(1)5
READ(CM)
REPEAT
READ(Yo)
READ(Y1)
READ(An)
M=0(1)3
READ(GM)
REPEAT
READ(R)
READ(S)
READ(T)
READ(O)
READ(P)
READ(Q)
M=5(1)21
READ(EM)
REPEAT
M=5(1)21
READ(FM)
REPEAT

A15=xSQRT(£)
D6=2/A15
H1=C1/C2
H2=C3/C2
Un=A11/A12
D7=xSQRT(£A2A4)
D8=xSQRT(£A1A3)
NEWLINE
A=xDIVIDE(Y1Y1,A6A6)
A=xEXP(A)
A8=AH2D7
Zn=Y1-Yo
B=xEXP(Zn/A8)
Co=BC3
H8=C3/Co
A8=xMOD(A8)
CAPTION
No=
PRINT(Co)0,4
CAPTION
L2=
PRINT(A8)0,4
```

FOR DOUBLE GAUSSIAN

```
A8=2AH2A2A4/Y1
A8=xMOD(A8)
Zn=Y1-Yo
B=xEXP(Zn/A8)
Co=BC3
H8=C3/Co
Do=Yo/A5
JUMPDOWN(R770)
A=D1
Do=Y1/A5
JUMPDOWN(R770)
B=D1
```

```
A=xDIVIDE(YoYo,A6A6)
A=xEXP(-A)
B=xDIVIDE(YoYo,A5A5)
B=xEXP(-B)
C=xDIVIDE(Y1Y1,A6A6)
C=xEXP(-C)
D=xDIVIDE(Y1Y1,A5A5)
D=xEXP(-D)
A=C-A
B=D-B
A=AA6/A15
B=BA5/A15
Do=Y1/A5
JUMPDOWN(R770)
C=Y1D1
Do=Yo/A5
JUMPDOWN(R770)
B=C-YoD1-B
Do=Y1/A6
JUMPDOWN(R770)
C=Y1D1
Do=Yo/A6
JUMPDOWN(R770)
A=C-YoD1-A
A=BC1-AC2
B=xEXP(-Zn/A8)
B20=CoA8-BCoA8+A
G7=0.01A8
G8=A8
 I=5
JUMPDOWN(R1)
A7=xMOD(E2)
CAPTION
L1=
PRINT(A7)0,4
B=D7H1/D8
B=xLOG(B)
C=xDIVIDE(1,4A1A3)
D=xDIVIDE(1,4A2A4)
C=C-D
B=B/C
C7=xSQRT(B)
CAPTION
XM(ERFC)=
PRINT(C7)0,4
B25=A8/A7
B=xLOG(B25)
C7=xDIVIDE(BA8,B25-1)
Yn=C7/Zn
CAPTION
YM(E)=
PRINT(Yn)3,4
```

For Double Gaussian use Statements below.

```
A=AC1D8-BC1D8
Do=Yo/A6
JUMPDOWN(R770)
B=D1
Do=Y1/A6
JUMPDOWN(R770)
B=BC2D7-D1C2D7
A=A-B
B=xEXP(-Zn/A8)
B20=CoA8-BCoA8+A
G7=0.01A8
G8=A8
I=5
JUMPDOWN(R1)
A7=E2
A7=xMOD(A7)
CAPTION
No=
PRINT(Co)0,4
CAPTION
L2=
PRINT(A8)0,4
CAPTION
L1=
PRINT(A7)0,4
B25=A8/A7
B=xDIVIDE(A2A4C1,A1A3C2)
B=xLOG(B)
C=xDIVIDE(1,4A1A3)
D=xDIVIDE(1,4A2A4)
C=C-D
B=B/C
C7=xSQRT(B)
CAPTION
XM(G)=
PRINT(C7)0,4
B=xLOG(B25)
C7=xDIVIDE(BA8,B25-1)
Yn=C7/Zn
```

```
C7=C7+Yo
CAPTION
XM(E)=
PRINT(C7)o,4
NEWLINE
NEWLINE
CAPTION
     X              N(X)
N=o(5)100
 X=o.o1NZn
A=xEXP(-X/A8)
B=xEXP(-X/A7)
A=ACo-BCo-C3
X=X+Yo
NEWLINE
PRINT(X)o,5
PRINT(A)o,5
REPEAT
NEWLINE

NEWLINE
CAPTION
COLLECTOR JUNCTION
NEWLINE
CAPTION
   A1           A2           D/L2          D              CTC/A
CAPTION
        VC
N=R(S)T
G7=G2
G8=G3
E4=NAoA13
A25=E4/A8
I=1
JUMPDOWN(R1)
A24=E2
JUMP41,A24=5o
D=xEXP(o.5A24)
E=xEXP(-o.5A24)
D=xDIVIDE(D+E,D-E)
D=o.5A24A24D-A24
Vn=DA8A8C3Un
Eo=A24A8-E4
NEWLINE
PRINT(Eo)o,4
PRINT(E4)o,4
PRINT(A24)2,3
D=A8A24
PRINT(D)o,4
D=A12/D
PRINT(D)o,4
PRINT(Vn)3,6
CAPTION
-SINGLE EXP
```

```
41)G7=Go
G8=G1
I=4
JUMPDOWN(R1)
Eo=E2
JUMP42,Eo=5o
 A24=Eo/A8+A25
B=xEXP(-A24)
C=BA24-BEo/A8+B+Eo/A8-1
D=xEXP(-A24A8/A7)
E=DA24B25-DEo/A7+D+Eo/A7-1
W=Zn-Eo
B=xEXP(-W/A8)
B=BC
D=xEXP(-W/A7)
C=A7/A8
D=CCDE
C=A24-2Eo/A8
B=B-D+0.5CH8A24
Vn=CoA8A8BUn
NEWLINE
PRINT(Eo)o,4
PRINT(E4)o,4
PRINT(A24)2,3
D=A8A24
PRINT(D)o,4
D=A12/D
PRINT(D)o,4
PRINT(Vn)3,6
CAPTION
- DOUBLE EXP
NEWLINE
REPEAT
```

Double Gaussian
Replaces from 42) to
First NEWLINE on next page

```
42)Do=Yo/A5
JUMPDOWN(R770)
D=1-D1
B=DD8H1
Do=Yo/A6
JUMPDOWN(R770)
C=1-D1
C=CD7
B=-B+C-H2Yo
G6=BC2/Yo
CAPTION
NE=
PRINT(G6)o,5
A=xDIVIDE(-YoYo,4A1A3)
A=xEXP(A)
A=xDIVIDE(AC1Yo,2A1A3)
B=xDIVIDE(YoYo,4A2A4)
B=xEXP(-B)
B=xDIVIDE(BC2Yo,2A2A4)
A=A-B
CAPTION
SG=
PRINT(A)o,4
CAPTION
S2=
B=CoB25/A8-Co/A8
PRINT(B)o,4
```

```
A=xDIVIDE(YoYo,A5A5)
A=xEXP(-A)
A=AC1/D8
B=xDIVIDE(YoYo,A6A6)
B=xEXP(-B)
B=A-BC2/D7
CAPTION
SERFC=
PRINT(B)o,4
A=CoB25/A8-Co/A8
CAPTION
S2=
PRINT(A)o,4

NEWLINE
NEWLINE
CAPTION
EMITTER JCTN
NEWLINE
CAPTION
   A1                A2              V1          V2          VE*
CAPTION
          CE/A          C1/A
N=O(P)Q
E4=NAoA13
H=E4
JUMPDOWN(R13)
NEWLINE
NEWLINE
PRINT(Eo)o,4
PRINT(E4)o,4
PRINT(D)2,5
PRINT(E)2,5
PRINT(Vn)2,5
D=*Eo+E4
D=A12/D
PRINT(D)o,4
D=A12/E4
PRINT(D)o,4
CAPTION
- ABR EMITTER

NEWLINE
I=2
JUMPDOWN(R1)
Eo=xMOD(E2)
JUMP44,Eo=5o
JUMPDOWN(R16)
PRINT(Eo)o,4
PRINT(E4)o,4
PRINT(V)2,5
PRINT(Vn)2,5
PRINT(Vo)2,5
```

```
E=Eo+E4
E=A12/E
PRINT(E)o,4
E=A12/E4
PRINT(E)o,4
CAPTION
-DBL. EXP EM.
REPEAT

44)NEWLINE
NEWLINE
CAPTION
MINORITY CARRIER DENSITY + TRANSIT TIME - D(N)
N=50(10)100
W=0.01NZn
NEWLINE
NEWLINE
CAPTION
W=
PRINT(W)o,4
Ho=W/A8
CAPTION
M2=
PRINT(Ho)2,4
NEWLINE
NEWLINE
CAPTION
     X              N/JW/Q
Jn=1(1)10
E4=0.01Jn
JUMPDOWN(R9)
REPEAT
*Jn=15(5)50
E4=0.01Jn
JUMPDOWN(R9)
REPEAT
REPEAT

NEWLINE
NEWLINE
CAPTION
DR AND DA APPROXIMATION
NEWLINE
NEWLINE
CAPTION
MINORITY CARRIER DENSITY
NEWLINE
N=50(10)100
W=0.01NZn
Ho=W/A8
NEWLINE
CAPTION
W=
PRINT(W)o,5
CAPTION
M2=
PRINT(Ho)2,4
Yn=C7/W-Yo/W
```

```
        CAPTION
        Yn=
        PRINT(Yn)0,4
        NEWLINE
        NEWLINE
        CAPTION
             DR          DA          X/W          N/JW/Q
        Jn=1(1)10
        E4=0.01Jn
        JUMPDOWN(R14)
        NEWLINE
        PRINT(D11)3,3
        PRINT(D12)3,3
        PRINT(E4)3,3
        JUMP22,E4>Yn
        PRINT(A)0,4
        JUMP23
        22)PRINT(X)0,4
        23)REPEAT
        Jn=15(5)100
        E4=0.01Jn
        JUMPDOWN(R14)
        NEWLINE
        PRINT(D11)3,3
        PRINT(D12)3,3
        PRINT(E4)3,3
        JUMP24,E4>Yn
        PRINT(A)0,4
        JUMP25
        24)PRINT(X)0,4
        25)REPEAT
        REPEAT

        NEWLINE
        NEWLINE
        CAPTION
        TRANSIT TIME
        NEWLINE
        NEWLINE
        N=50(10)100
        W=0.01NZn
        Ho=W/A8
        Yn=C7/W-Yo/W
        ***NEWLINE
        NEWLINE
        CAPTION
        W=
**      PRINT(W)0,4
        CAPTION
        M2=
        PRINT(Ho)0,4
```

```
CAPTION
Yn=
PRINT(Yn)0,5
NEWLINE
NEWLINE
CAPTION
    DR        DA              X/W             T/WW/DR             T
Jn=1(1)10
E4=0.01Jn
JUMPDOWN(R15)
NEWLINE
PRINT(D11)3,3
PRINT(D12)3,3
PRINT(E4)3,3
PRINT(D15)0,5
A=WWD15/D11
PRINT(A)0,5
REPEAT
Jn=15(5)50
E4=0.01Jn
JUMPDOWN(R15)
NEWLINE
PRINT(D11)3,3
PRINT(D12)3,3
PRINT(E4)3,3
PRINT(D15)0,5
A=WWD15/D11
PRINT(A)0,5
REPEAT
REPEAT
END
xEXP
xLOG
CLOSE

.03075324200
.07036604749
.10715922047
.13957067793
.16626920582
.18616100002
.19843148533
.20257824193
.19843148533
.18616100002
.16626920582
.13957067793
.10715922047
.07036604749
.03075324200
```

```
-.98799251802
-.93727339240
-.84820658341
-.72441773136
-.57097217261
-.39415134708
-.20119409400
0.00000000000
.20119409400
.39415134708
.57097217261
.72441773136
.84820658341
.93727339240
.98799251802

0.01
3.4,-13
3.4,-13
3.22453,3
2.75027,4
6.62220,-5
1.93400,-4
296
1.38,-23
1.6025,-19
1.0625,-12
1.0,-4
1.0,21
5.0,18
5.0,15
9.415,19
1,15
1.5,-4
4.5,-4
 1.0,-5
1.0,-11
3.0,-4
0.001
30
10
20
450
1
1
20
```

REST OF DATA AS IN APPENDIX A.4

A.7 DETAILED EQUATIONS FOR INPUT AND OUTPUT ADMITTANCE

The detailed equations based on the circuits of Fig. 4.3 are as follows:

Case A: Common Base input admittance

$$R_{ib} = \frac{\frac{1}{r'_{bb}} + \theta_3}{\left(\frac{1}{r'_{bb}} + \theta_3\right)^2 + \theta_4^2} + \frac{\left(\frac{1}{r'_{bb}} + \theta_3\right)^2 + \theta_4^2}{\frac{1}{r'_{bb}} + \theta_3} \cdot \left[\frac{1}{\omega C_{te}} + \frac{\theta_4}{\left(\frac{1}{r'_{bb}} + \theta_3\right) + \theta_4}\right]^2 \qquad \text{A.7.1}$$

where $$\theta_3 = \frac{r'_{cc} + \theta_5}{(r'_{cc} + \theta_5)^2 + (\omega C_{tc_1} r_c \theta_5)^2}$$

$$\theta_4 = \frac{\omega C_{tc_1} r_c \theta_5}{(r'_{cc} + \theta_5)^2 + (\omega C_{tc_1} r_c \theta_5)^2}$$

$$\theta_5 = \frac{r_c}{1 + \omega^2 C_{tc_1}^2 r_c^2}$$

$$C_{ib} = C_{seb} + C_{sec} + \frac{\frac{1}{\omega^2 C_{te}} + \frac{C_{tc_1}}{\theta_6^2 + \omega^2 C_{tc_1}^2}}{\left[\frac{\theta_6}{\theta_6^2 + \omega^2 C_{tc_1}^2}\right]^2 + \left[\frac{1}{\omega C_{te}} + \frac{\omega C_{tc_1}}{\theta_6^2 + \omega^2 C_{tc_1}^2}\right]^2} \qquad \text{A.7.2}$$

where $$\theta_6 = \frac{1}{r'_{bb}} + \frac{1}{r_c} + \omega^2 C_{tc_1}^2 r'_{cc}$$

Case B: Common emitter input admittance

$$R_{ie} = r'_{bb} + \frac{\theta_3}{\theta_3^2 + (\omega C_{te} + \theta_4)^2} + \frac{\left[\frac{\omega C_{te} + \theta_4 \quad \ldots\ldots}{\theta_3^2 + (\omega C_{te} + \theta_4)^2}\right]^2}{r'_{bb} + \frac{\theta_3}{\theta_3^2 + (\omega C_{te} + \theta_4)^2}} \qquad \text{A.7.3}$$

$$C_{ie} = C_{tc} + C_{seb} + C_{sec} + \frac{\frac{C_{te} + \theta_4/\omega}{\theta_3^2 + (\omega C_{te} + \theta_4)}}{\left\{r'_{bb} + \frac{\theta_3}{\theta_3^2 + (\omega C_{te} + \theta_4)^2}\right\}^2 + \left\{\frac{\omega C_{te} + \theta_4}{\theta_3^2 + (\omega C_{te} + \theta_4)}\right\}^2} \qquad \text{A.7.4}$$

Case C: Common base output admittance

$$R_{ob} = \theta_7 + \theta_8^2 / \theta_7 \qquad \text{A.7.5}$$

$$C_{ob} = C_{tc_2} + C_{scb} + C_{sec} + \frac{\theta_4 / \omega}{\theta_3^2 + \theta_4^2} \qquad \text{A.7.6}$$

where $\theta_7 = r'_{cc} + \theta_5 + \dfrac{r'_{bb}}{1 + (\omega C_{te}\, r'_{bb})^2}$

$$\theta_8 = \omega C_{tc_1}\, r_c\, \theta_5 + \frac{\omega C_{te}\, r'^2_{bb}}{1 + (\omega C_{te}\, r'_{bb})^2}$$

A.8 EVALUATION OF INTEGRAL IN TRANSIT TIME EXPRESSION

The integral term in eqn. 4.4.4 can be represented in general form as:

$$-\int_c^d \frac{e^{aY}}{1 - e^{-bY}}\, dY$$

where $a = \gamma m_2$ and $b = (\gamma - 1)m_2$. The upper limit d is either y_m or 1, while the lower limit c is either Y_1 or Y_m.

The above integral may be evaluated by effecting a change of variable:

Let $Z = e^{bY}$, therefore $dZ = bZ\, dY$ giving $dY = \frac{1}{b}\frac{dZ}{Z}$; $e^{aY} = Z^{a/b}$

The integral becomes:

$$\frac{1}{b}\int_{Z_c}^{Z_d} \frac{Z^{\frac{a}{b} - 1}}{Z - 1}\, dZ$$

This integral may be evaluated when γ is 2 or 3. When $\gamma = 2$: $a = 2m_2$ and $b = m_2$.

The integral is now:

$$\frac{1}{m_2}\int_{Z_c}^{Z_d} \frac{Z}{Z - 1}\, dZ = \frac{1}{m_2}\int_{Z_c}^{Z_d} \left(1 + \frac{1}{Z - 1}\right) dZ$$

$$= \frac{1}{m_2}\left[(Z_d - Z_c) + \ln\left|\frac{Z_d - 1}{Z_c - 1}\right|\right]$$

Substituting $Z_d = e^{m_2 d}$ and $Z_c = e^{m_2 c}$, the solution is:

$$\frac{1}{m_2}\left[(e^{m_2 d} - e^{m_2 c}) + \ln\left|\frac{e^{m_2 d} - 1}{e^{m_2 c} - 1}\right|\right] \quad . \qquad (A)$$

When $\gamma = 3$: $a = 3m_2$, $b = m_2$, $Z_d = e^{2m_2 d}$, $Z_c = e^{2m_2 c}$.

For this case the integral reads:

$$\frac{1}{2m_2} \int_{Z_c}^{Z_d} \frac{\sqrt{Z}}{Z - 1} \, dZ$$

This integral may be evaluated to give

$$\frac{1}{2m_2} \left[2 \left(\sqrt{Z_d} - \sqrt{Z_c}\right) - \ln \left| \frac{\sqrt{Z_d} + 1}{\sqrt{Z_d} - 1} \right| + \ln \left| \frac{\sqrt{Z_c} + 1}{\sqrt{Z_c} - 1} \right| \right]$$

Combining the two ln terms and substituting the values of Z_c and Z_d gives:

$$\frac{1}{2m_2} \left[2\left(e^{m_2 d} - e^{m_2 c}\right) + \ln \left| \frac{(e^{m_2 d} - 1)(e^{m_2 c} + 1)}{(e^{m_2 d} + 1)(e^{m_2 c} - 1)} \right| \right] \qquad \text{(B)}$$

When either solution (A) or (B) is required in the determination of base transit time, the appropriate values of c and d must be substituted.

A.9 Program to Determine Double Exponential Model

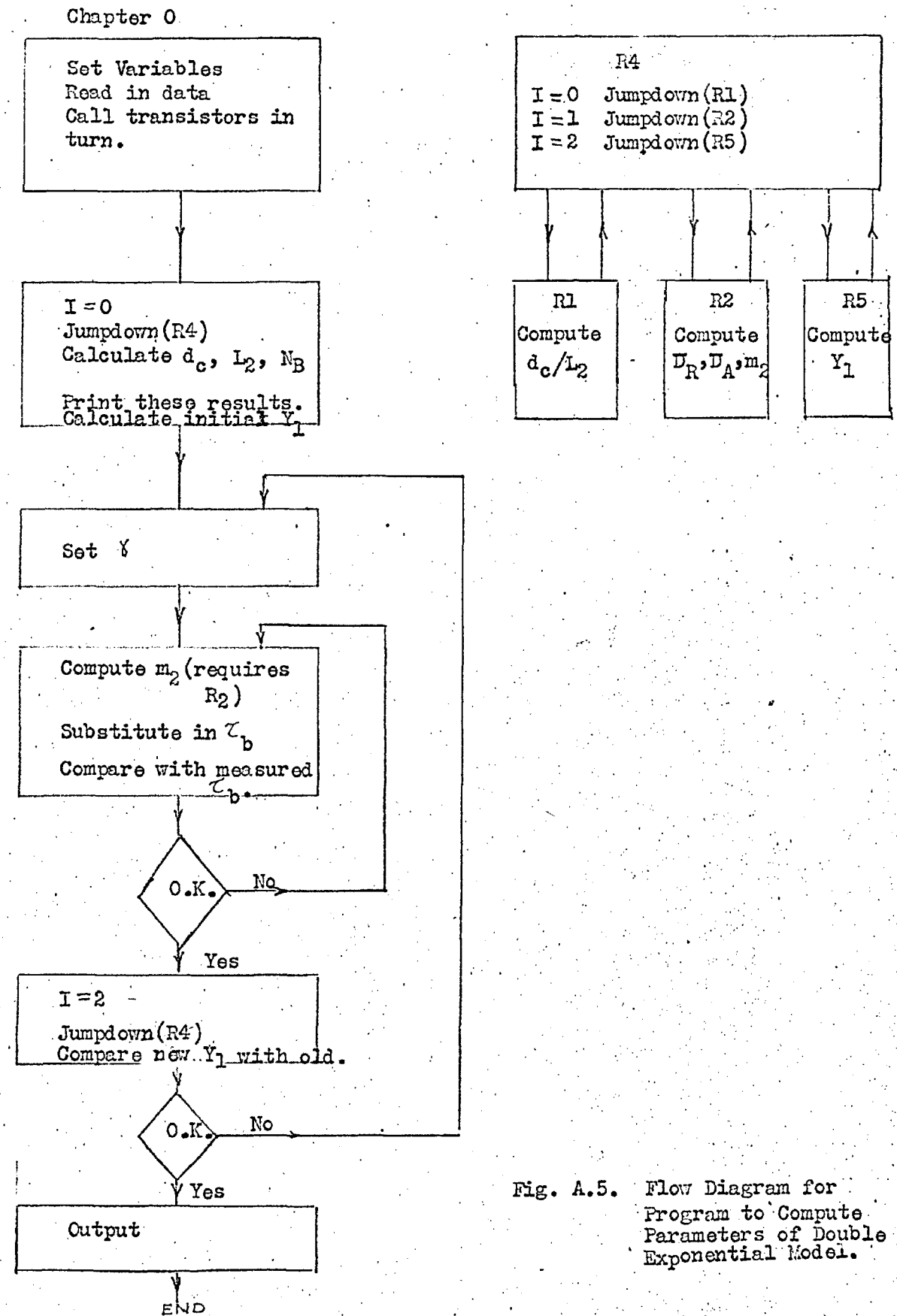


Fig. A.5. Flow Diagram for Program to Compute Parameters of Double Exponential Model.

```
JOB
LXK43PA1, THOMAS RUN71 7/5/66
COMPUTING 25000 INSTRUCTIONS
OUTPUT
0 LINE PRINTER 250 LINES
STORE 20 BLOCKS
COMPILER EMA
MAIN→500
AUXILIARY(0,0)
DEPTH 3
DUMPS 0
TITLE
DBLE EXP. PARAMETERS -DIODE LAW + TRANSIT T.

ROUTINE1
B=C21A
B=xDIVIDE(C12+B,G3)
B=BA11/A12
C=AAA
C=1/C
D=xEXP(.5A)
E=xEXP(-.5A)
D=xDIVIDE(D+E,D-E)
D=.5AAD-A
B=B-CD
RETURN
xEXP
**

ROUTINE2
A13=En-1
A15=A
A16=AA3
B=xEXP(A15)
A17=BA5/A8
Y1=Y4/A16
B=xMOD(En)
B=xLOG(B)
D7=BA3/A13
C=xEXP(-D7/A3)
D=xEXP(-EnD7/A3)
B=A3-CA3+A3/En-DA3/En
Cn=BA17/D7+A5
B=D0/Cn
B=xMOD(B)
B=xLOG(B)
B=xEXP(BD2)
D10=BD1
D9=A5/A17
B=xEXP(-A15)
C=xEXP(-D7/A3)
B=C-B
C=xEXP(-EnA15)
D=xEXP(-EnD7/A3)
C=D-C
B=BA3+CA3/En
D8=xDIVIDE(BA17,A16-D7)
```

```
Cn=D8+A5
B=Do/Cn
B=xMOD(B)
B=xLOG(B)
B=xEXP(BD2)
D11=BD1
A20=D10/D11

A18=D7/A16
B=xEXP(-EnA15Y1)
C=xEXP(-A15Y1)
D=B/En-C-D9A15Y1
E=xEXP(-EnA15A18)
C=xEXP(-A15A18)
E=E/En-C-D9A15A18
E=E-EA20
C=xEXP(-EnA15)
F=xEXP(-A15)
C=C/En-F-D9A15
C=CA20
D4=E+C-D
D4=xMOD(D4)
D5=xDIVIDE(AoD10,A3A10A17)
B=D4-D5
RETURN
xEXP
xLOG
**

ROUTINE3
M=1(1)15
D=o.5XMA18-o.5XMY1+o.5A18+o.5Y1
B=xEXP(-DAA15)
C=xEXP(-DA15)
E=C-B-D9
B=xDIVIDE(B,AA15)
B=B-C/A15-DD9
C=xEXP(-AA15A18)
F=xEXP(-A15A18)
C=xDIVIDE(C,AA15)
C=C-F/A15-D9A18
A21=xEXP(-A15)
A22=xEXP(-AA15)
A23=xDIVIDE(A22,AA15)
A19=A23-A21/A15-D9
B=C-CA20+A19A20-B
B=B/E
C=o.5A18-o.5Y1
ZM=CBWM
REPEAT
M=2(1)15
ZM=ZM+Z(M-1)
REPEAT
D6=ZM
```

```
M=1(1)15
D=0.5XM-0.5XMA18+0.5+0.5A18
B=xEXP(-DAA15)
C=xEXP(-DA15)
E=C-B-D9
B=xDIVIDE(B,AA15)
B=B-C/A15-DD9
B=A19-B
B=B/E
C=0.5-0.5A18
ZM=BCWM
REPEAT
M=2(1)15
ZM=ZM+Z(M-1)
REPEAT
D6=ZMA20+D6
D3=D6A16A16/D10
D3=xMOD(D3)
D13=G5-D3
RETURN
**

ROUTINE4
E1=C24
A=E1
JUMP3,I=1
JUMP30,I=2
2)JUMPDOWN(R1)
JUMP4
3)JUMPDOWN(R2)
JUMP4
30)JUMPDOWN(R5)
4)F1=B
E3=C25
17)A=E3
JUMP7,I=1
JUMP31,I=2
6)JUMPDOWN(R1)
JUMP8
7)JUMPDOWN(R2)
JUMP8
31)JUMPDOWN(R5)
8)F3=B
E2=5
C=F1F3
JUMP16,C>0
9)E2=0.5E1+0.5E3
A=E2
JUMP12,I=1
JUMP32,I=2
11)JUMPDOWN(R1)
JUMP13
12)JUMPDOWN(R2)
JUMP13
32)JUMPDOWN(R5)
13)F2=B
```

```
Y=E3-E1
Y=Y/E3
An=.001
JUMP15,An>Y
C=F1F2
JUMP14,0>C
F1=F2
E1=E2
JUMP9
14)F3=F2
E3=E2
JUMP9
16)JUMP15,E3>5C25
E3=1.5E3
JUMP17
15)RETURN
**

ROUTINE5
C=xEXP(2A15Yo/A16)
D=xEXP(2A15YoEn/A16)
B=xEXP(-AA15)
B=BC-B
C=xEXP(-AA15En)
C=CD-C
B=B-C/En
B=B-2D9A15Yo/A16
RETURN
**

CHAPTERo
A→26
W→15
X→15
Y→5
Z→15
B→312
C→25
E→22
F→22
G→8
D→16
M=1(1)15
READ(WM)
REPEAT
M=1(1)15
READ(XM)
REPEAT
READ(A12)
READ(A24)
READ(C13)
READ(C14)
READ(Go)
READ(G1)
READ(K)
```

```
READ(Do)
READ(D1)
READ(D2)
Q=1(1)K
READ(BQ)
READ(B(Q+26))
READ(B(Q+52))
READ(B(Q+78))
READ(B(Q+104))
READ(B(Q+130))
READ(B(Q+156))
READ(B(Q+182))
READ(B(Q+208))
READ(B(Q+234))
READ(B(Q+260))
READ(B(Q+286))
REPEAT

Q=1(1)K
Ao=B(Q)
A1=B(Q+26)
A11=B(Q+52)
A9=B(Q+78)
C11=B(Q+104)
C3=B(Q+130)
C9=B(Q+156)
C12=B(Q+182)
C16=B(Q+208)
C18=B(Q+234)
A10=B(Q+260)
G2=B(Q+286)
NEWLINE
NEWLINE
A2=Ao/A1
F4=C3/A11
A=F4F4F4
G3=C9/A
C21=A24C11/A12
C24=C13
C25=C14
I=o
CAPTION
D/L2=
JUMPDOWN(R4)
A4=E2
PRINT(A4)3,3
G4=A1/F4
A3=G4/A4
A5=xDIVIDE(G3,A4G4G4)
CAPTION
D=
PRINT(G4)o,4
CAPTION
L2=
PRINT(A3)o,4
```

```
CAPTION
NB=
 PRINT(A5)o,4
B=G4/G2
G5=C18-B
A=xEXP(-A4)
A=1-A
A8=A/A4
Yo=o.5AoA11/A9
Y4=Yo

J=o
S=o
En=2.o
19)I=1
C24=Go
C25=G1
G8=Y4
JUMPDOWN(R4)
A15=E2
A16=A15A3
A=En
JUMPDOWN(R3)
D14=D13/G5
D=xMOD(D14)
JUMP26,o.o1>D
JUMP26,J>1oo
JUMP21,J>o
2o)D15=D14
G6=En
En=En+o.1En
J=J+1
JUMP19
21)C=D14D15
JUMP23,o>C
 B=xMOD(D15)
JUMP2o,B>D
22)D15=D14
G6=En
En=En-o.1En
J=J+1
JUMP27,1≥En
JUMP19
23)G7=En
D16=D14
24)J=J+1
JUMP26,J>3o
En=o.5G6+o.5G7
JUMPDOWN(R4)
A15=E2
A16=A3A15
A=En
JUMPDOWN(R3)
D14=D13/G5
```

```
C=G7-G6
C=C/G7
C=xMOD(C)
JUMP26,0.01>C
C=D14D15
JUMP25,0>C
G6=En
D15=D14
JUMP24
25)G7=En
D16=D14
JUMP24
26)B=AoAoAo
Y5=C16/B
Y3=A17En/A3-A17/A3
C24=0.5Yo/A16
C25=2Yo/A16
I=2
JUMPDOWN(R4)
Y4=E2A16
C=Y4/G8-1
C=xMOD(C)
S=S+1
JUMP50,3>S
JUMP27,J>100
50)JUMP27,S>8
J=0
JUMP19,C>0.01
27)Yn=Y4/A16
Y2=2Yo-Y4

CAPTION
L2/L1=
PRINT(En)3,4
CAPTION
M2=
PRINT(A15)0,4
CAPTION
Ao=
PRINT(Yo)0,4
NEWLINE
CAPTION
W=
PRINT(A16)0,4
CAPTION
No=
PRINT(A17)0,4
CAPTION
A2=
PRINT(Y4)0,4
CAPTION
A1=
PRINT(Y2)0,4
CAPTION
DR=
PRINT(D10)3,4
```

```
CAPTION
DA=
PRINT(D11)3,4
CAPTION
YM=
PRINT(A18)3,4
NEWLINE
CAPTION
Y1=
PRINT(Yn)3,5
CAPTION
S1=
PRINT(Y5)0,4
CAPTION
To=
PRINT(G5)0,5
CAPTION
S2=
PRINT(Y3)0,4
REPEAT
END
xEXP
xLOG
CLOSE

FIRST TWO BLOCKS OF DATA AS IN APPENDIX A.6
-USED FOR INTEGRATION BY GAUSSIAN QUADRATURE

1.6025,-19
1.38,-23
0.05
20.0
1.0001
6.0
1       -UP TO 26 TRANSISTORS MAY BE INCLUDED
6.0,16
13.5
0.25

1.126,-3
4.93,-3
1.06248,-12
1.19,-10
295.5
1.13,-11
1.469,12
10.43
8.93,12
1.40,-9
2.79,-15
1.6,7

→
***Z
```